NASA/TM-20210017631/REV1

Flight Test Data for Prototype Air-Ground Control and Non-Payload Communications Radio Link

Kurt Shalkhauser and Joseph Ishac
Glenn Research Center, Cleveland, Ohio

Steven Bretmersky
MTI Systems, Inc., Cleveland, Ohio

Michael W. Neale
Advantage Consulting and Engineering Services Corporation, Washington, DC

Brian Frantz
HX5, LLC, Brook Park, Ohio

Michael Cauley and Dennis Iannicca
Glenn Research Center, Cleveland, Ohio

Christine Chevalier and David Stewart
HX5, LLC, Brook Park, Ohio

Robert Dimond and Evan Hanau
Peerless Technologies Corporation, Fairview Park, Ohio

This Revised Copy, numbered as NASA/TM-20210017631/REV1, March 2023, supersedes the previous version, NASA/TM-20210017631, December 2021, in its entirety.

March 2023

NASA STI Program . . . in Profile

Since its founding, NASA has been dedicated to the advancement of aeronautics and space science. The NASA Scientific and Technical Information (STI) Program plays a key part in helping NASA maintain this important role.

The NASA STI Program operates under the auspices of the Agency Chief Information Officer. It collects, organizes, provides for archiving, and disseminates NASA's STI. The NASA STI Program provides access to the NASA Technical Report Server—Registered (NTRS Reg) and NASA Technical Report Server—Public (NTRS) thus providing one of the largest collections of aeronautical and space science STI in the world. Results are published in both non-NASA channels and by NASA in the NASA STI Report Series, which includes the following report types:

- TECHNICAL PUBLICATION. Reports of completed research or a major significant phase of research that present the results of NASA programs and include extensive data or theoretical analysis. Includes compilations of significant scientific and technical data and information deemed to be of continuing reference value. NASA counter-part of peer-reviewed formal professional papers, but has less stringent limitations on manuscript length and extent of graphic presentations.

- TECHNICAL MEMORANDUM. Scientific and technical findings that are preliminary or of specialized interest, e.g., "quick-release" reports, working papers, and bibliographies that contain minimal annotation. Does not contain extensive analysis.

- CONTRACTOR REPORT. Scientific and technical findings by NASA-sponsored contractors and grantees.

- CONFERENCE PUBLICATION. Collected papers from scientific and technical conferences, symposia, seminars, or other meetings sponsored or co-sponsored by NASA.

- SPECIAL PUBLICATION. Scientific, technical, or historical information from NASA programs, projects, and missions, often concerned with subjects having substantial public interest.

- TECHNICAL TRANSLATION. English-language translations of foreign scientific and technical material pertinent to NASA's mission.

For more information about the NASA STI program, see the following:

- Access the NASA STI program home page at http://www.sti.nasa.gov

- E-mail your question to help@sti.nasa.gov

- Fax your question to the NASA STI Information Desk at 757-864-6500

- Telephone the NASA STI Information Desk at 757-864-9658

- Write to:
  NASA STI Program
  Mail Stop 148
  NASA Langley Research Center
  Hampton, VA 23681-2199

NASA/TM-20210017631/REV1

Flight Test Data for Prototype Air-Ground Control and Non-Payload Communications Radio Link

Kurt Shalkhauser and Joseph Ishac
Glenn Research Center, Cleveland, Ohio

Steven Bretmersky
MTI Systems, Inc., Cleveland, Ohio

Michael W. Neale
Advantage Consulting and Engineering Services Corporation, Washington, DC

Brian Frantz
HX5, LLC, Brook Park, Ohio

Michael Cauley and Dennis Iannicca
Glenn Research Center, Cleveland, Ohio

Christine Chevalier and David Stewart
HX5, LLC, Brook Park, Ohio

Robert Dimond and Evan Hanau
Peerless Technologies Corporation, Fairview Park, Ohio

This Revised Copy, numbered as NASA/TM-20210017631/REV1, March 2023, supersedes the previous version, NASA/TM-20210017631, December 2021, in its entirety.

National Aeronautics and
Space Administration

Glenn Research Center
Cleveland, Ohio 44135

March 2023

Acknowledgments

This report was prepared under the Unmanned Aircraft Systems Integration in the National Airspace System (UAS in the NAS) Project in coordination with Radio Technical Commission for Aeronautics (RTCA) Special Committee (SC) 228 Working Group 2. Michael W. Neale from Advantage Consulting and Engineering Services (ACES) Corporation was supported by the Federal Aviation Administration. The authors acknowledge the members of the UAS in the NAS Command and Control (C2) Subproject team who have contributed to this report and to the extensive flight test activities it describes. They include Daniel Young (Peerless Technologies Corporation) and Donna Clements (HX5, LLC). The project would not have been possible without the support of the pilots Kurt Blankenship, James Demers, Mark Russell, and Aaron Swank; the flight engineers Jeff Polack and Matt Fakler; and the entire maintenance staff. Additionally, the research conducted throughout the C2 Subproject would not have been possible without the capabilities of NASA601, the Lockheed Corporation model S–3B Viking aircraft owned by NASA Glenn Research Center (aircraft registration number N601NA). This twin-turbofan jet research aircraft was used extensively for all of the dual-band channel sounding measurements, developmental Control and Non-Payload Communications (CNPC) radio flight tests, CNPC radio validation flight tests, and site surveys required under the UAS C2 efforts. Built in 1978, this venerable aircraft was the last S–3B assembled by Lockheed Corporation and was the only S–3B still in service throughout the NASA UAS in the NAS Project. This aircraft has now been decommissioned and is enjoying full retirement at the San Diego Air and Space Museum.

Revised Copy

This Revised Copy, numbered as NASA/TM-20210017631/REV1, March 2023, supersedes the previous version, NASA/TM-20210017631, December 2021, in its entirety.

An incorrect version of NASA/TM-20210017631 was published in October 2021. Modifications to this Revised Copy address errors, omissions, and inconsistencies to the text and figures. The acknowledgments section has been revised, and an authorship note has been inserted.

Authorship note:
The authorship of this Technical Memorandum was updated in September 2022. Based on an analysis/investigation by the NASA Glenn Research Center Research Integrity Officer into the contributors to this report, the updated order of the authors reflects the best estimate of their contributions.

Level of Review: This material has been technically reviewed by technical management.

This report is available in electronic form at http://www.sti.nasa.gov/ and http://ntrs.nasa.gov/

Preface

This document was originally prepared in coordination with Radio Technical Commission for Aeronautics (RTCA) Special Committee (SC) 228 Working Group 2 in the investigation of a radio communications link between an unmanned aircraft and fixed ground station. The data and analysis in this report were published in their entirety as Appendix O of DO–362A, "Command and Control (C2) Data Link Minimum Operational Performance Standard (MOPS) (Terrestrial)" (RTCA, Inc., Command and Control (C2) Data Link Minimum Operational Performance Standards (MOPS) (Terrestrial), RTCA DO–362A, 2020) and were used extensively in the preparation of that standard. The appendix is being republished here as an independent document so that its contents are available to a wider audience.

Contents

Flight Test Data for Prototype Air-Ground Control and Non-Payload Communications Radio Link

Kurt A. Shalkhauser* and Joseph Ishac
National Aeronautics and Space Administration
Glenn Research Center
Cleveland, Ohio 44135

Steven C. Bretmersky
MTI Systems, Inc.
Cleveland, Ohio 44135

Michael W. Neale
Advantage Consulting and Engineering Services Corporation
Washington, DC 20004

Brian Frantz
HX5, LLC
Brook Park, Ohio 44142

Michael Cauley and Dennis Iannicca*
National Aeronautics and Space Administration
Glenn Research Center
Cleveland, Ohio 44135

Christine Chevalier and David Stewart
HX5, LLC
Brook Park, Ohio 44142

Robert Dimond and Evan Hanau
Peerless Technologies Corporation
Fairview Park, Ohio 44126

Summary

Extensive flight testing was conducted over flat terrain, hilly terrain, and open freshwater settings to examine performance of an air-ground command and control radio link for unmanned aerial vehicles. The flight data collected on bidirectional radio range, signal fading, and transmitted data loss were necessary to validate a proposed air-ground radio waveform that was being considered by a U.S. standards organization. The NASA test system operated at C-band frequencies and utilized a prototype, software-defined radio developed in cooperation with a commercial avionics supplier. Results are presented for multiple altitudes, ranges, and flight conditions, indicating the signal fade depths, occurrence rates, and durations for each flight environment.

* Retired.

1.0 Introduction

Researchers at the NASA Glenn Research Center conducted a series of flight tests under the Unmanned Aircraft Systems Integration in the National Airspace System (UAS-in-the-NAS) Project to specifically examine radio signal propagation and data flow at C-band frequencies. This report presents data recorded during flight tests of Gaussian Minimum Shift Keying (GMSK) Control and Non-Payload Communications (CNPC) Link System radios operating in a bidirectional, air-to-ground arrangement. Data is presented for test flights over smooth plains, slightly rolling plains, and open water settings at various altitudes, ranges, and ascent and descent angles. Excess path loss (EPL), availability (A%), average fade duration (AFD), and level crossing rates (LCR) calculated from the flight test results are presented in Section 4.0. Data in this report has been used to validate the Technical Requirements in Subsection 2.2.2 of the Minimum Operational Performance Standards (MOPS) (Ref. 1) including 2.2.1.12 Channel Model for Receiver Performance Verification and serves as the basis for the Link Budget Analysis in Appendix L and for the Desired/Undesired Signal Analysis in Appendix R.

The validation flight tests were conducted during the period from October 2019 to March 2020 in airspace above Ohio, U.S.A. This report includes a compilation of data from the validation flight tests, along with descriptions of the airborne and ground-based test systems. Additional information on the prototype radios, their performance, and the system test configuration is presented in the technical memorandum entitled "Control and Non-Payload Communications Generation 7 Radio Flight Test Report" (Ref. 2).

2.0 General Description of Measurement System

An overview diagram of the validation test system is presented in Figure 1. The primary elements of the system are the test aircraft (described in Section 2.1) and the ground equipment (described in Section 2.2), both of which were monitored and controlled by a centralized test operations center at NASA Glenn Research Center. One CNPC Link Radio System was installed in the test aircraft and one installed at the ground site to establish bidirectional radio connectivity, allowing researchers to simultaneously monitor both air-to-ground and ground-to-air signal propagation characteristics and radio performance. The radios operated at a selectable frequency within the 5,030- to 5,091-MHz band (C-band).

In order to capture signal propagation data in specific terrain settings, the ground radio system (GRS), ground support equipment, and the test antenna were temporarily positioned in three unique geographic locations. An aircraft flight pattern was designed and flown at each location to allow direct comparison of propagation performance. Azimuth and elevation angles of the ground antenna were adjusted to maintain a desired angle above ground topography, to achieve unobstructed line of sight to the aircraft, and to exploit the surface roughness in the foreground of the ground antenna. The GRS equipment was operated with a customized, self-supporting trailer with an extendable antenna mast. For flight tests over open, flat terrain (referred to as "smooth plains") (Ref. 3), the mobile equipment trailer was positioned at the southern boundary of NASA's Plum Brook Station facility[1] in Perkins Township, Ohio. For flight tests over hilly terrain (referred to as "slightly rolling plains") (Ref. 3), the same GRS equipment was positioned on the tarmac of the Ohio University Gordon K. Bush Airport in Albany, Ohio (airport designation: KUNI). For the over-water tests, the GRS equipment was positioned at the extreme western shoreline of Lake Erie in Sandusky, Ohio. At each site, the GRS test system was equipped with internet

[1]Now NASA's Neil A. Armstrong Test Facility.

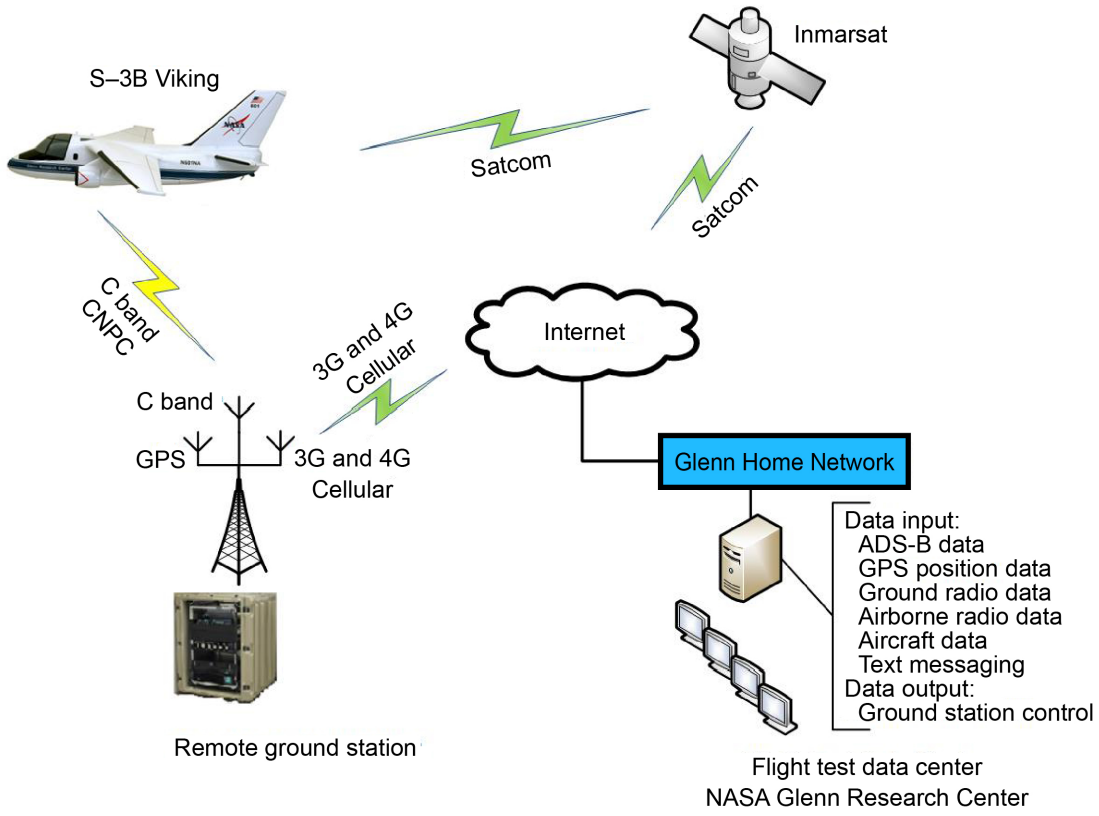

Figure 1.—Control and Non-Payload Communications (CNPC) Minimum Operational Performance Standard baseline radio test system. Automatic Dependent Surveillance-Broadcast (ADS-B). Global Positioning System (GPS). Satellite communication (Satcom).

connections for remote control, monitoring, programming, and test operations. A commercial, satellite-based communications link was used to coordinate test operations between the GRS locations, the Glenn test operations center, and the test aircraft.

2.1 Description of Airborne Platform Used in Validation Testing

A Lockheed model S–3B Viking aircraft owned by NASA Glenn Research Center (Federal Aviation Administration (FAA) aircraft registration number N601NA) was used for all of the MOPS CNPC Link System flight tests. The twin-turbofan jet research aircraft had been used extensively for L- and C-band channel sounding measurements preceding this radio investigation and for numerous developmental CNPC Link System flight tests.

The S–3B aircraft possessed multiple features supporting the MOPS CNPC Link System flight validation testing:

1. A high-mounted, cantilever wing provided an unobstructed radio line-of-sight path between airborne and ground test antennas during level flight and light banking. Wingspan: 68 ft 8 in.
2. A long-range flight (endurance) capability provided typical flight durations of 2- to 4 h.
3. A large, pressurized cabin accommodated a crew of four persons, which includes a pilot, co-pilot, and two research personnel.
4. A commercial satellite communications link provided experiment coordination between ground and airborne flight test personnel.
5. In-cabin equipment racks with ample research electrical power accommodations were available.

6. Excellent flight stability and maneuverability including roll and pitch stability within ±2°; standard rate turns at 20° to 30° aircraft banking, maximum 60° bank turns, and sustained 10° bank (slip) was possible.
7. Fully retractable landing gear and minimal underside fuselage contour provided minimum obstruction to the CNPC antenna hemispherical field of view.
8. The maximum (true) airspeed was 360 kn (414 mph, 185 m/s) at 29,000 ft (8,839 m).
9. The cruise speed was 250 kn (287 mph, 128 m/s).
10. The minimum airspeed was 120 kn (138 mph, 61 m/s).
11. The range was over 1,000 nmi.
12. The service ceiling was at 29,000 ft. (8,839 m).

The airborne research equipment consisted of one prototype C-band CNPC–5000E[2] airborne radio system (ARS), attendant radiofrequency (RF) components, a laboratory-grade RF high-power amplifier, electrical power supply electronics, a Global Positioning System (GPS) and time server equipment, an avionics-bus interface system, computers, and networking equipment. These components, shown in Figure 2, were installed into two 19-in.-wide equipment racks within the pressurized volume in the rear of the aircraft.

A flight-certified, C-band, low-profile, omnidirectional, 1/4-wave monopole antenna was permanently mounted on the underside of the S–3B aircraft to support both the transmit and receive functions of the ARS. The antenna was connected through the pressure bulkhead to the radio by a single customized, aircraft-grade, fully shielded, low-insertion-loss coaxial cable. When landing gear is stowed for level flight, the antenna field of view (in the “downward” or nadir direction) is a full hemisphere that is unobstructed by protuberances from the aircraft. Figure 3 shows the location of the CNPC antenna and underside fuselage geometry of the S–3B test aircraft. The antenna is positioned slightly right of the aircraft centerline to reduce coupling to adjacent aircraft antennas.

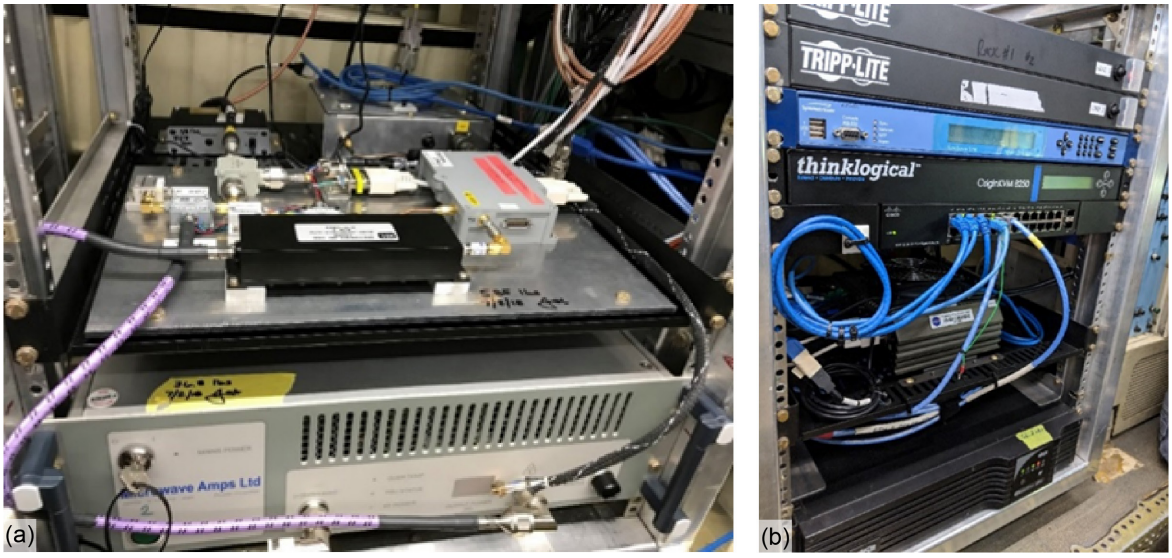

Figure 2.—Control and Non-Payload Communications (CNPC) radio. (a) CNPC–5000E radio shown with attendant radiofrequency components and high-power amplifier (HPA). (b) Aircraft computer, networking, and time base equipment.

[2]Radio hardware developed in conjunction with Collins Aerospace under NASA Cooperative Research Agreement NNC11AA01A.

Figure 3.—NASA S–3B Viking test aircraft showing antenna mounting location.

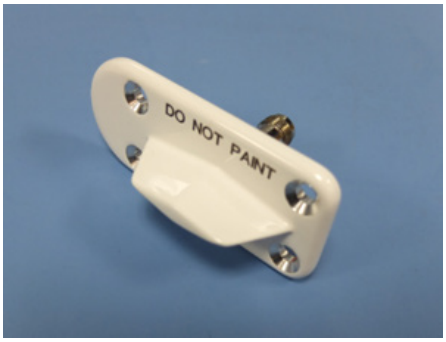

Figure 4.—C-band aircraft antenna.

The aircraft antenna used in the CNPC flight tests is shown in Figure 4. The antenna was a commercially available model that provided omnidirectional RF performance suitable for conducting the flight tests but did not necessarily meet the antenna requirements stated in Reference 1. Gain patterns for the aircraft antenna are presented in Section 2.3.

2.2 Description of Ground Equipment Used in Validation Testing

The ground equipment used in the validation testing was prepared and operated by Glenn. Like the ARS test system, the ground system consisted of one C-band prototype CNPC–5000E radio with attendant RF, high-power amplifier (HPA), networking, and time base equipment. The ground equipment connected to the internet through either a hard-wired host-site network or a 3G/4G cellular network, allowing full control and monitoring of the GRS from the Glenn test operations center in Cleveland, Ohio.

Figure 5 shows a block diagram of the main elements of the ground station (GS) and GRS. The blue boxes represent the prototype CNPC radio and attendant devices. These components are grouped inside a broken-line box to indicate all the functions that would typically reside internally to a CNPC radio. The green components are interface and support equipment specific to the NASA test system.

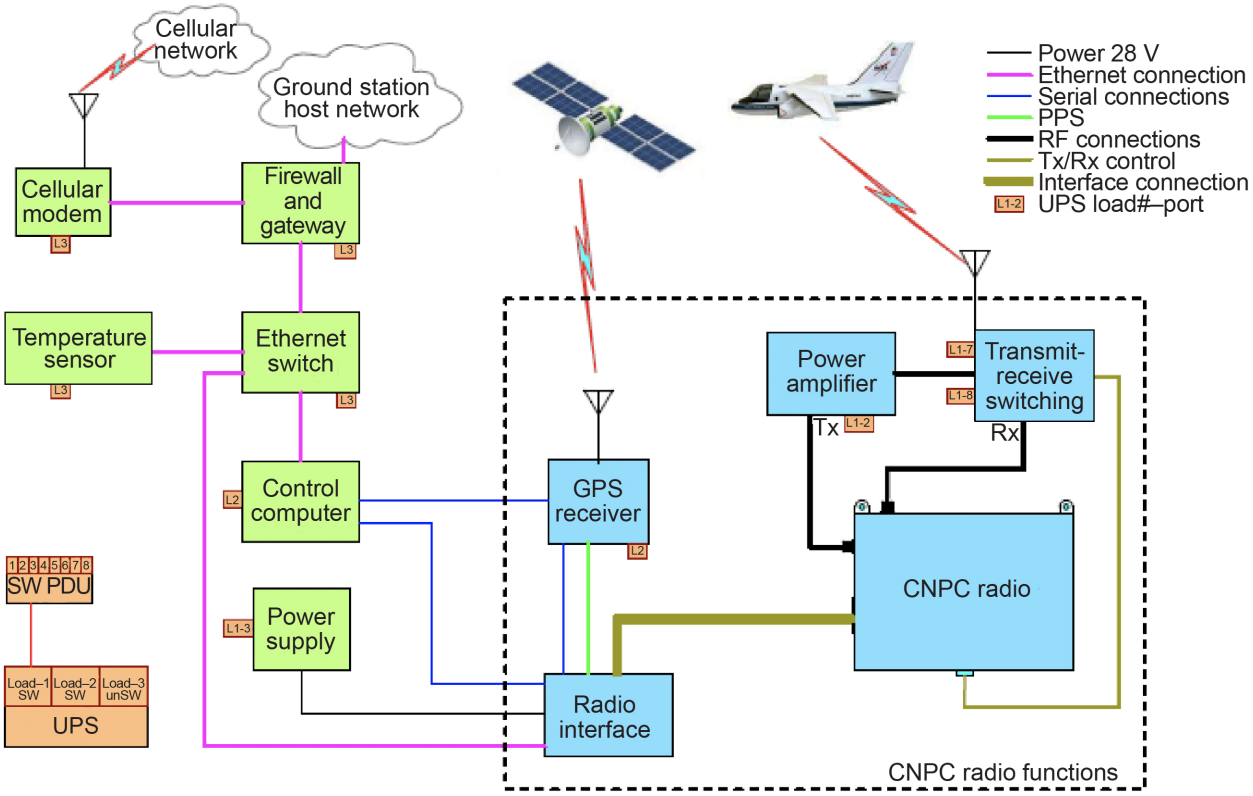

Figure 5.—NASA ground equipment. Control and Non-Payload Communications (CNPC). Global Positioning System (GPS). Pulse per second (PPS). Power distribution unit (PDU). Radiofrequency (RF). Receive (Rx). Switched (SW). Transmit (Tx). Uninterruptible power supply (UPS).

The small form factor, prototype CNPC radio used in the flight tests did not contain an internal transmit and receive (T/R) antenna switch or transmit amplifier. To provide these functions, NASA Glenn designed and assembled a T/R circuit (Figure 6) that contained components to merge the radio transmit and receive signal connections into one antenna port. The T/R circuit also provided a bandpass filter to prohibit out-of-band emissions. The high-speed electronic switches controlled the transmitted and received RF signal flow paths to synchronize with the 20-Hz time-division duplex rate of the CNPC radio.

A commercially available solid-state, rack-mounted, 120-W HPA was included in the GRS to compensate for insertion losses of the RF components and cabling. The HPA was operated in its linear amplification region well below its saturation level, where it produced nominally 10 W of signal power at the radio tray antenna port, appropriate for flight testing.

A GPS antenna delivered a coded signal to the ground radio, which is used as a time server for the computer and cellular modem. This allowed all ground equipment to be time synchronized with the aircraft and flight test operations center. This synchronization was necessary for accurately recording the precise spatial and geometric relationship of the ARS to the GRS, as well as measuring data flow latency throughout the network.

Figure 7 shows the ground equipment installed into a ruggedized transport case. Antenna coaxial cables, mains power cable, and a network cable exit the case to external locations.

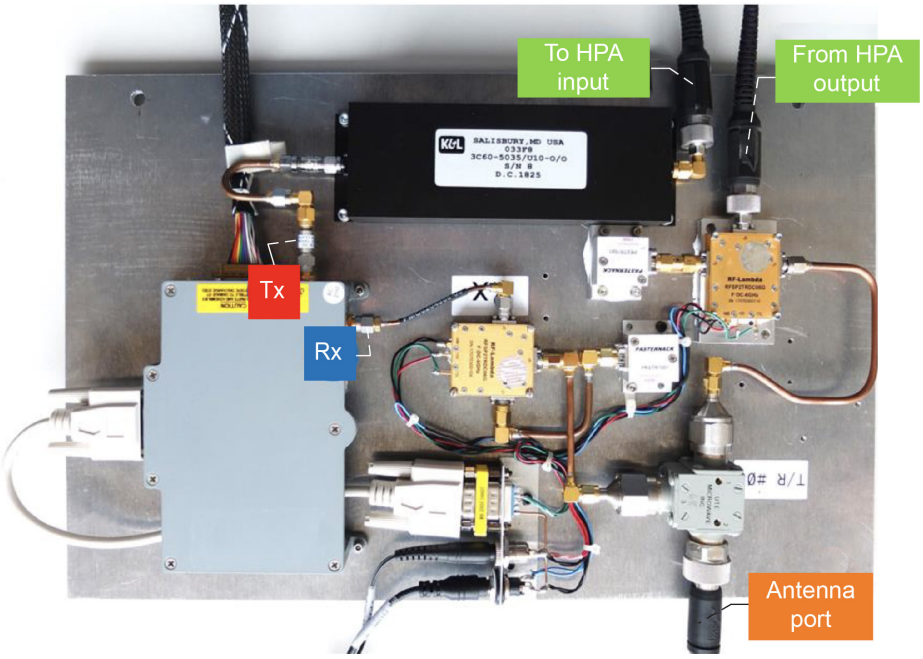

Figure 6.—Transmit (Tx) and receive (Rx) switching, bandpass filter, and radio. High-power amplifier (HPA).

Figure 7.—Ground radio system (GRS) transportable equipment.

The antenna used at the GS for the CNPC flight tests is shown in Figure 8. The antenna is a commercially available, linearly polarized, lensed horn fed through a rectangular waveguide section from a right-angle coaxial launcher. The antenna has an H-plane 3-dB beamwidth of nominally 30°, resulting in the ability to achieve a directional beam to reduce multipath reception and improve directivity. The antenna was mounted to a pan and tilt mechanism at the top of the mobile tower mast for precise azimuth and elevation alignment at each test location. Gain patterns for the aircraft antenna are presented in Section 2.3.

2.2.1 Ground Site Locations

Ground site selection for the validation testing was influenced by many factors. Still, it was primarily driven by local terrain features and the ability to establish the point-to-point CNPC Link System connection between the airborne radio and the ground radio in that particular terrestrial setting. Unique propagation and dispersive signal propagation conditions were desired in each location. Special attention was given to line-of-sight obstructions and terrain surface roughness in the areas up to 1 km immediately in front of the ground antenna where primary RF signal reflections would occur.

Frequency authorizations were obtained for the NASA flight test operations in areas covering most of the Ohio, U.S.A. region. Validation testing occurred in these flight zones, indicated by the 140-km-radius circles shown in Figure 9. Both the transportable GRS and flight ARS operated within these authorized areas. Table I lists location details for the ground sites used in the validation testing.

Figure 8.—Installed ground station directional antenna.

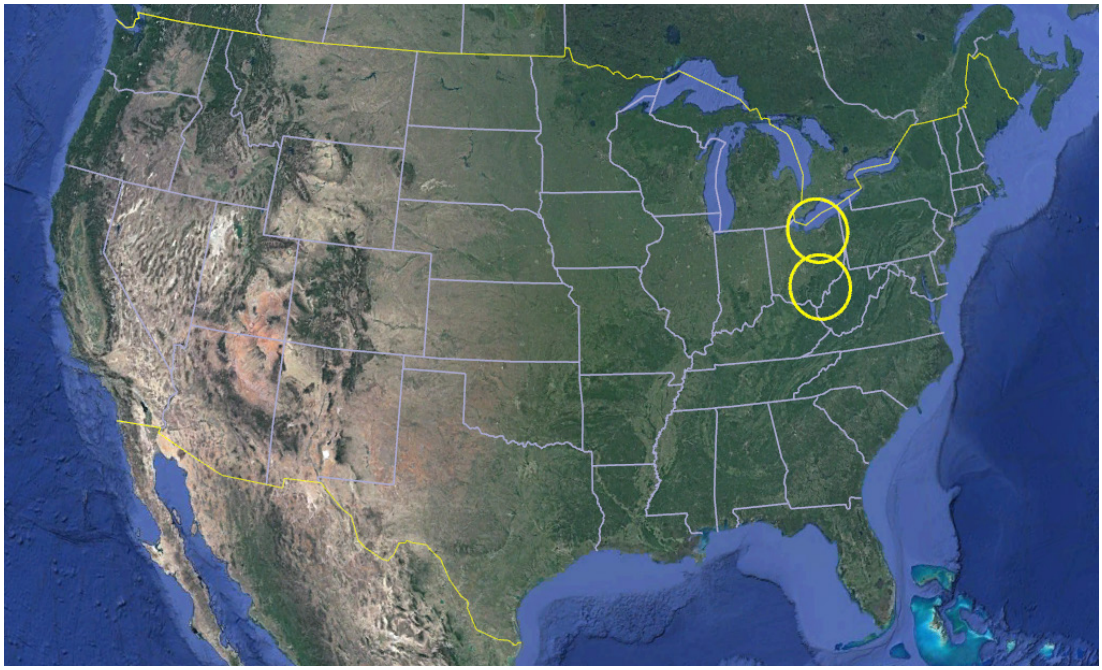

Figure 9.—U.S. map identifying test locations with Control and Non-Payload Communications frequency authorizations with 140-km-radius flight zones shown. Image ©2020 GoogleEarth.

TABLE I.—VALIDATION FLIGHT TEST GROUND SITE LOCATIONS

Test date	Ground station location	Latitude, longitude	Setting	Ground elevation above mean sea level, ft	Antenna height above ground level, ft
10/8/2019	NASA Plum Brook Station[a] Perkins Township, Ohio	41°20'22.50" N 82°38'59.60" W	Smooth plains	623	51.3
12/3/2019	Cedar Point Sandusky, Ohio	41°28'41.89" N 82°40'35.59" W	Open, freshwater	569	51.3
12/5/2019					
12/6/2019					
12/11/2019	Ohio University Airport Albany, Ohio	39°12'44.40" N 82°13'23.40" W	Slightly rolling plains	763	51.3
12/12/2019					

[a]Now NASA's Neil A. Armstrong Test Facility.

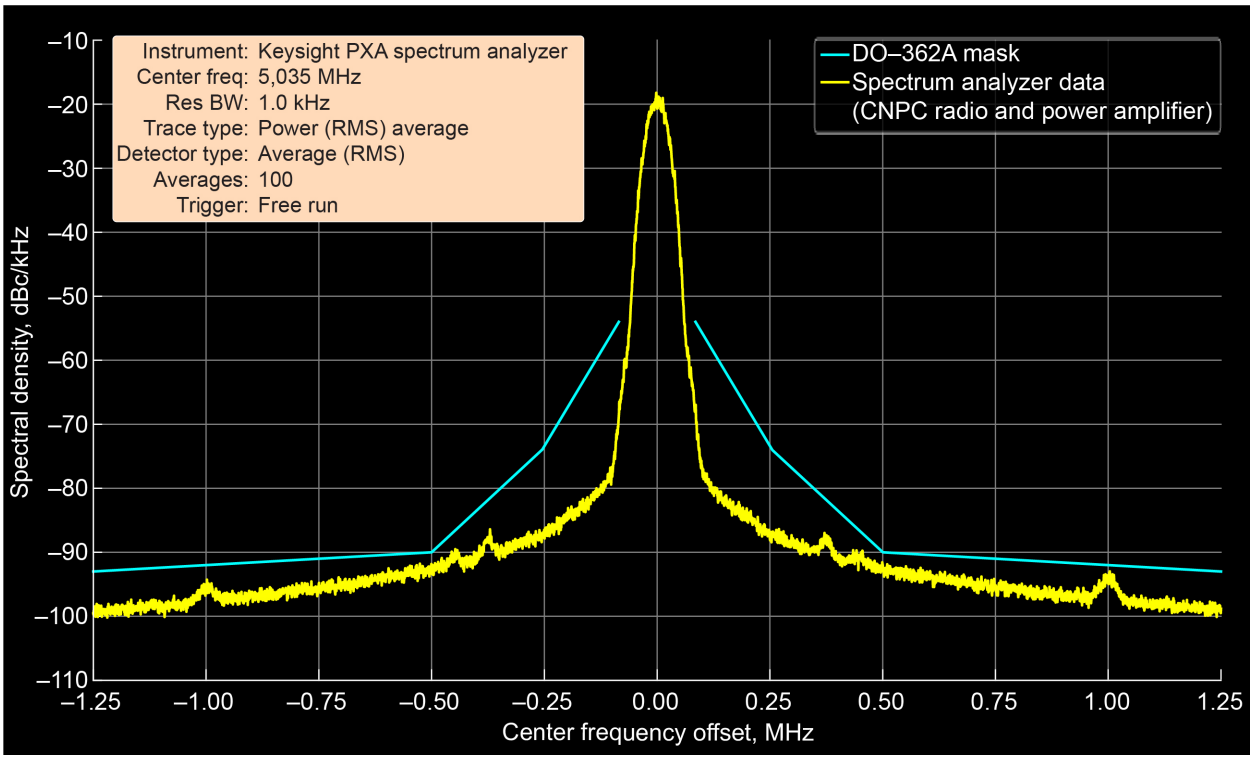

Figure 10.—Control and Non-Payload Communications (CNPC) radio output signal, 90-kHz mode.

2.2.2 Control and Non-Payload Communications Link System Transmission Spectrum

The prototype CNPC Link System radios operated using GMSK modulation to produce an output signal spectra similar to that shown in Figure 10. The trace shown is for CNPC–5000E radio serial number E10 operating at the 5,035-MHz center frequency. The ordinate axis is for scale only. The radios were operated in data class 3 service with the 170-kHz channel bandwidth waveform, offering a symbol rate of 103,500 symbols per second.

For all validation flight tests, the prototype CNPC Link System radios were operated within their respective frequency authorizations at a center frequency of 5,035 MHz for both uplinks and downlinks. For the validation flight tests, the ARS and GRS were operated at an output power level of 10-W average envelope power. Table II shows the transmit power parameters and antenna cable losses for each radio system.

TABLE II.—GROUND SITE RADIO ANTENNA TYPES AND RADIO OUTPUT POWER LEVELS

Application	CNPC radio serial number	Power level at transmit and receive output port (leading to antenna)		Antenna cable radiofrequency losses at 5,035 MHz, S21, dB	Notes
		dBm	W		
Airborne radio system	E10	40	10	3.2	5-dBi omnidirectional monopole blade
Ground radio system	E09	40	10	6.5	15.2-dBi directional horn

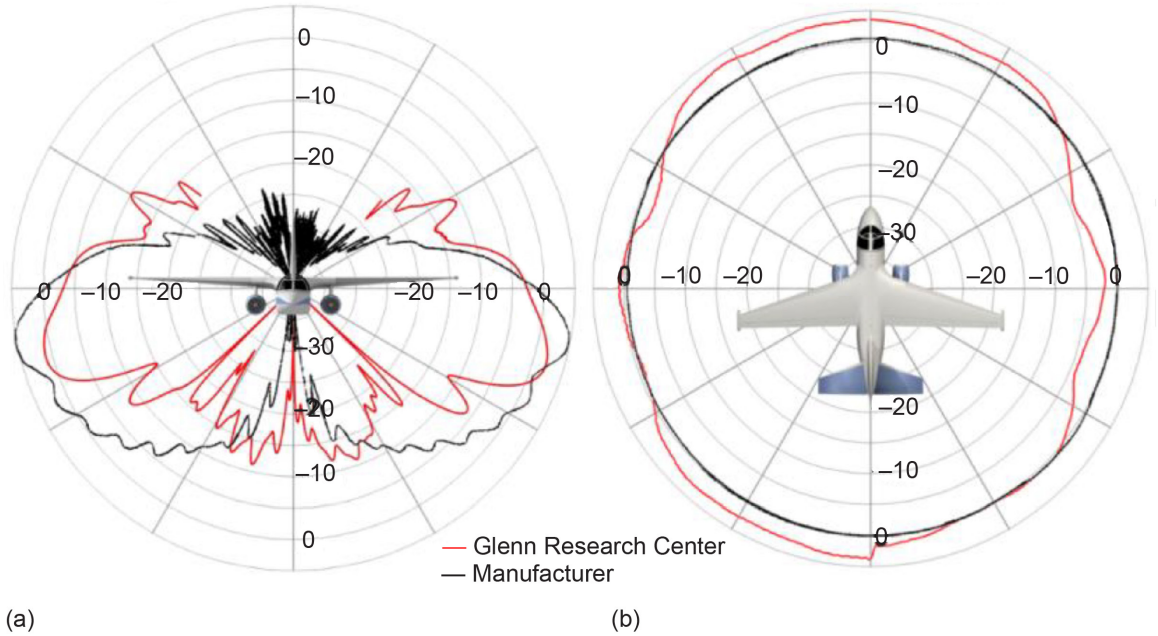

Figure 11.—C-band aircraft antenna gain patterns (dBi). (a) Vertical plane. (b) Horizontal plane.

2.3 Antenna Performance

Antennas utilized in the flight tests were purchased through commercial vendors and were selected to provide practical performance and ready availability. For the aircraft, an antenna certified for high-speed operations was required, and several commercial options were available. Several types of antennas were also available for the GS. For the CNPC flight tests, a waveguide conical horn antenna was used in order to provide a needed signal gain in the air-ground link, as well as to produce a directional beam for multipath signal investigations.

Gain patterns for the aircraft and ground radio antennas are provided in Figure 11 and Figure 12. The patterns were measured in an anechoically treated antenna range under laboratory conditions. When available, the manufacturer's performance data is included for comparison. The antenna performance plots are provided for general assessment only, as antenna gain performance would likely change once installed onto an aircraft or tower structure.

For airport surface operations testing, Glenn used a commercially available C-band, full-wave dipole, omnidirectional, GS antenna shown in Figure 13. Due to the close proximity of the GS to the airport property, the antenna was required to have a wide azimuthal coverage, thereby eliminating the use of the directional antenna. The dipole antenna was positioned vertically and elevated to a height of 15 ft above ground level for the taxi tests.

The performance of the antenna was measured in Glenn's Far-Field Antenna Range, as shown in Figure 14. A gain of 3.76 dBi was measured, similar to, but slightly less than, the manufacturer's specification of 4.15 dBi.

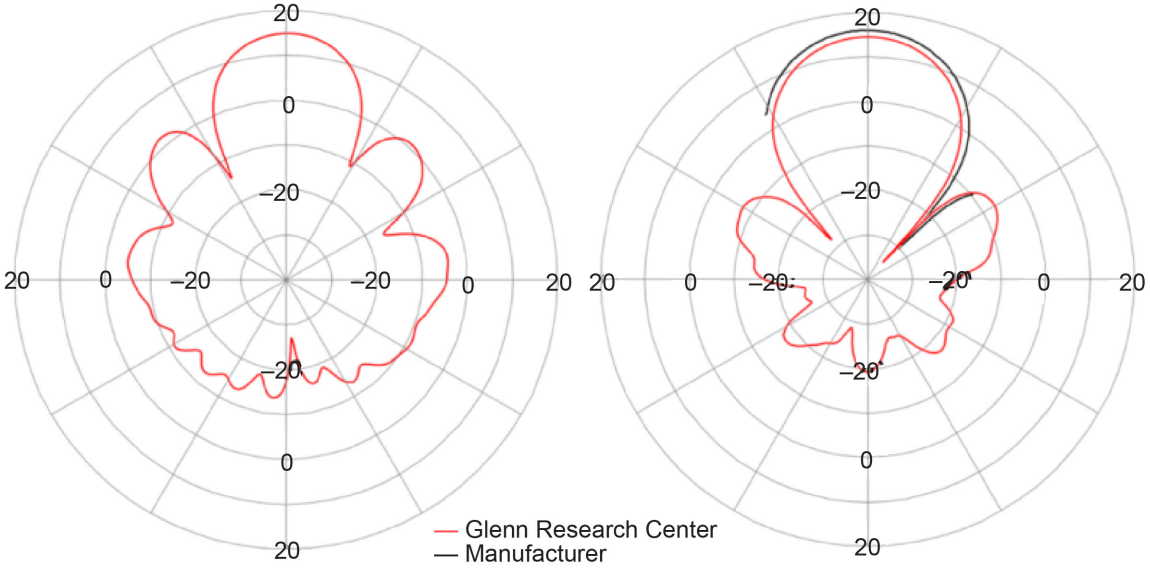

Figure 12.—C-band ground directional antenna gain patterns (dBi). (a) Vertical plane. (b) Horizontal plane.

Figure 13.—Ground station C-band omnidirectional antenna.

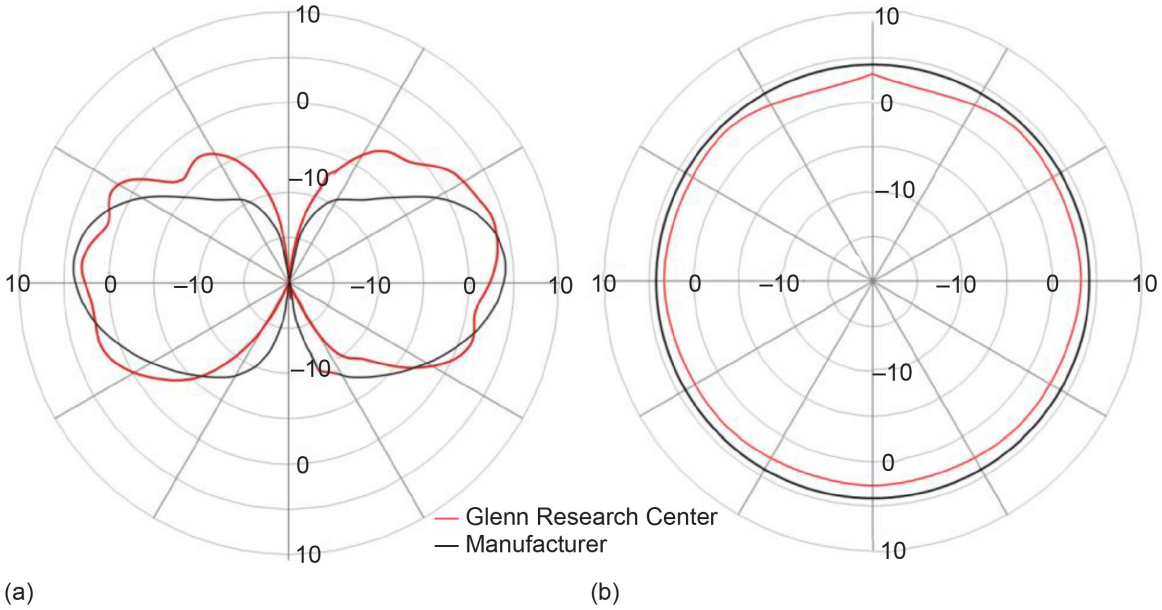

Figure 14.—C-band ground station omnidirectional antenna gain patterns (dBi). (a) Vertical plane. (b) Horizontal plane.

3.0 Validation Test Flightpath General Description

The planned flightpath was purposely the same for each of the three validation test settings to allow direct comparison of electromagnetic propagation over the diverse terrain conditions. Flight altitudes required slight tailoring in land areas to account for ground elevation changes. The azimuthal direction of the flightpath and GRS antenna pointing direction was adjusted to avoid ground obstructions and achieve desired ground surface conditions. Careful planning allowed the flight to be executed above the desired terrain, avoid ground obstructions, observe frequency authorization restrictions, and meet limitations imposed by FAA and local air traffic control authorities. Flight areas are shown in Figure 15.

For each test flight, the NASA research aircraft was piloted between pairs of preselected waypoints at fixed range from the GS. Aircraft altitude, attitude, and airspeed were held constant between waypoints to create a one-way flight “segment” of a nominally 1.5- to 4.0-min duration. After completing a flight segment, the aircraft reversed direction and traveled the same flightpath between waypoints, but in the opposite direction. This technique intended to determine the impact of asymmetrical installation of the antenna on the aircraft. During these flight segments, the aircraft traveled transverse to the direction of RF radiation from the GS, thereby presenting the port and starboard sides of the aircraft to the GS antenna.

The test aircraft flew the path between each pair of waypoints not only in two directions, but also at multiple altitudes to capture the effects of terrain obstruction, multipath reflections, and signal dispersion. Flight segments were arranged at 15-, 30-, 45-, and 60-nmi range from the GS at altitudes that would achieve 1.0°, 1.5°, 2.0°, and 3.0° elevation angles of above ground level.

In addition to transverse flightpaths, inbound and outbound segments were flown at each test location along the GRS antenna centerline on 1.0°, 1.5°, 2.0°, and 3.0° elevation angles. A summary of as-flown flight altitudes, ranges, and flightpaths is presented in Table III. The altitudes flown during the test were adjusted to the nearest 500 ft to meet FAA flight rules.

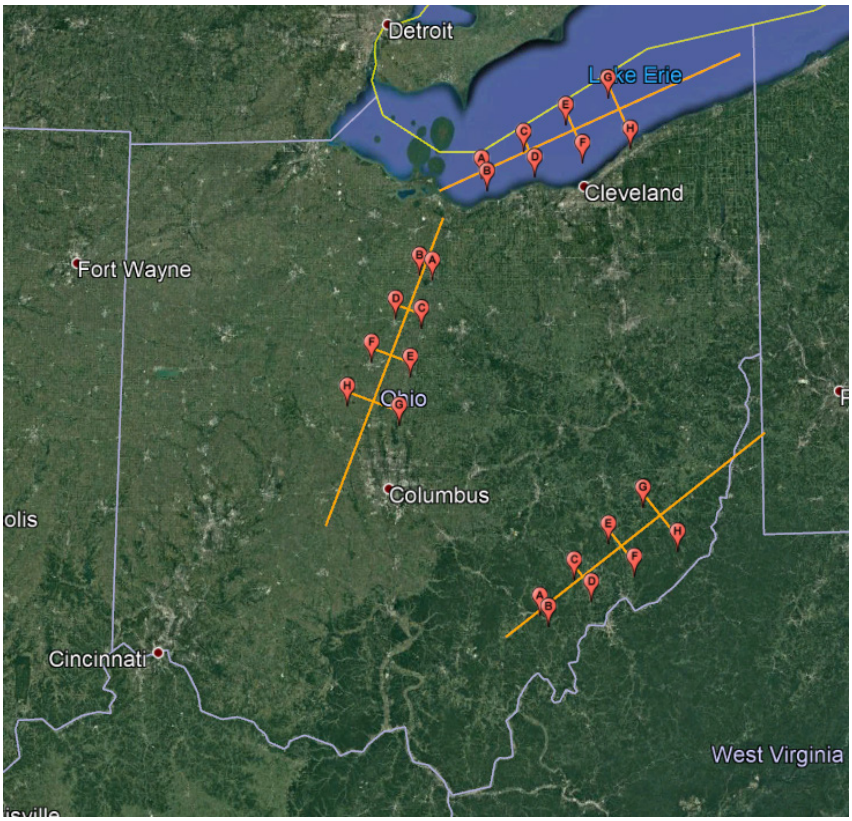

Figure 15.—Ohio flight test areas. Image ©2020 GoogleEarth.

TABLE III.—VALIDATION FLIGHT TEST SUMMARY

Waypoints	A, B	C, D	E, F	G, H	Inbound track (descending)	Outbound track (ascending)
Range, nmi	15	30	45	60		
Elevation angle	Altitude over terrain, above mean sea level, ft				Maximum range from GRS, nmi	
Flat terrain						
1.0°	2,500	5,000	7,500	10,500	60	60
1.5°	3,500	6,500	10,000	14,000	60	60
2.0°	4,000	8,000	12,500	17,500	55	60
3.0°	Not performed					
Hilly terrain						
1.0°	3,000	5,500	8,000	11,500	75	75
1.5°	3,500	7,000	10,500	15,000	70	60
2.0°	4,500	8,500	13,500	18,500	60	60
3.0°	6,000	11,500	17,500	--------	70	60
Open freshwater						
1.0°	2,000	4,000	6,500	9,000	75	75
1.5°	3,000	5,500	8,500	12,000	65	65
2.0°	3,500	7,000	11,000	15,500	70	60
3.0°	5,000	10,500	15,500	--------	65	60

3.1 Validation Flight Test Data Format Description

CNPC Link System prototype radio performance data from the validation test campaign is presented in the following subsections. Section 3.2 presents data collected over smooth plains on October 8, 2019. Section 3.3 presents data collected over slightly rolling plains on March 11 and 12, 2019. Section 3.4 presents data collected over open freshwater on March 3, 5, and 6, 2019.

Each flight segment highlighted in a flight track plot corresponds directly to data plots for both ground-to-air and air-to-ground radio links. Separate data plots are presented for each direction of aircraft travel between the waypoints, for each test altitude, and for 15-, 30-, 45-, and 60-nmi range from the GS.

Received signal strength values were measured at the radio receivers and are plotted in blue and red traces for both the ground-to-air "uplink" and air-to-ground "downlink" path. The signal strength data are measured for each data frame (at a rate of 20 times per second, or every 50 ms), then plotted as an average value every 200 ms as necessary for the EPL analysis in Section 4.0. Signal strength values are time synchronized and plotted with the aircraft flight position and attitude data, which is presented once per second. The CNPC radios were operated with the data class 3 waveform for a point-to-point, 170-kHz-wide data channel at the 103,500 symbol rate.

Estimated signal strength values for the uplink and downlink paths are plotted alongside the empirical flight data as gray and black traces. These estimates are calculated using the temperature-compensated power levels, GS and aircraft antenna gains, cable losses, and free space path loss. The aircraft and GS antenna gains are computed from measurement-enhanced, three-dimensional antenna models at the specific phi and theta angles determined from the GS and aircraft locations, GS antenna orientation, and the aircraft heading, pitch, and roll. The free space path loss is based on the slant range distance between the aircraft and GS. The difference between the measured received signal strength and estimated received signal strength forms the basis of the excess path loss analysis described in Section 4.0.

Directly below the signal strength traces are the percentages of data frame losses averaged over 1 s at the ground and aircraft receivers. Where the CNPC Link System was transferring all data to the receiving radio with zero decoding errors, the performance is presented as a 0-percent loss and no trace is visible on the grid. Where errors occurred, the lost frame data results in a visible vertical line ranging from 0 to 100 percent, where the latter represents a total loss of the link. The second trace on each loss graticule is detection failure, which indicates when the received signal is sufficiently corrupted or of such low signal power that it cannot be viably detected by the radio.

Aircraft parameters are plotted in the lowest portion of each figure. The range plot is the slant range between the ground station and aircraft, calculated from the GPS data of the aircraft and the ground station. Because each path between waypoints was flown as a line segment rather than as an arc segment, the range plot predictably shows small variation across the test period. Aircraft altitude and roll angle are acquired from aircraft onboard instrumentation. All data in all traces is time synchronized using GPS-based timing information.

3.2 Validation Flight Test Data for Smooth Plains Terrain Setting, October 8, 2019

Figure 16 presents the flight track of the NASA aircraft over smooth plains in north-central Ohio. The orange trace is the complete flightpath of the aircraft, including all reversals, ascent and descent maneuvers, and range changes. Figure 17 is the same flight track viewed from an oblique perspective to show the flightpath at various test altitudes. Waypoints are identified with alphabet characters A to H. The flight segments between waypoints are highlighted in yellow, which precisely represents the locations where RF data was captured for evaluation. For this location, the GRS was positioned at the southern perimeter of NASA's Plum Brook Station facility in Perkins Township, Ohio.

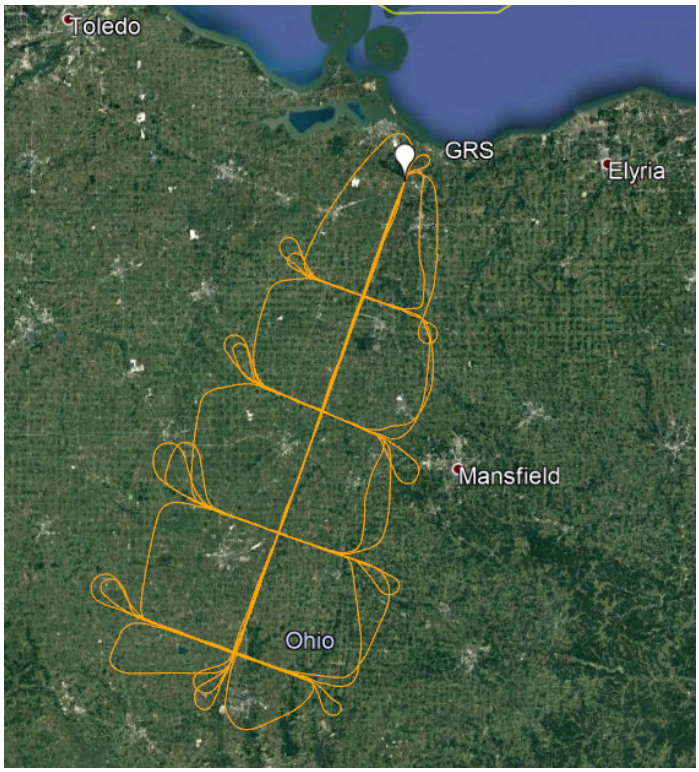

Figure 16.—Flightpath over smooth plains terrain October 8, 2019. Image ©2020 GoogleEarth.

Figure 17.—Perspective view of flightpath over smooth plains terrain highlighting data capture segments, October 8, 2019. Image ©2020 GoogleEarth.

C-band validation flight test data over smooth plains terrain is presented in Figure 18 to Figure 47. Crosstrack plots are arranged for elevation angles of 1.0°, 1.5°, and 2.0°, followed by ascent and descent plots.

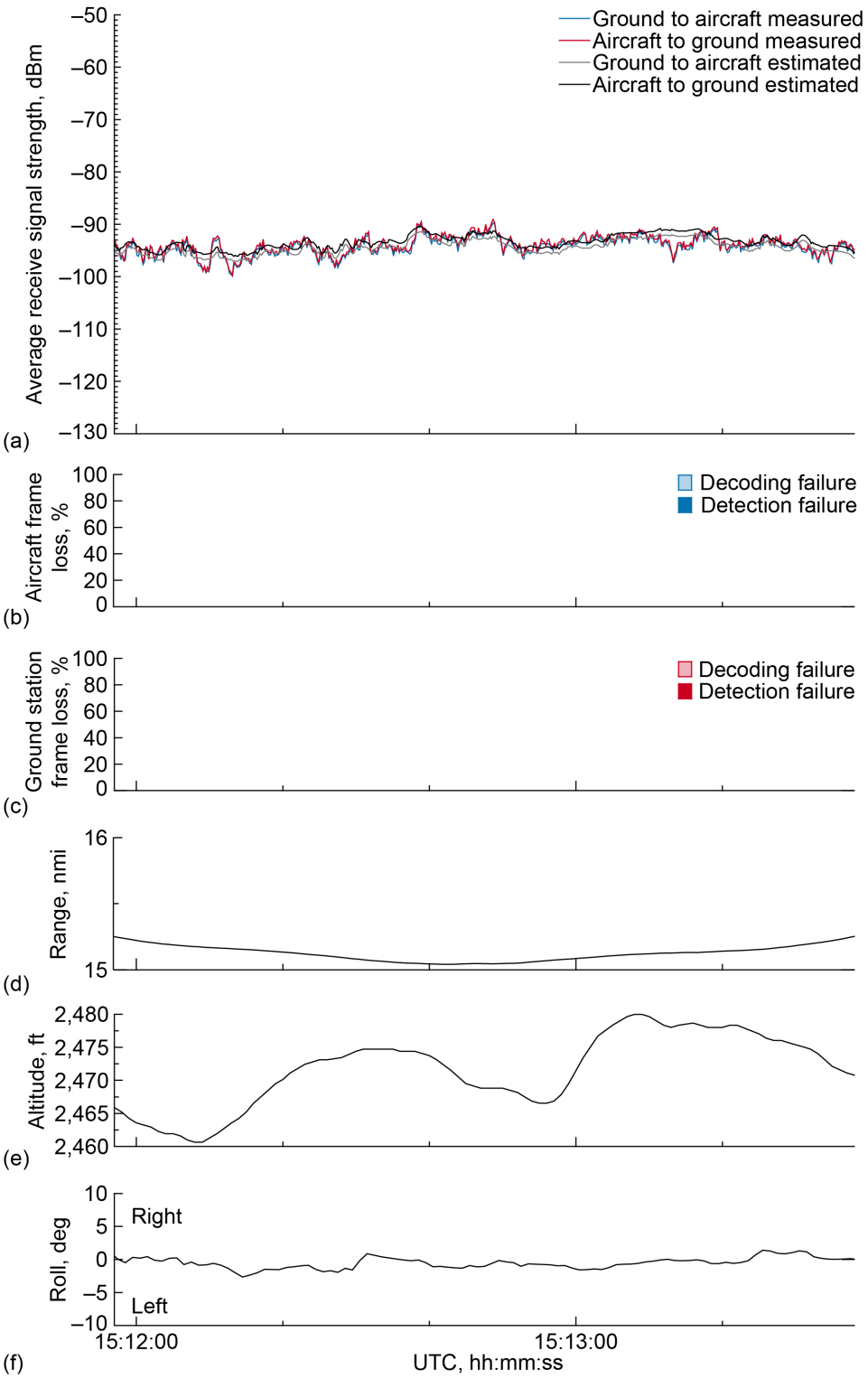

Figure 18.—Signal strength and frame loss over smooth plains terrain at 15-nmi range and 2,500-ft altitude, 1.0° antenna elevation, traveling from waypoint A to waypoint B. (a) Average receive signal strength. (b) Aircraft frame loss. (c) Ground station frame loss. (d) Range. (e) Altitude. (f) Roll.

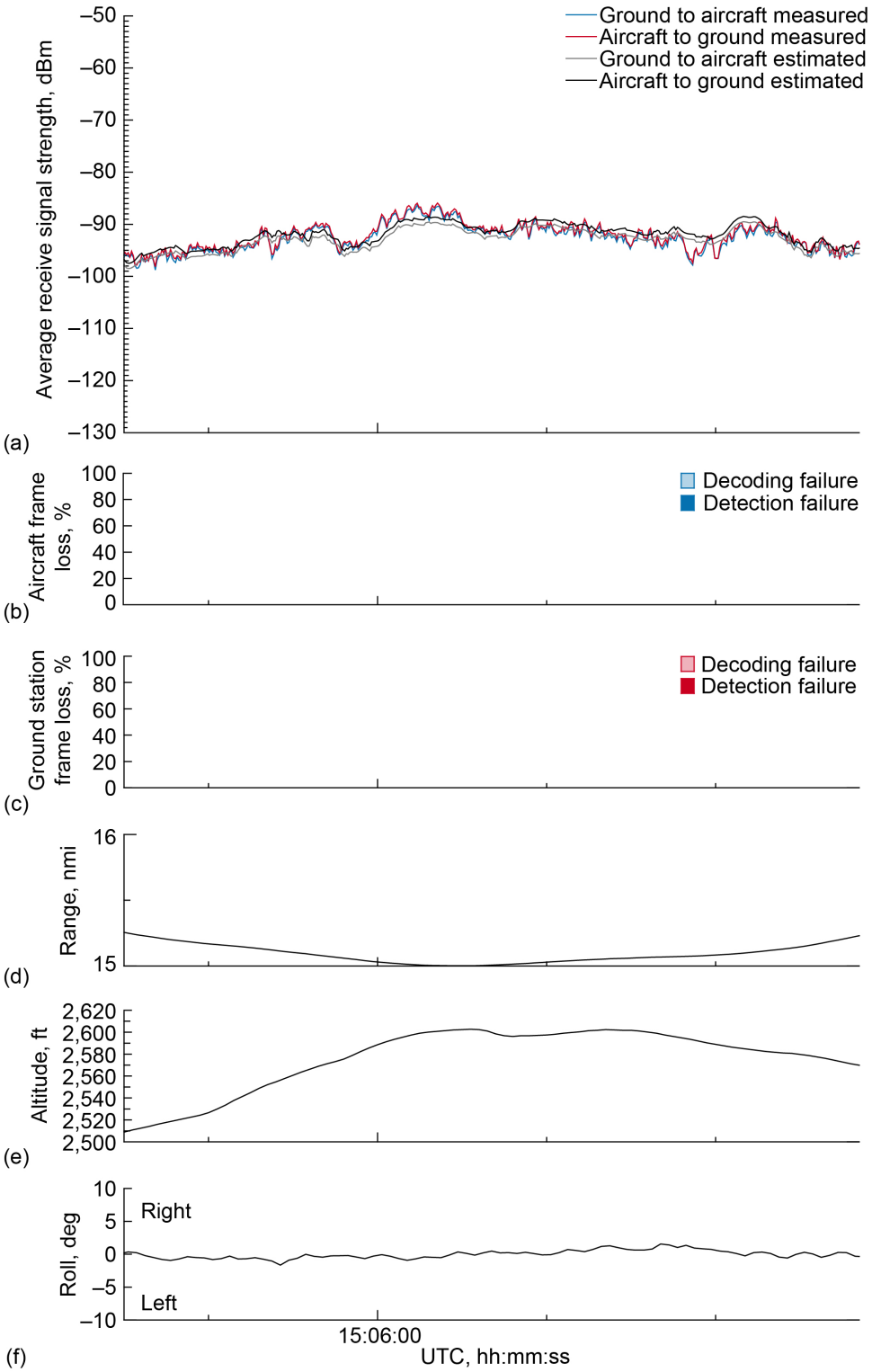

Figure 19.—Signal strength and frame loss over smooth plains terrain at 15-nmi range and 2,500-ft altitude, 1.0° antenna elevation, traveling from waypoint B to waypoint A. (a) Average receive signal strength. (b) Aircraft frame loss. (c) Ground station frame loss. (d) Range. (e) Altitude. (f) Roll.

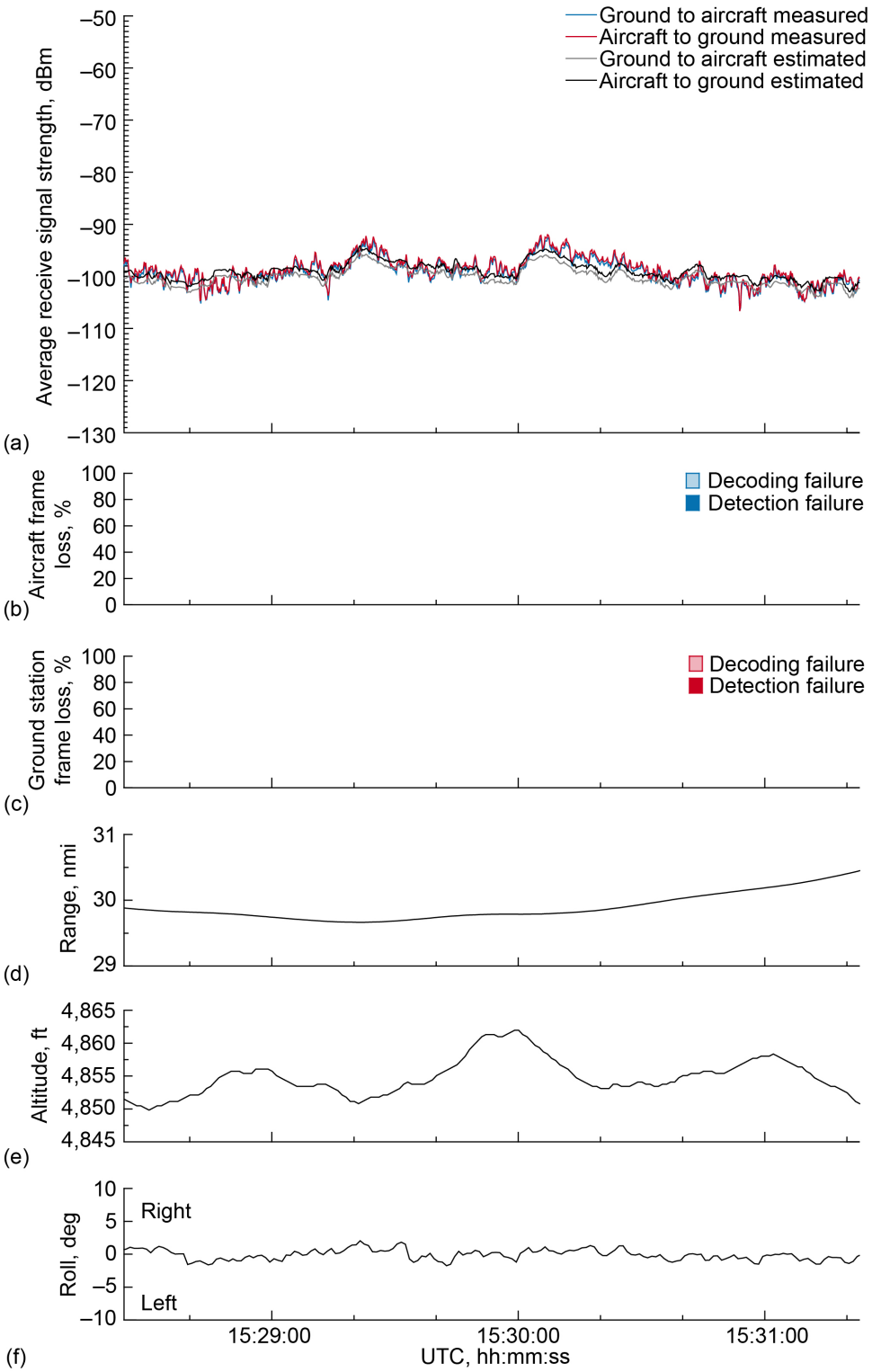

Figure 20.—Signal strength and frame loss over smooth plains terrain at 30-nmi range and 5,000-ft altitude, 1.0° antenna elevation, traveling from waypoint C to waypoint D. (a) Average receive signal strength. (b) Aircraft frame loss. (c) Ground station frame loss. (d) Range. (e) Altitude. (f) Roll.

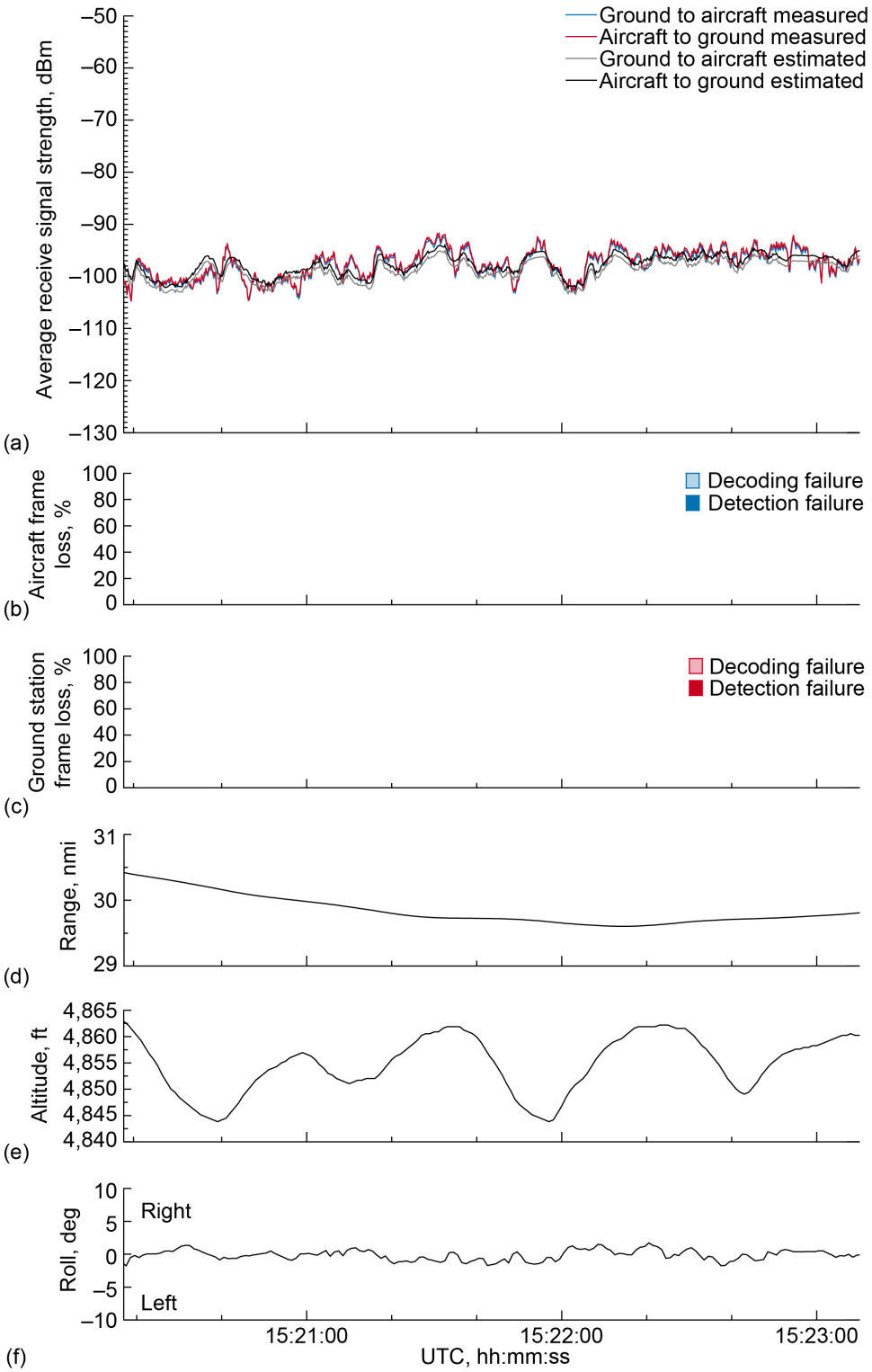

Figure 21.—Signal strength and frame loss over smooth plains terrain at 30-nmi range and 5,000-ft altitude, 1.0° antenna elevation, traveling from waypoint D to waypoint C. (a) Average receive signal strength. (b) Aircraft frame loss. (c) Ground station frame loss. (d) Range. (e) Altitude. (f) Roll.

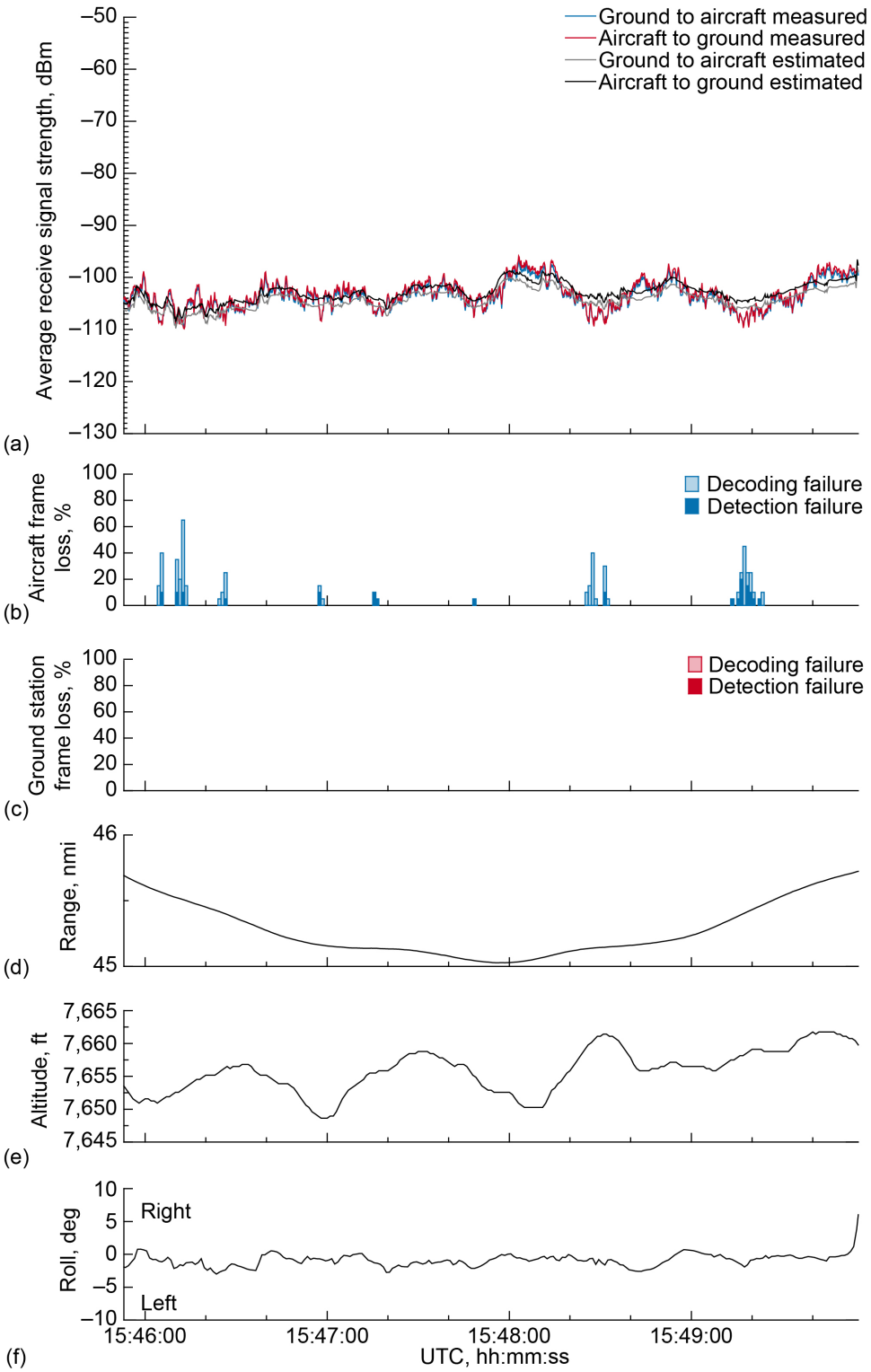

Figure 22.—Signal strength and frame loss over smooth plains terrain at 45-nmi range and 7,500-ft altitude, 1.0° antenna elevation, traveling from waypoint E to waypoint F. (a) Average receive signal strength. (b) Aircraft frame loss. (c) Ground station frame loss. (d) Range. (e) Altitude. (f) Roll.

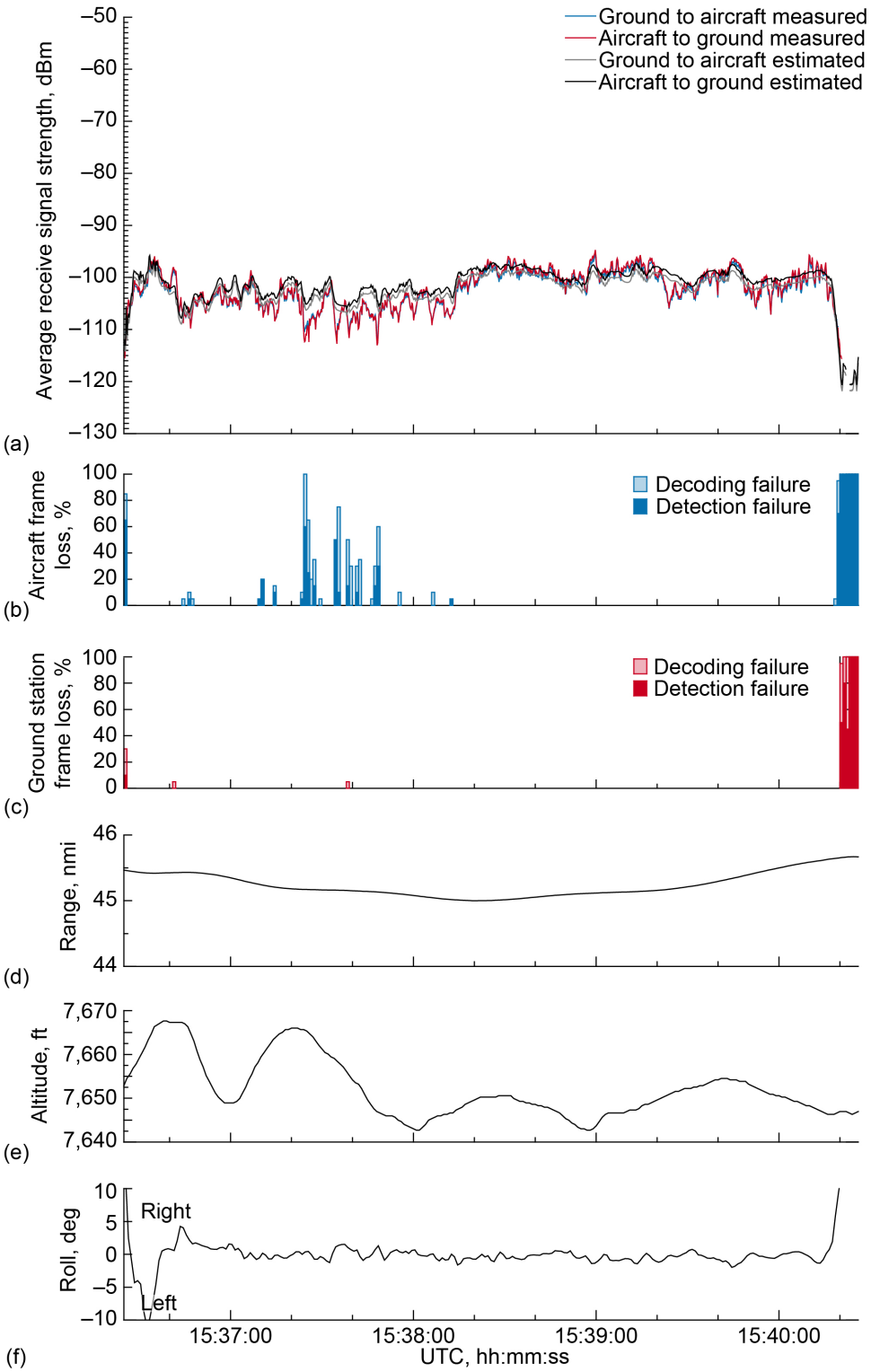

Figure 23.—Signal strength and frame loss over smooth plains terrain at 45-nmi range and 7,500-ft altitude, 1.0° antenna elevation, traveling from waypoint F to waypoint E. (a) Average receive signal strength. (b) Aircraft frame loss. (c) Ground station frame loss. (d) Range. (e) Altitude. (f) Roll.

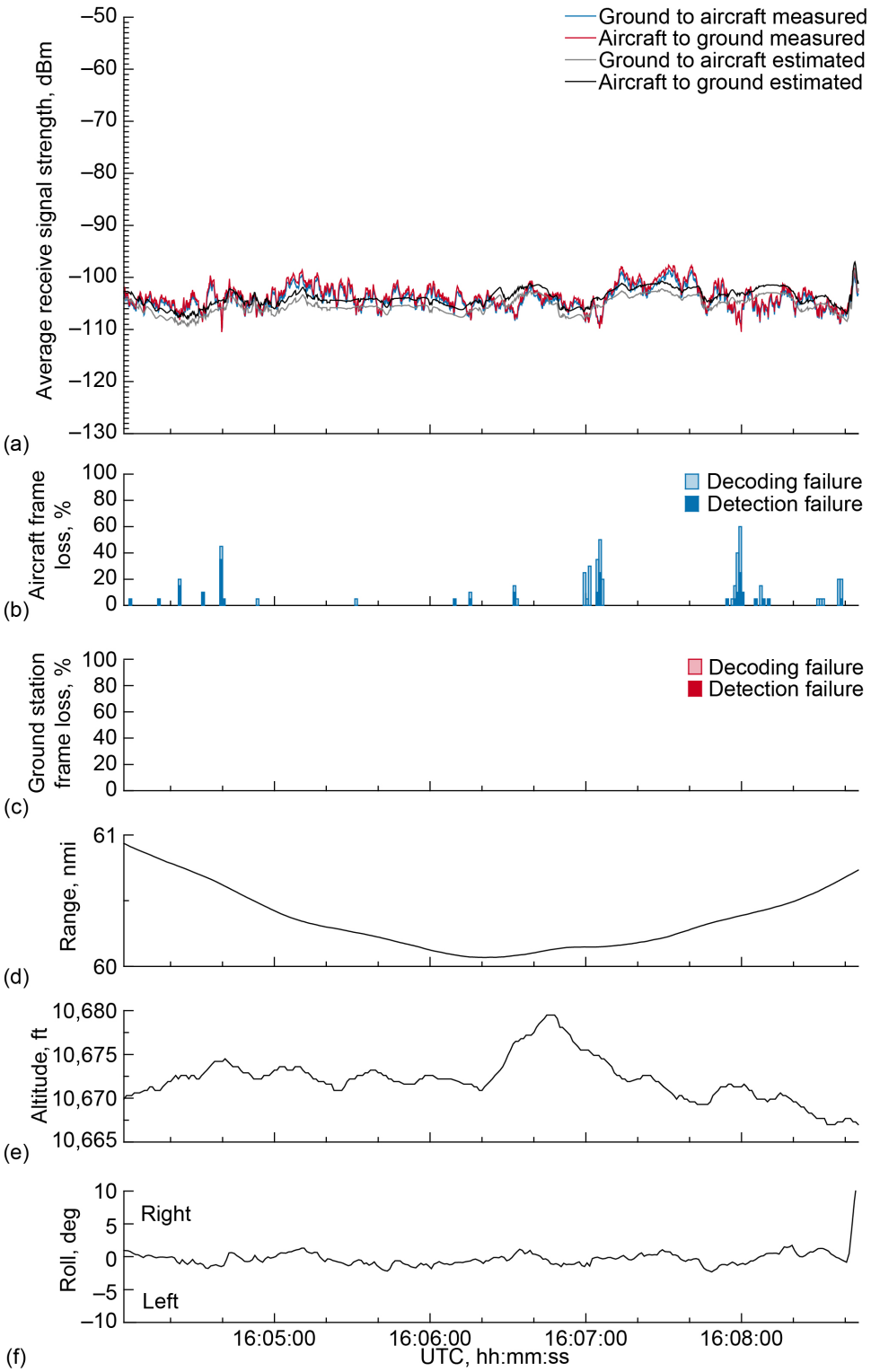

Figure 24.—Signal strength and frame loss over smooth plains terrain at 60-nmi range and 10,500-ft altitude, 1.0° antenna elevation, traveling from waypoint G to waypoint H. (a) Average receive signal strength. (b) Aircraft frame loss. (c) Ground station frame loss. (d) Range. (e) Altitude. (f) Roll.

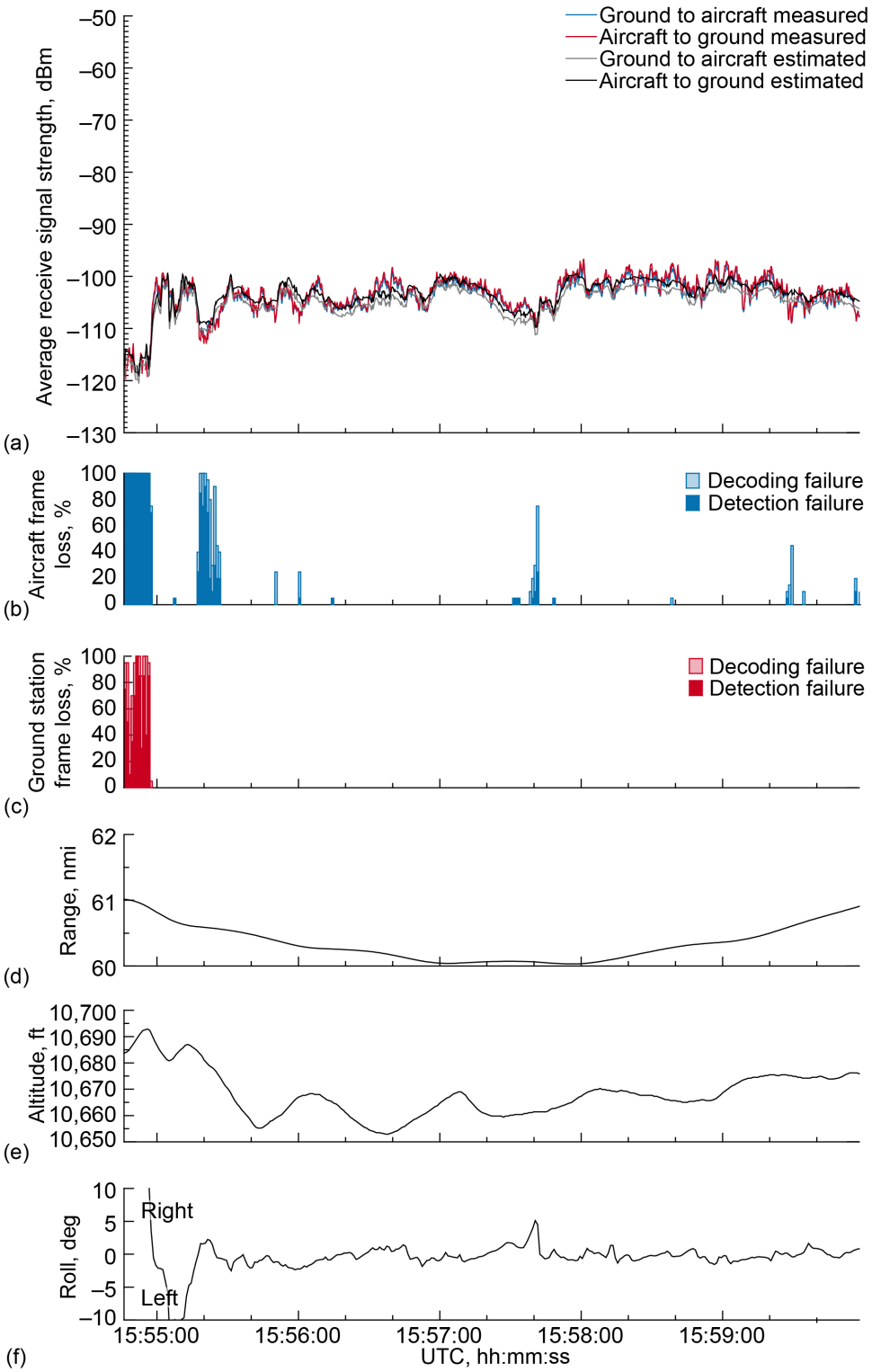

Figure 25.—Signal strength and frame loss over smooth plains terrain at 60-nmi range and 10,500-ft altitude, 1.0° antenna elevation, traveling from waypoint H to waypoint G. (a) Average receive signal strength. (b) Aircraft frame loss. (c) Ground station frame loss. (d) Range. (e) Altitude. (f) Roll.

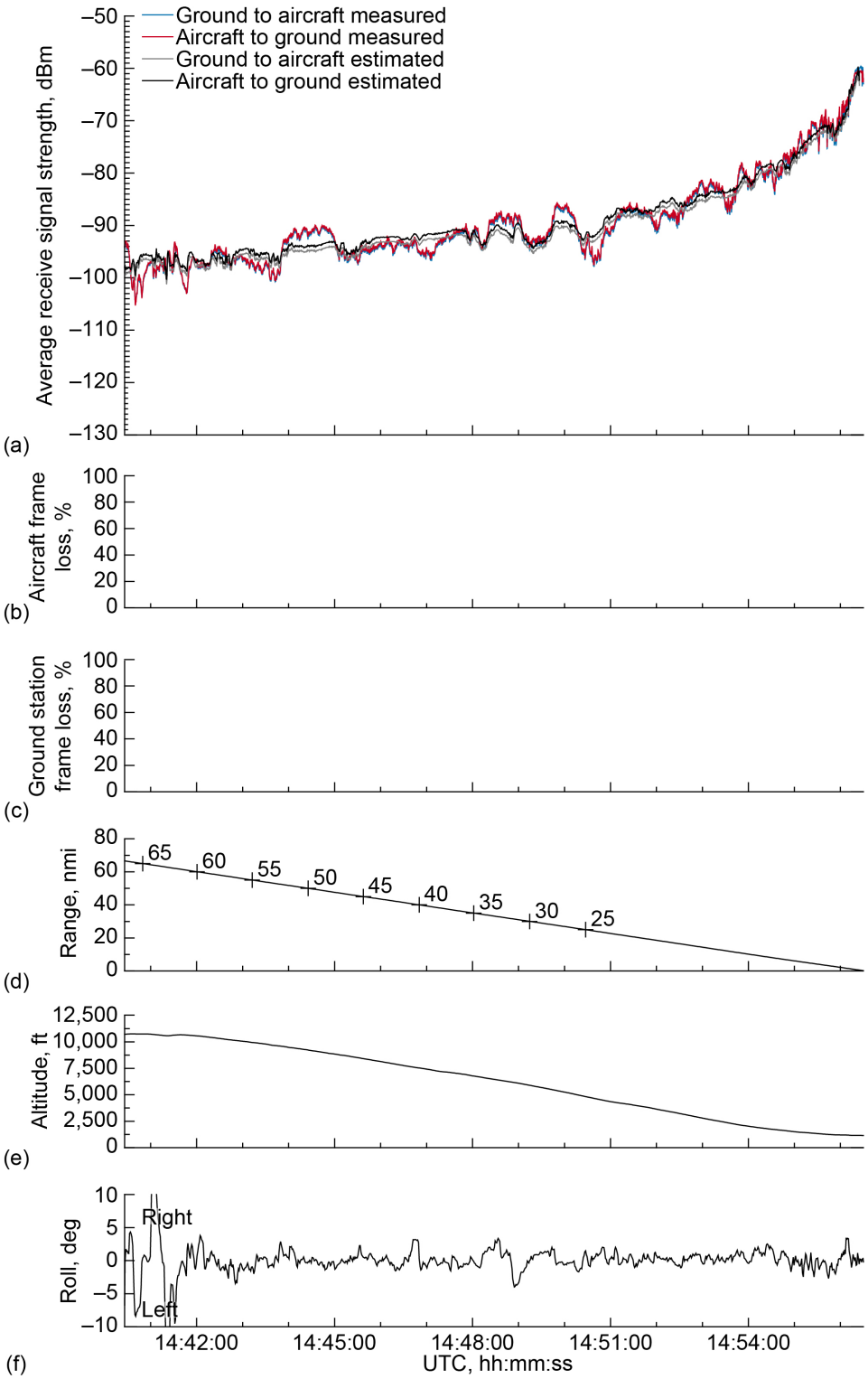

Figure 26.—Signal strength and frame loss over smooth plains terrain during inbound, descending track on 1.0° glide slope, traveling toward ground station. (a) Average receive signal strength. (b) Aircraft frame loss. (c) Ground station frame loss. (d) Range. (e) Altitude. (f) Roll.

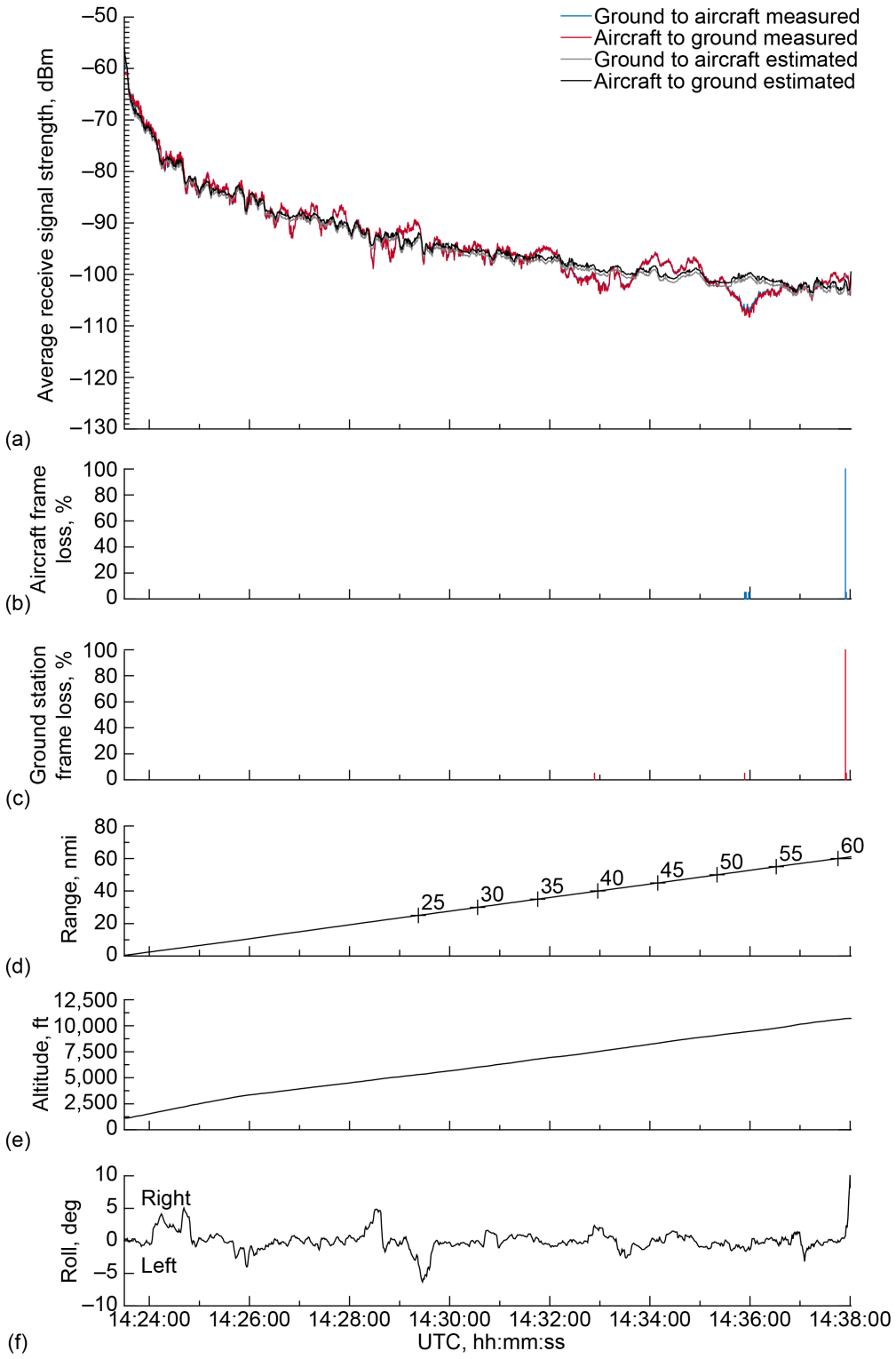

Figure 27.—Signal strength and frame loss over smooth plains terrain during outbound, ascending track on 1.0° glide slope, traveling away from ground station. (a) Average receive signal strength. (b) Aircraft frame loss. (c) Ground station frame loss. (d) Range. (e) Altitude. (f) Roll.

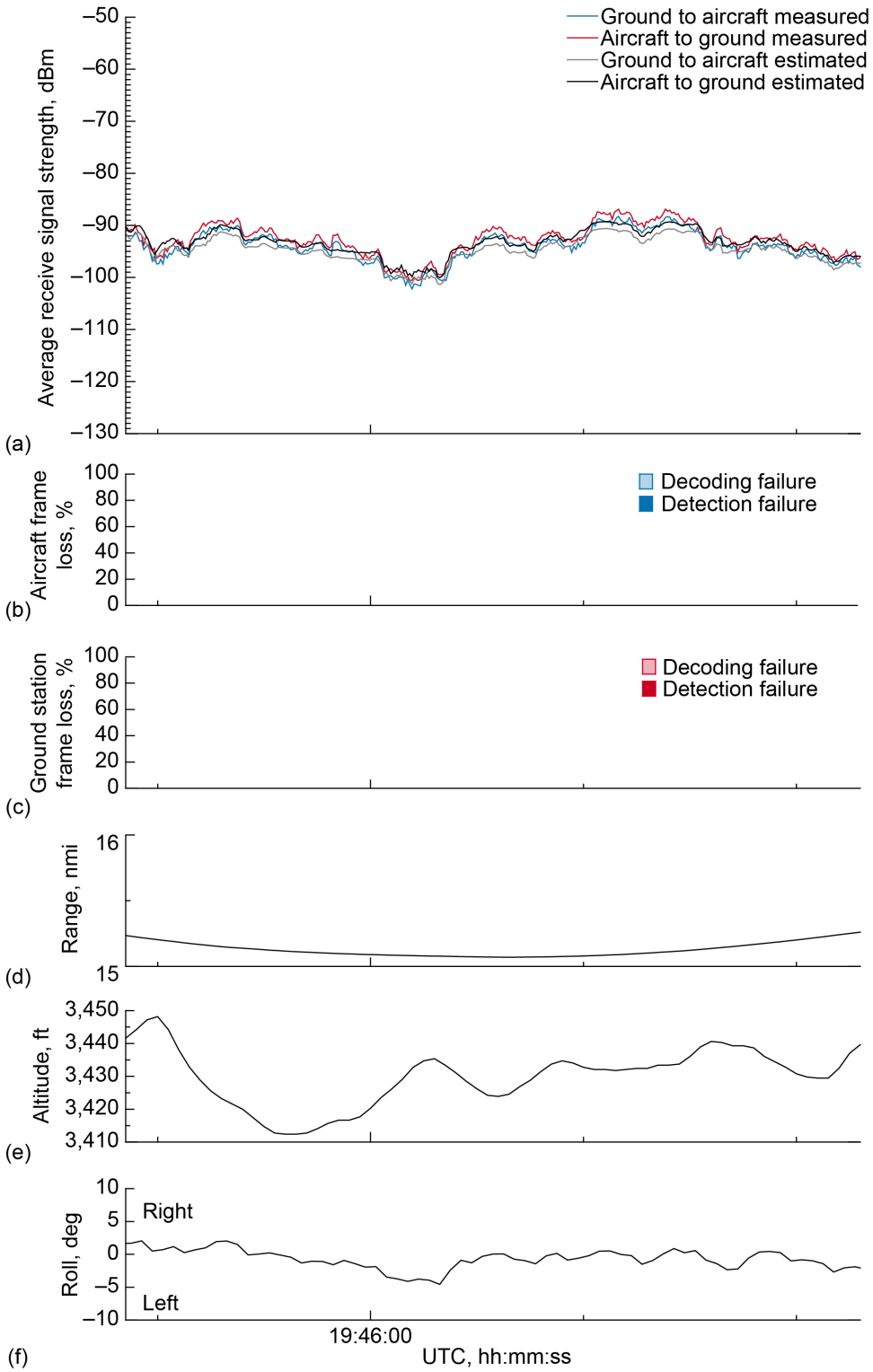

Figure 28.—Signal strength and frame loss over smooth plains terrain at 15-nmi range and 3,500-ft altitude, 1.5° antenna elevation, traveling from waypoint A to waypoint B. (a) Average receive signal strength. (b) Aircraft frame loss. (c) Ground station frame loss. (d) Range. (e) Altitude. (f) Roll.

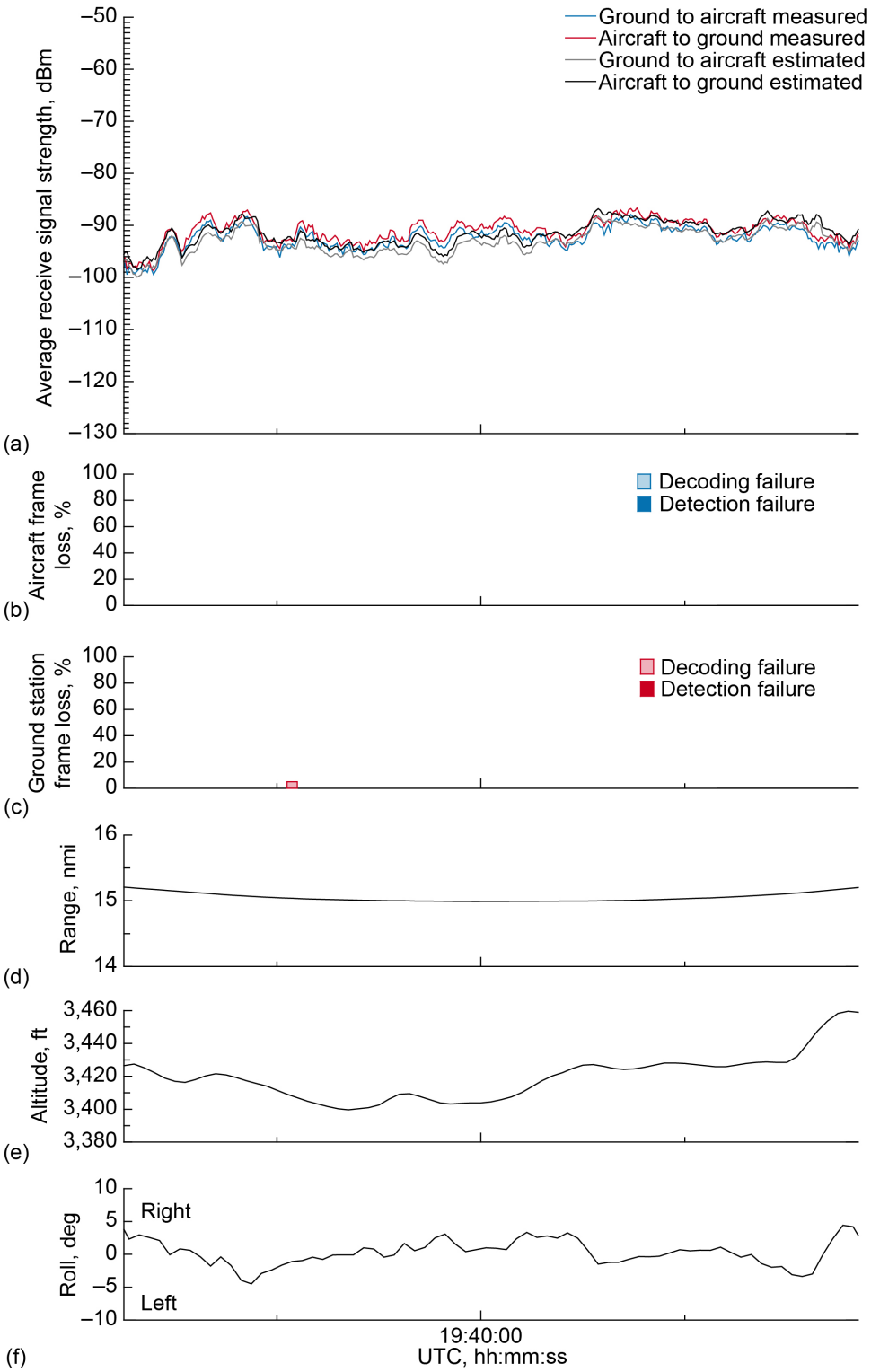

Figure 29.—Signal strength and frame loss over smooth plains terrain at 15-nmi range and 3,500-ft altitude, 1.5° antenna elevation, traveling from waypoint B to waypoint A. (a) Average receive signal strength. (b) Aircraft frame loss. (c) Ground station frame loss. (d) Range. (e) Altitude. (f) Roll.

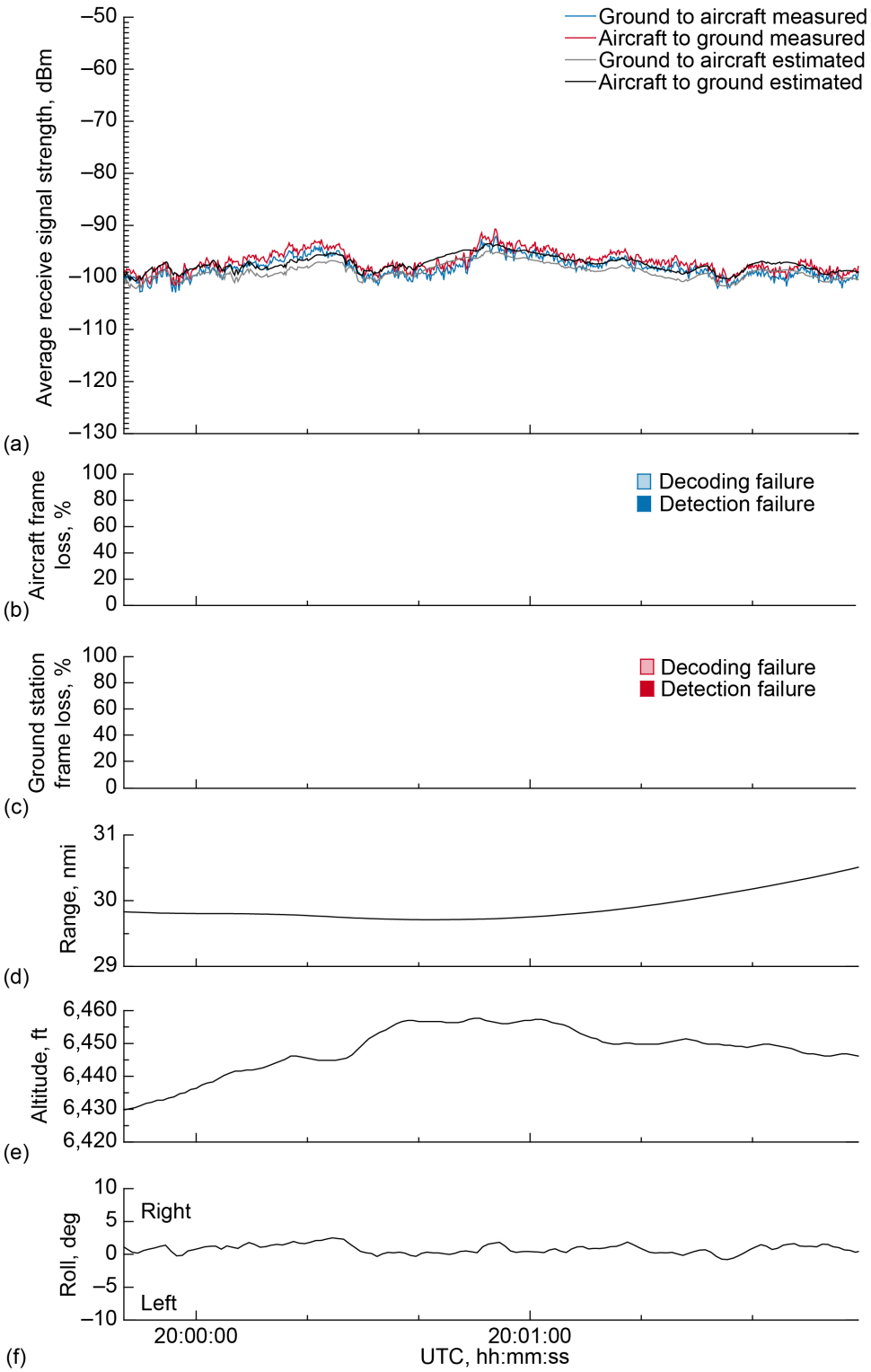

Figure 30.—Signal strength and frame loss over smooth plains terrain at 30-nmi range and 6,500-ft altitude, 1.5° antenna elevation, traveling from waypoint C to waypoint D. (a) Average receive signal strength. (b) Aircraft frame loss. (c) Ground station frame loss. (d) Range. (e) Altitude. (f) Roll.

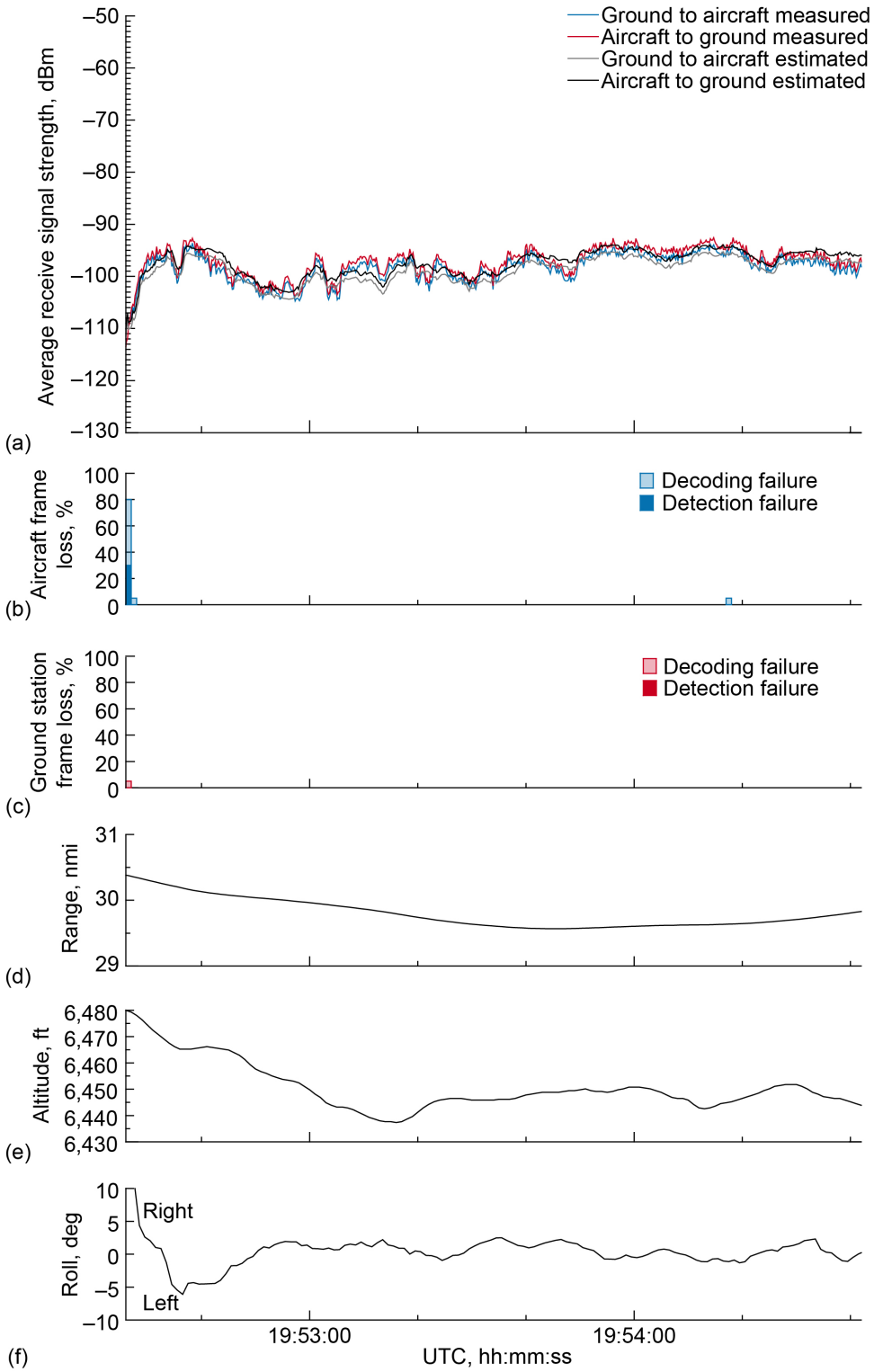

Figure 31.—Signal strength and frame loss over smooth plains terrain at 30-nmi range and 6,500-ft altitude, 1.5° antenna elevation, traveling from waypoint D to waypoint C. (a) Average receive signal strength. (b) Aircraft frame loss. (c) Ground station frame loss. (d) Range. (e) Altitude. (f) Roll.

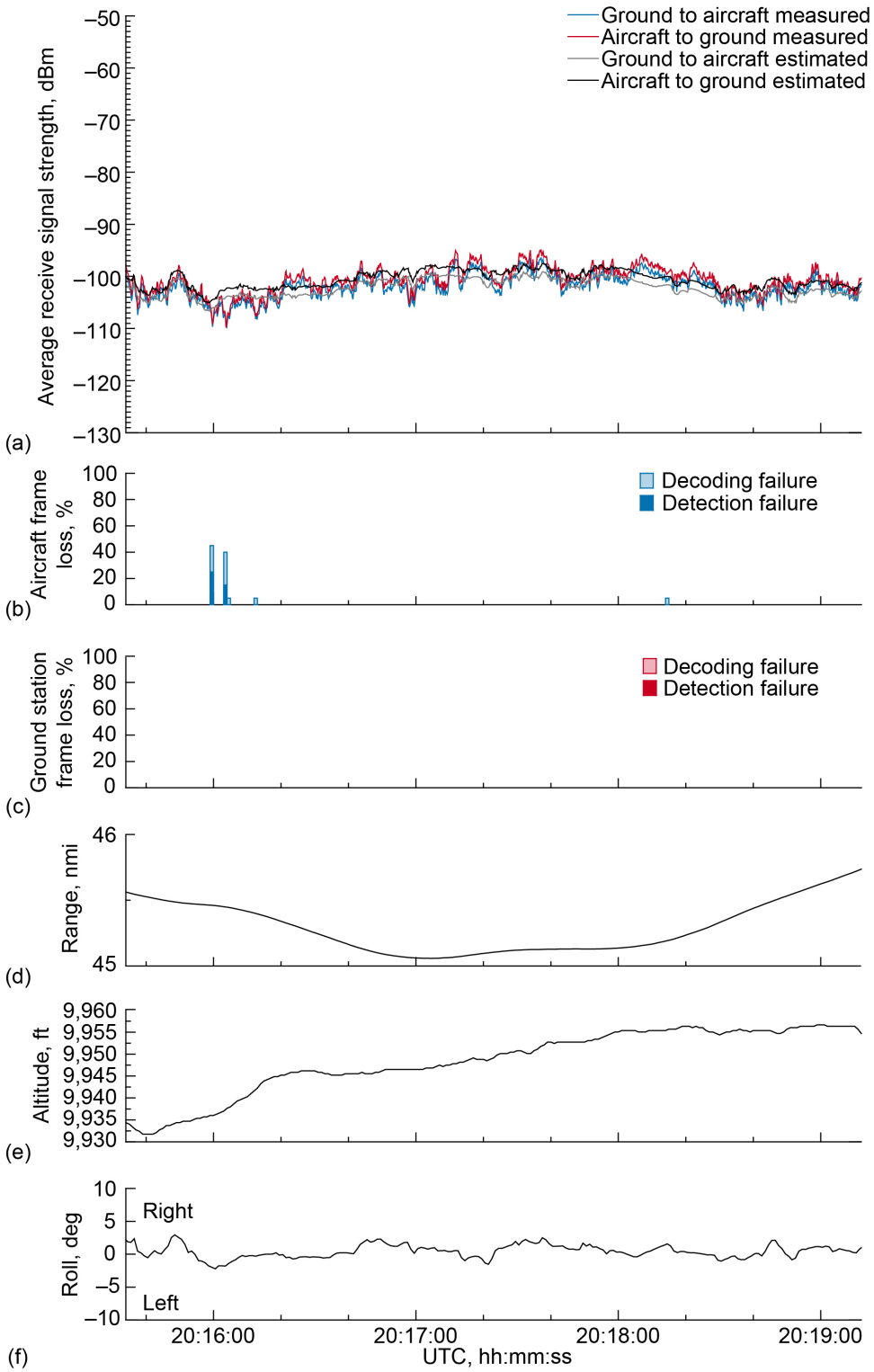

Figure 32.—Signal strength and frame loss over smooth plains terrain at 45-nmi range and 10,000-ft altitude, 1.5° antenna elevation, traveling from waypoint E to waypoint F. (a) Average receive signal strength. (b) Aircraft frame loss. (c) Ground station frame loss. (d) Range. (e) Altitude. (f) Roll.

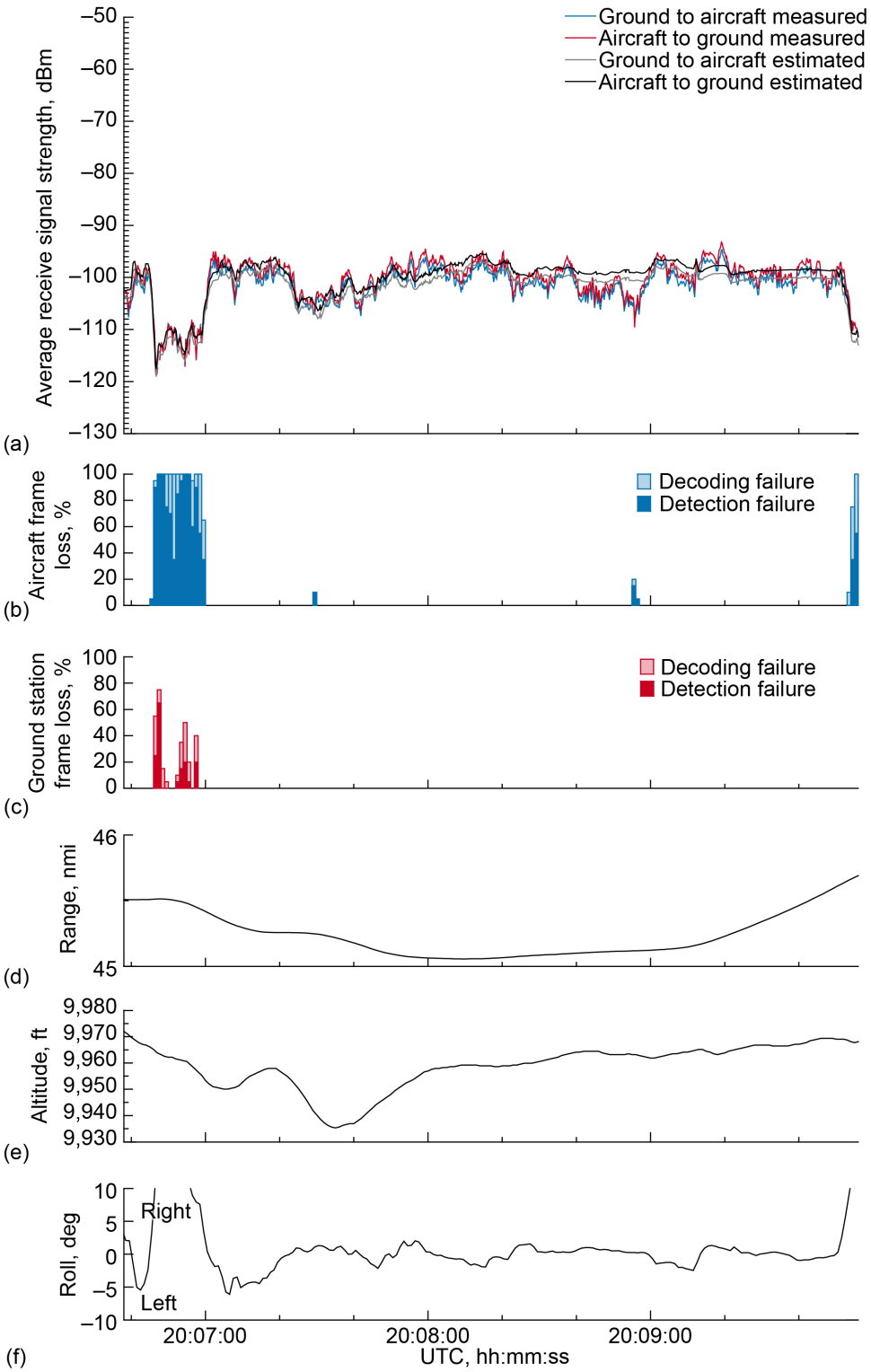

Figure 33.—Signal strength and frame loss over smooth plains terrain at 45-nmi range and 10,000-ft altitude, 1.5° antenna elevation, traveling from waypoint F to waypoint E. (a) Average receive signal strength. (b) Aircraft frame loss. (c) Ground station frame loss. (d) Range. (e) Altitude. (f) Roll.

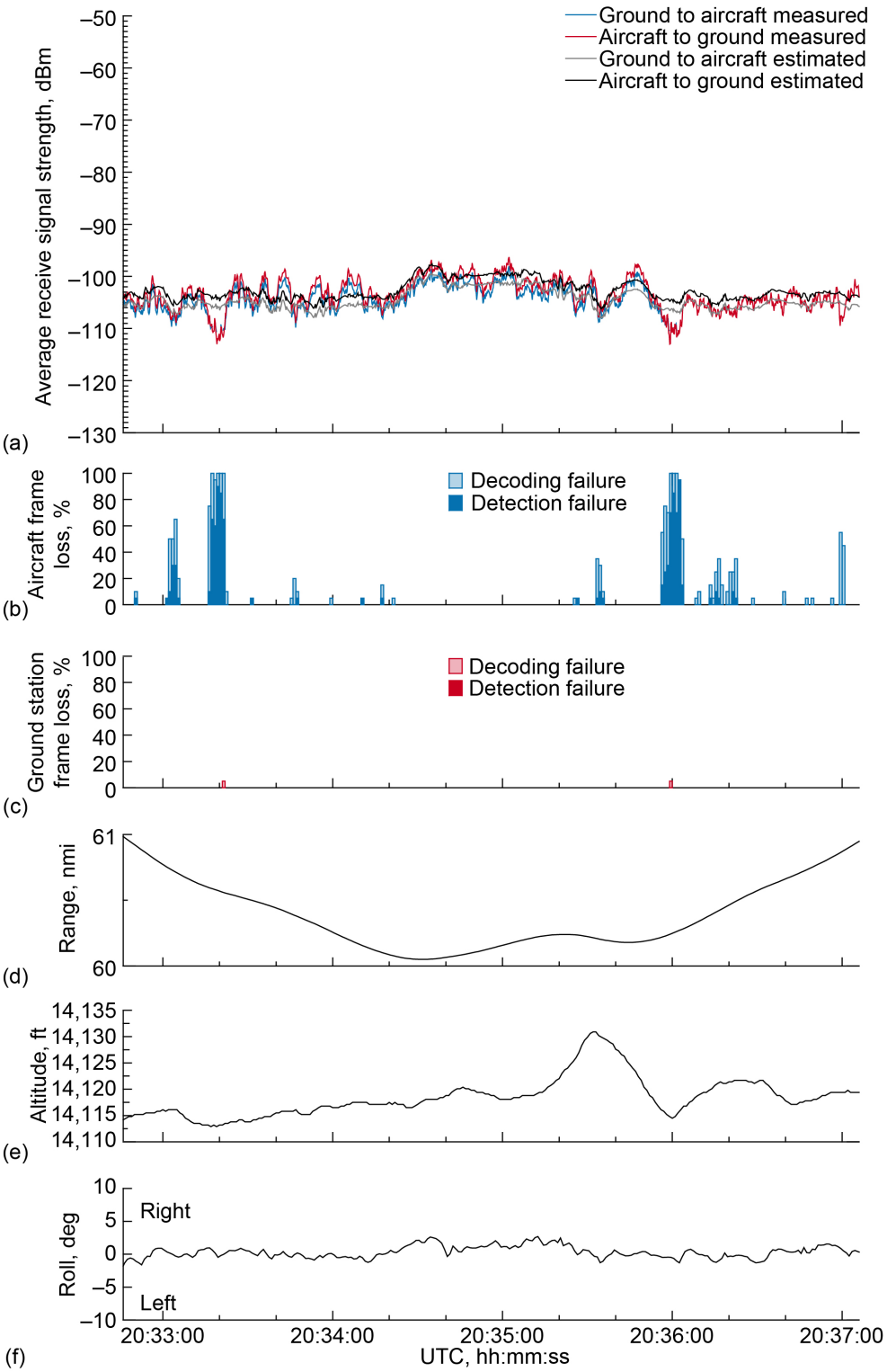

Figure 34.—Signal strength and frame loss over smooth plains terrain at 60-nmi range and 14,000-ft altitude, 1.5° antenna elevation, traveling from waypoint G to waypoint H. (a) Average receive signal strength. (b) Aircraft frame loss. (c) Ground station frame loss. (d) Range. (e) Altitude. (f) Roll.

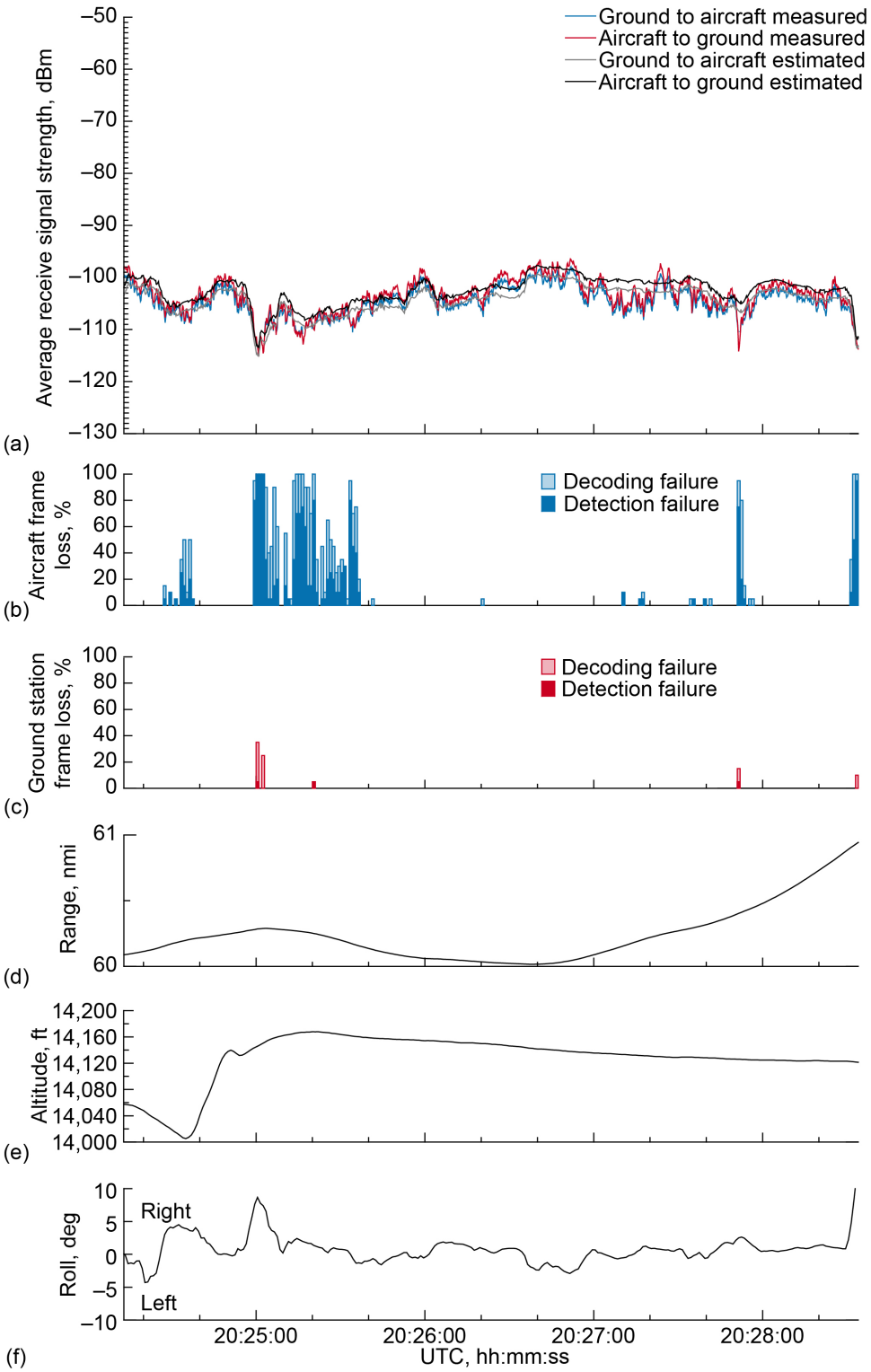

Figure 35.—Signal strength and frame loss over smooth plains terrain at 60-nmi range and 14,000-ft altitude, 1.5° antenna elevation, traveling from waypoint H to waypoint G. (a) Average receive signal strength. (b) Aircraft frame loss. (c) Ground station frame loss. (d) Range. (e) Altitude. (f) Roll.

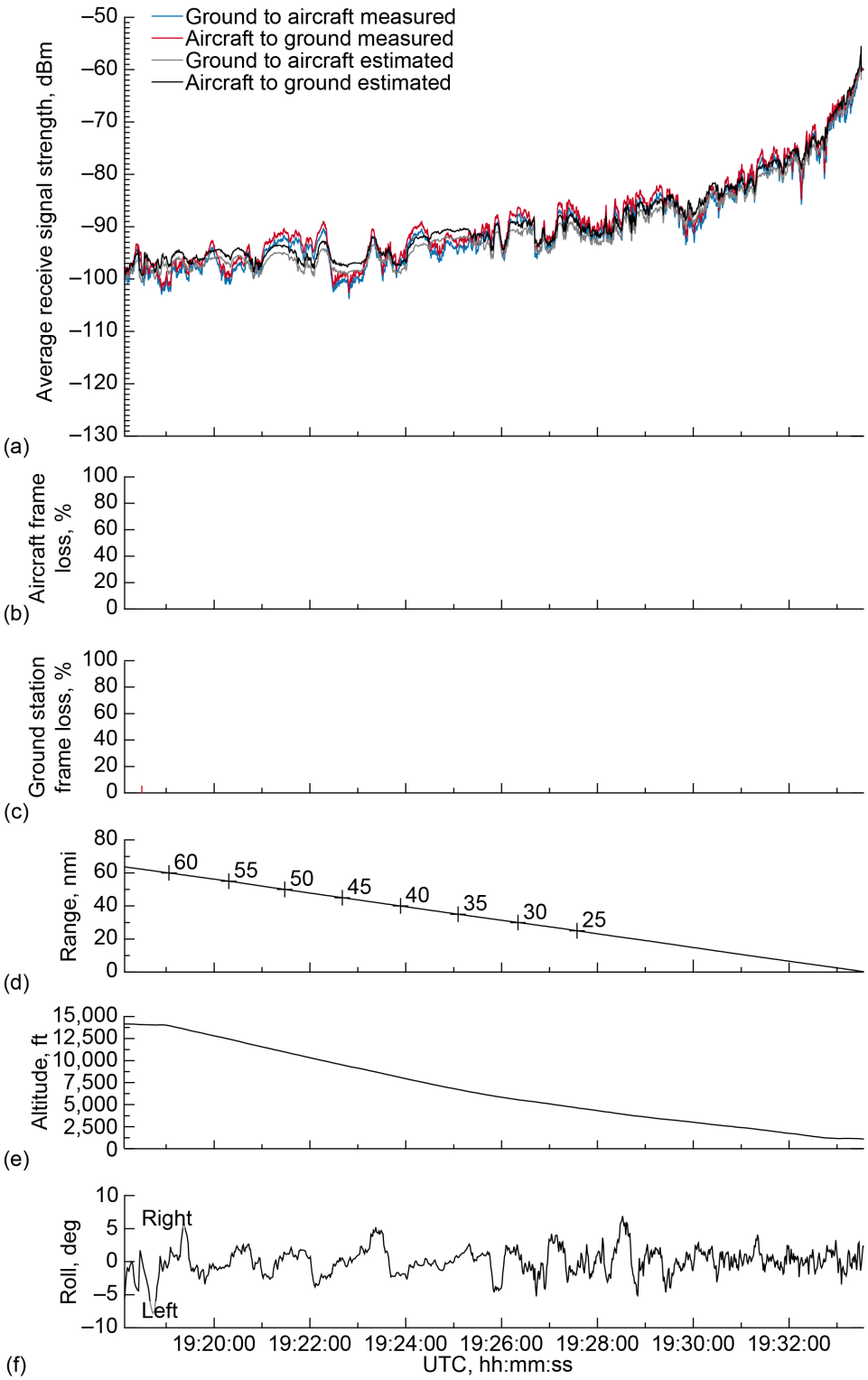

Figure 36.—Signal strength and frame loss over smooth plains terrain during inbound, descending track on 1.5° glide slope, traveling toward ground station. (a) Average receive signal strength. (b) Aircraft frame loss. (c) Ground station frame loss. (d) Range. (e) Altitude. (f) Roll.

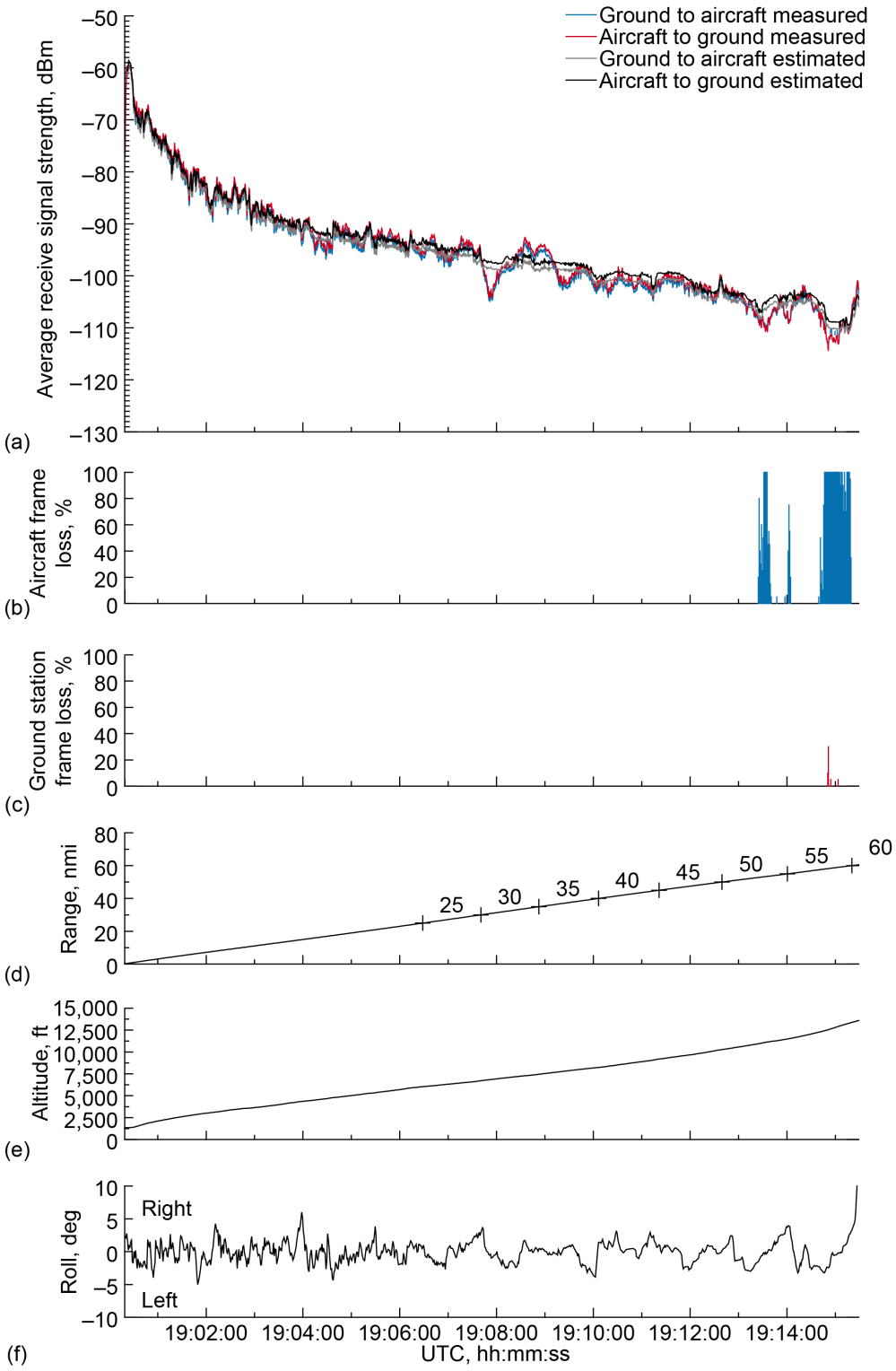

Figure 37.—Signal strength and frame loss over smooth plains terrain during outbound, ascending track on 1.5° glide slope, traveling away from ground station. (a) Average receive signal strength. (b) Aircraft frame loss. (c) Ground station frame loss. (d) Range. (e) Altitude. (f) Roll.

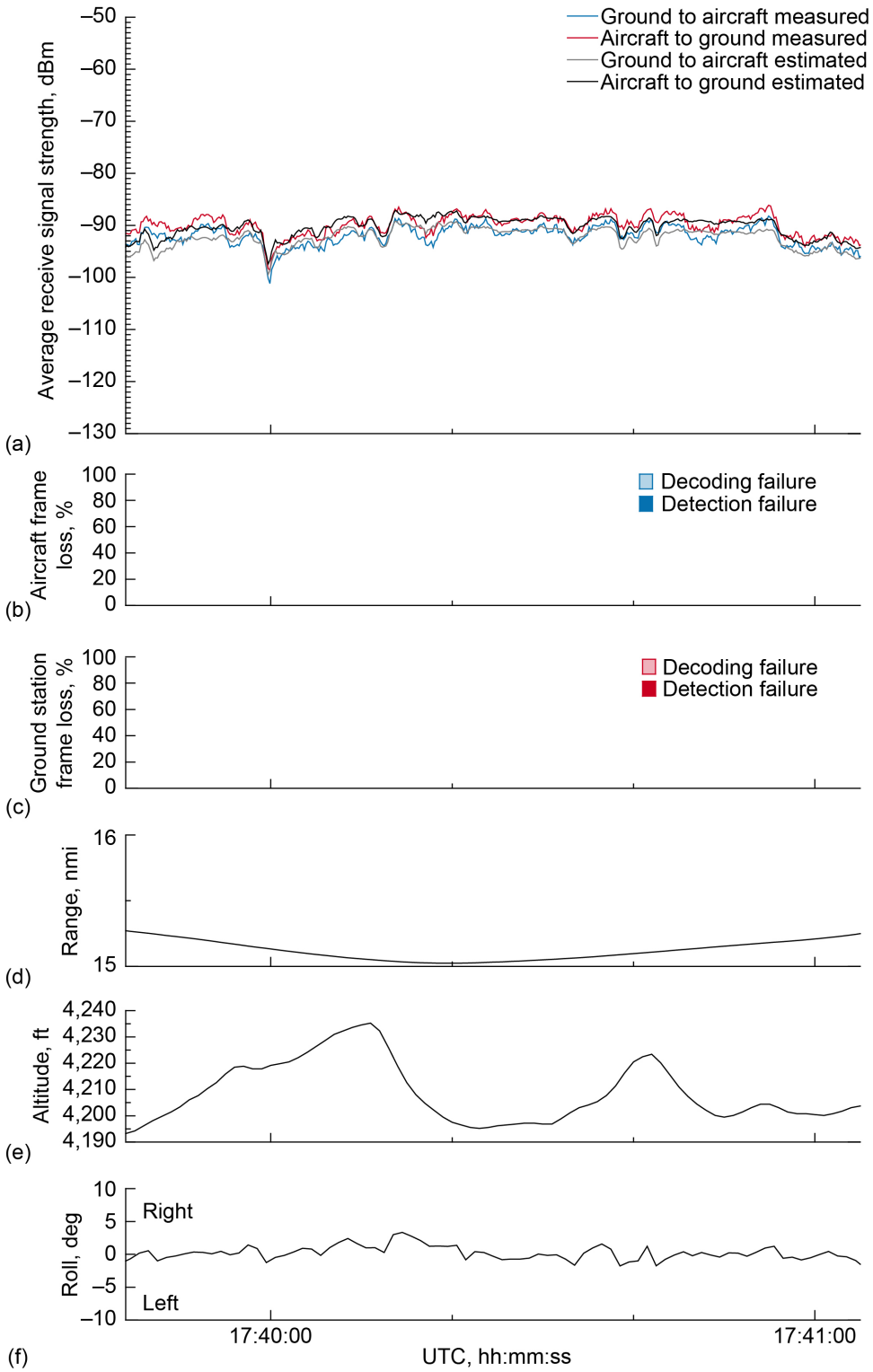

Figure 38.—Signal strength and frame loss over smooth plains terrain at 15-nmi range and 4,000-ft altitude, 2.0° antenna elevation, traveling from waypoint A to waypoint B. (a) Average receive signal strength. (b) Aircraft frame loss. (c) Ground station frame loss. (d) Range. (e) Altitude. (f) Roll.

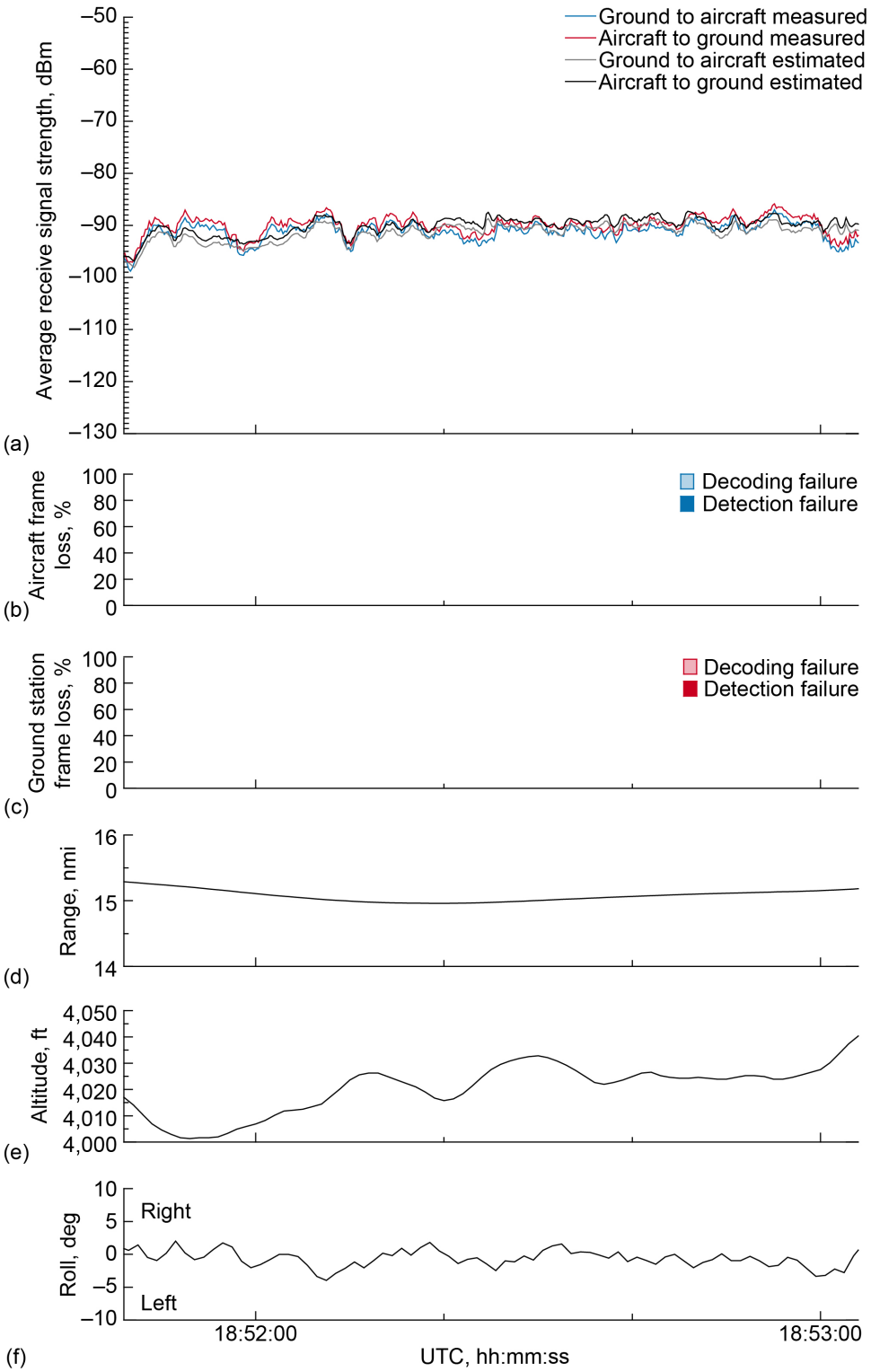

Figure 39.—Signal strength and frame loss over smooth plains terrain at 15-nmi range and 4,000-ft altitude, 2.0° antenna elevation, traveling from waypoint B to waypoint A. (a) Average receive signal strength. (b) Aircraft frame loss. (c) Ground station frame loss. (d) Range. (e) Altitude. (f) Roll.

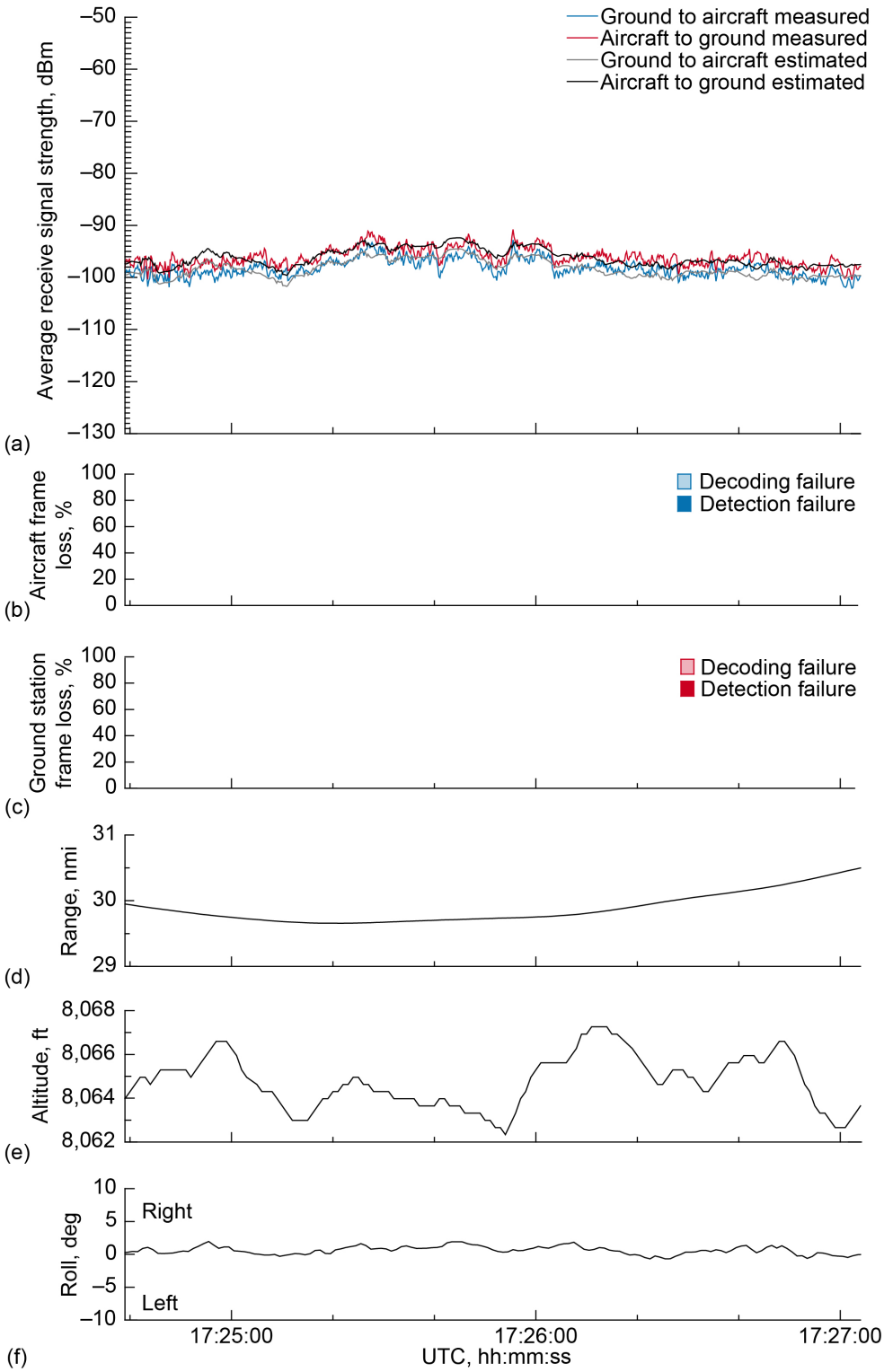

Figure 40.—Signal strength and frame loss over smooth plains terrain at 30-nmi range and 8,000-ft altitude, 2.0° antenna elevation, traveling from waypoint C to waypoint D. (a) Average receive signal strength. (b) Aircraft frame loss. (c) Ground station frame loss. (d) Range. (e) Altitude. (f) Roll.

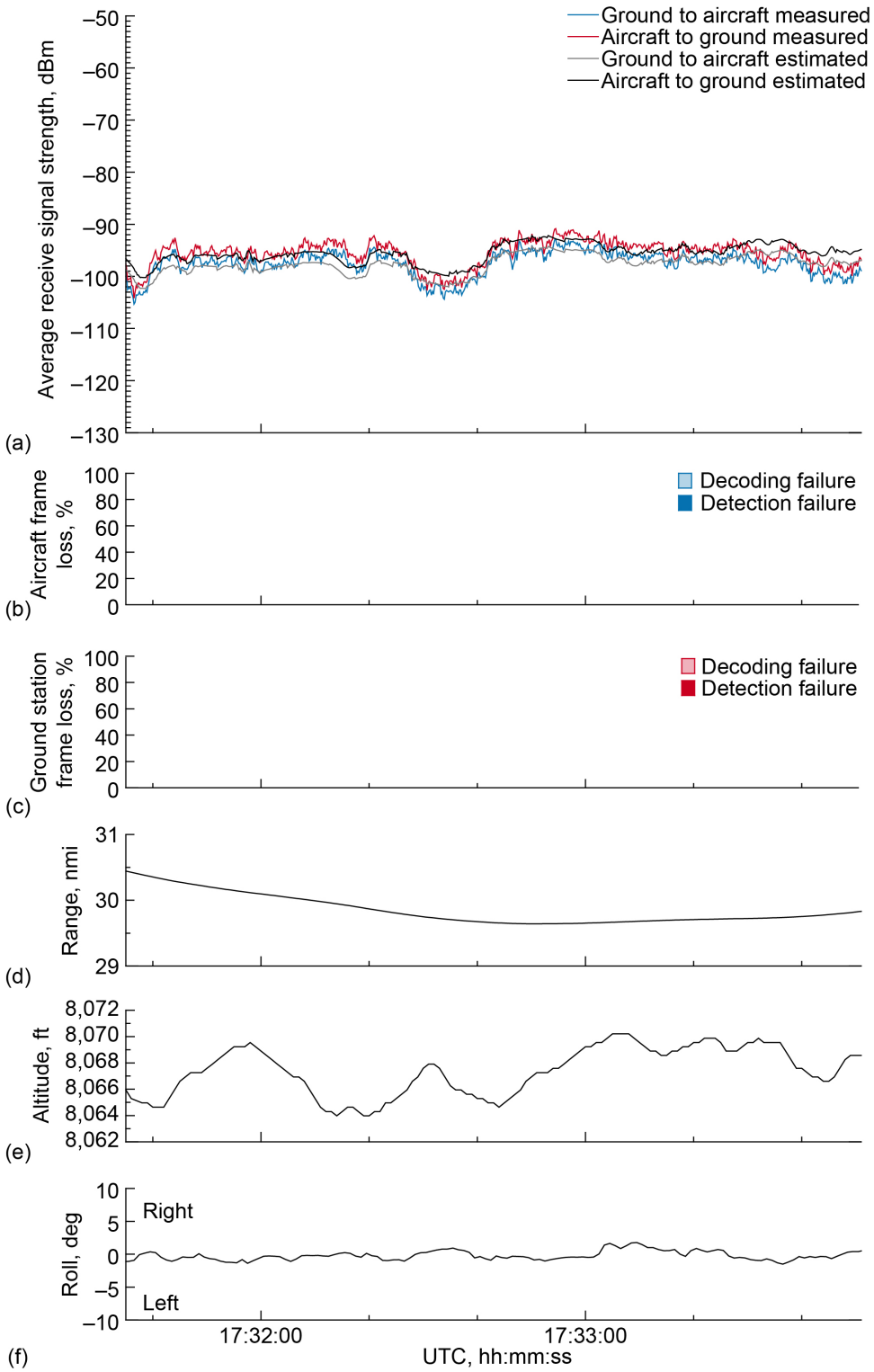

Figure 41.—Signal strength and frame loss over smooth plains terrain at 30-nmi range and 8,000-ft altitude, 2.0° antenna elevation, traveling from waypoint D to waypoint C. (a) Average receive signal strength. (b) Aircraft frame loss. (c) Ground station frame loss. (d) Range. (e) Altitude. (f) Roll.

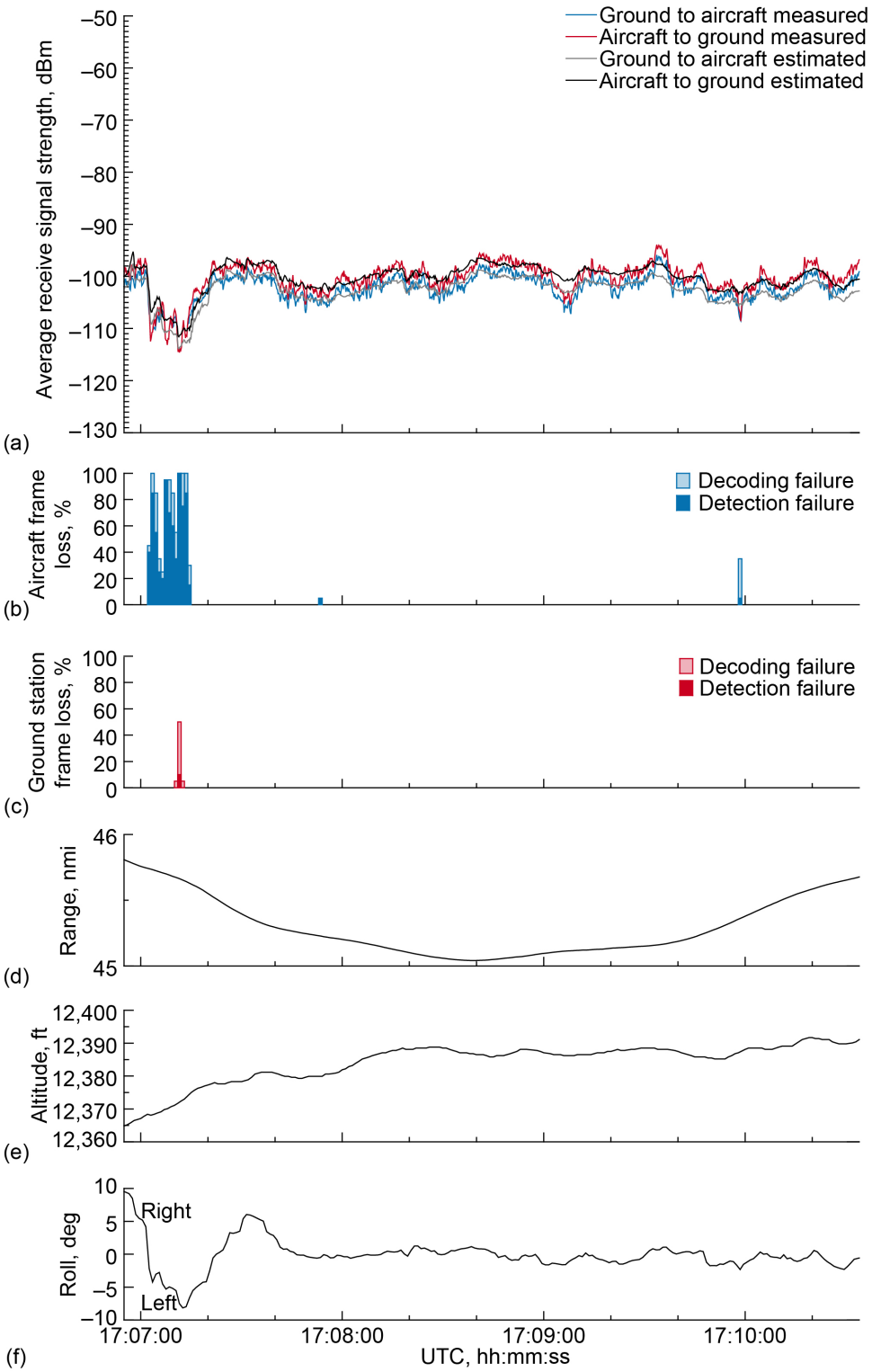

Figure 42.—Signal strength and frame loss over smooth plains terrain at 45-nmi range and 12,500-ft altitude, 2.0° antenna elevation, traveling from waypoint E to waypoint F. (a) Average receive signal strength. (b) Aircraft frame loss. (c) Ground station frame loss. (d) Range. (e) Altitude. (f) Roll.

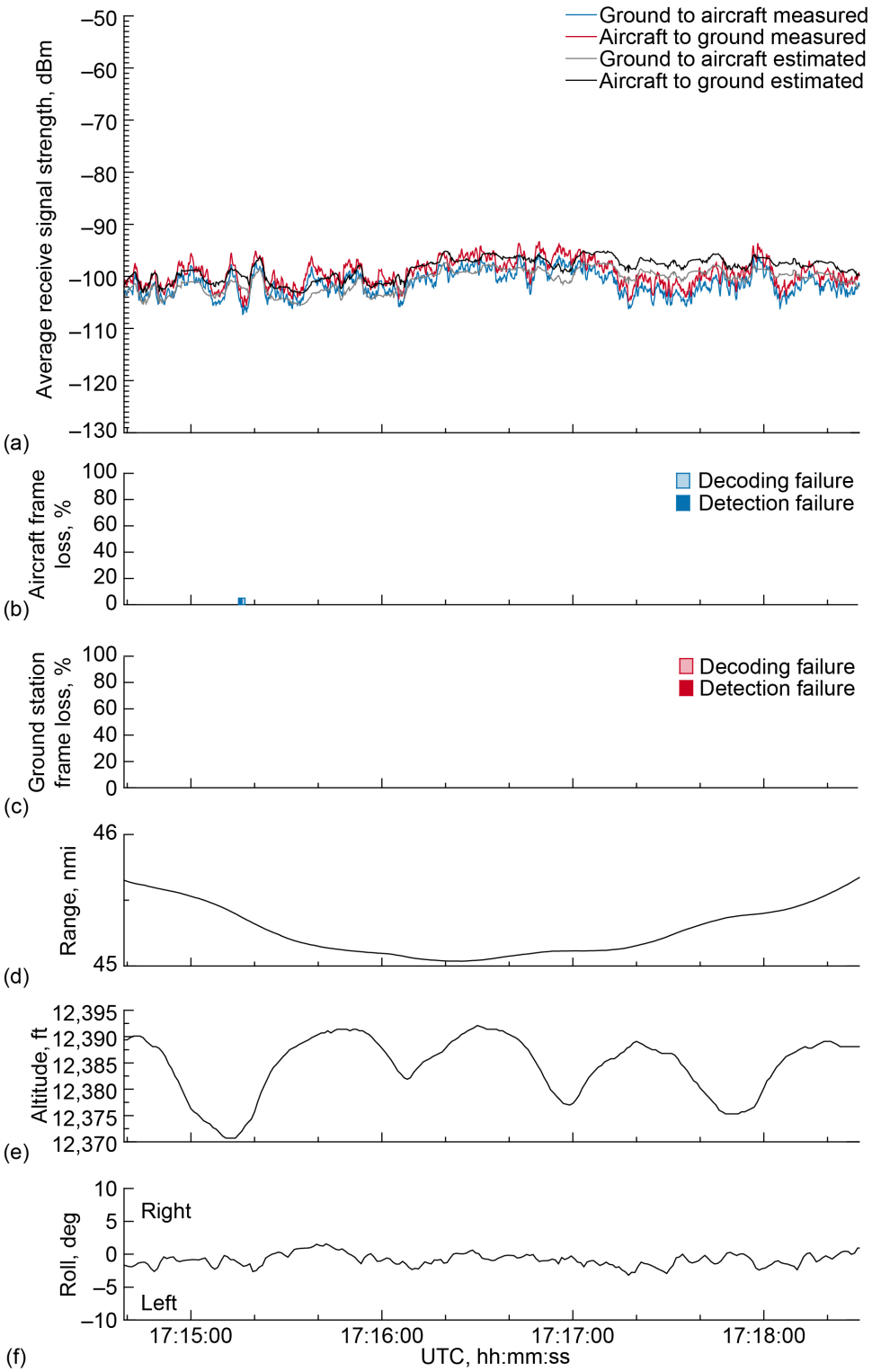

Figure 43.—Signal strength and frame loss over smooth plains terrain at 45-nmi range and 12,500-ft altitude, 2.0° antenna elevation, traveling from waypoint F to waypoint E. (a) Average receive signal strength. (b) Aircraft frame loss. (c) Ground station frame loss. (d) Range. (e) Altitude. (f) Roll.

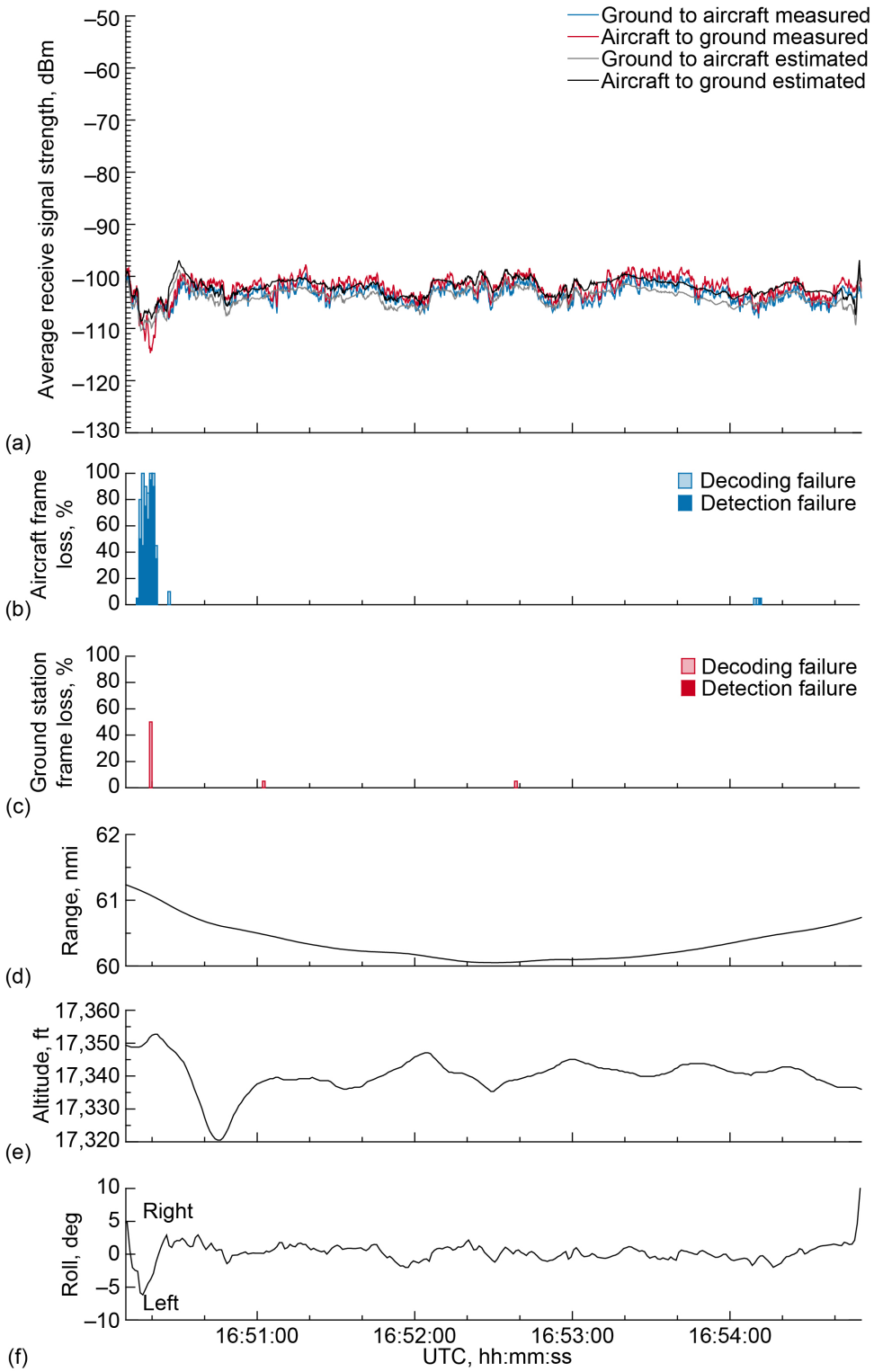

Figure 44.—Signal strength and frame loss over smooth plains terrain at 60-nmi range and 17,500-ft altitude, 2.0° antenna elevation, traveling from waypoint G to waypoint H. (a) Average receive signal strength. (b) Aircraft frame loss. (c) Ground station frame loss. (d) Range. (e) Altitude. (f) Roll.

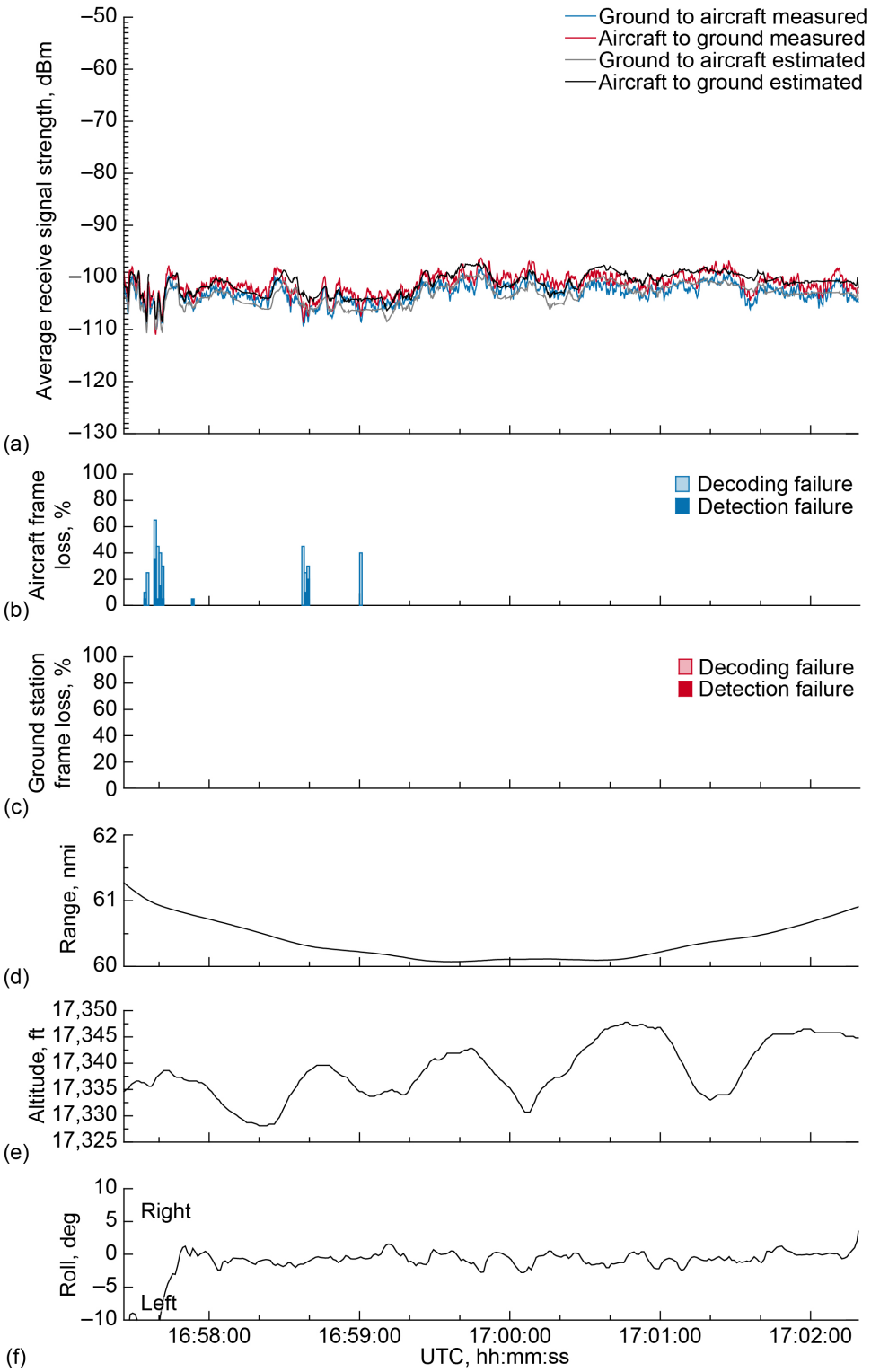

Figure 45.—Signal strength and frame loss over smooth plains terrain at 60-nmi range and 17,500-ft altitude, 2.0° antenna elevation, traveling from waypoint H to waypoint G. (a) Average receive signal strength. (b) Aircraft frame loss. (c) Ground station frame loss. (d) Range. (e) Altitude. (f) Roll.

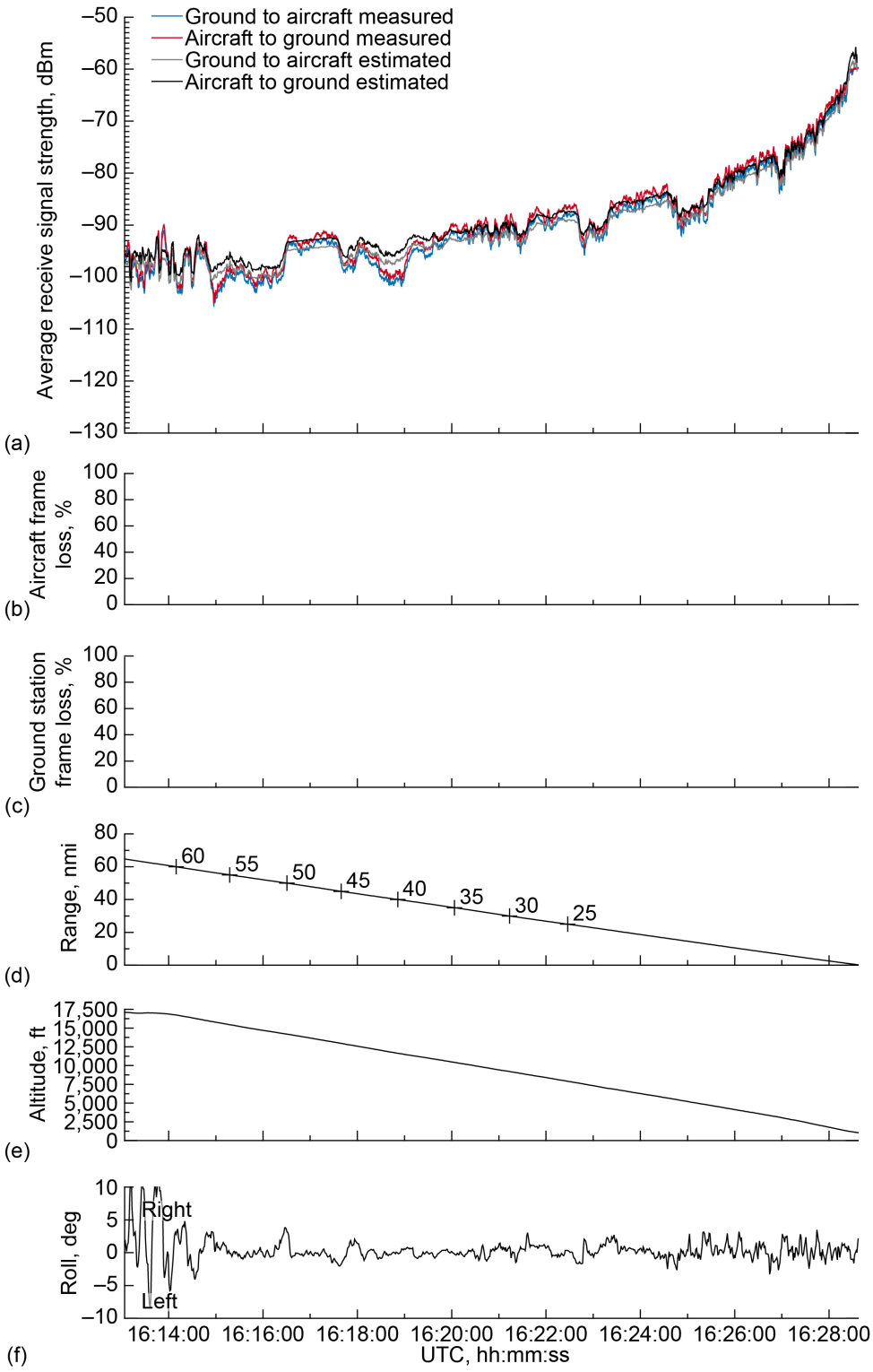

Figure 46.—Signal strength and frame loss over smooth plains terrain during inbound, descending track on 2.0° glide slope, traveling toward ground station. (a) Average receive signal strength. (b) Aircraft frame loss. (c) Ground station frame loss. (d) Range. (e) Altitude. (f) Roll.

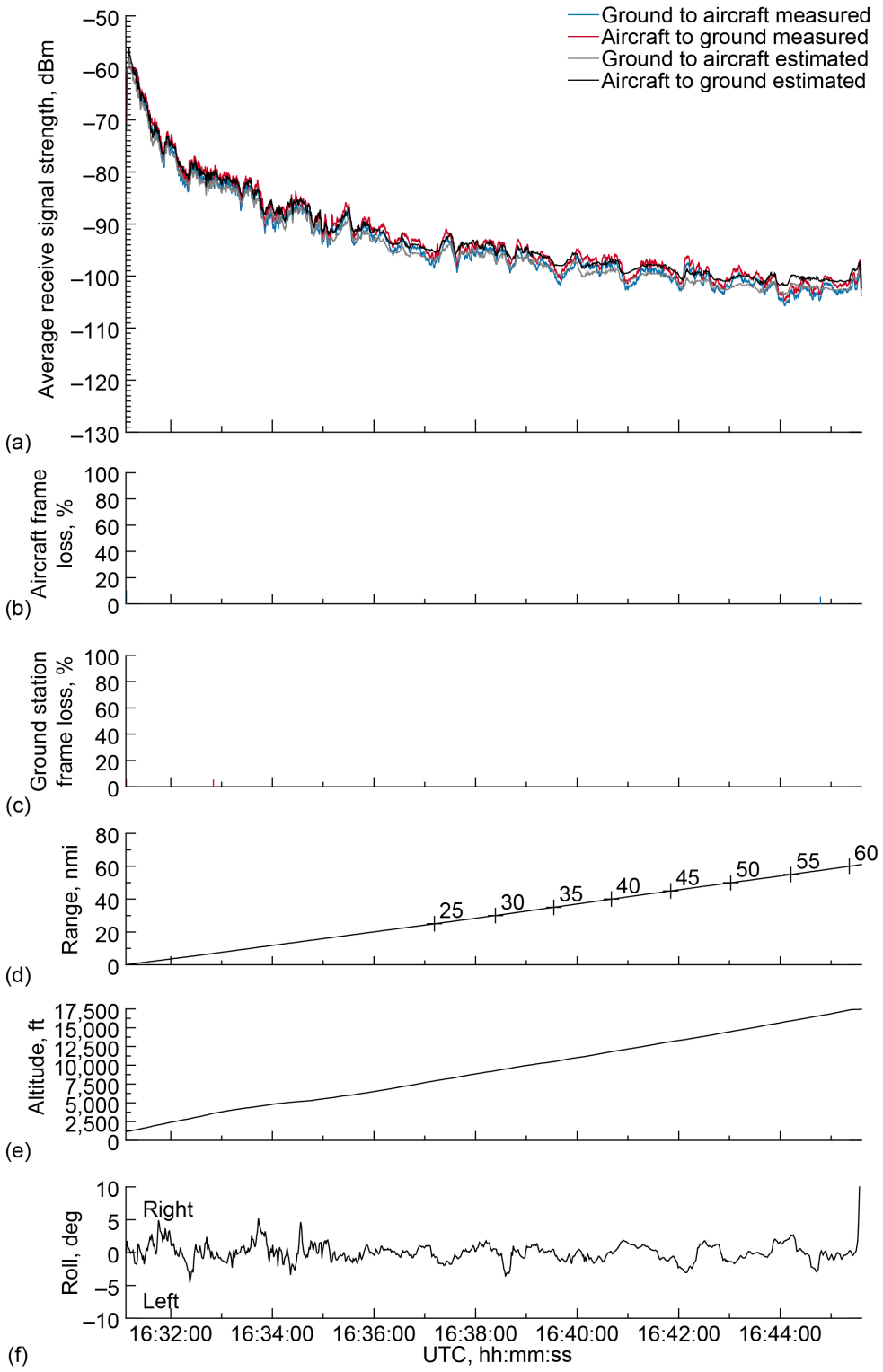

Figure 47.—Signal strength and frame loss over smooth plains terrain during outbound, ascending track on 2.0° glide slope, traveling away from ground station. (a) Average receive signal strength. (b) Aircraft frame loss. (c) Ground station frame loss. (d) Range. (e) Altitude. (f) Roll.

3.3 Validation Flight Test Data for Slightly Rolling Terrain Setting, December 11 and 12, 2019

Figure 48 presents the flight track of the NASA aircraft over slightly rolling plains in the airspace east of Athens, Ohio. The orange trace is the complete flightpath of the aircraft, including all reversals, ascent and descent maneuvers, and range changes. Figure 49 is the same flight track viewed from an oblique perspective to show the flightpath at various test altitudes. Waypoints are identified with alphabet characters A to H. The flight segments between waypoints are highlighted in yellow, which precisely represents the locations where RF data was captured for evaluation. For this terrain setting, the GRS was positioned on the open tarmac of the Ohio University Airport in Albany, Ohio.

C-band validation flight test data over slightly rolling plains is presented in Figure 50 to Figure 90. Crosstrack plots are arranged for elevation angles of 1.0°, 1.5°, 2.0°, and 3.0° followed by ascent and descent plots.

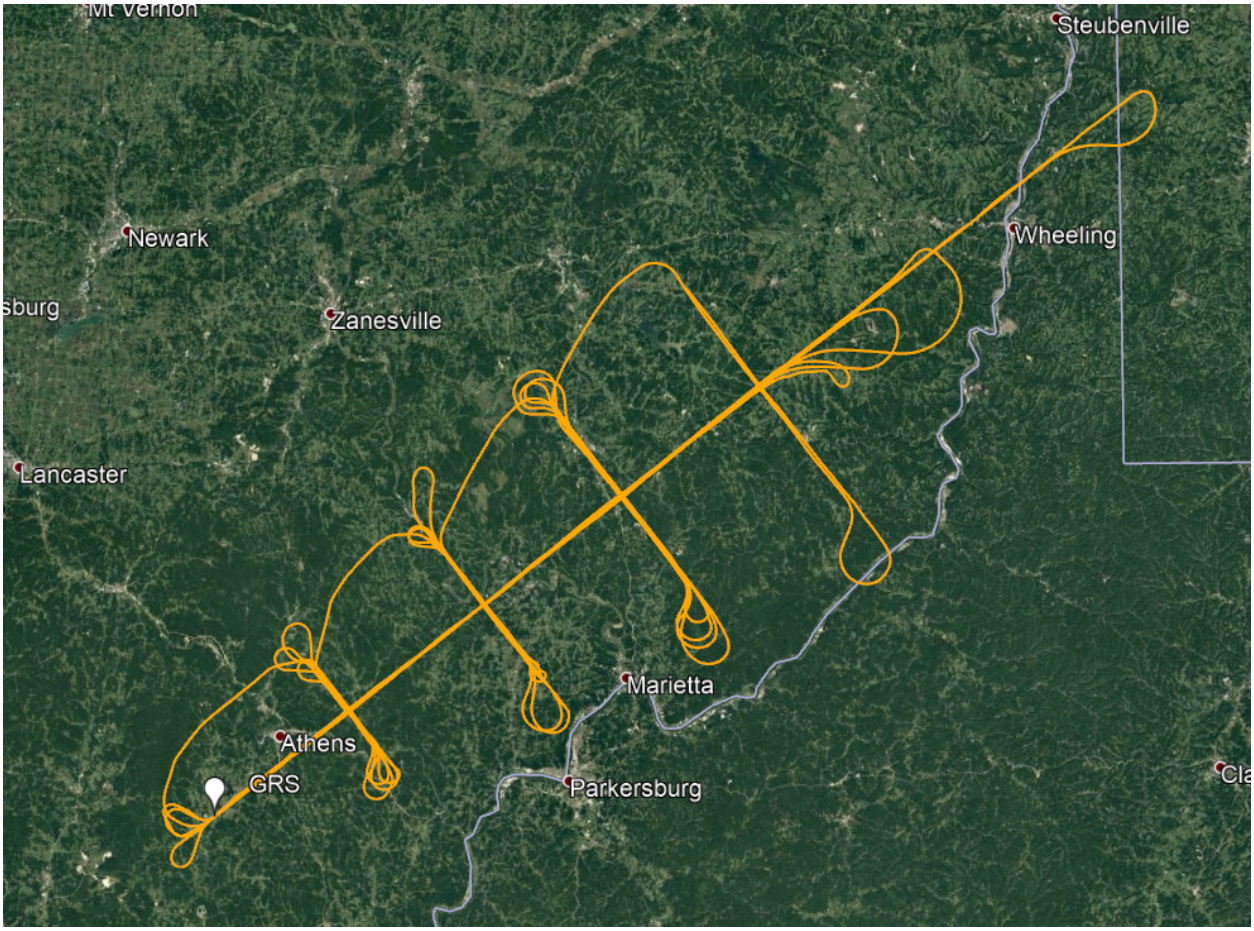

Figure 48.—Flightpath over slightly rolling terrain December 11, 2019. Image ©2020 GoogleEarth.

Figure 49.—Perspective view of flightpath over slightly rolling terrain highlighting data capture segments for December 11, 2019. Image ©2020 GoogleEarth.

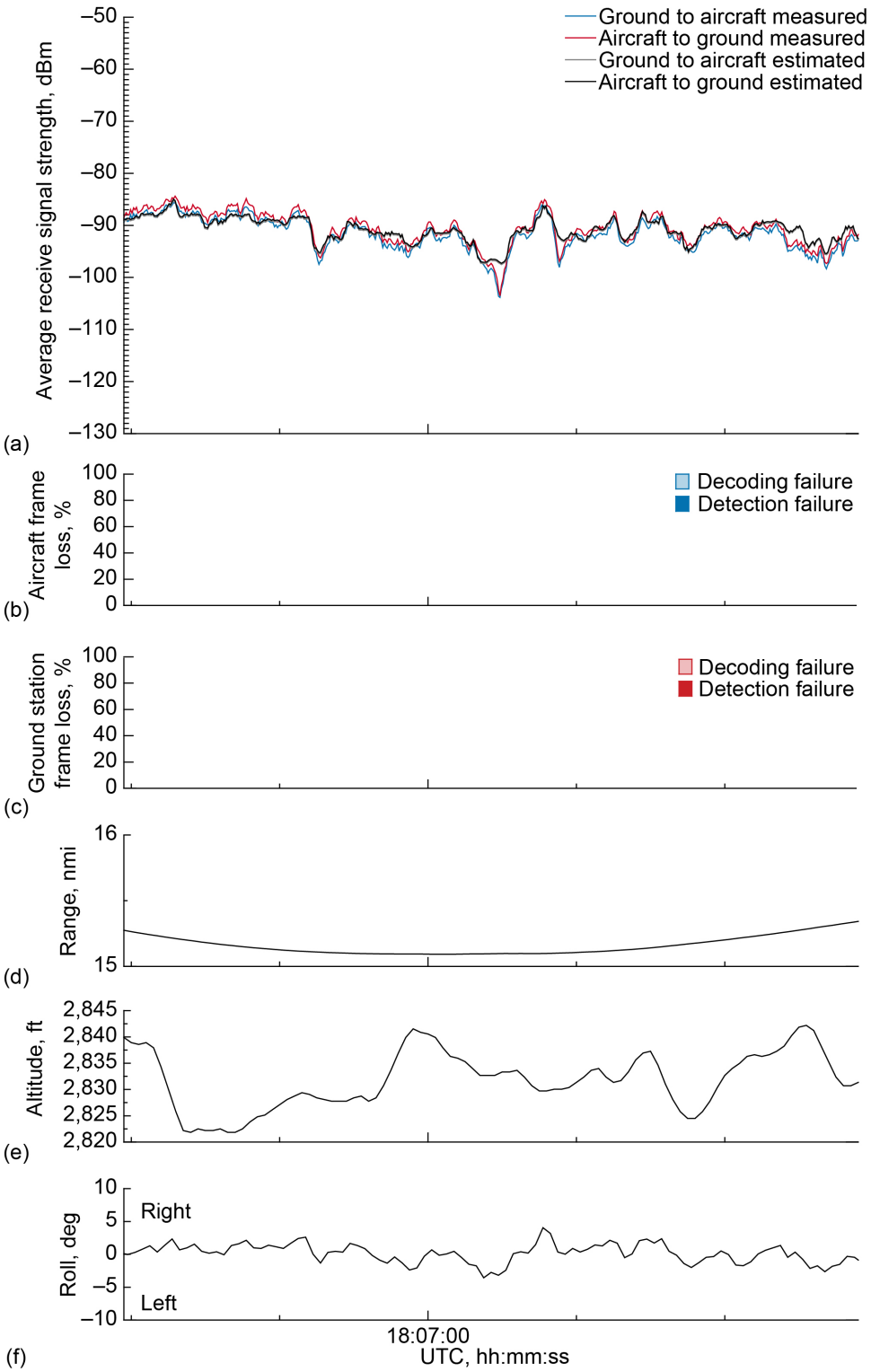

Figure 50.—Signal strength and frame loss over slightly rolling terrain at 15-nmi range and 3,000-ft altitude, 1.0° antenna elevation, traveling from waypoint A to waypoint B. (a) Average receive signal strength. (b) Aircraft frame loss. (c) Ground station frame loss. (d) Range. (e) Altitude. (f) Roll.

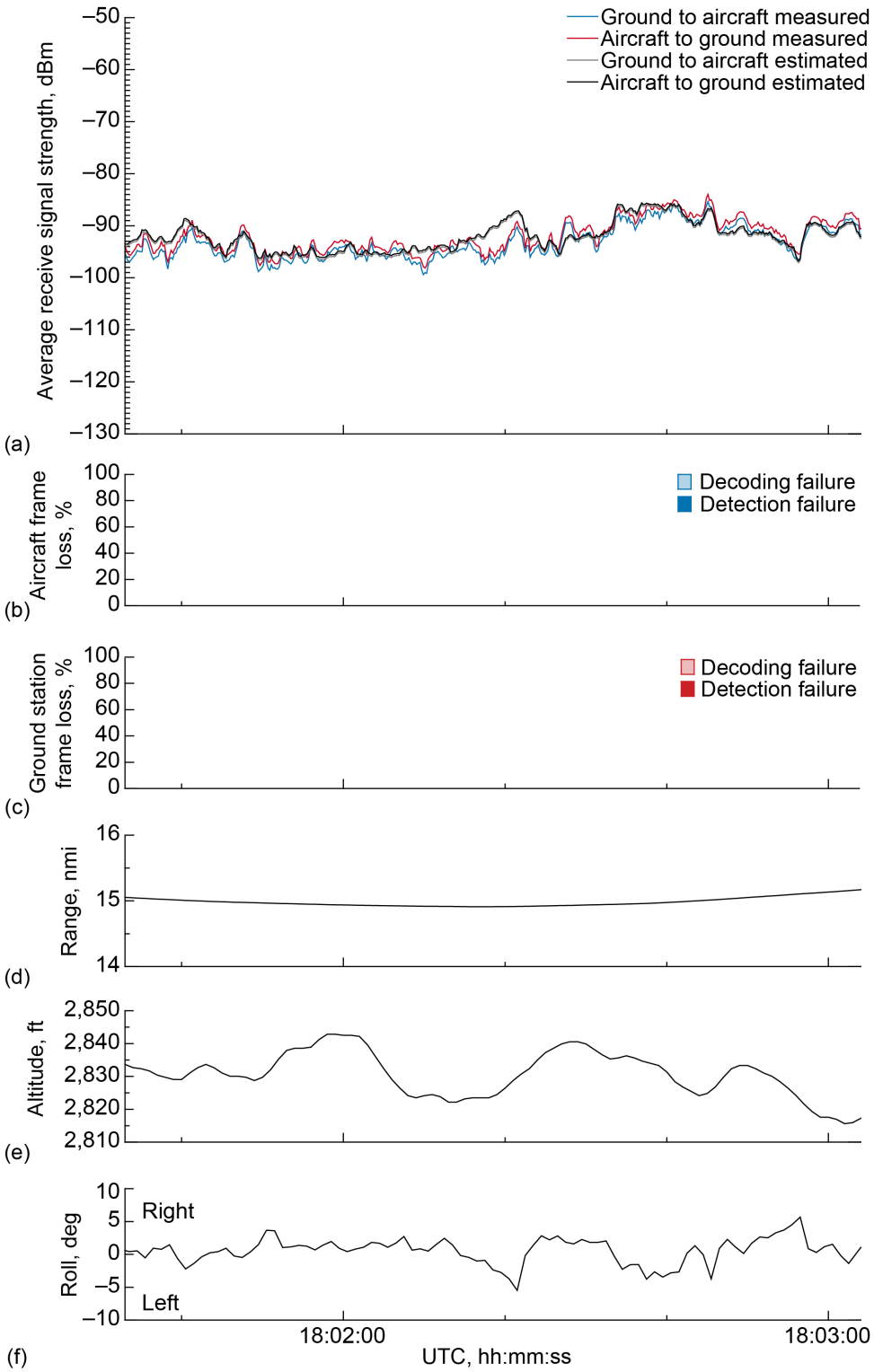

Figure 51.—Signal strength and frame loss over slightly rolling terrain at 15-nmi range and 3,000-ft altitude, 1.0° antenna elevation, traveling from waypoint B to waypoint A. (a) Average receive signal strength. (b) Aircraft frame loss. (c) Ground station frame loss. (d) Range. (e) Altitude. (f) Roll.

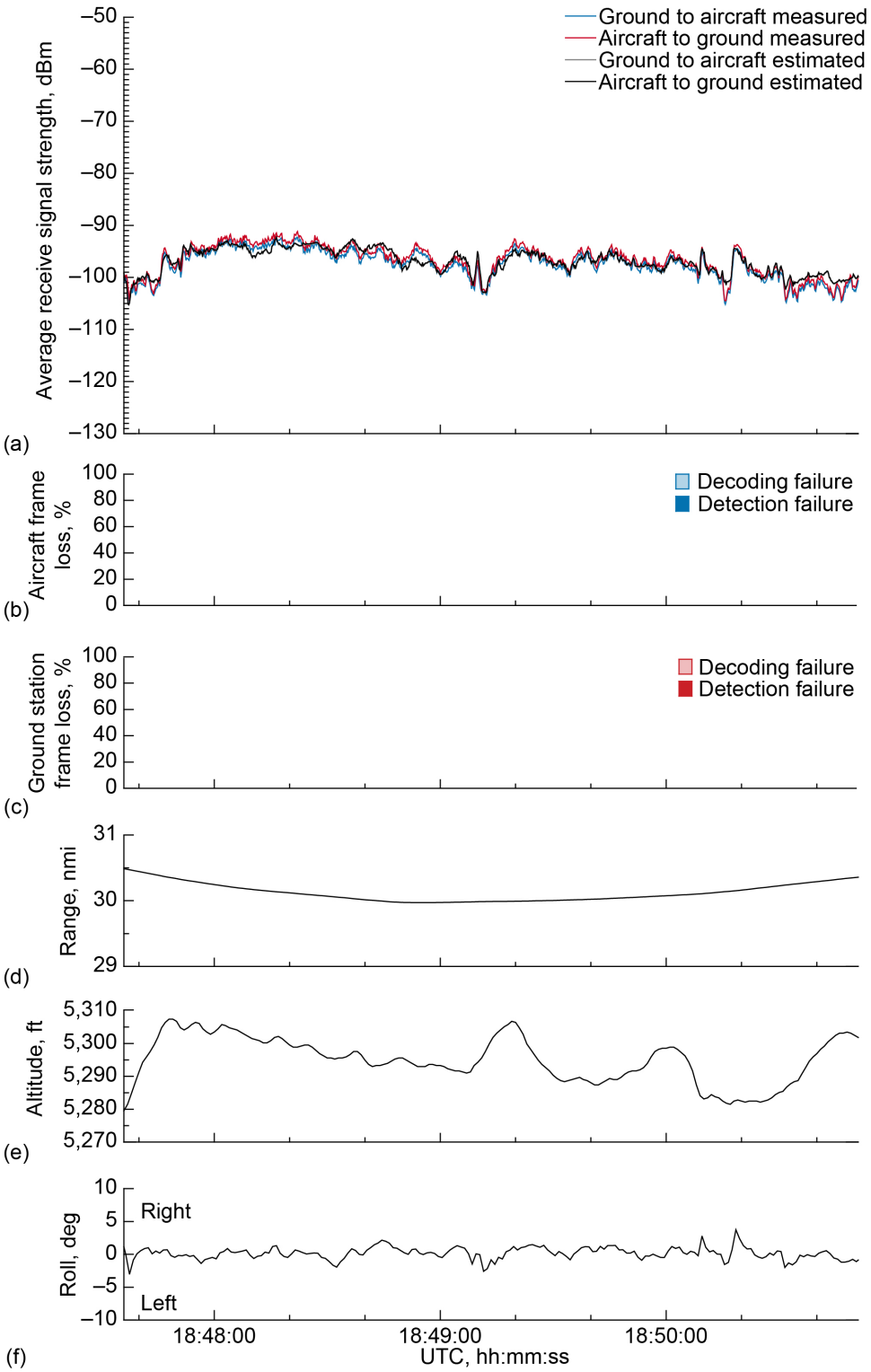

Figure 52.—Signal strength and frame loss over slightly rolling terrain at 30-nmi range and 5,500-ft altitude, 1.0° antenna elevation, traveling from waypoint C to waypoint D. (a) Average receive signal strength. (b) Aircraft frame loss. (c) Ground station frame loss. (d) Range. (e) Altitude. (f) Roll.

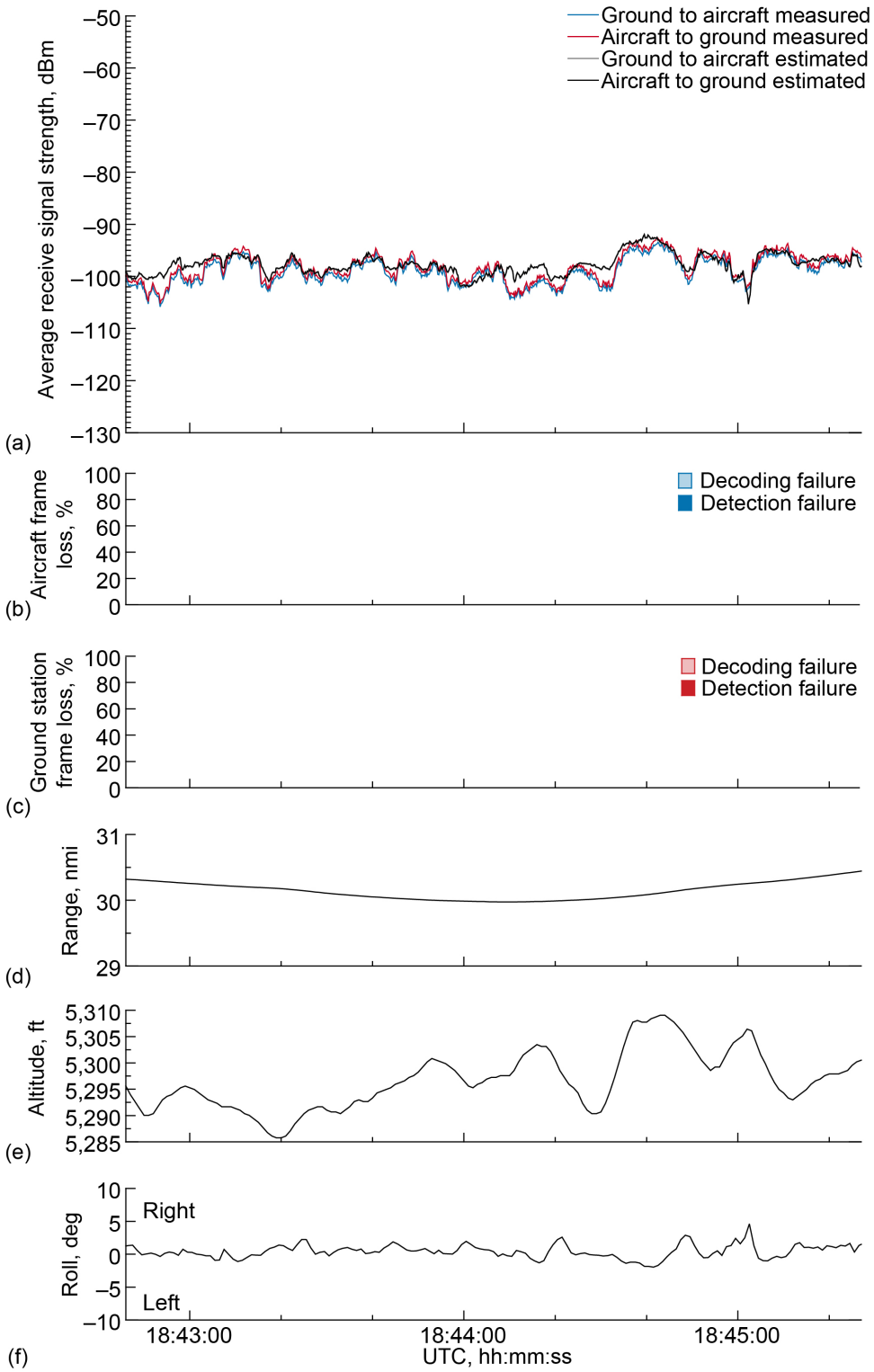

Figure 53.—Signal strength and frame loss over slightly rolling terrain at 30-nmi range and 5,500-ft altitude, 1.0° antenna elevation, traveling from waypoint D to waypoint C. (a) Average receive signal strength. (b) Aircraft frame loss. (c) Ground station frame loss. (d) Range. (e) Altitude. (f) Roll.

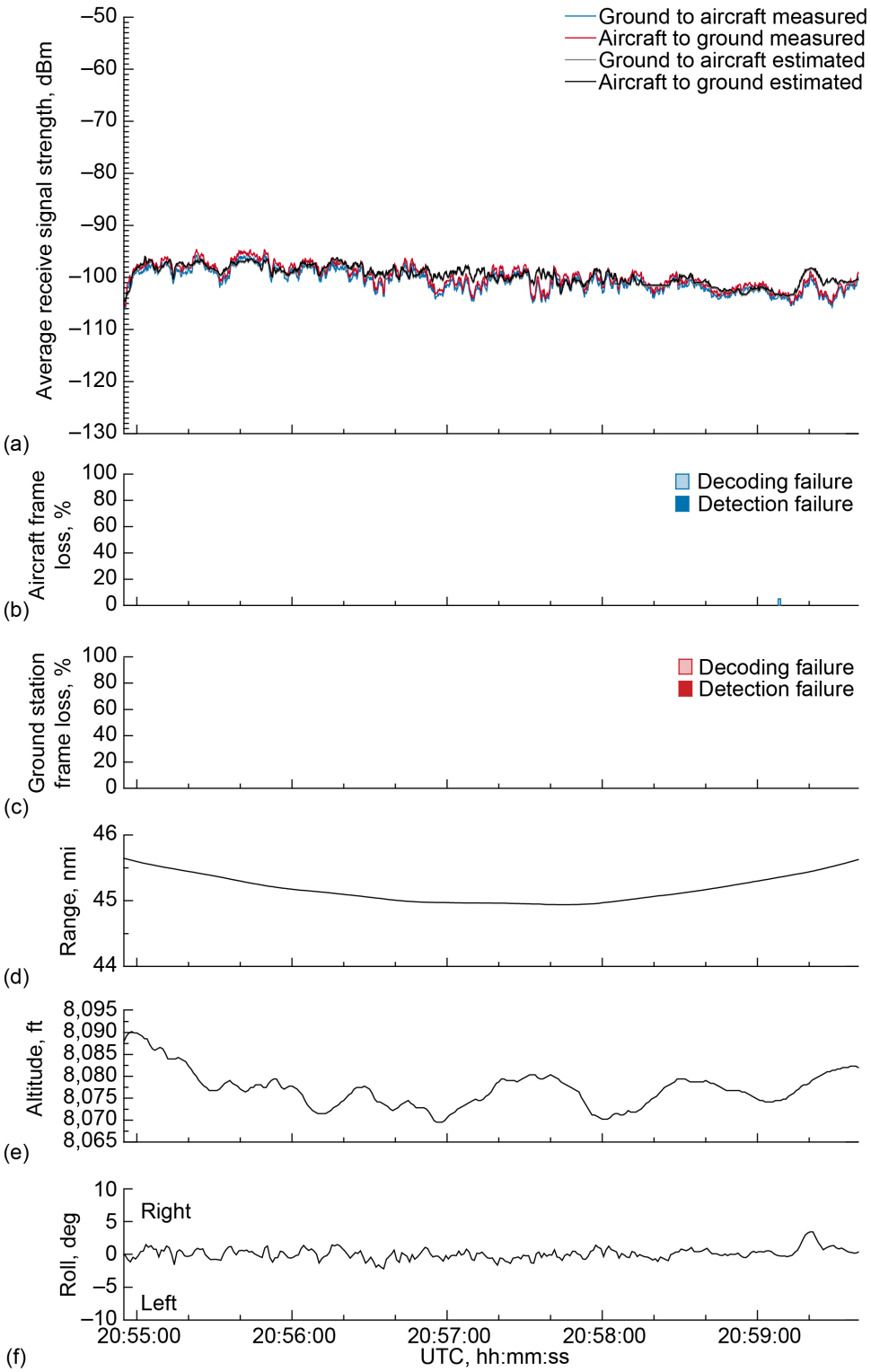

Figure 54.—Signal strength and frame loss over slightly rolling terrain at 45-nmi range and 8,000-ft altitude, 1.0° antenna elevation, traveling from waypoint E to waypoint F. (a) Average receive signal strength. (b) Aircraft frame loss. (c) Ground station frame loss. (d) Range. (e) Altitude. (f) Roll.

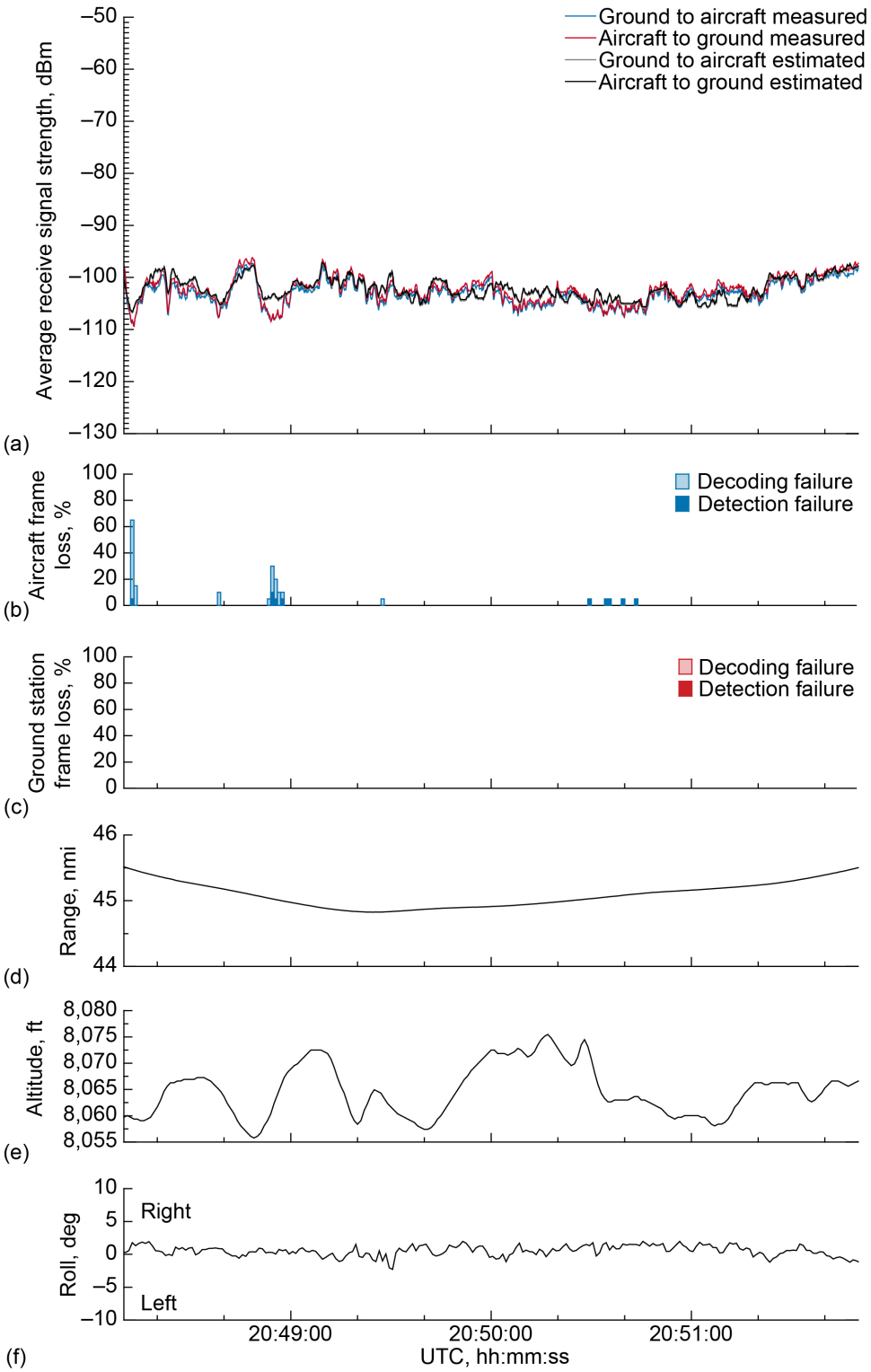

Figure 55.—Signal strength and frame loss over slightly rolling terrain at 45-nmi range and 8,000-ft altitude, 1.0° antenna elevation, traveling from waypoint F to waypoint E. (a) Average receive signal strength. (b) Aircraft frame loss. (c) Ground station frame loss. (d) Range. (e) Altitude. (f) Roll.

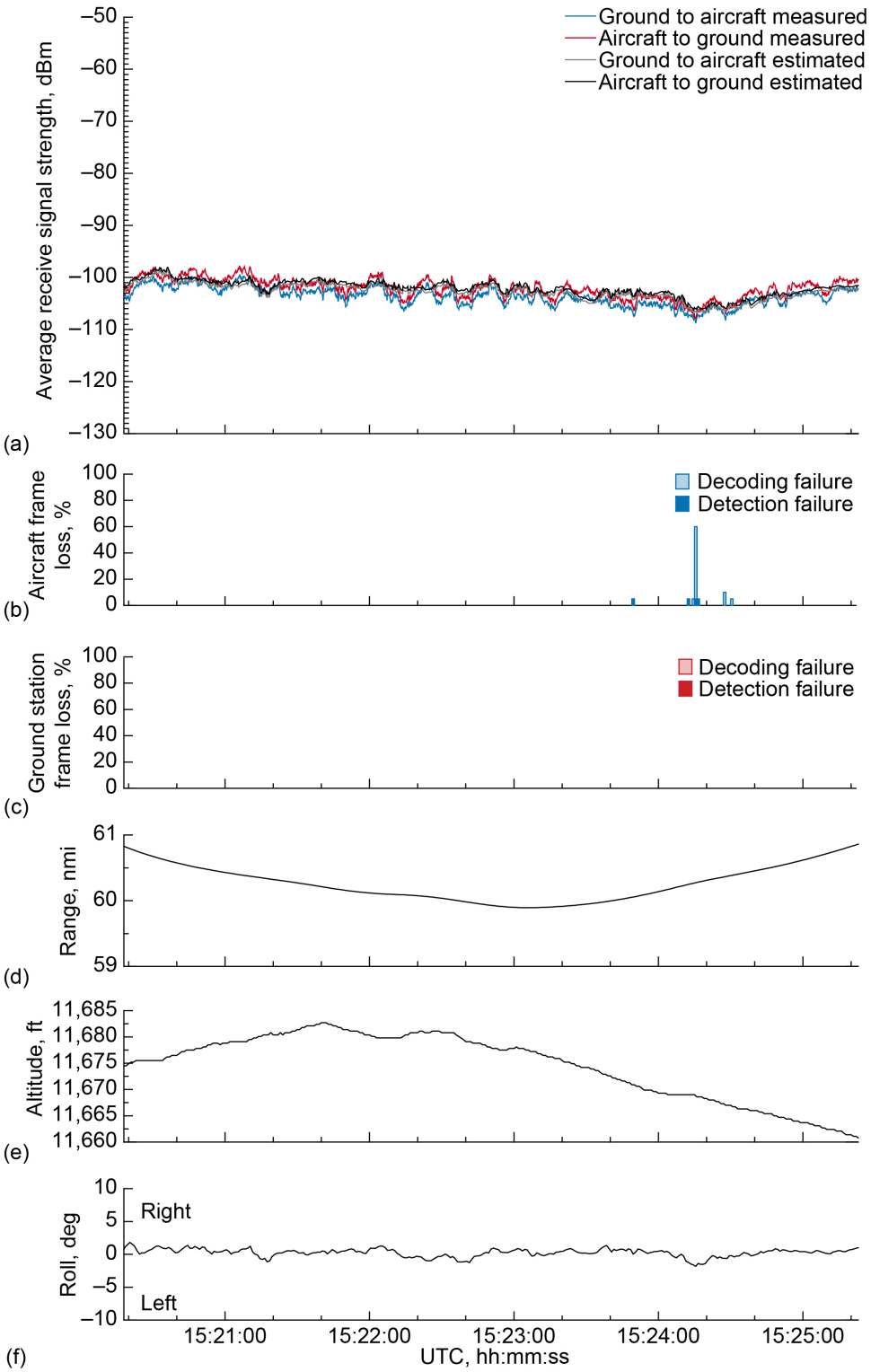

Figure 56.—Signal strength and frame loss over slightly rolling terrain at 60-nmi range and 11,500-ft altitude, 1.0° antenna elevation, traveling from waypoint G to waypoint H. (a) Average receive signal strength. (b) Aircraft frame loss. (c) Ground station frame loss. (d) Range. (e) Altitude. (f) Roll.

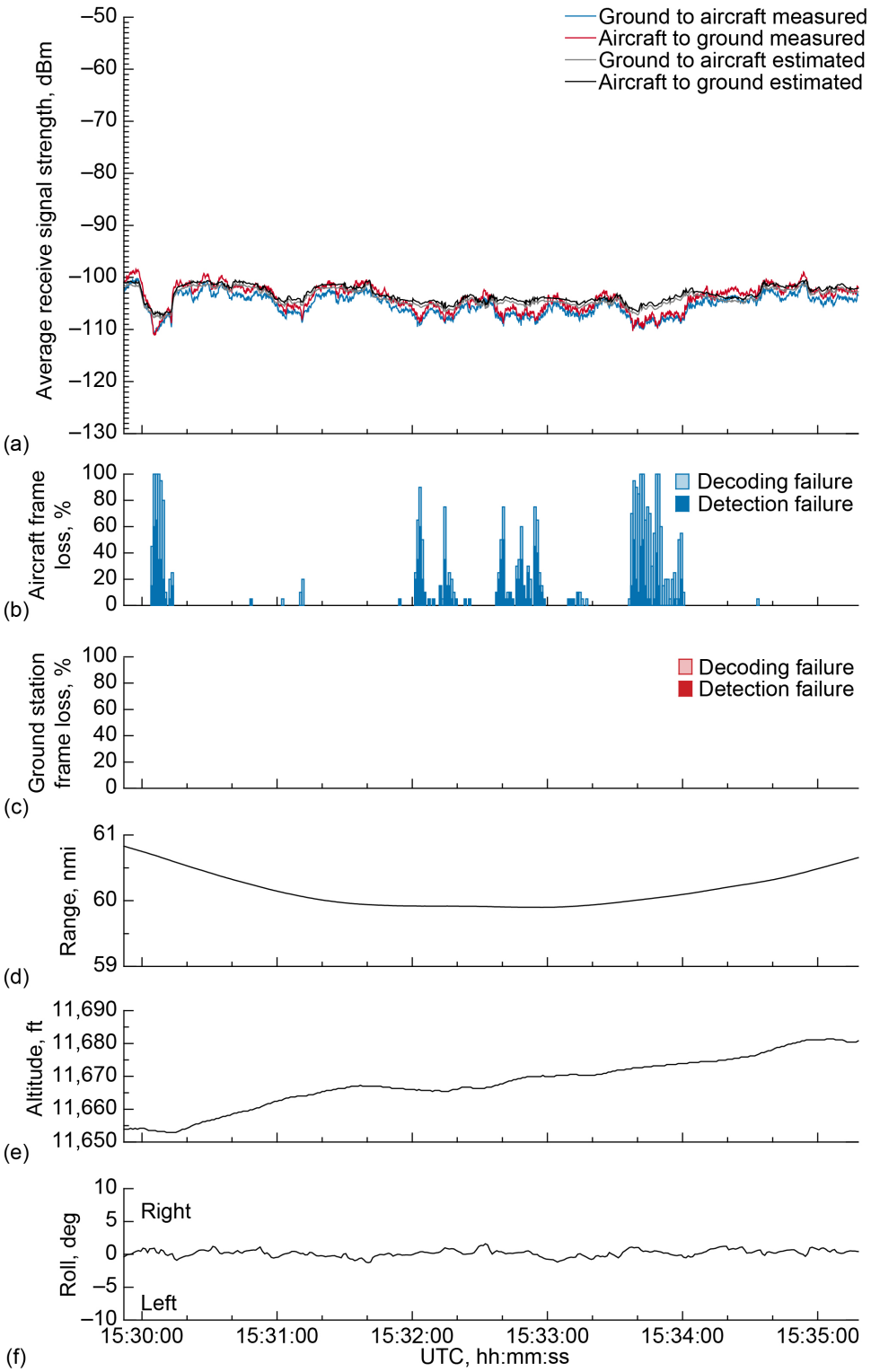

Figure 57.—Signal strength and frame loss over slightly rolling terrain at 60-nmi range and 11,500-ft altitude, 1.0° antenna elevation, traveling from waypoint H to waypoint G. (a) Average receive signal strength. (b) Aircraft frame loss. (c) Ground station frame loss. (d) Range. (e) Altitude. (f) Roll.

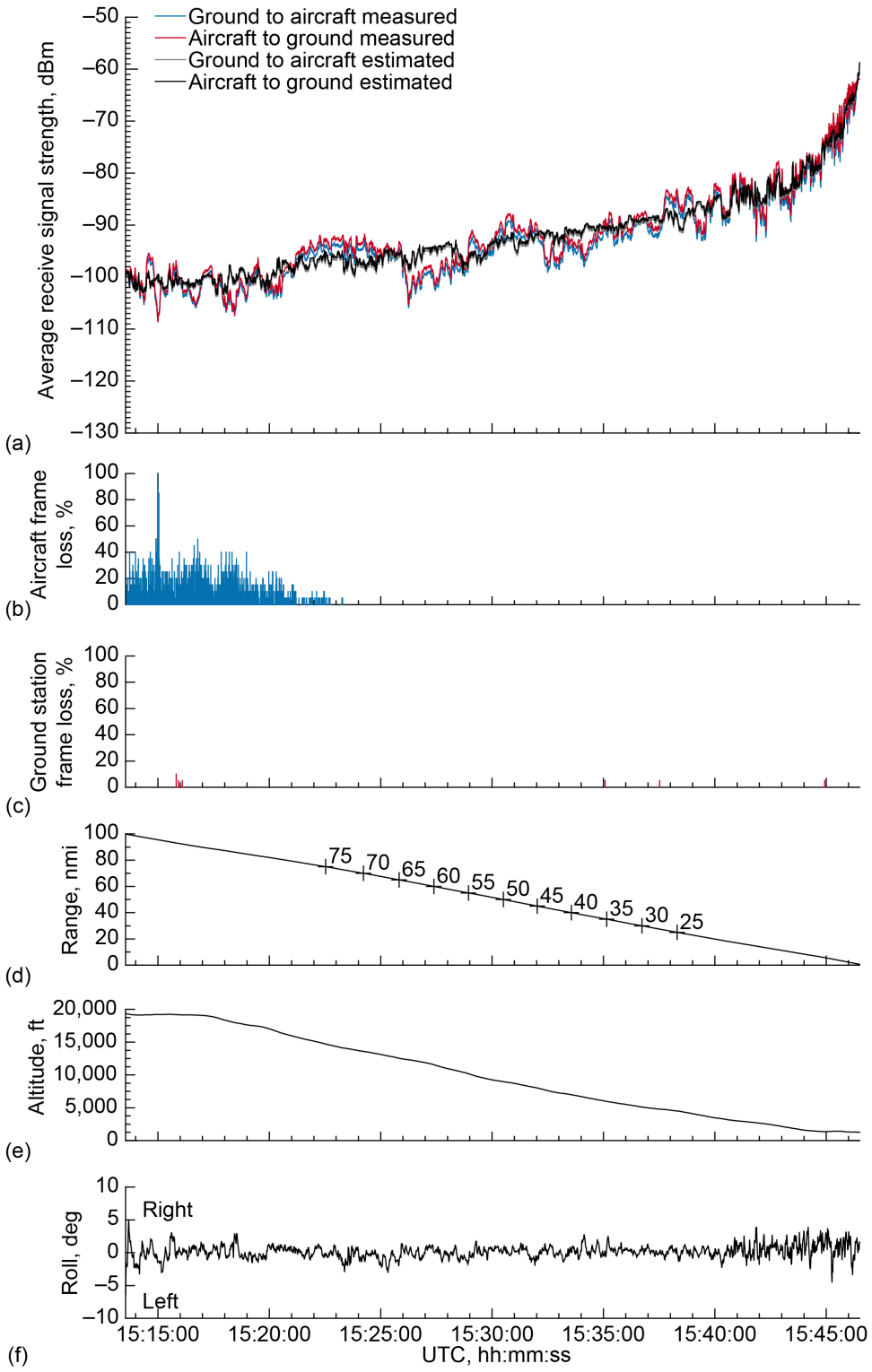

Figure 58.—Signal strength and frame loss over slightly rolling terrain during inbound, descending track on 1.0° glide slope, traveling toward ground station. (a) Average receive signal strength. (b) Aircraft frame loss. (c) Ground station frame loss. (d) Range. (e) Altitude. (f) Roll.

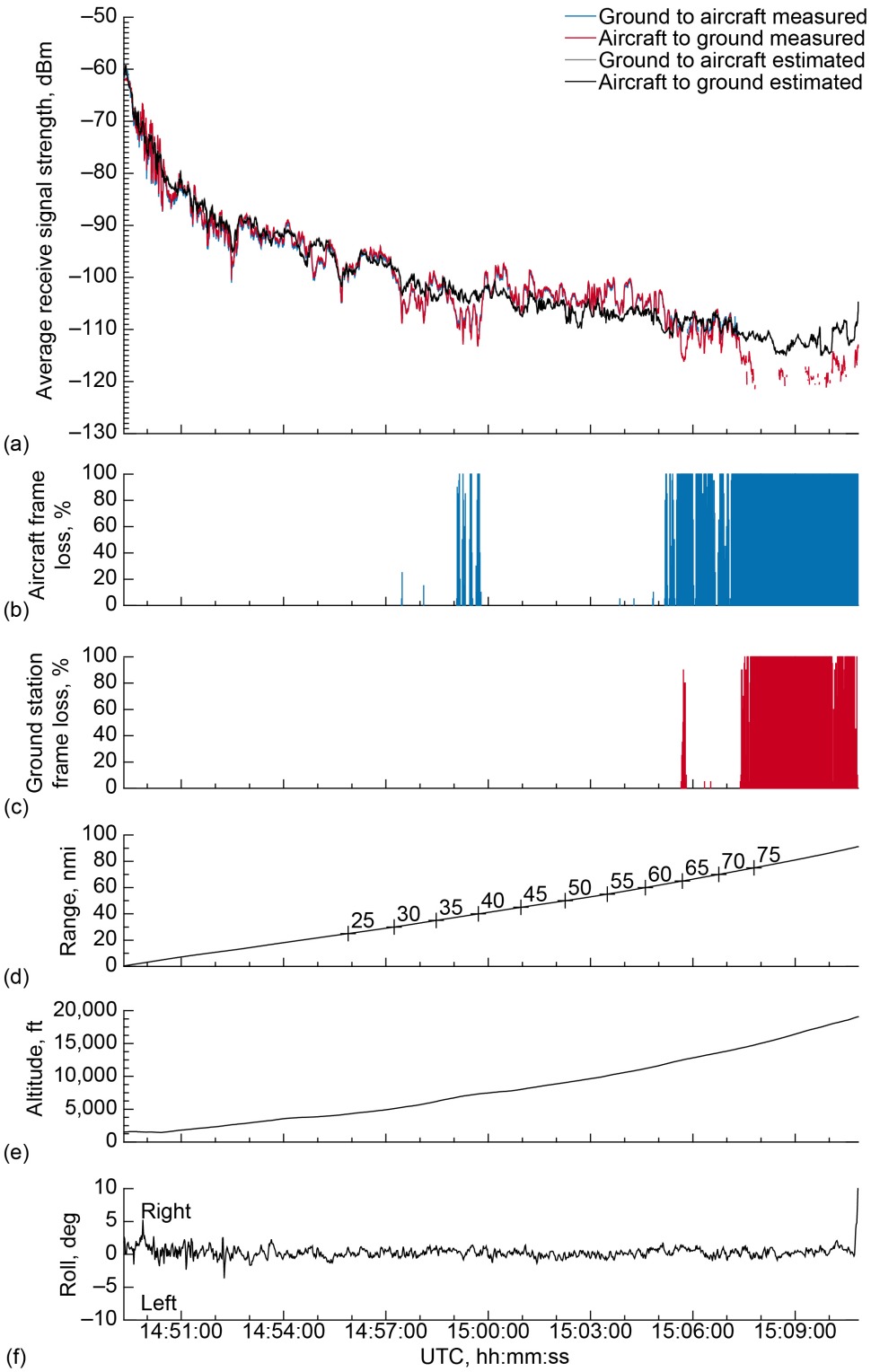

Figure 59.—Signal strength and frame loss over slightly rolling terrain during outbound, ascending track on 1.0° glide slope, traveling away from ground station. (a) Average receive signal strength. (b) Aircraft frame loss. (c) Ground station frame loss. (d) Range. (e) Altitude. (f) Roll.

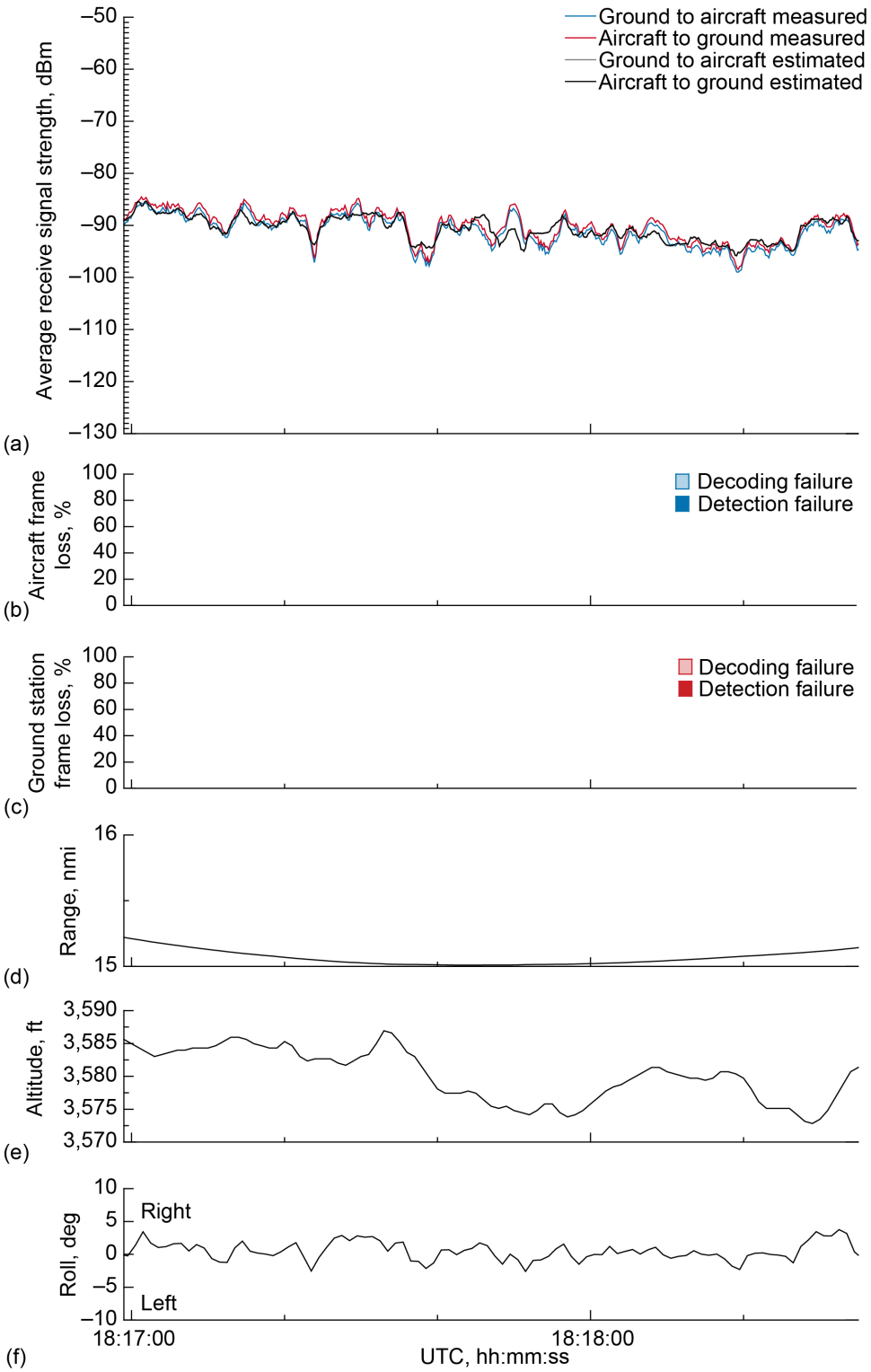

Figure 60.—Signal strength and frame loss over slightly rolling terrain at 15-nmi range and 3,500-ft altitude, 1.5° antenna elevation, traveling from waypoint A to waypoint B. (a) Average receive signal strength. (b) Aircraft frame loss. (c) Ground station frame loss. (d) Range. (e) Altitude. (f) Roll.

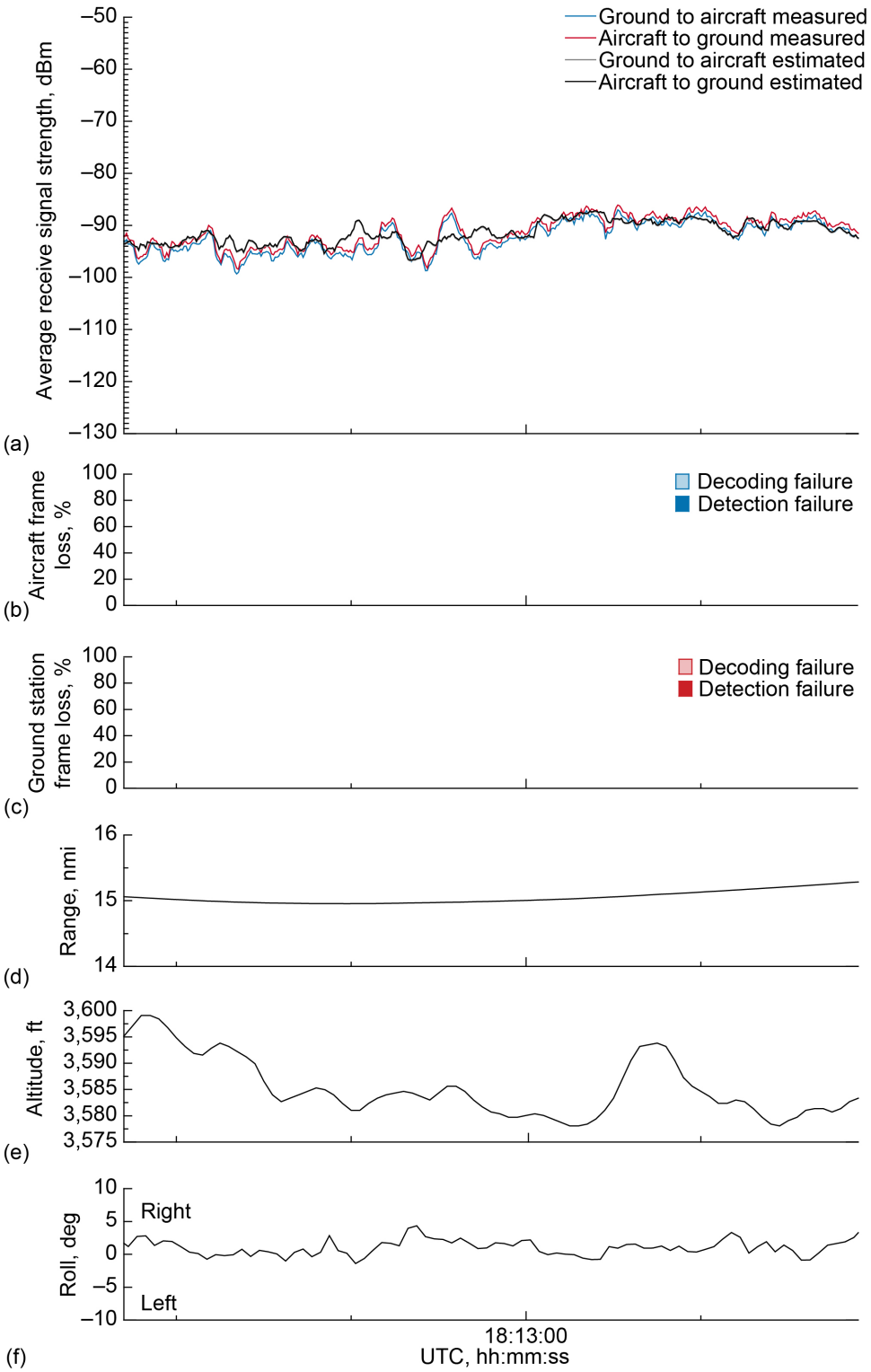

Figure 61.—Signal strength and frame loss over slightly rolling terrain at 15-nmi range and 3,500-ft altitude, 1.5° antenna elevation, traveling from waypoint B to waypoint A. (a) Average receive signal strength. (b) Aircraft frame loss. (c) Ground station frame loss. (d) Range. (e) Altitude. (f) Roll.

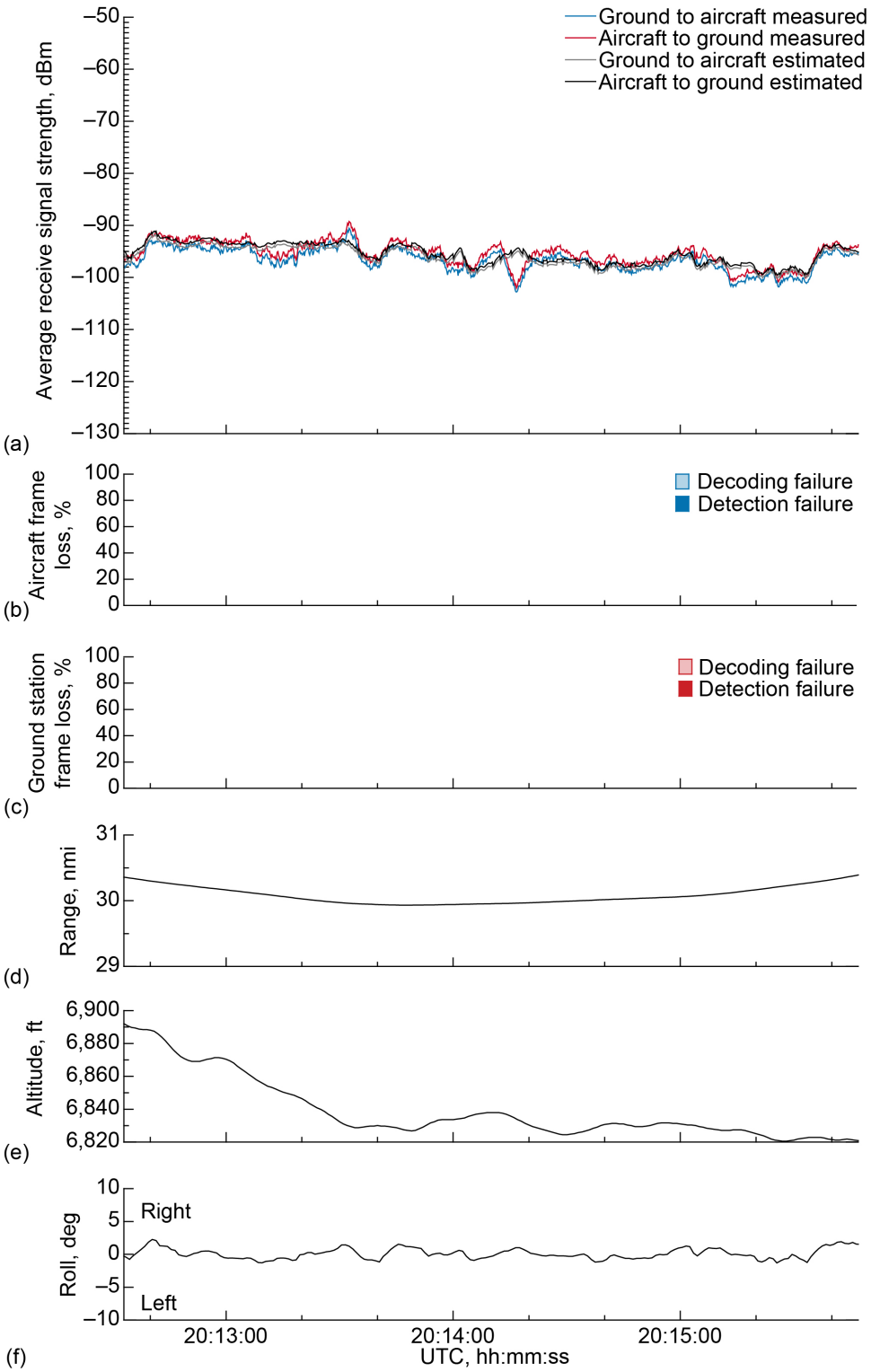

Figure 62.—Signal strength and frame loss over slightly rolling terrain at 30-nmi range and 7,000-ft altitude, 1.5° antenna elevation, traveling from waypoint C to waypoint D. (a) Average receive signal strength. (b) Aircraft frame loss. (c) Ground station frame loss. (d) Range. (e) Altitude. (f) Roll.

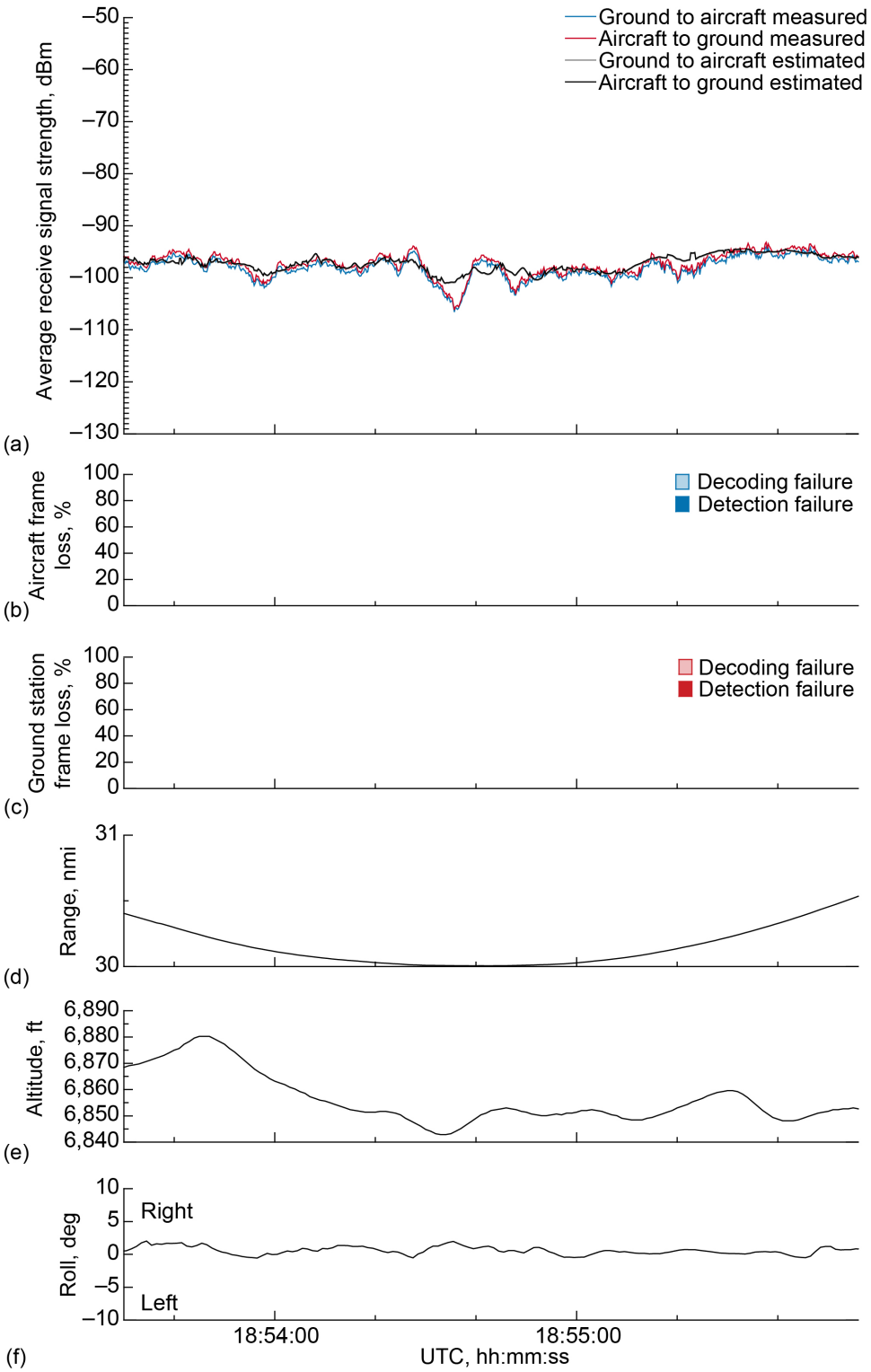

Figure 63.—Signal strength and frame loss over slightly rolling terrain at 30-nmi range and 7,000-ft altitude, 1.5° antenna elevation, traveling from waypoint D to waypoint C. (a) Average receive signal strength. (b) Aircraft frame loss. (c) Ground station frame loss. (d) Range. (e) Altitude. (f) Roll.

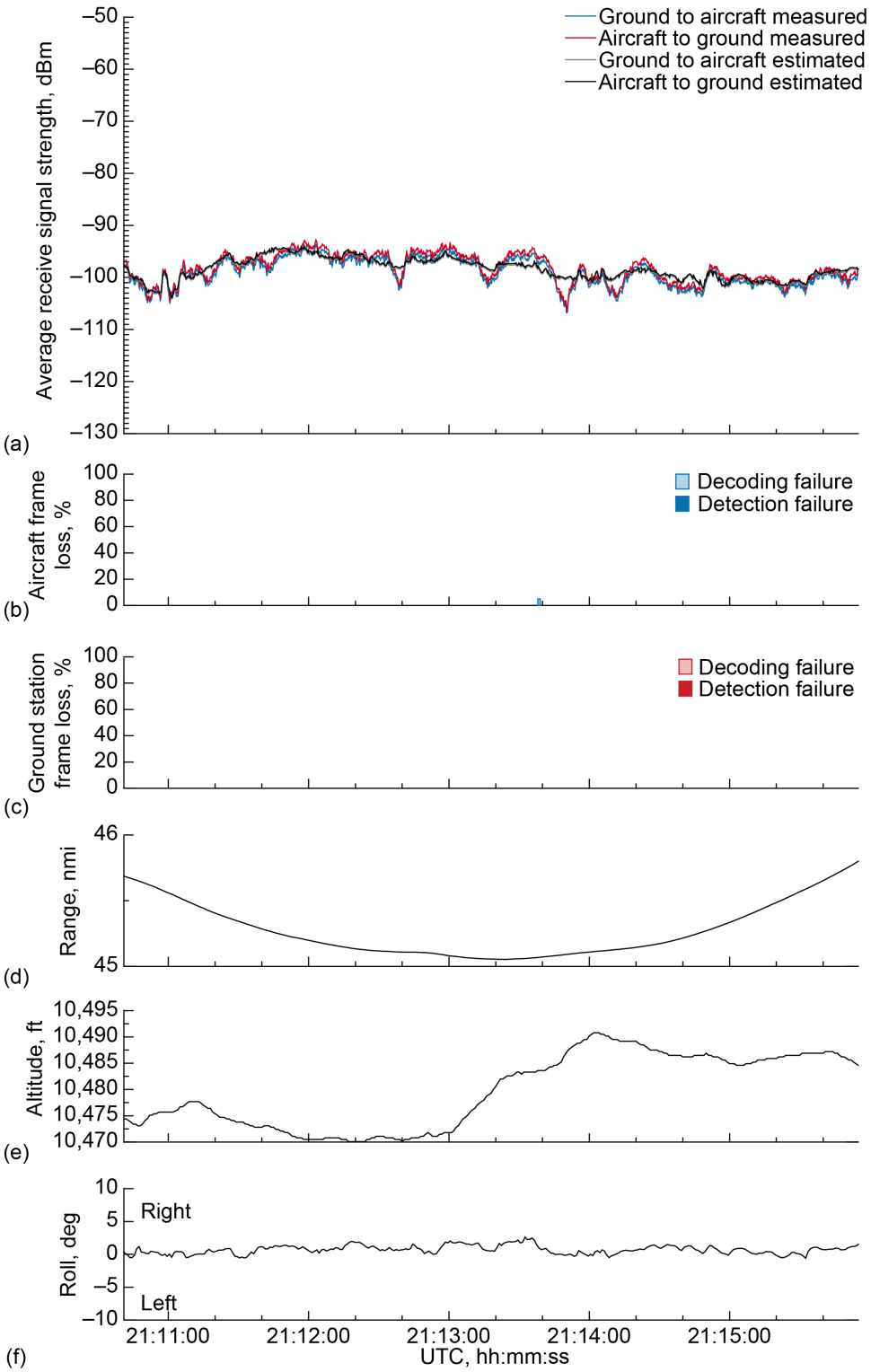

Figure 64.—Signal strength and frame loss over slightly rolling terrain at 45-nmi range and 10,500-ft altitude, 1.5° antenna elevation, traveling from waypoint E to waypoint F. (a) Average receive signal strength. (b) Aircraft frame loss. (c) Ground station frame loss. (d) Range. (e) Altitude. (f) Roll.

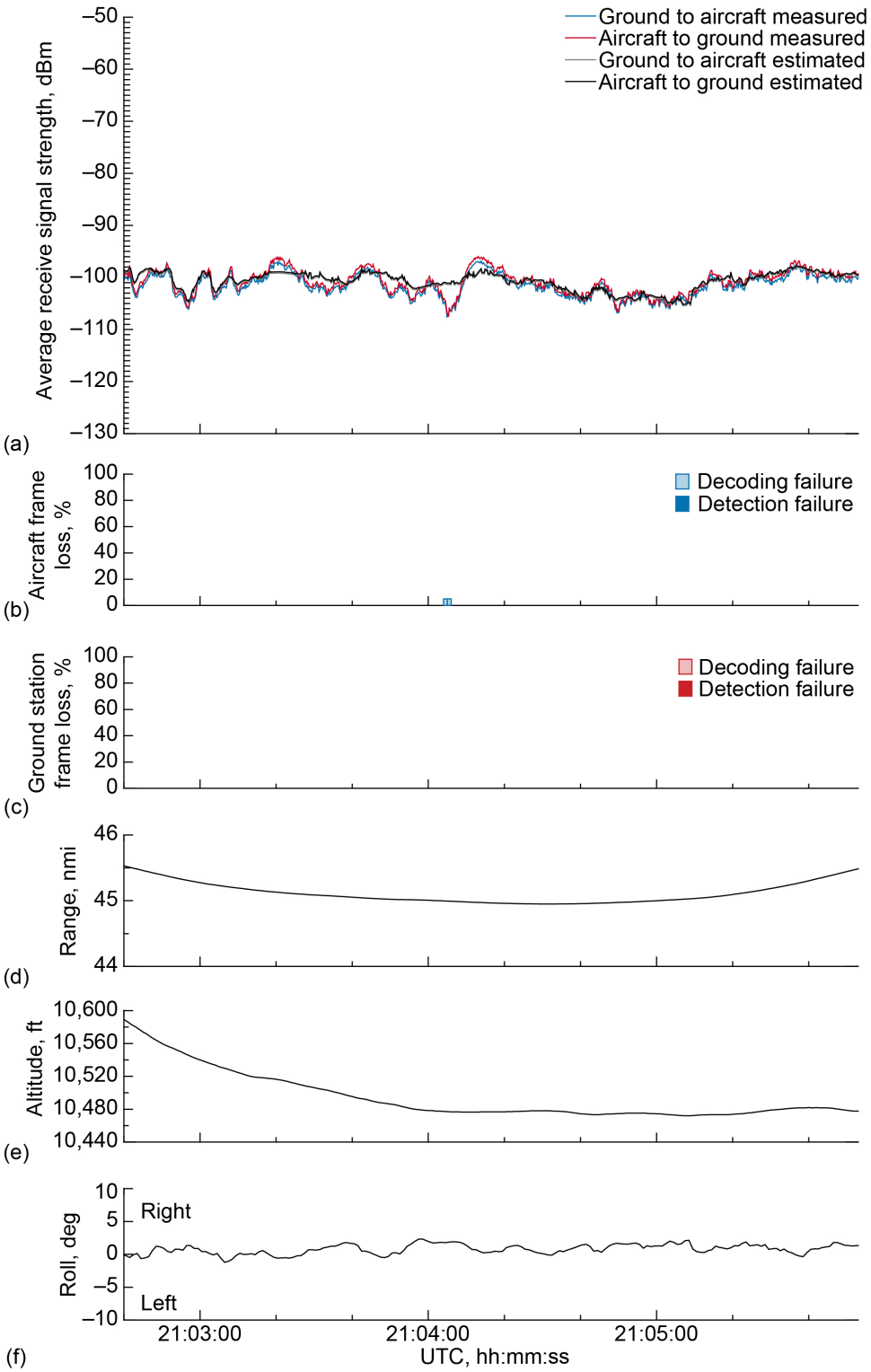

Figure 65.—Signal strength and frame loss over slightly rolling terrain at 45-nmi range and 10,500-ft altitude, 1.5° antenna elevation, traveling from waypoint F to waypoint E. (a) Average receive signal strength. (b) Aircraft frame loss. (c) Ground station frame loss. (d) Range. (e) Altitude. (f) Roll.

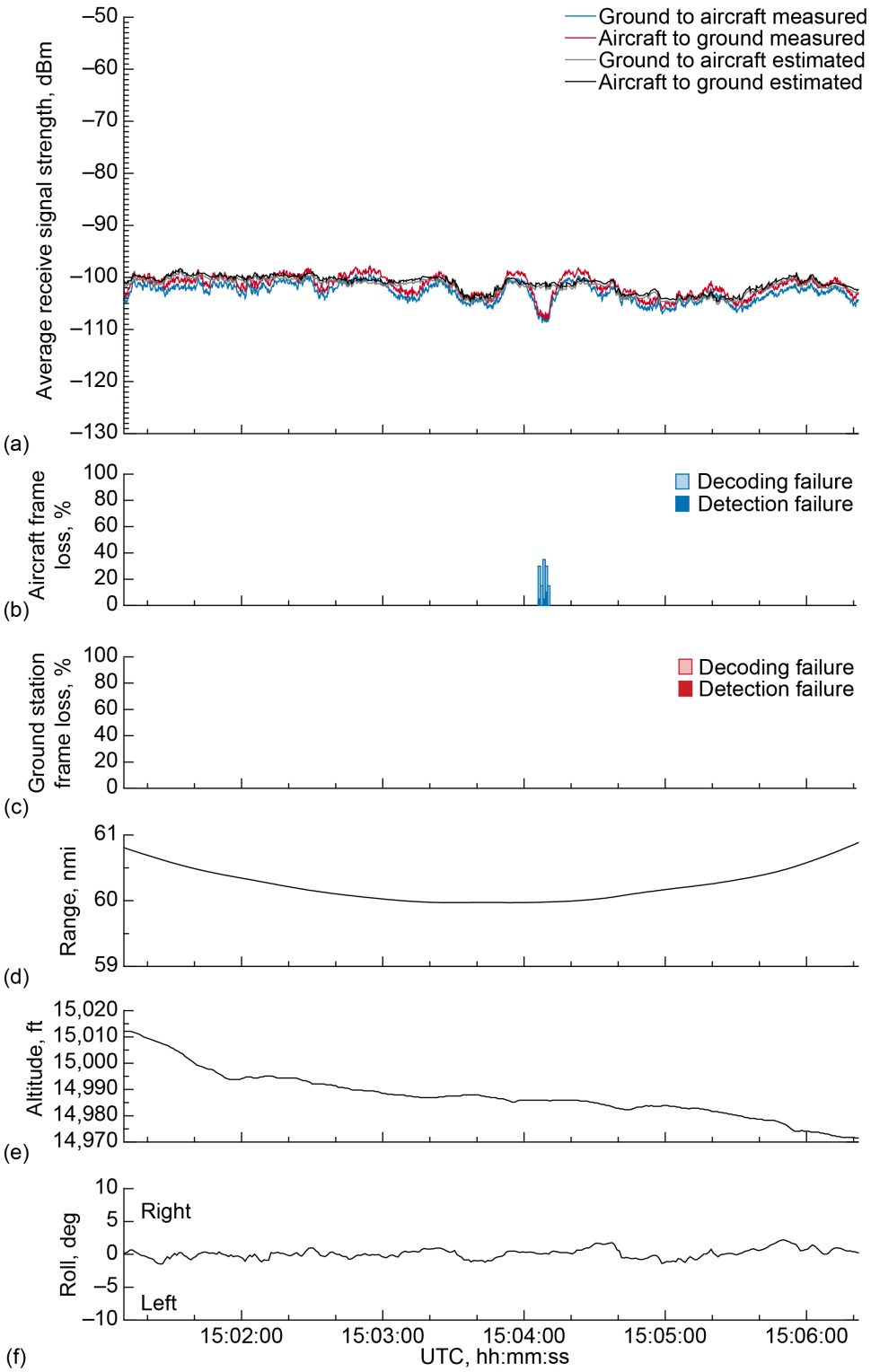

Figure 66.—Signal strength and frame loss over slightly rolling terrain at 60-nmi range and 15,000-ft altitude, 1.5° antenna elevation, traveling from waypoint G to waypoint H. (a) Average receive signal strength. (b) Aircraft frame loss. (c) Ground station frame loss. (d) Range. (e) Altitude. (f) Roll.

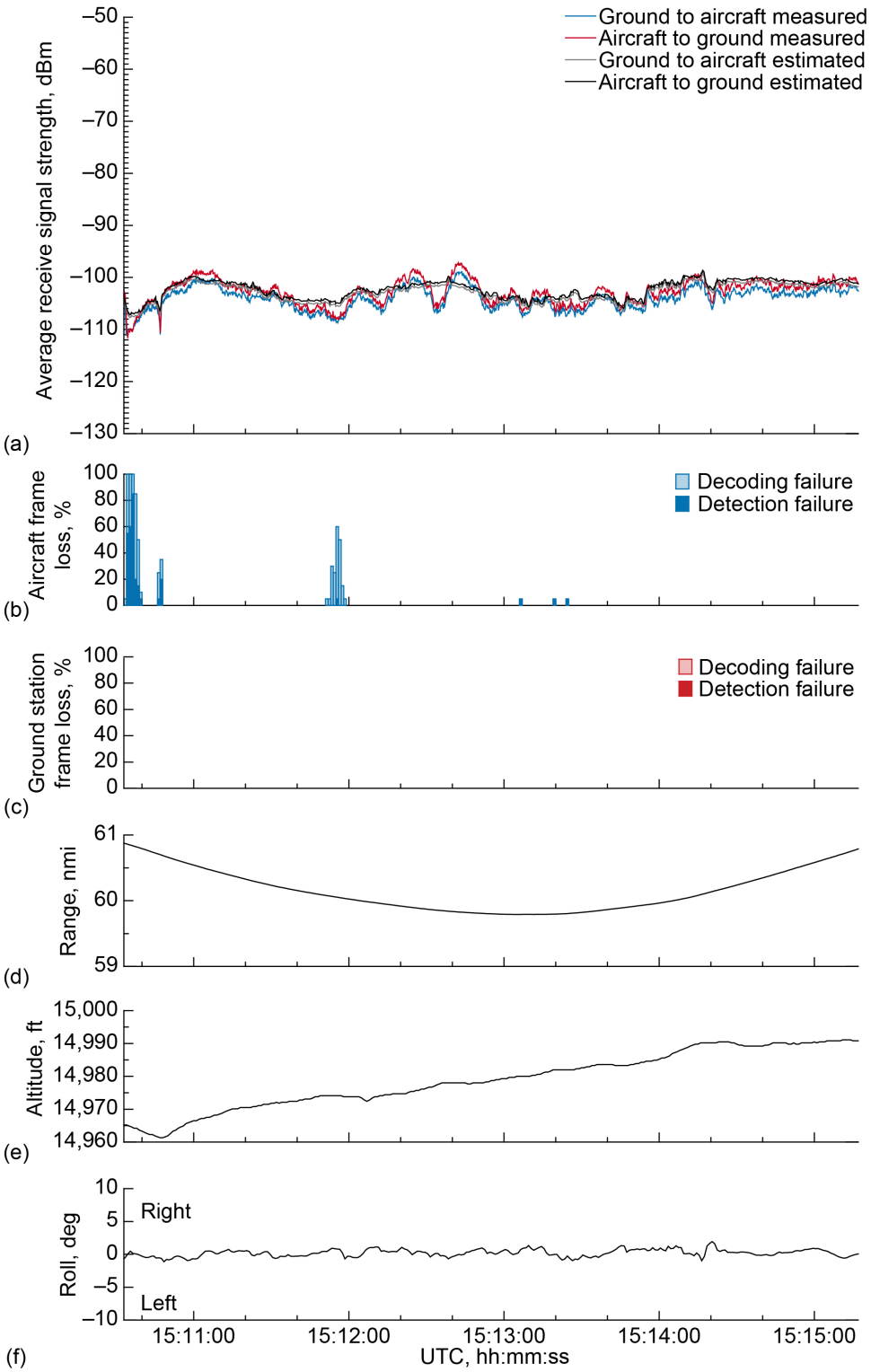

Figure 67.—Signal strength and frame loss over slightly rolling terrain at 60-nmi range and 15,000-ft altitude, 1.5° antenna elevation, traveling from waypoint H to waypoint G. (a) Average receive signal strength. (b) Aircraft frame loss. (c) Ground station frame loss. (d) Range. (e) Altitude. (f) Roll.

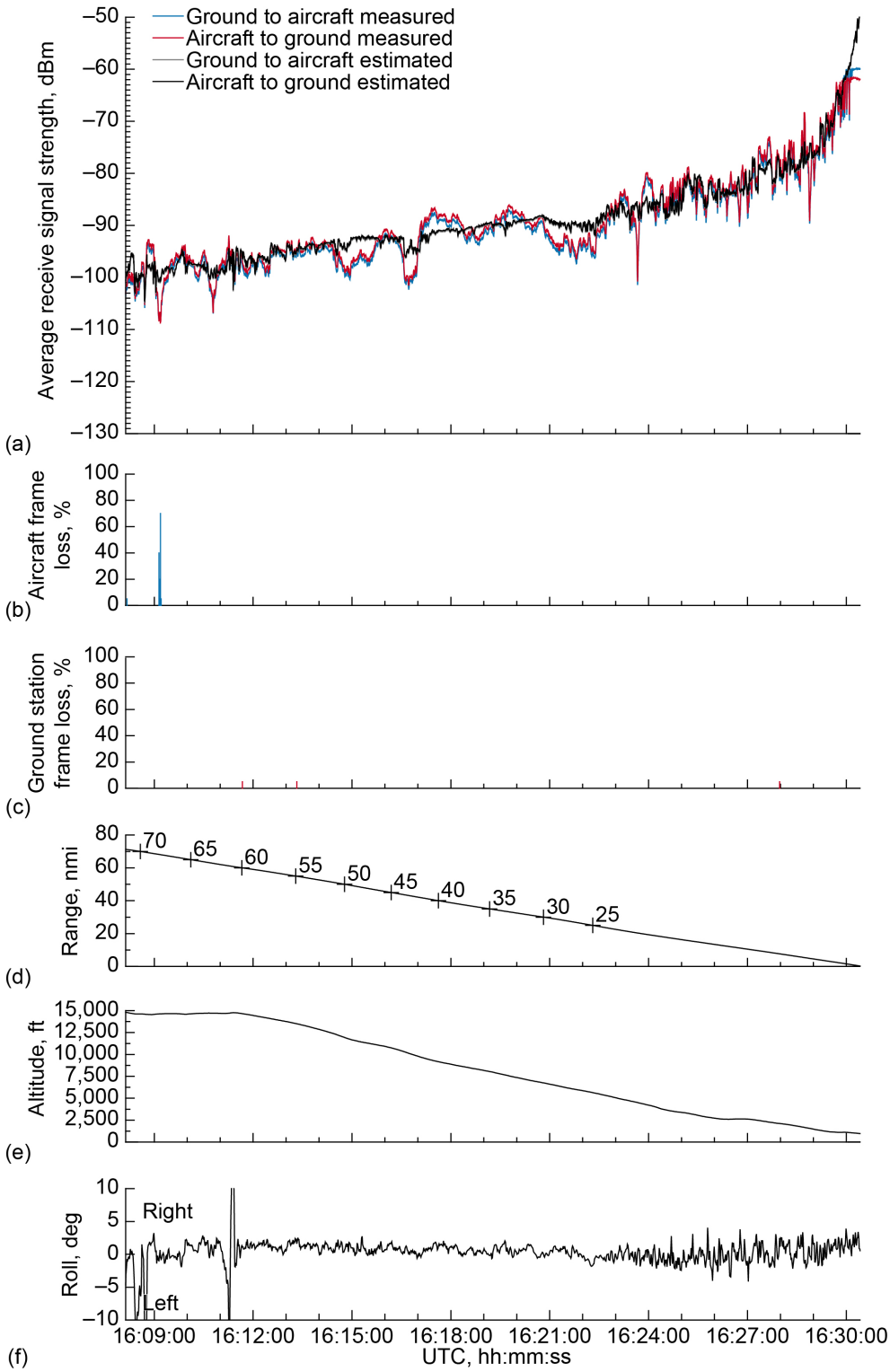

Figure 68.—Signal strength and frame loss over slightly rolling terrain during inbound, descending track on 1.5° glide slope, traveling toward ground station. (a) Average receive signal strength. (b) Aircraft frame loss. (c) Ground station frame loss. (d) Range. (e) Altitude. (f) Roll.

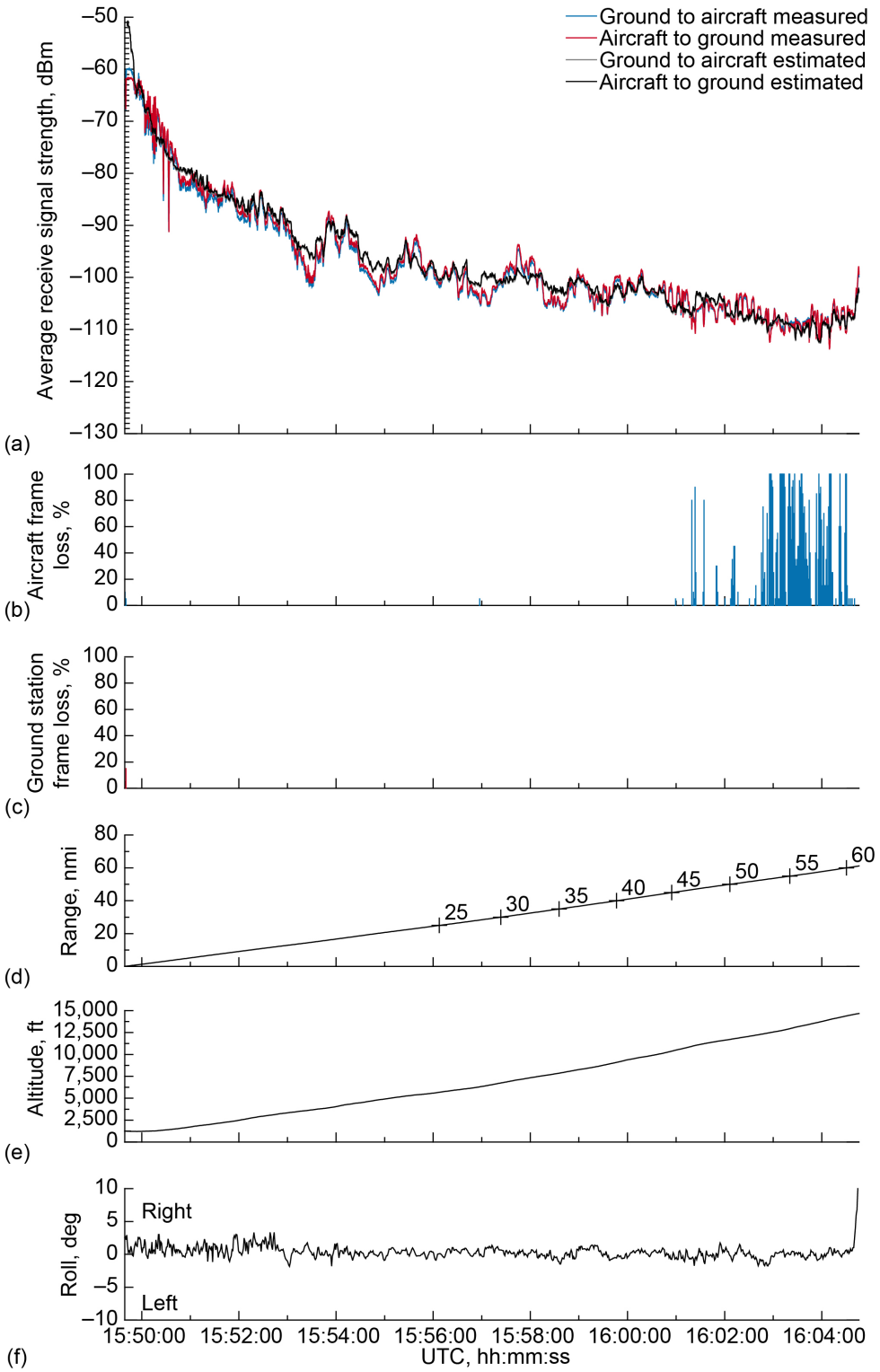

Figure 69.—Signal strength and frame loss over slightly rolling terrain during outbound, ascending track on 1.5° glide slope, traveling away from ground station. (a) Average receive signal strength. (b) Aircraft frame loss. (c) Ground station frame loss. (d) Range. (e) Altitude. (f) Roll.

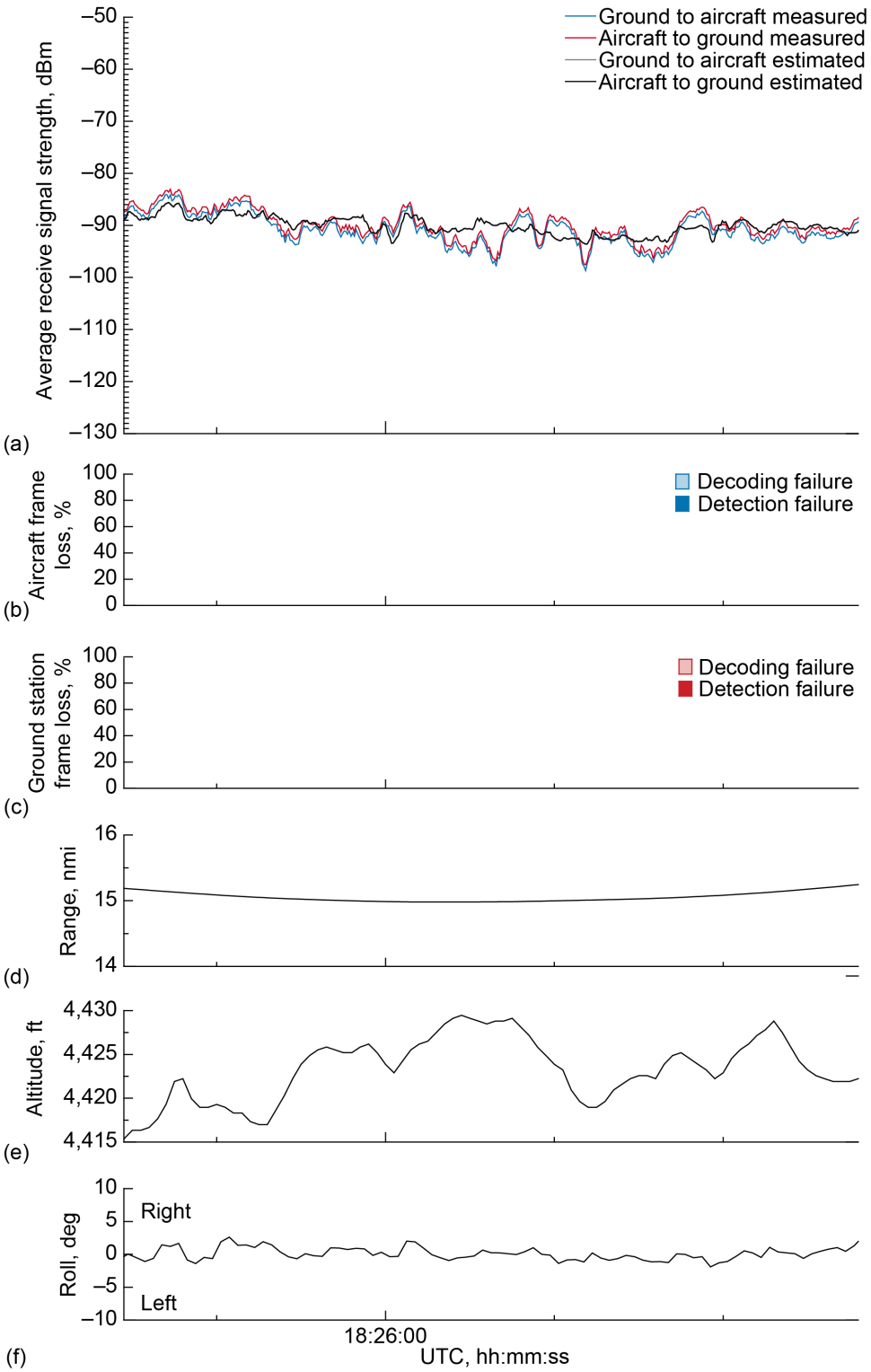

Figure 70.—Signal strength and frame loss over slightly rolling terrain at 15-nmi range and 4,500-ft altitude, 2.0° antenna elevation, traveling from waypoint A to waypoint B. (a) Average receive signal strength. (b) Aircraft frame loss. (c) Ground station frame loss. (d) Range. (e) Altitude. (f) Roll.

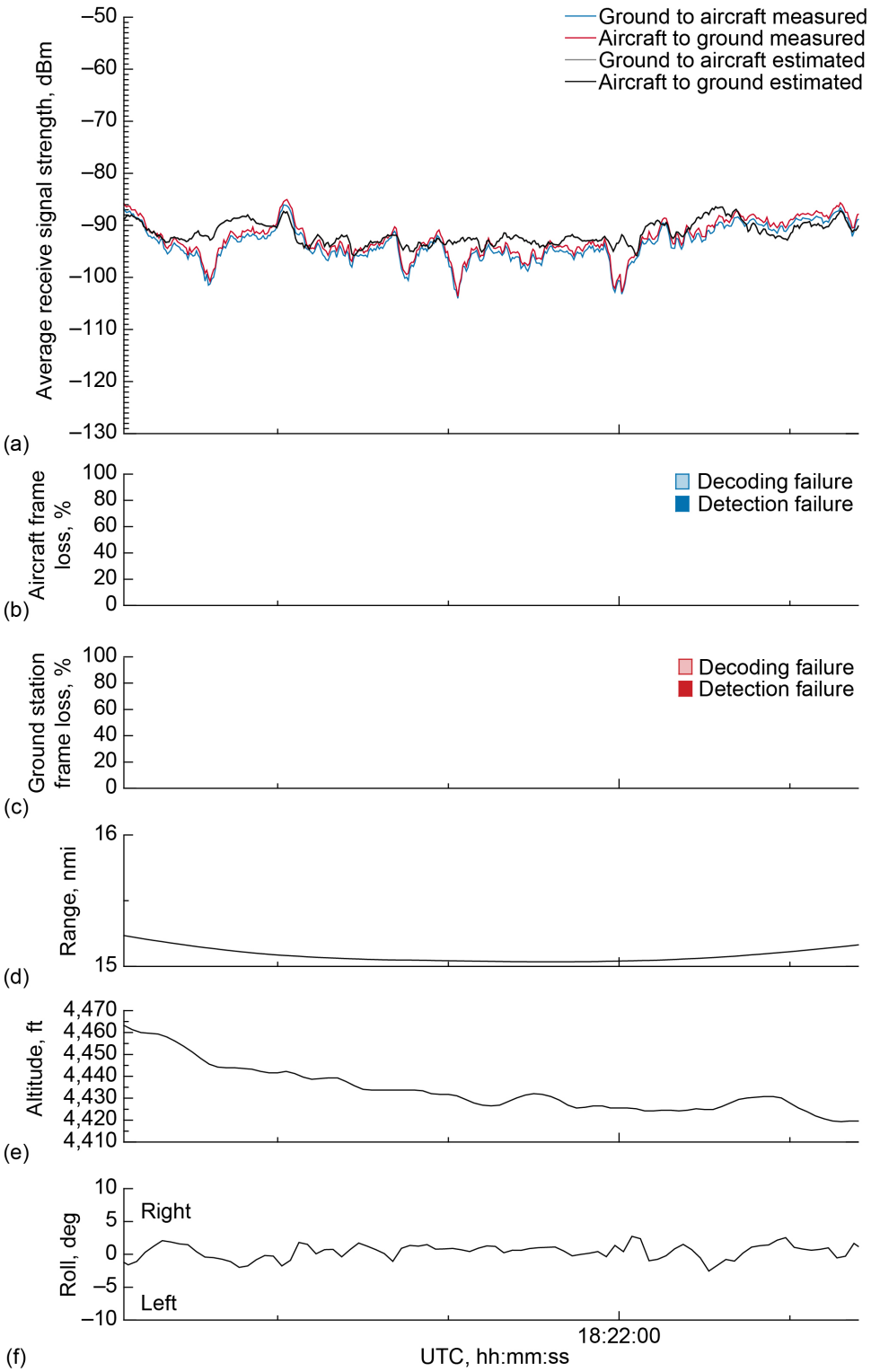

Figure 71.—Signal strength and frame loss over slightly rolling terrain at 15-nmi range and 4,500-ft altitude, 2.0° antenna elevation, traveling from waypoint B to waypoint A. (a) Average receive signal strength. (b) Aircraft frame loss. (c) Ground station frame loss. (d) Range. (e) Altitude. (f) Roll.

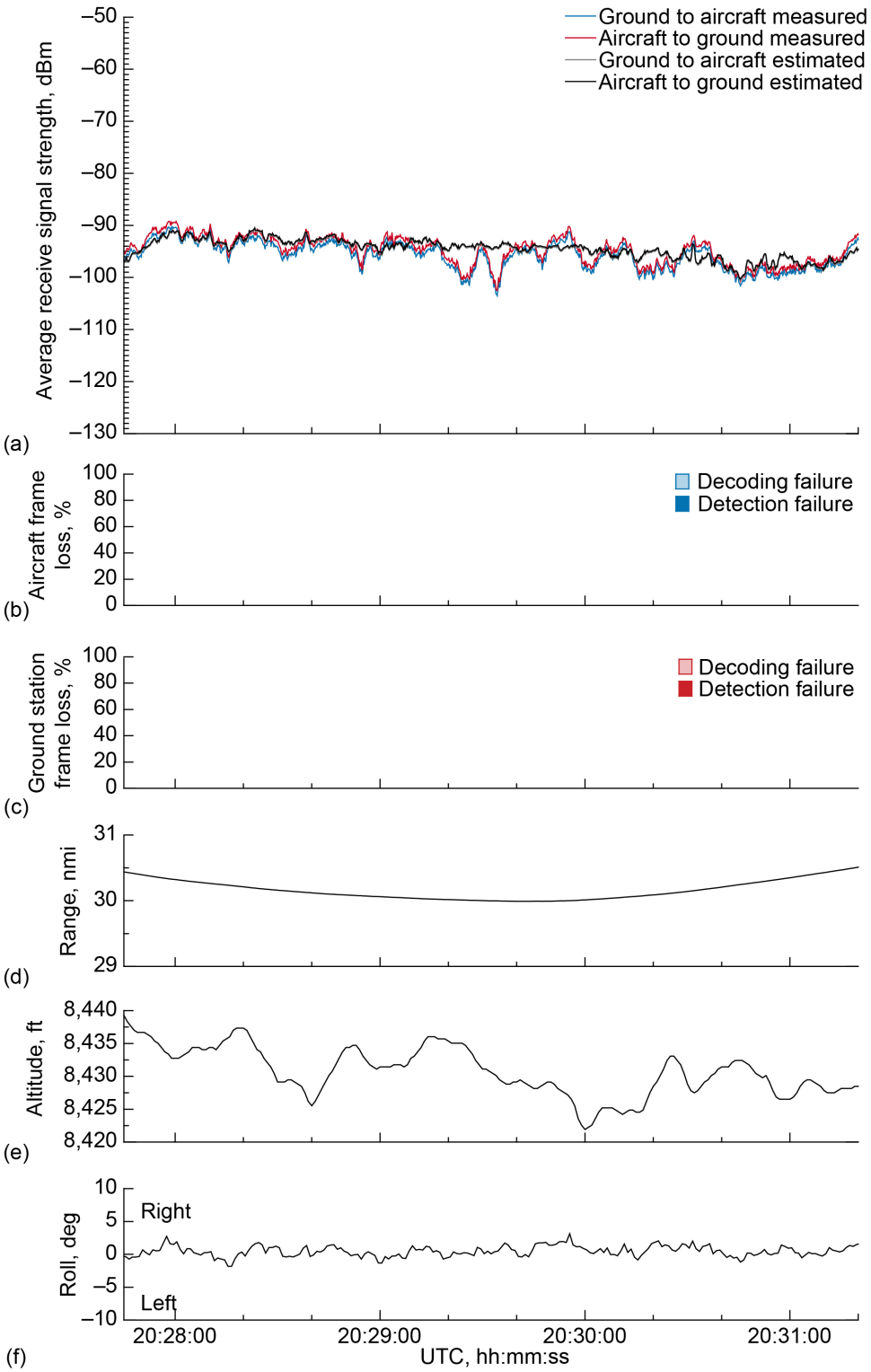

Figure 72.—Signal strength and frame loss over slightly rolling terrain at 30-nmi range and 8,500-ft altitude, 2.0° antenna elevation, traveling from waypoint C to waypoint D. (a) Average receive signal strength. (b) Aircraft frame loss. (c) Ground station frame loss. (d) Range. (e) Altitude. (f) Roll.

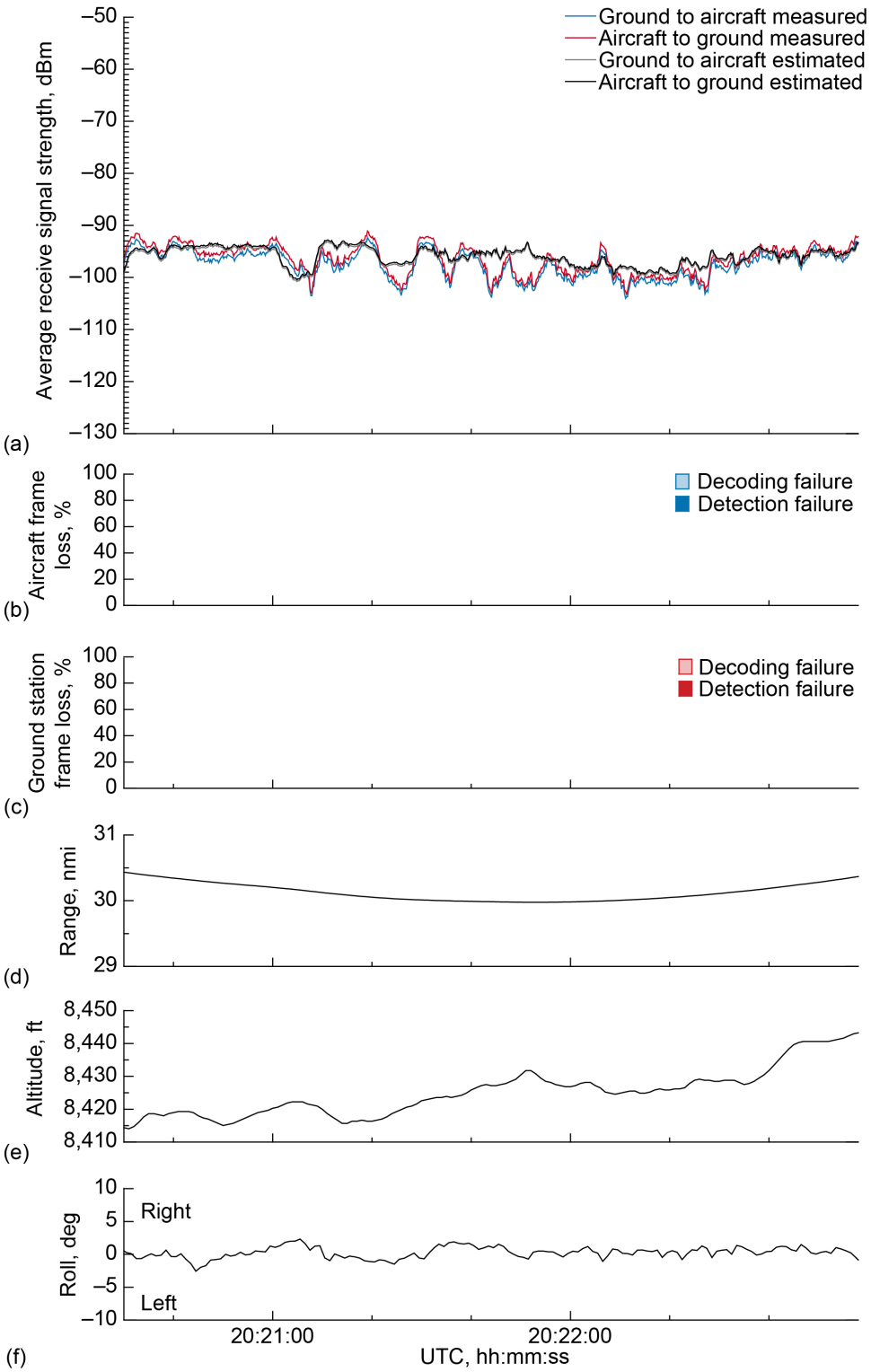

Figure 73.—Signal strength and frame loss over slightly rolling terrain at 30-nmi range and 8,500-ft altitude, 2.0° antenna elevation, traveling from waypoint D to waypoint C. (a) Average receive signal strength. (b) Aircraft frame loss. (c) Ground station frame loss. (d) Range. (e) Altitude. (f) Roll.

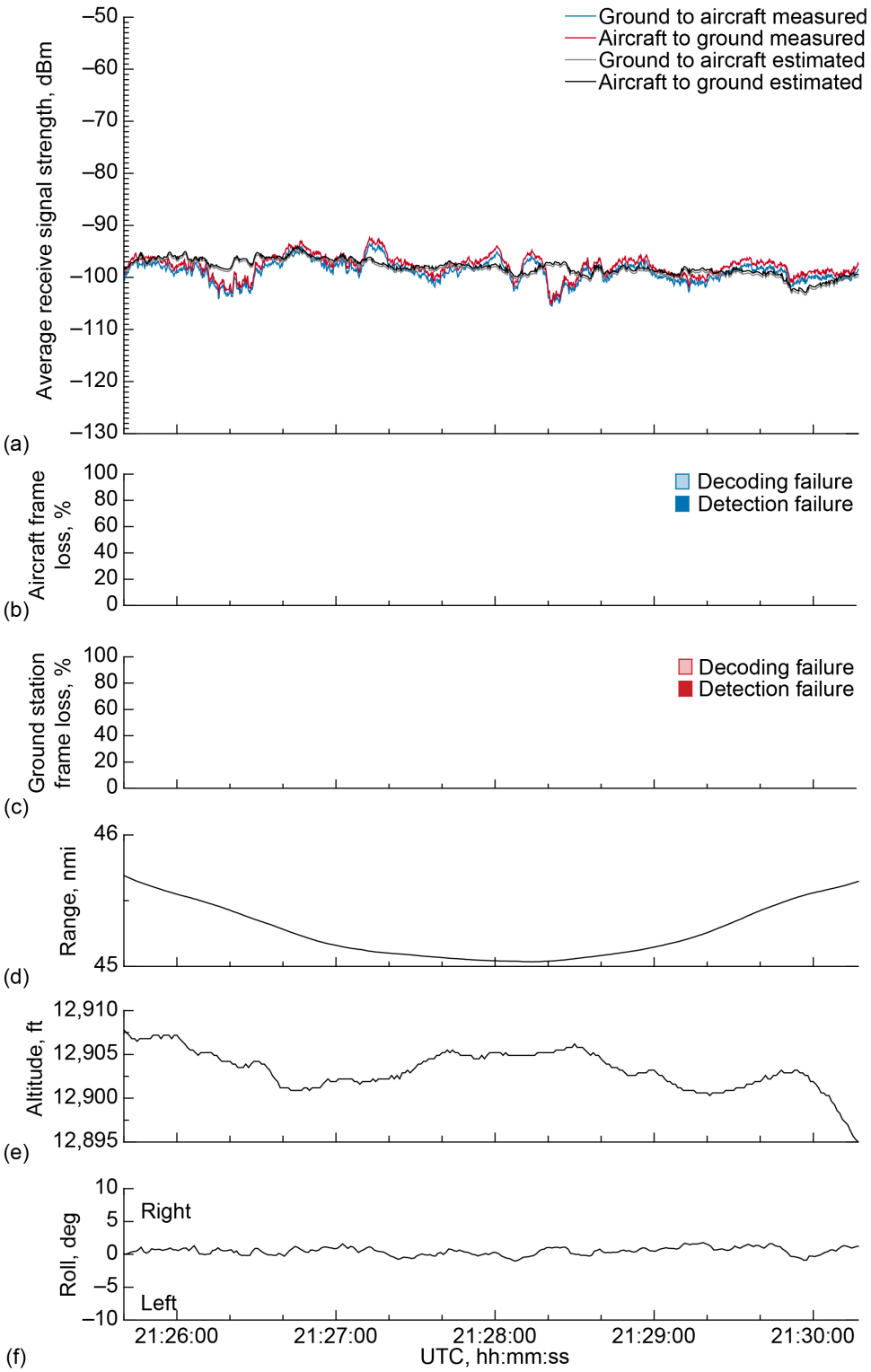

Figure 74.—Signal strength and frame loss over slightly rolling terrain at 45-nmi range and 13,000-ft altitude, 2.0° antenna elevation, traveling from waypoint E to waypoint F. (a) Average receive signal strength. (b) Aircraft frame loss. (c) Ground station frame loss. (d) Range. (e) Altitude. (f) Roll.

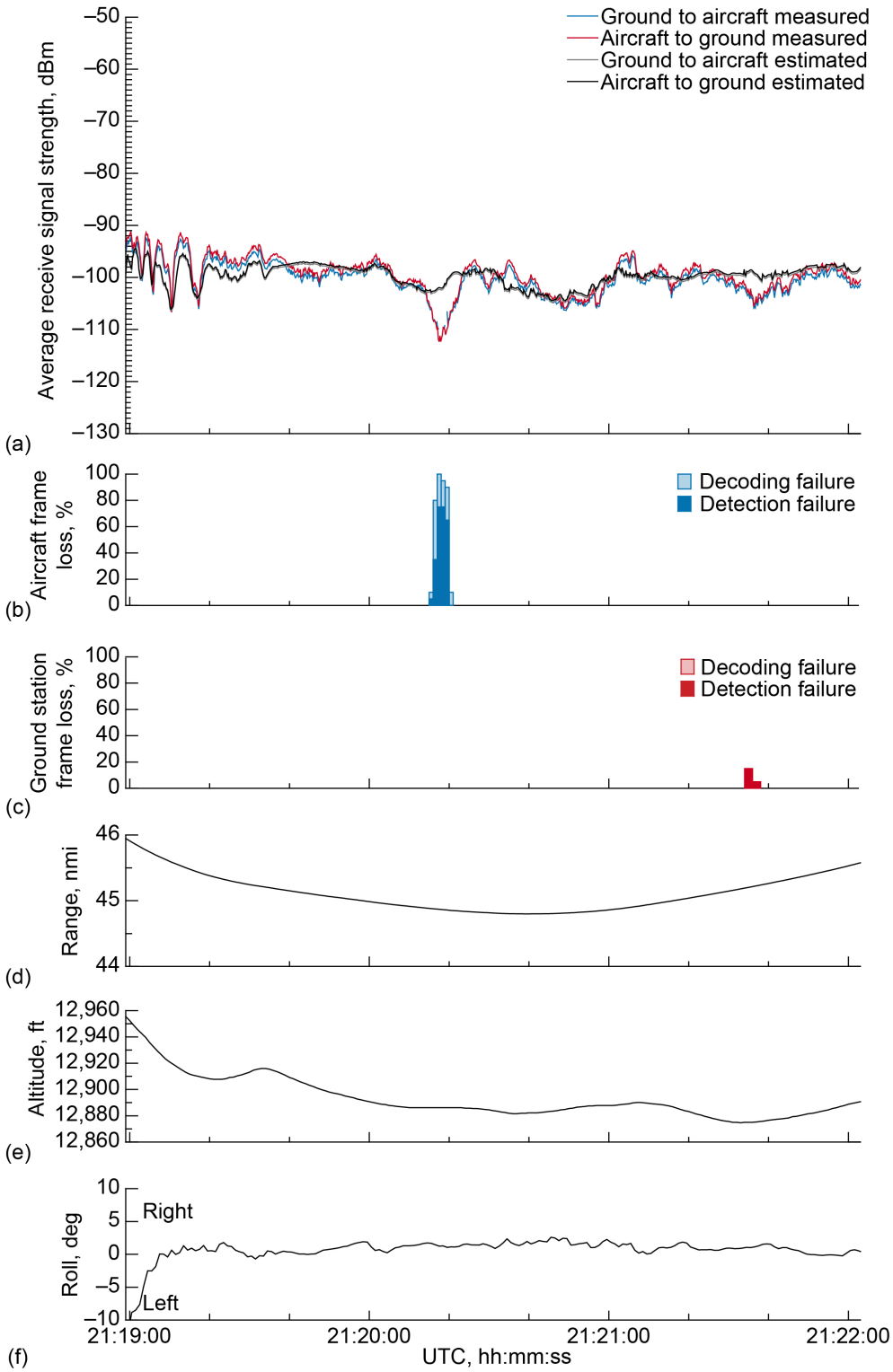

Figure 75.—Signal strength and frame loss over slightly rolling terrain at 45-nmi range and 13,000-ft altitude, 2.0° antenna elevation, traveling from waypoint F to waypoint E. (a) Average receive signal strength. (b) Aircraft frame loss. (c) Ground station frame loss. (d) Range. (e) Altitude. (f) Roll.

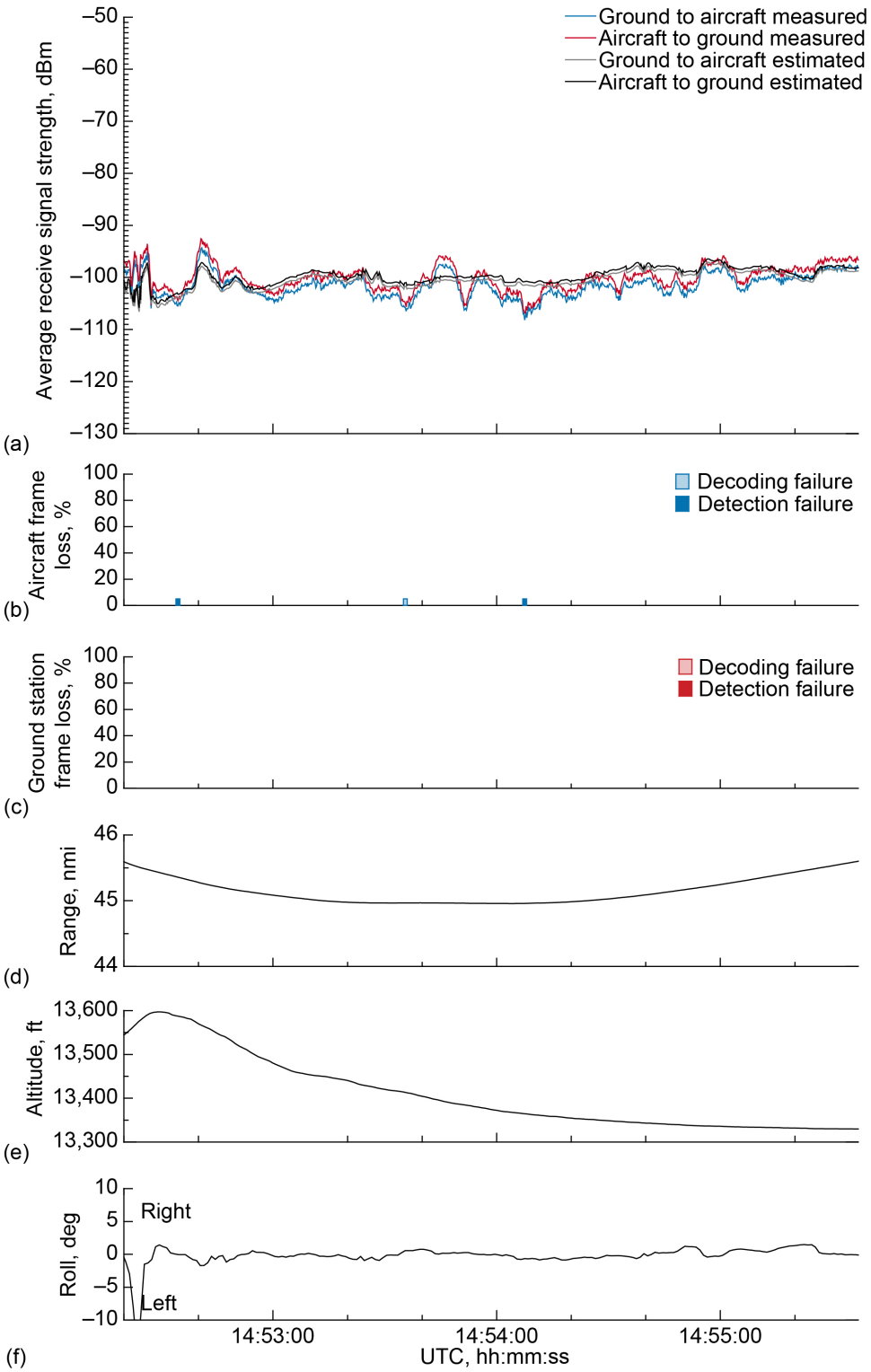

Figure 76.—Signal strength and frame loss over slightly rolling terrain at 45-nmi range and 13,500-ft altitude, 2.0° antenna elevation, traveling from waypoint F to waypoint E. (a) Average receive signal strength. (b) Aircraft frame loss. (c) Ground station frame loss. (d) Range. (e) Altitude. (f) Roll.

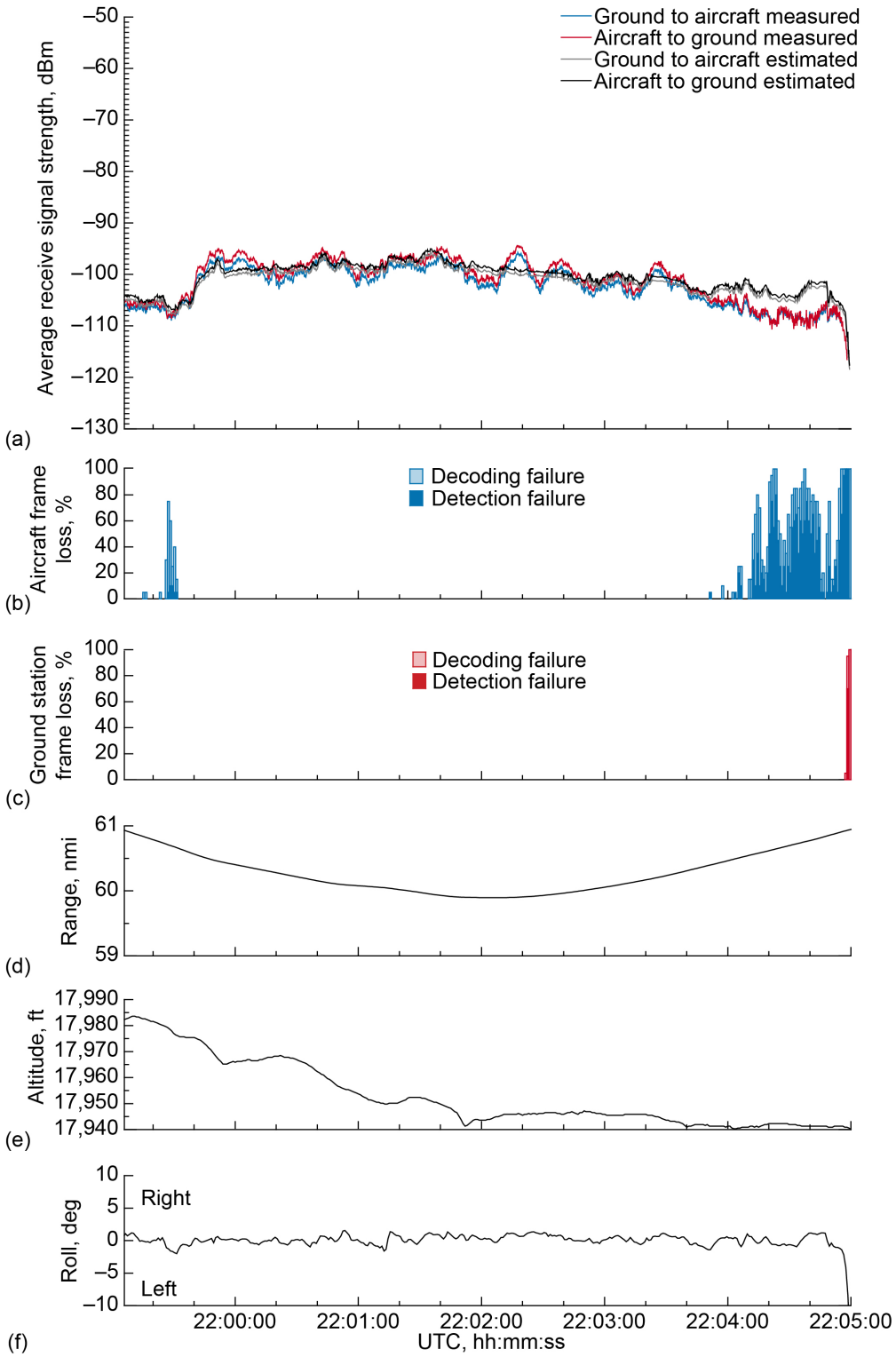

Figure 77.—Signal strength and frame loss over slightly rolling terrain at 60-nmi range and 18,000-ft altitude, 2.0° antenna elevation, traveling from waypoint G to waypoint H. (a) Average receive signal strength. (b) Aircraft frame loss. (c) Ground station frame loss. (d) Range. (e) Altitude. (f) Roll.

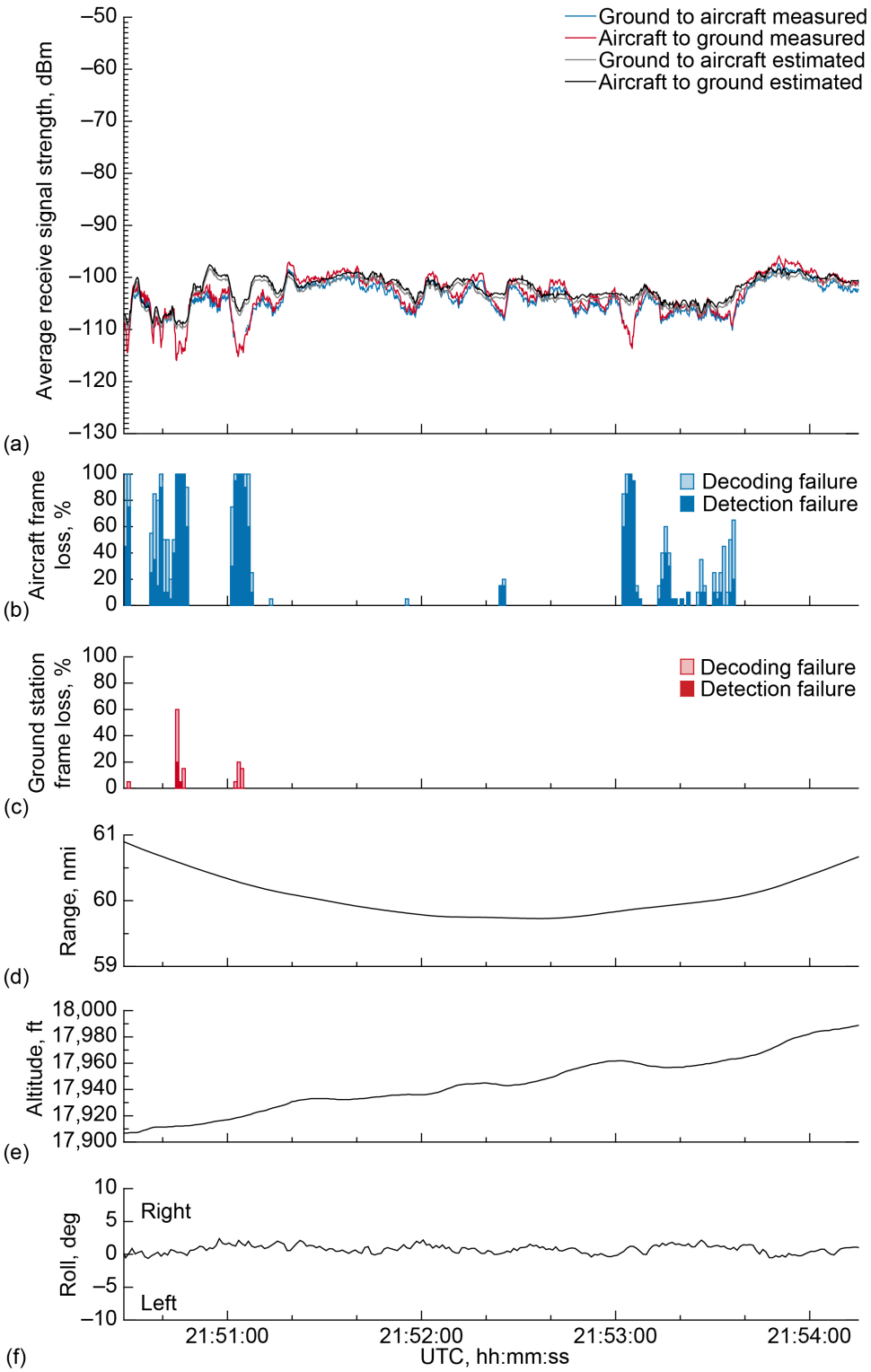

Figure 78.—Signal strength and frame loss over slightly rolling terrain at 60-nmi range and 18,000-ft altitude, 2.0° antenna elevation, traveling from waypoint H to waypoint G. (a) Average receive signal strength. (b) Aircraft frame loss. (c) Ground station frame loss. (d) Range. (e) Altitude. (f) Roll.

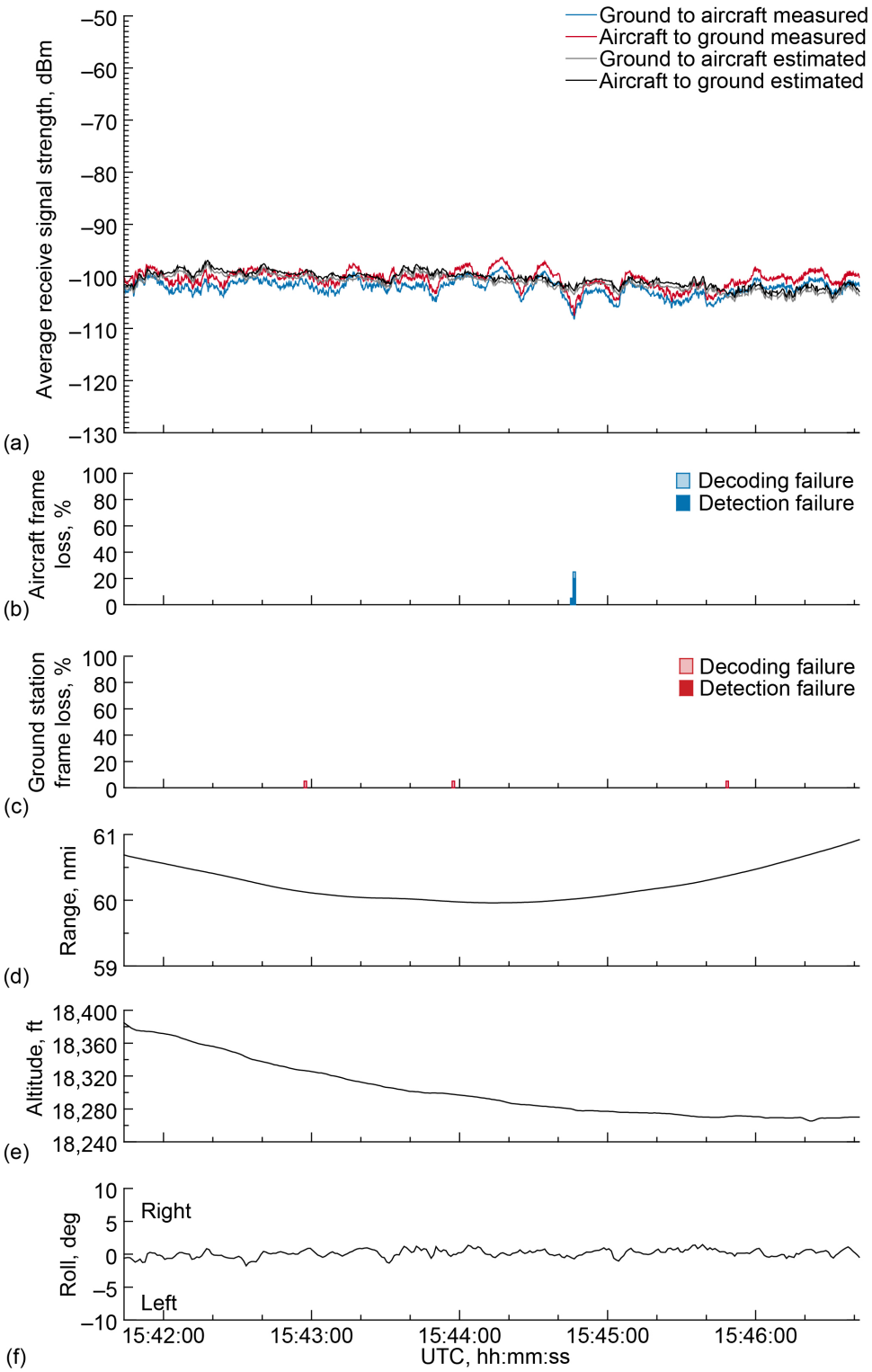

Figure 79.—Signal strength and frame loss over slightly rolling terrain at 60-nmi range and 18,500-ft altitude, 2.0° antenna elevation, traveling from waypoint G to waypoint H. (a) Average receive signal strength. (b) Aircraft frame loss. (c) Ground station frame loss. (d) Range. (e) Altitude. (f) Roll.

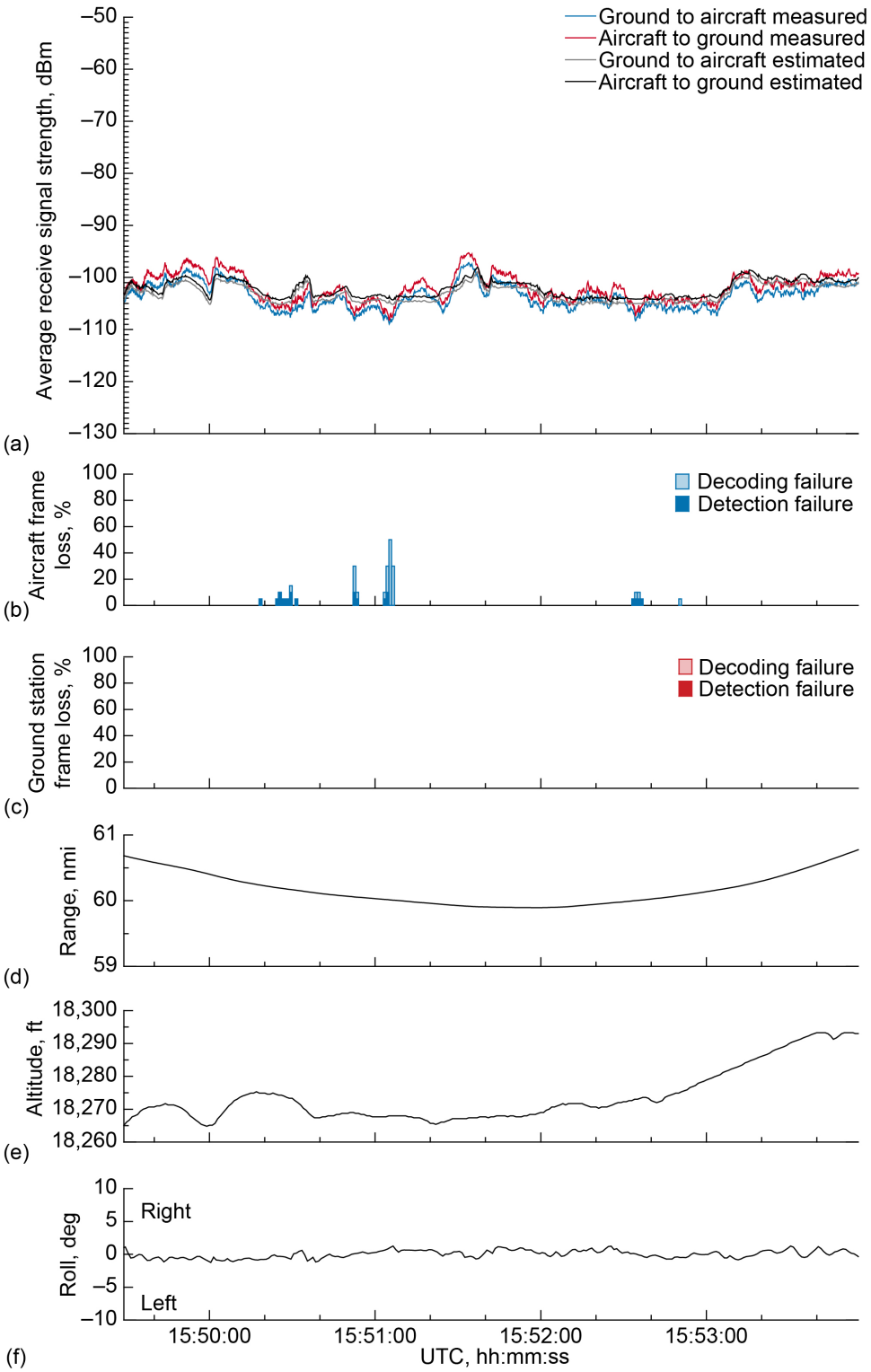

Figure 80.—Signal strength and frame loss over slightly rolling terrain at 60-nmi range and 18,500-ft altitude, 2.0° antenna elevation, traveling from waypoint H to waypoint G. (a) Average receive signal strength. (b) Aircraft frame loss. (c) Ground station frame loss. (d) Range. (e) Altitude. (f) Roll.

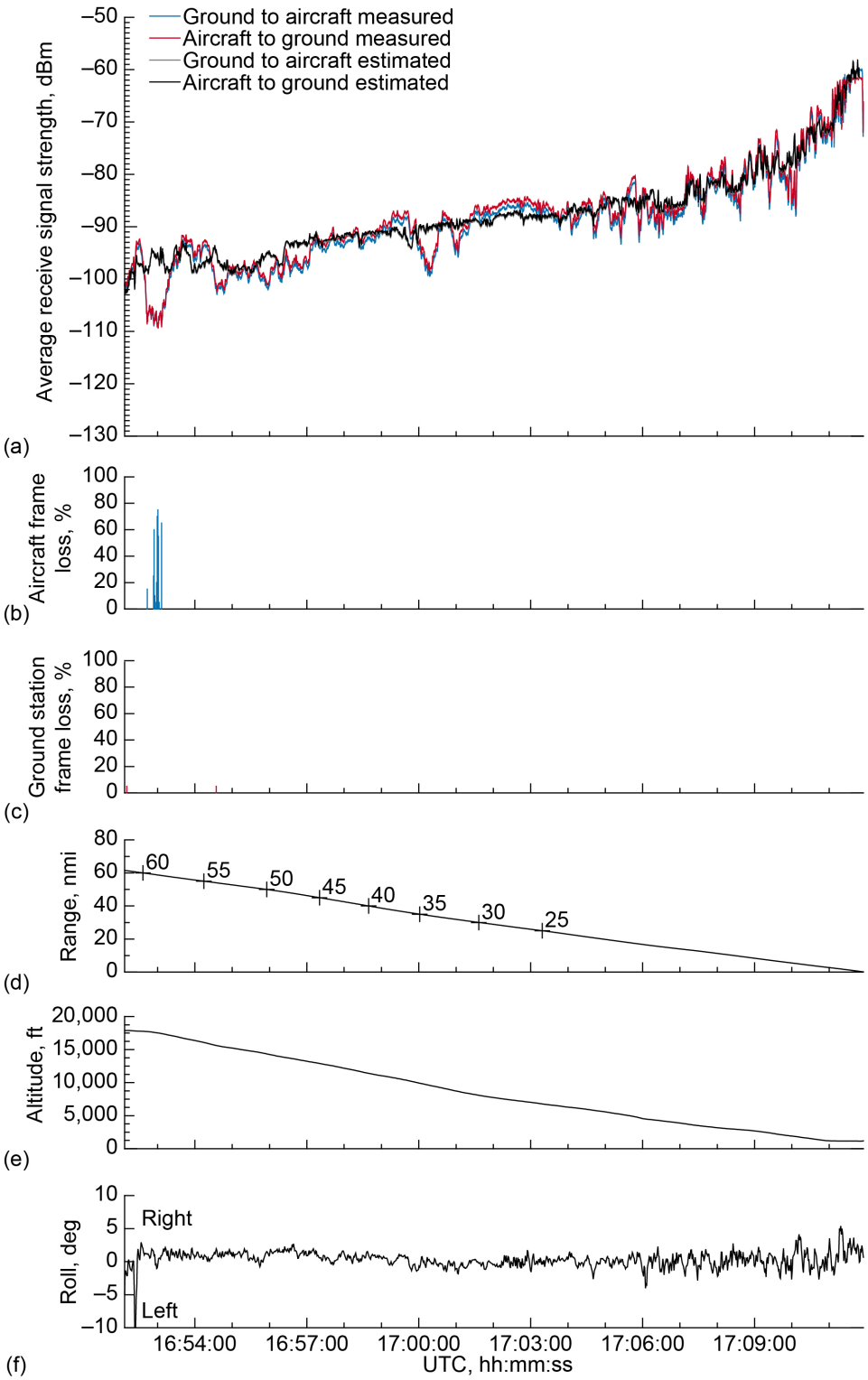

Figure 81.—Signal strength and frame loss over slightly rolling terrain during inbound, descending track on 2.0° glide slope, traveling toward ground station. (a) Average receive signal strength. (b) Aircraft frame loss. (c) Ground station frame loss. (d) Range. (e) Altitude. (f) Roll.

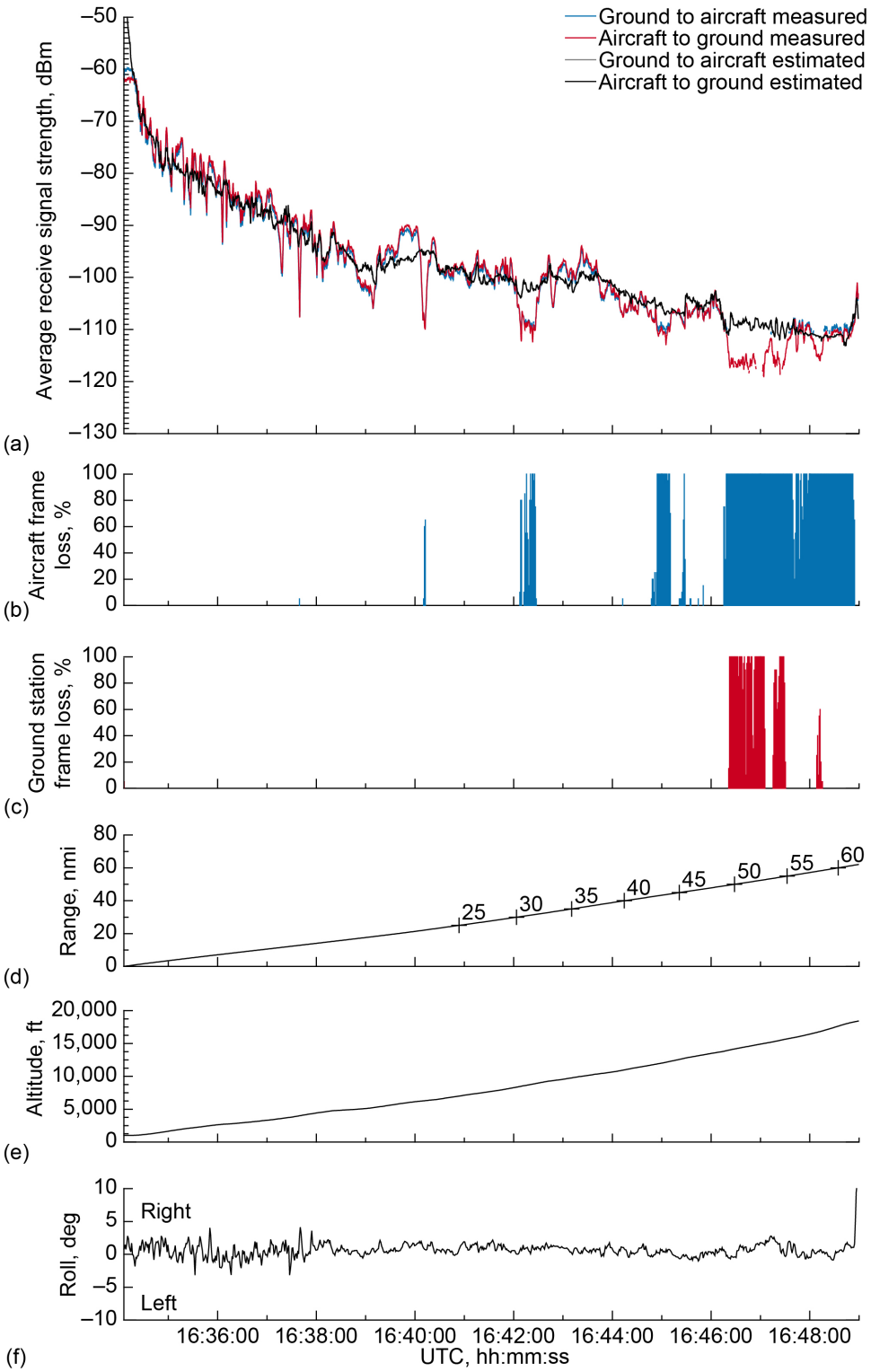

Figure 82.—Signal strength and frame loss over slightly rolling terrain during outbound, ascending track on 2.0° glide slope, traveling away from ground station. (a) Average receive signal strength. (b) Aircraft frame loss. (c) Ground station frame loss. (d) Range. (e) Altitude. (f) Roll.

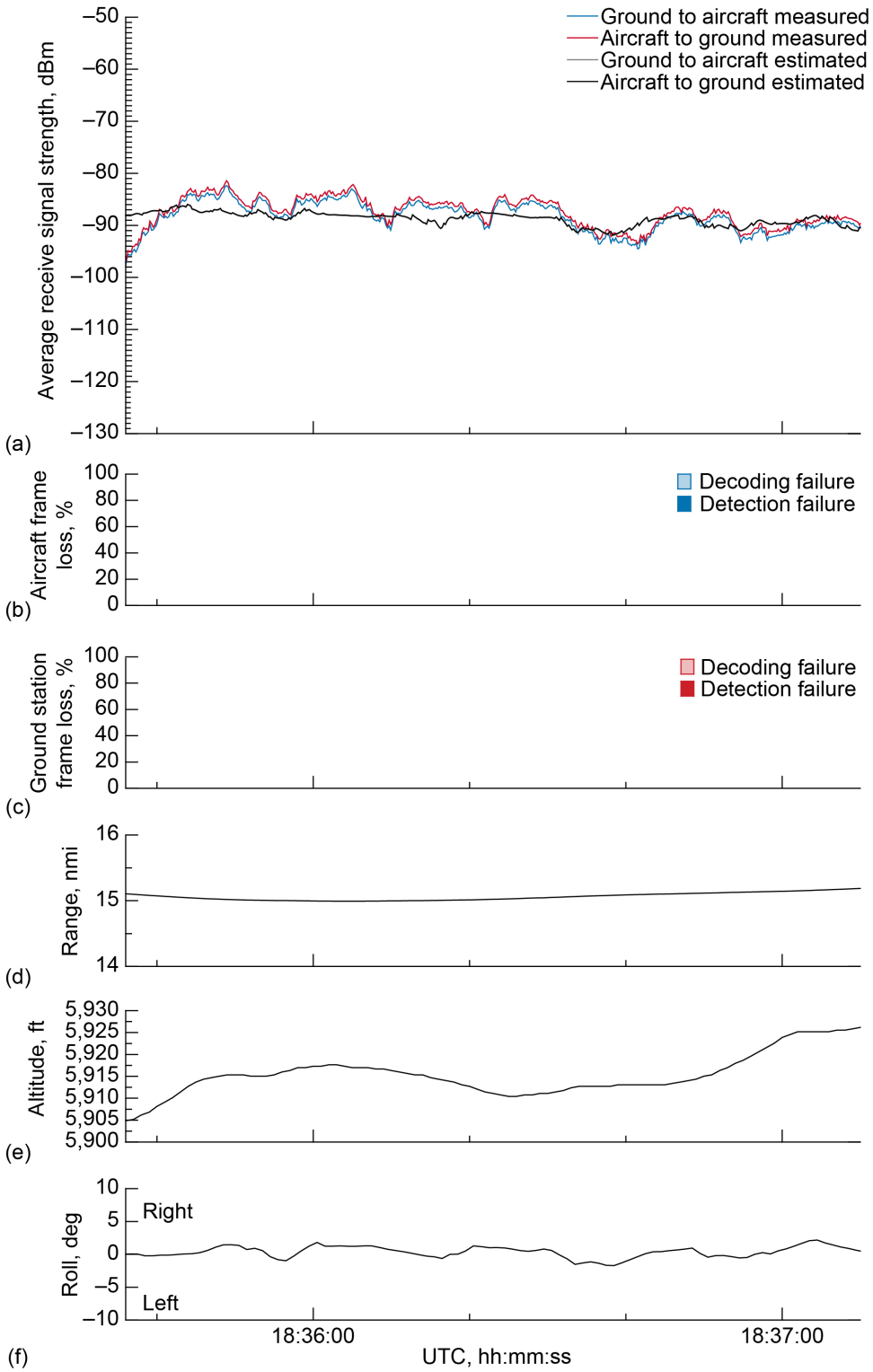

Figure 83.—Signal strength and frame loss over slightly rolling terrain at 15-nmi range and 6,000-ft altitude, 3.0° antenna elevation, traveling from waypoint A to waypoint B. (a) Average receive signal strength. (b) Aircraft frame loss. (c) Ground station frame loss. (d) Range. (e) Altitude. (f) Roll.

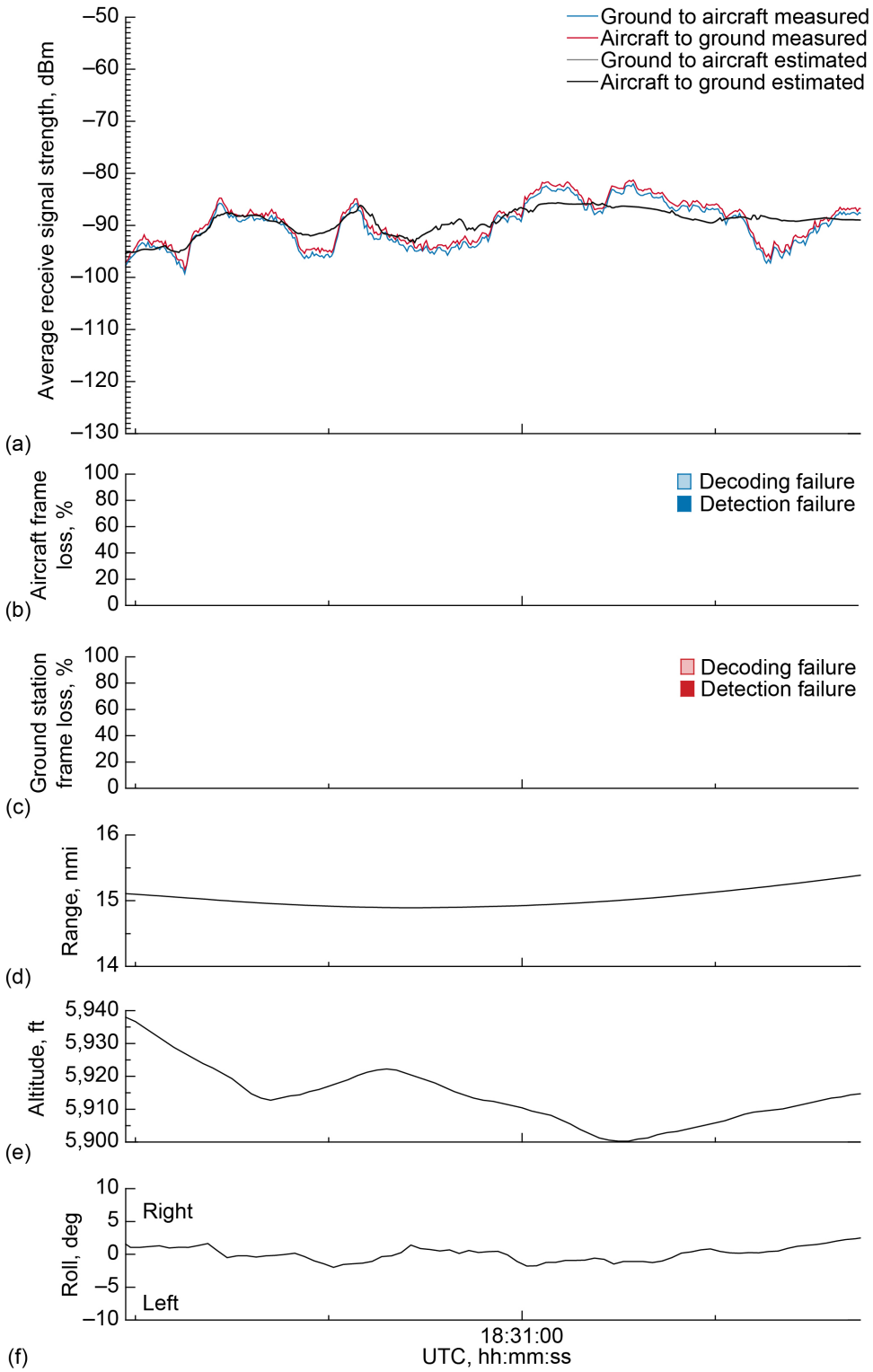

Figure 84.—Signal strength and frame loss over slightly rolling terrain at 15-nmi range and 6,000-ft altitude, 3.0° antenna elevation, traveling from waypoint B to waypoint A. (a) Average receive signal strength. (b) Aircraft frame loss. (c) Ground station frame loss. (d) Range. (e) Altitude. (f) Roll.

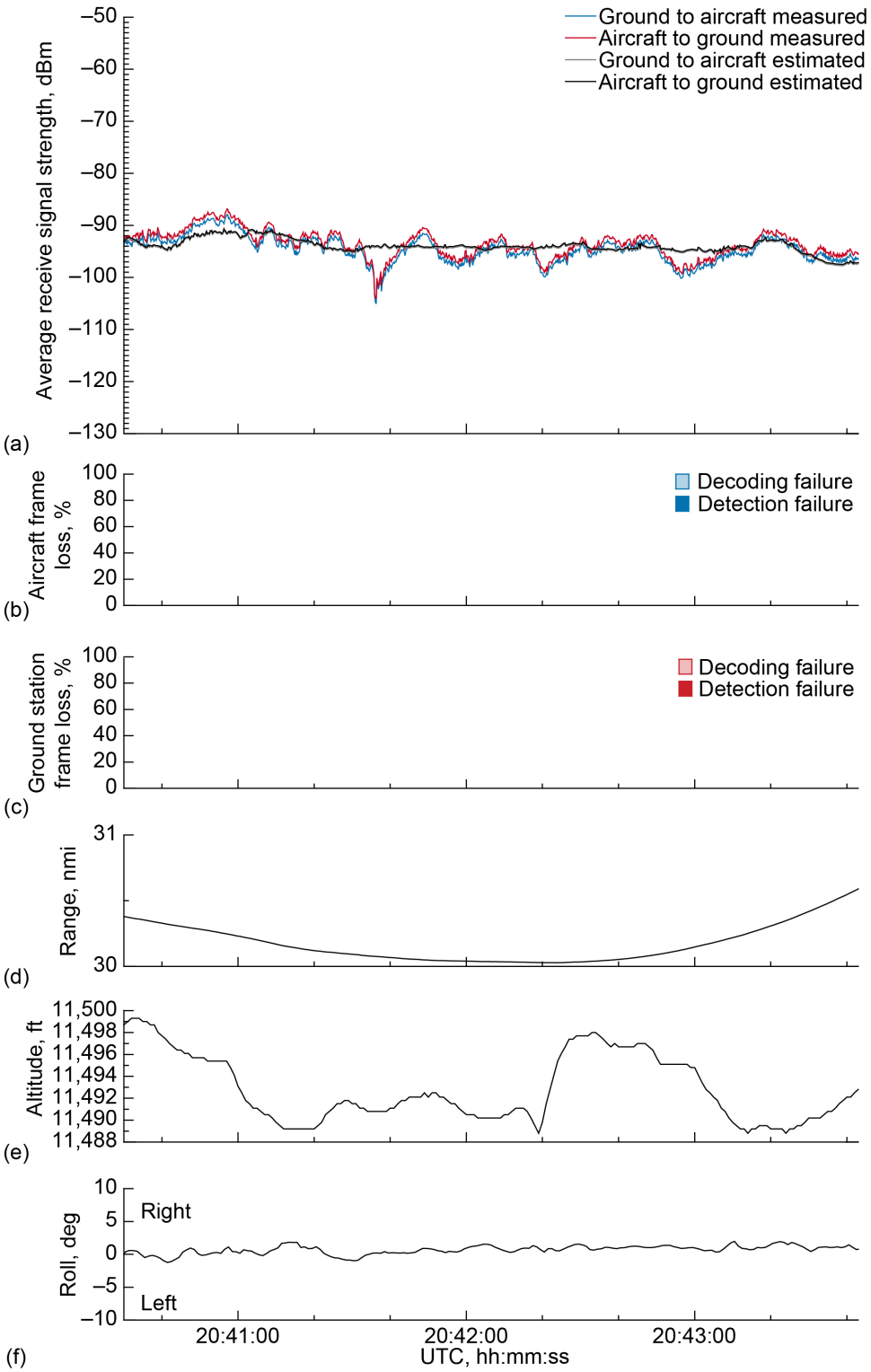

Figure 85.—Signal strength and frame loss over slightly rolling terrain at 30-nmi range and 11,500-ft altitude, 3.0° antenna elevation, traveling from waypoint C to waypoint D. (a) Average receive signal strength. (b) Aircraft frame loss. (c) Ground station frame loss. (d) Range. (e) Altitude. (f) Roll.

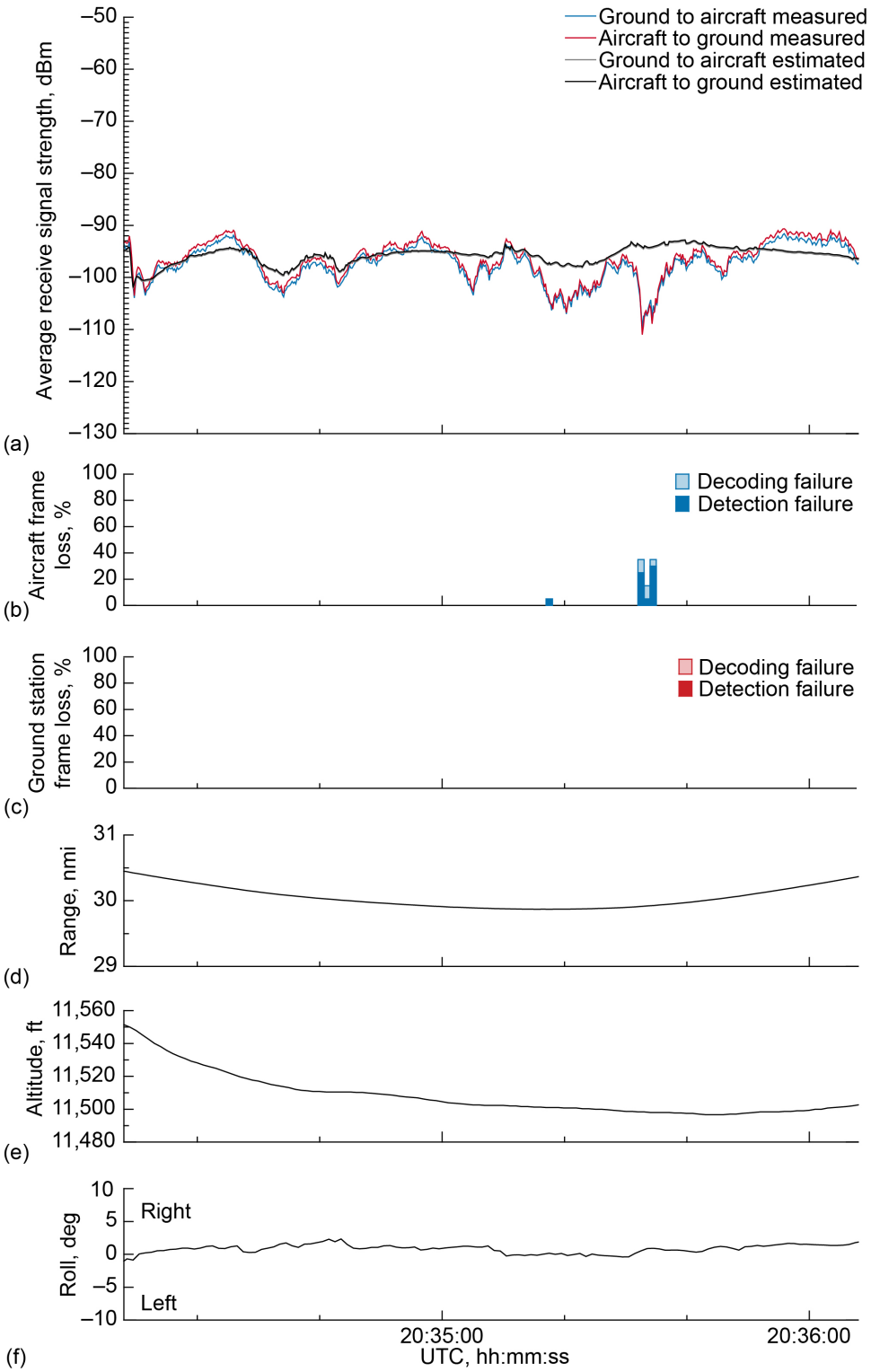

Figure 86.—Signal strength and frame loss over slightly rolling terrain at 30-nmi range and 11,500-ft altitude, 3.0° antenna elevation, traveling from waypoint D to waypoint C. (a) Average receive signal strength. (b) Aircraft frame loss. (c) Ground station frame loss. (d) Range. (e) Altitude. (f) Roll.

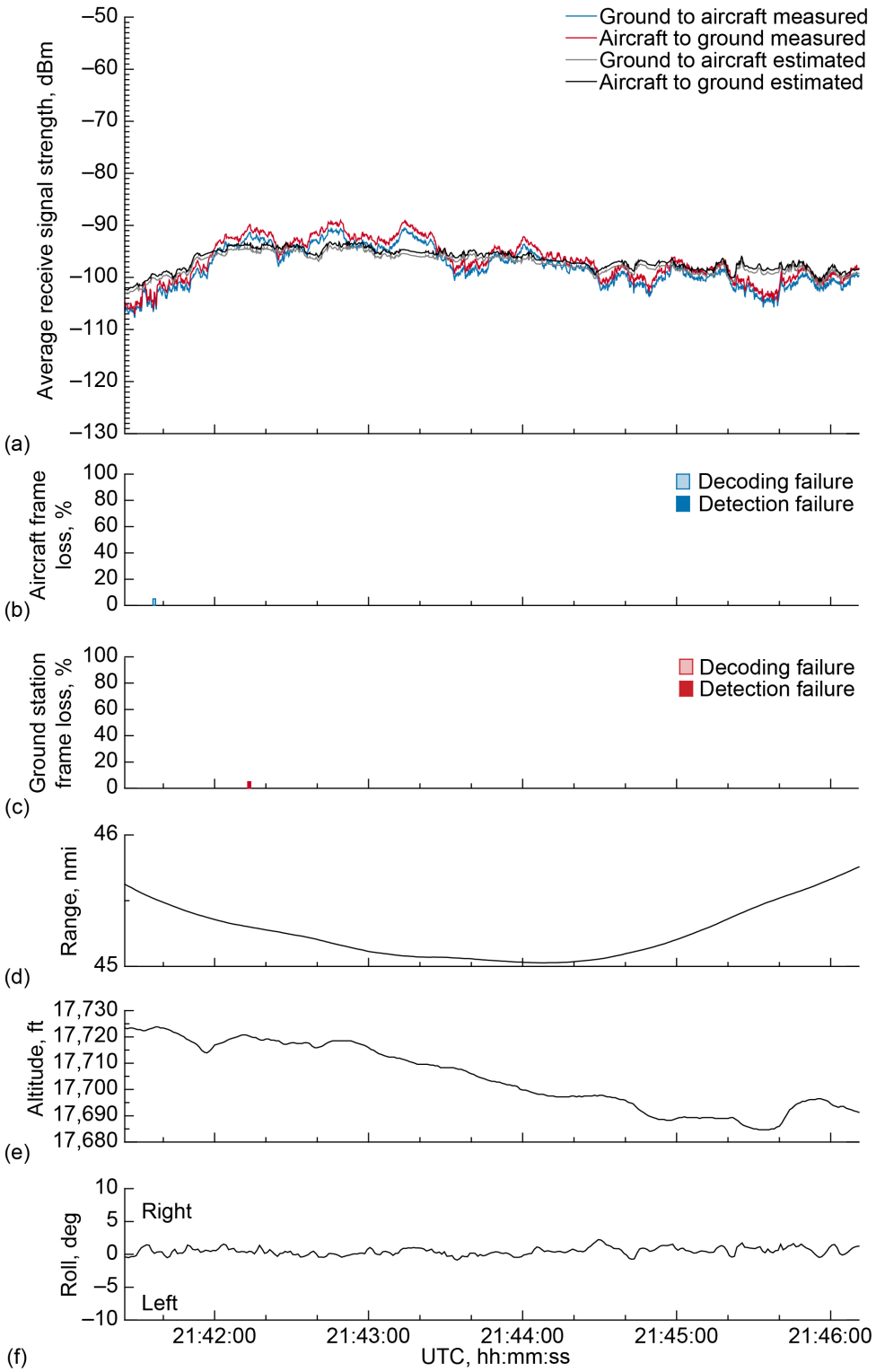

Figure 87.—Signal strength and frame loss over slightly rolling terrain at 45-nmi range and 17,500-ft altitude, 3.0° antenna elevation, traveling from waypoint E to waypoint F. (a) Average receive signal strength. (b) Aircraft frame loss. (c) Ground station frame loss. (d) Range. (e) Altitude. (f) Roll.

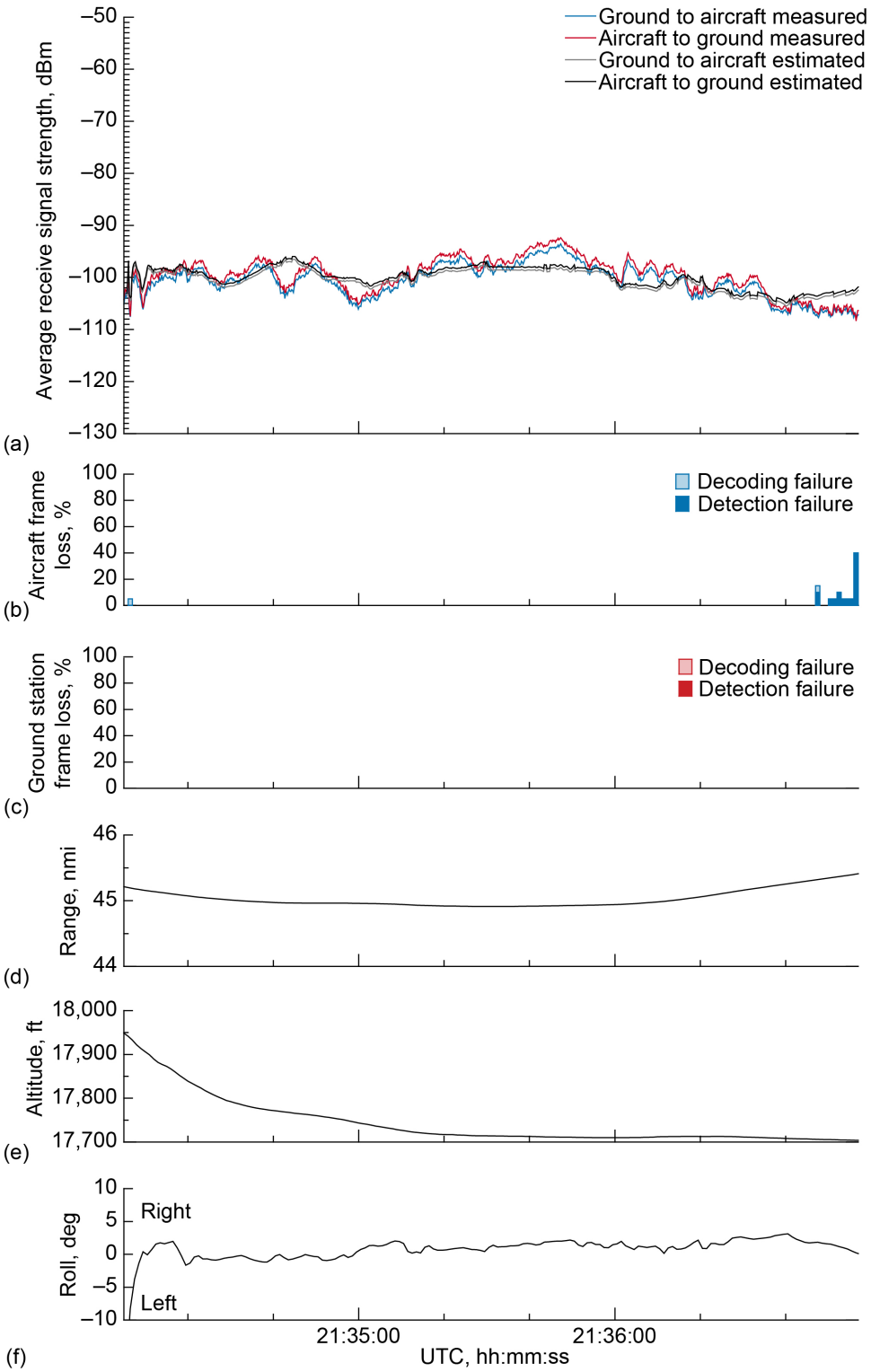

Figure 88.—Signal strength and frame loss over slightly rolling terrain at 45-nmi range and 17,500-ft altitude, 3.0° antenna elevation, traveling from waypoint F to waypoint E. (a) Average receive signal strength. (b) Aircraft frame loss. (c) Ground station frame loss. (d) Range. (e) Altitude. (f) Roll.

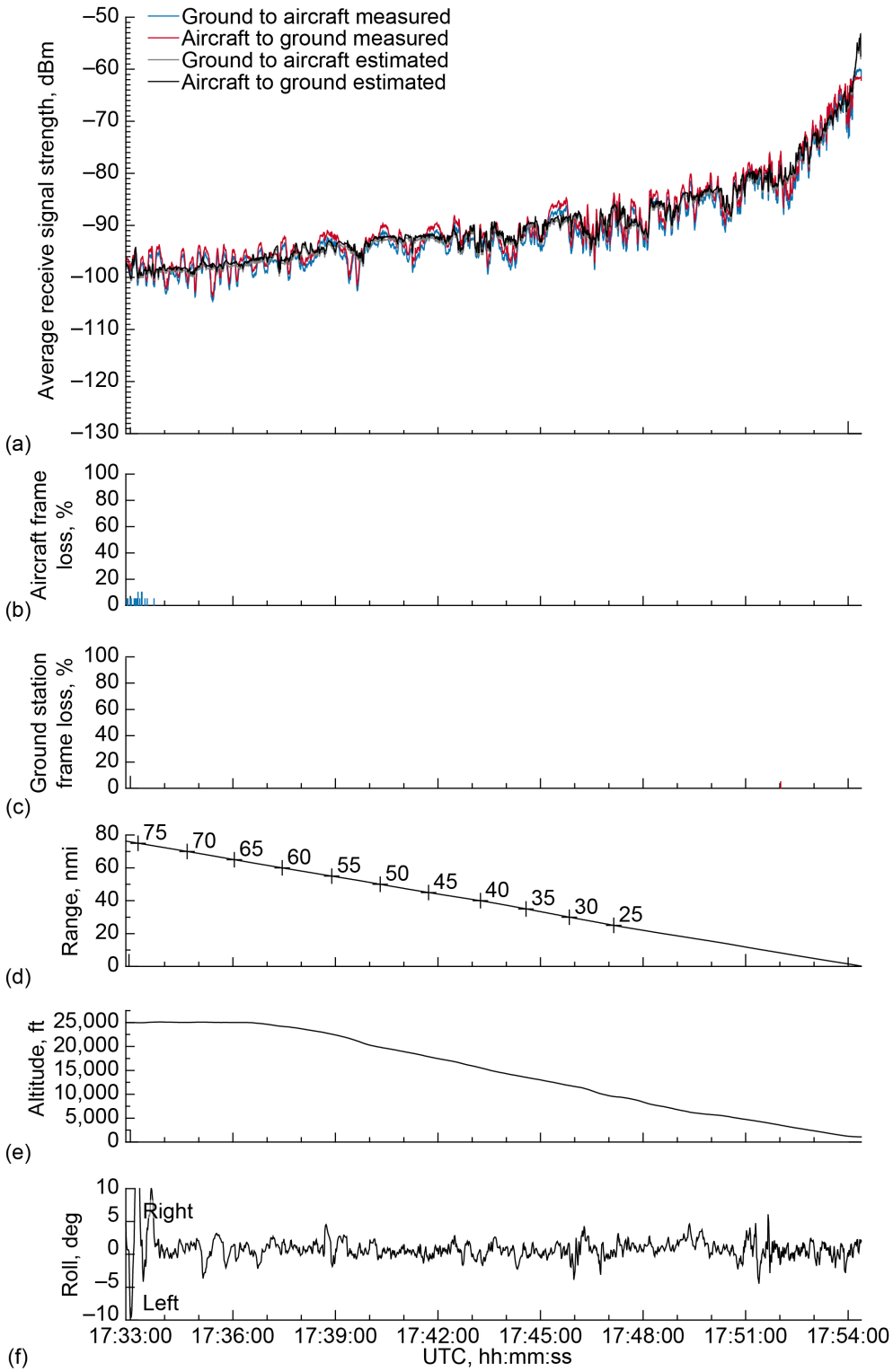

Figure 89.—Signal strength and frame loss over slightly rolling terrain during inbound, descending track on 3.0° glide slope, traveling toward ground station. (a) Average receive signal strength. (b) Aircraft frame loss. (c) Ground station frame loss. (d) Range. (e) Altitude. (f) Roll.

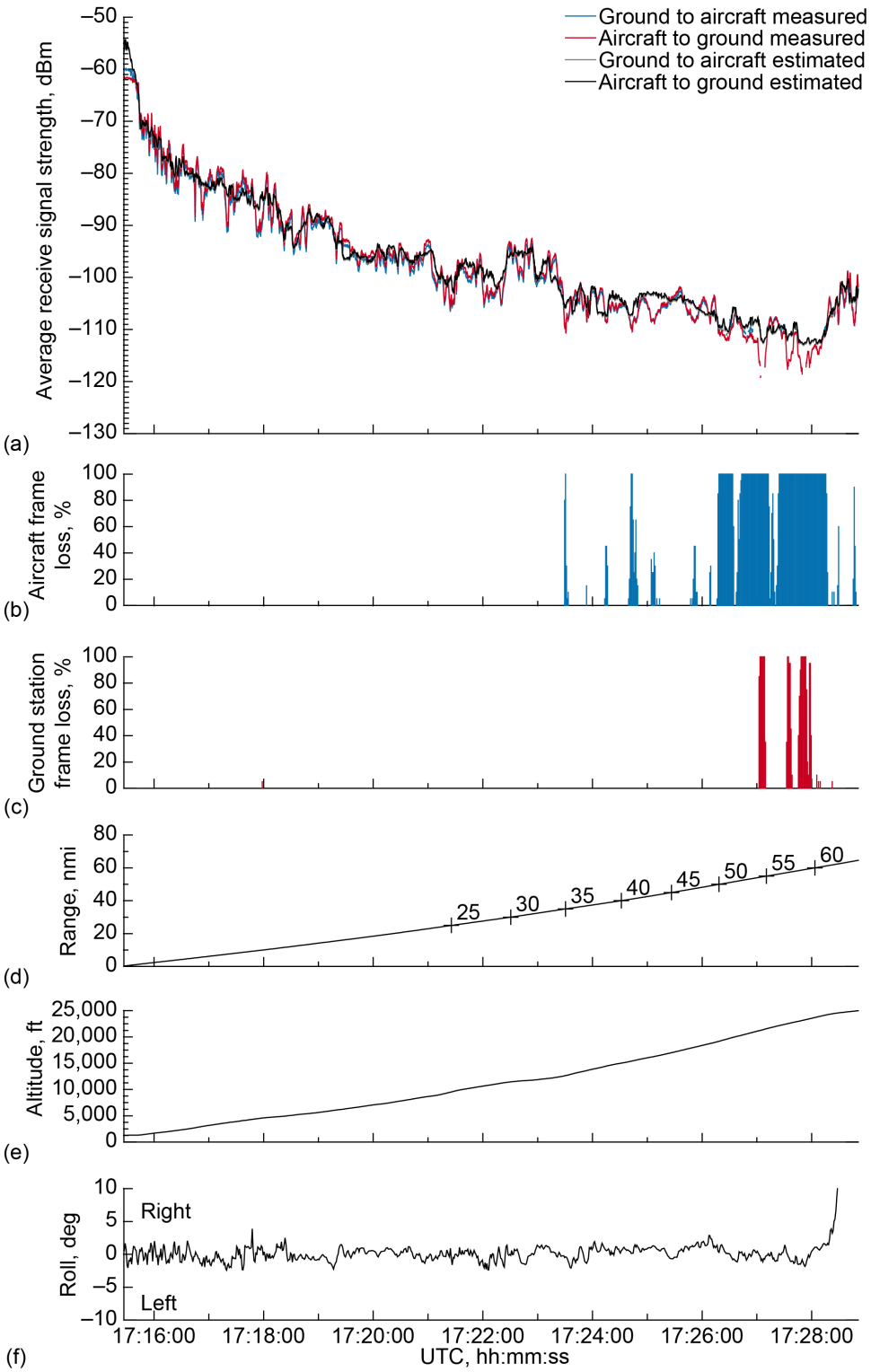

Figure 90.—Signal strength and frame loss over slightly rolling terrain during outbound, ascending track on 3.0° glide slope, traveling away from ground station. (a) Average receive signal strength. (b) Aircraft frame loss. (c) Ground station frame loss. (d) Range. (e) Altitude. (f) Roll.

3.4 Validation Flight Test Data for Open Water Setting, March 3, 5, and 6, 2019

Figure 91 presents the flight track of the NASA aircraft over the open water airspace above Lake Erie, north of Cleveland, Ohio. The orange trace is the complete flightpath of the aircraft, including all reversals, ascent and descent maneuvers, and range changes. Figure 92 is the same flight track viewed from an oblique perspective to show the flightpath at various test altitudes. Waypoints are identified with alphabet characters A to H. The flight segments between waypoints are highlighted in yellow, which precisely represents the locations where RF data was captured for evaluation. For this setting, the GRS was positioned at the shoreline along the western edge of Lake Erie. The surface of the open water carried 1- to 3-ft waves as the result of the east-northeast breeze.

The northern end of each crosstrack flightpath shows a heavily folded reversal made by the aircraft. This was due to the limits imposed by the frequency authorization for this test campaign, which prohibits the aircraft radio from transmitting in Canadian airspace.

C-band validation flight test data over open freshwater is presented in Figure 93 to Figure 141. Crosstrack plots are arranged for elevation angles of 1.0°, 1.5°, 2.0°, and 3.0° followed by ascent and descent plots.

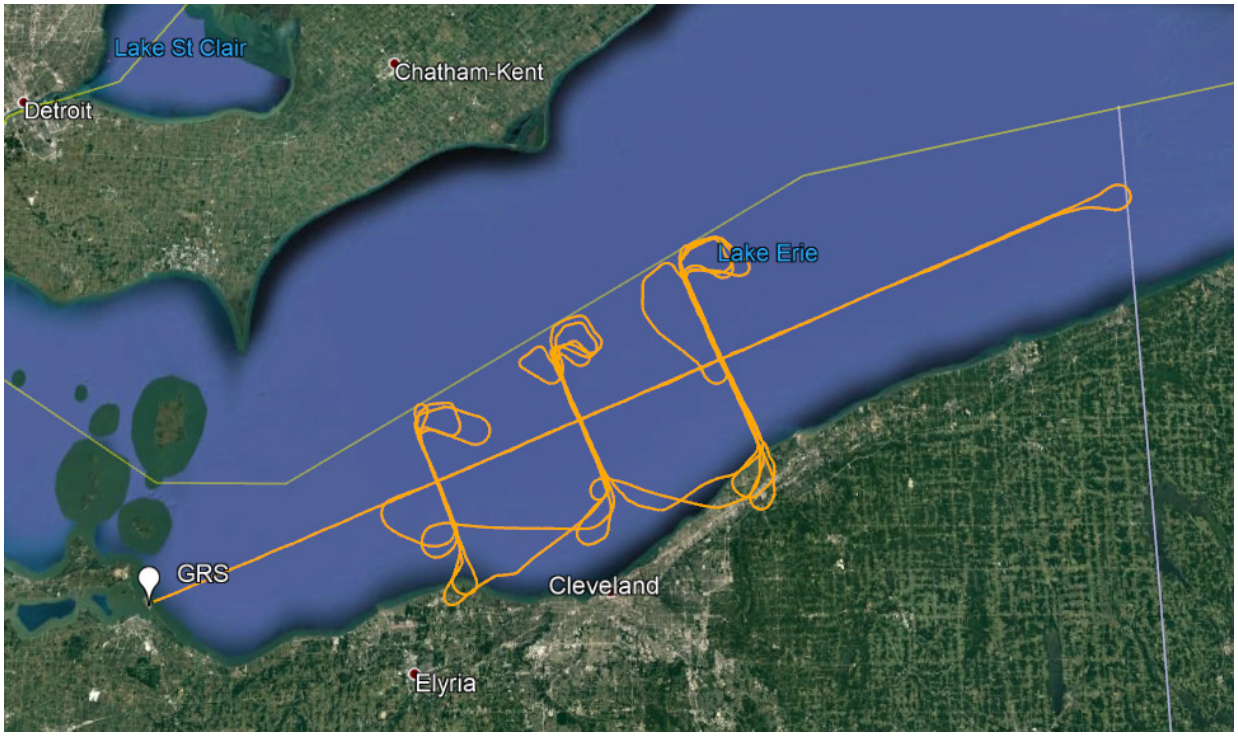

Figure 91.—Flightpath over freshwater December 3, 2019 (orange trace). International boundary indicated by yellow line. Image ©2020 GoogleEarth.

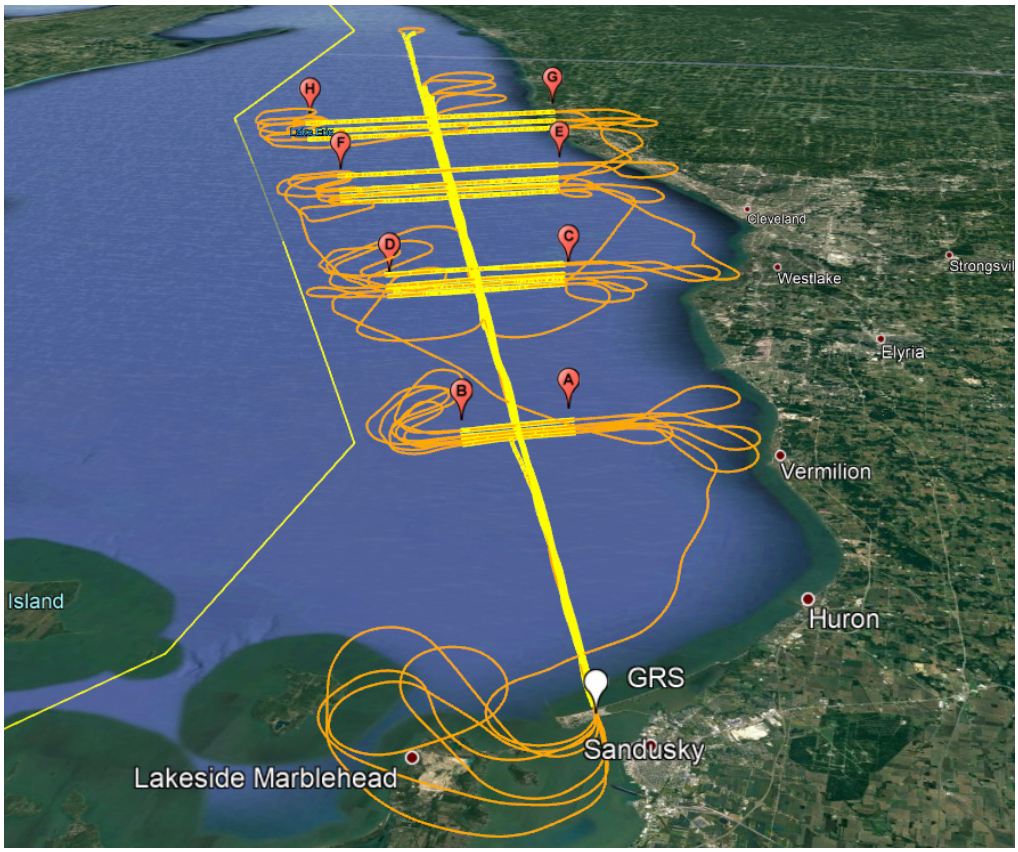

Figure 92.—Perspective view of flightpath over freshwater highlighting data capture segments December 3 and 5, 2019. Image ©2020 GoogleEarth.

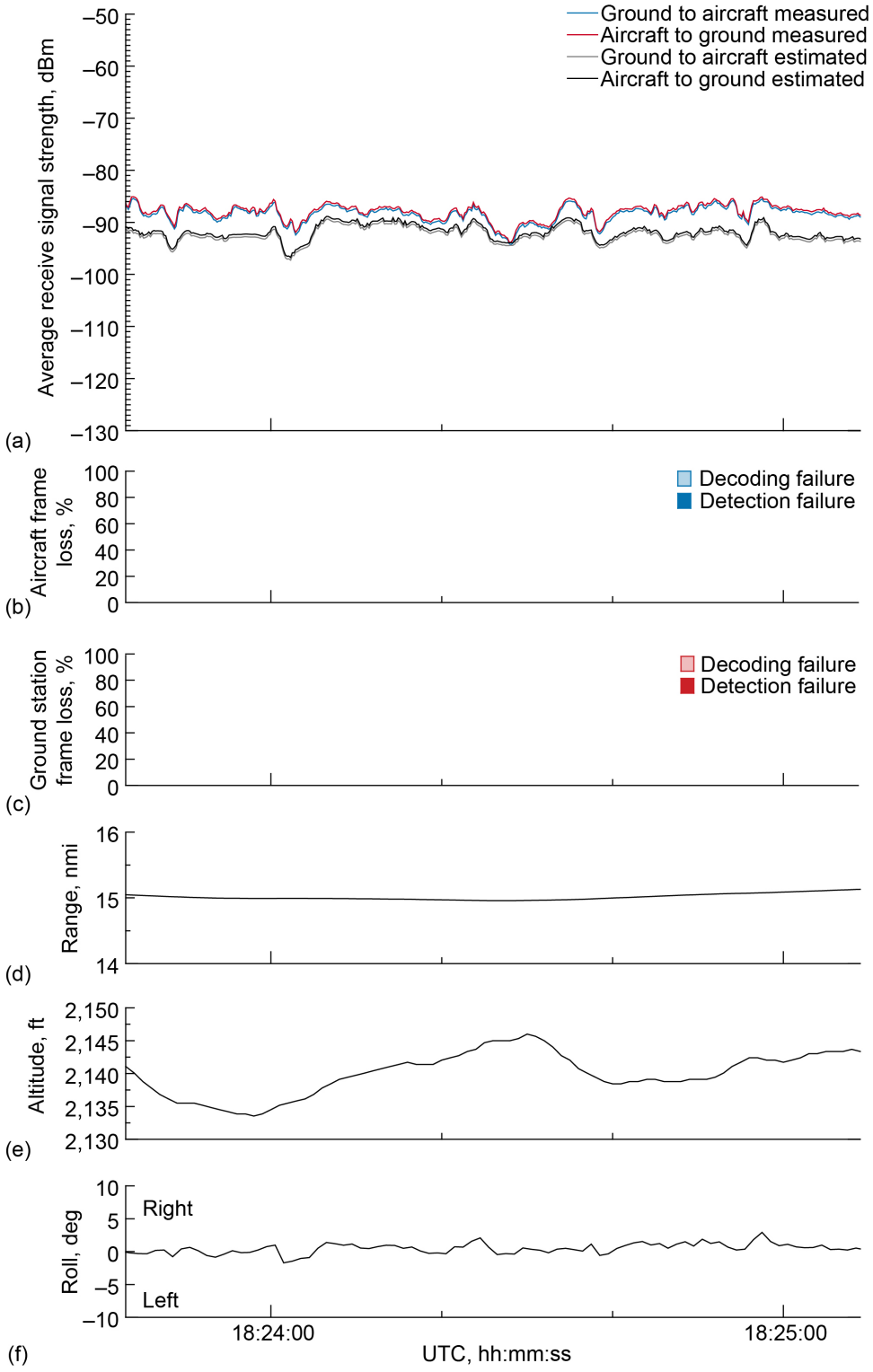

Figure 93.—Signal strength and frame loss over open freshwater at 15-nmi range and 2,000-ft altitude, 1.0° antenna elevation, traveling from waypoint A to waypoint B. (a) Average receive signal strength. (b) Aircraft frame loss. (c) Ground station frame loss. (d) Range. (e) Altitude. (f) Roll.

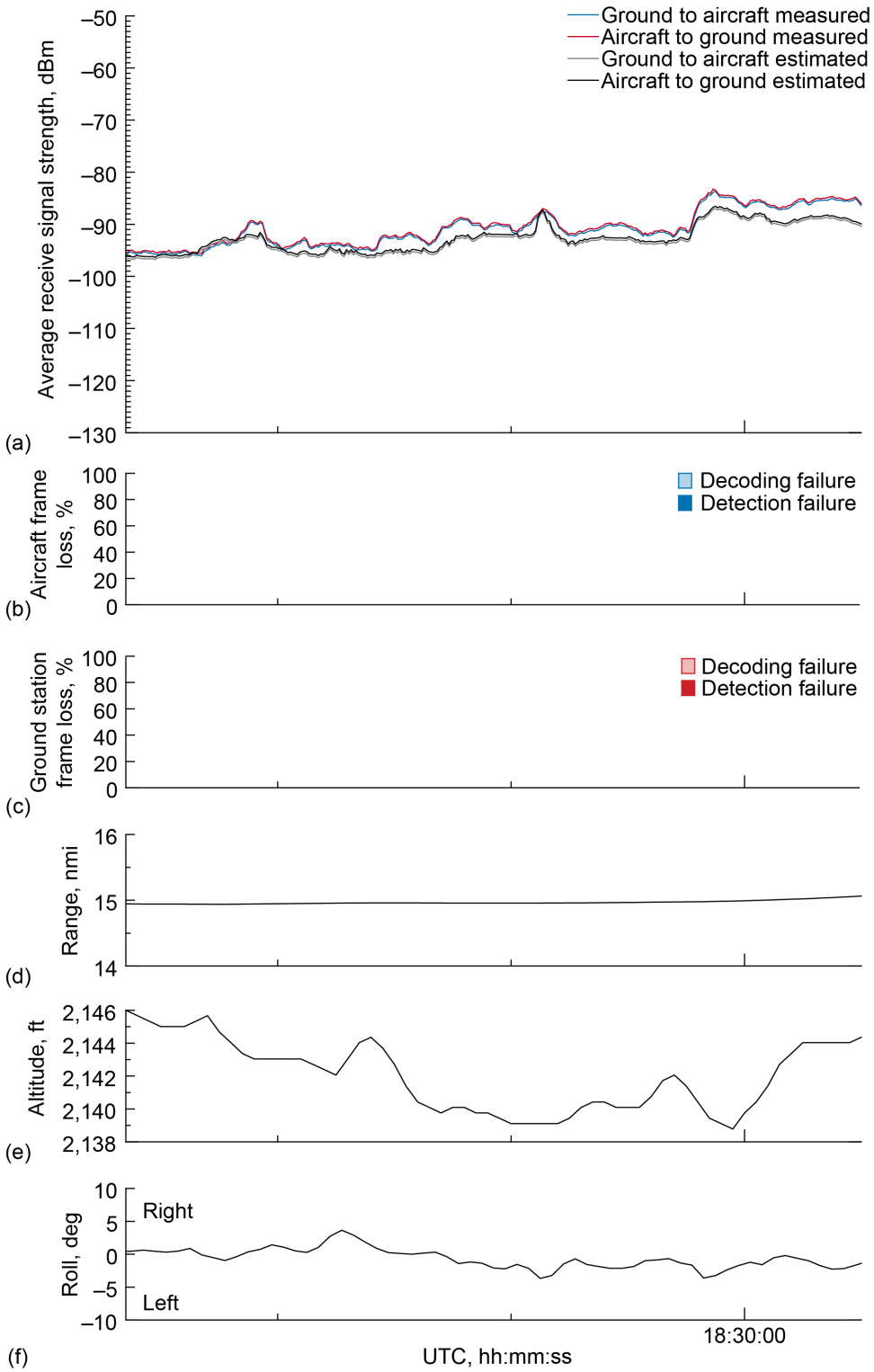

Figure 94.—Signal strength and frame loss over open freshwater at 15-nmi range and 2,000-ft altitude, 1.0° antenna elevation, traveling from waypoint B to waypoint A. (a) Average receive signal strength. (b) Aircraft frame loss. (c) Ground station frame loss. (d) Range. (e) Altitude. (f) Roll.

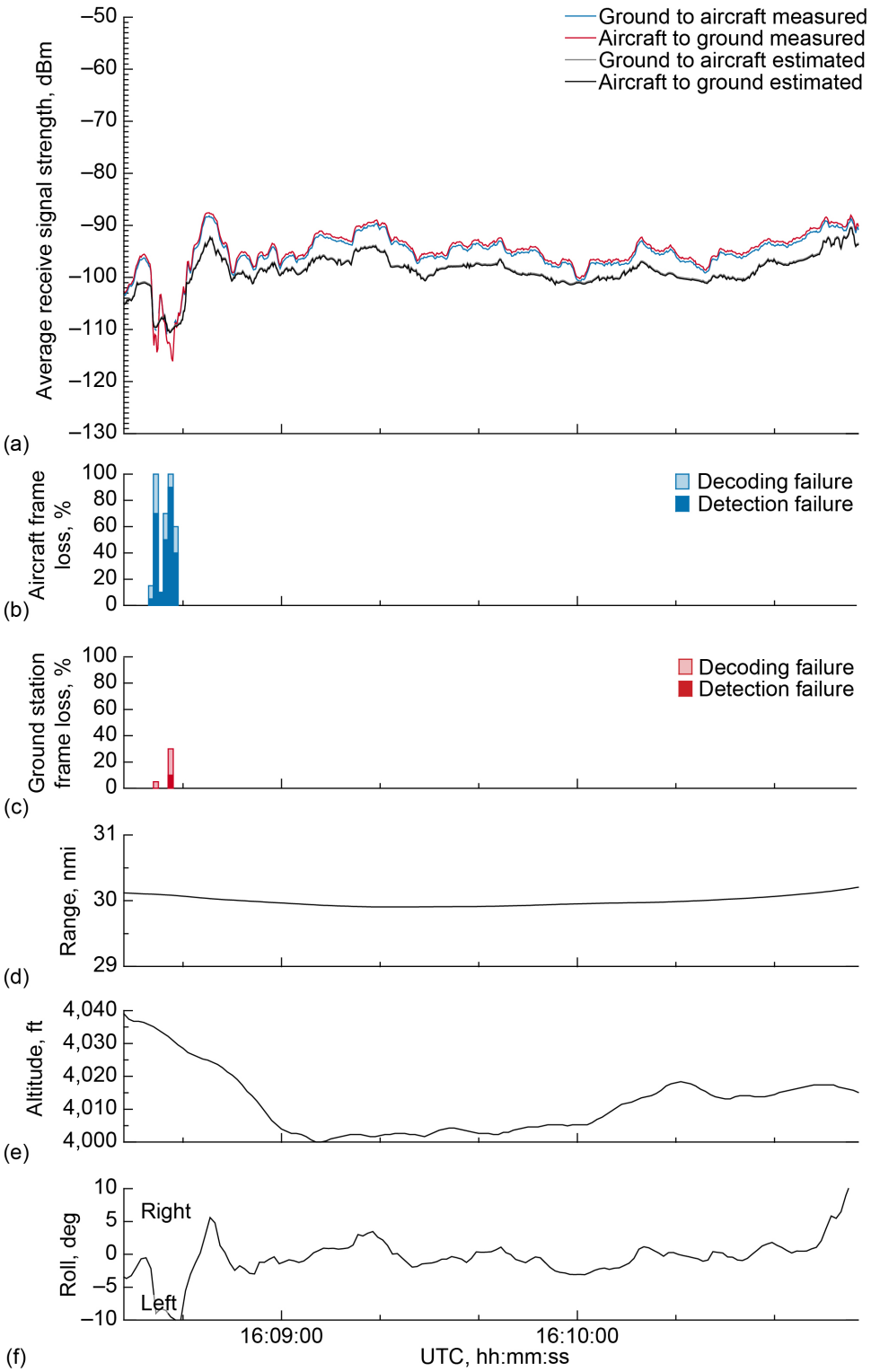

Figure 95.—Signal strength and frame loss over open freshwater at 30-nmi range and 4,000-ft altitude, 1.0° antenna elevation, traveling from waypoint C to waypoint D. (a) Average receive signal strength. (b) Aircraft frame loss. (c) Ground station frame loss. (d) Range. (e) Altitude. (f) Roll.

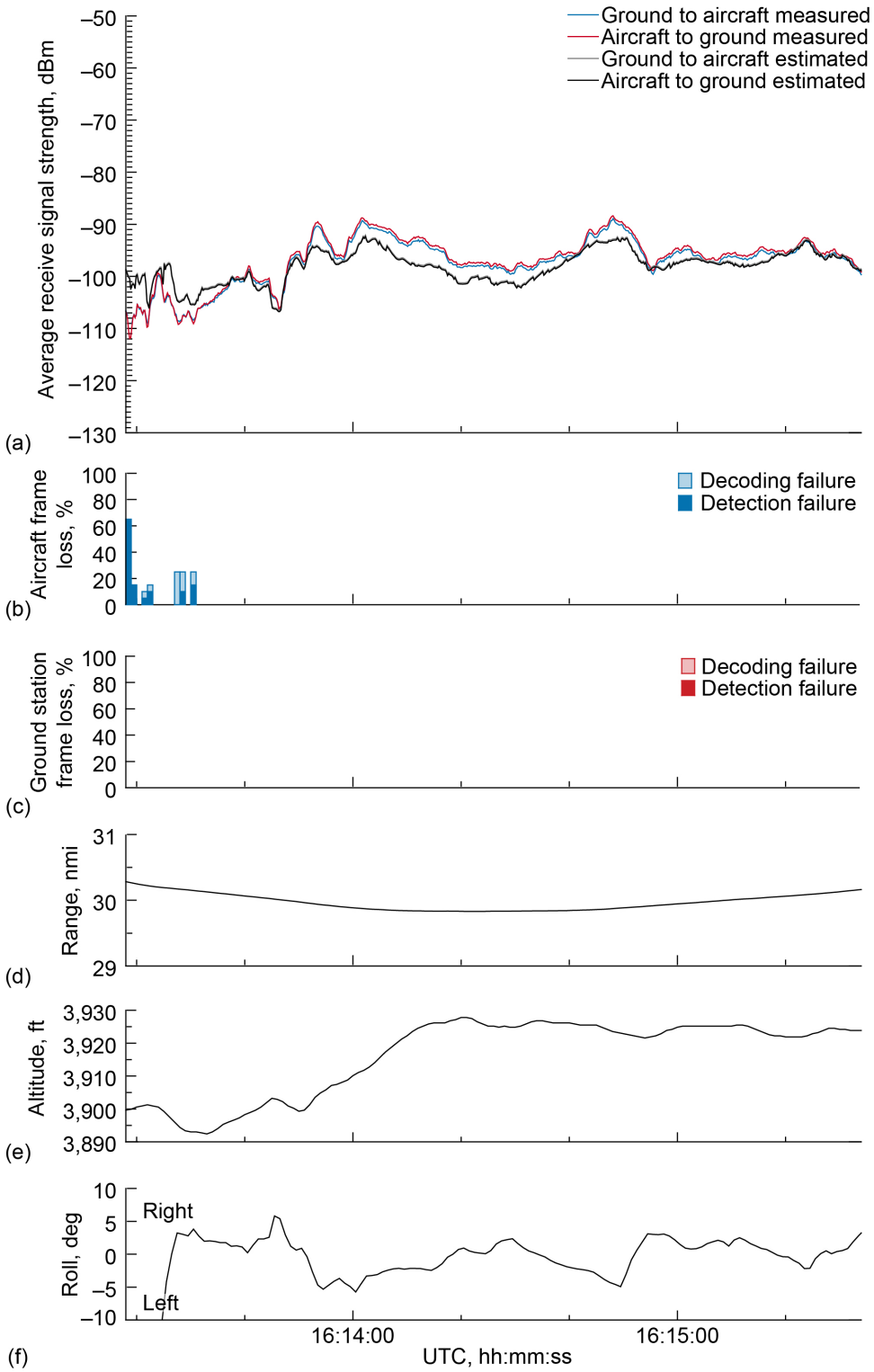

Figure 96.—Signal strength and frame loss over open freshwater at 30-nmi range and 4,000-ft altitude, 1.0° antenna elevation, traveling from waypoint D to waypoint C. (a) Average receive signal strength. (b) Aircraft frame loss. (c) Ground station frame loss. (d) Range. (e) Altitude. (f) Roll.

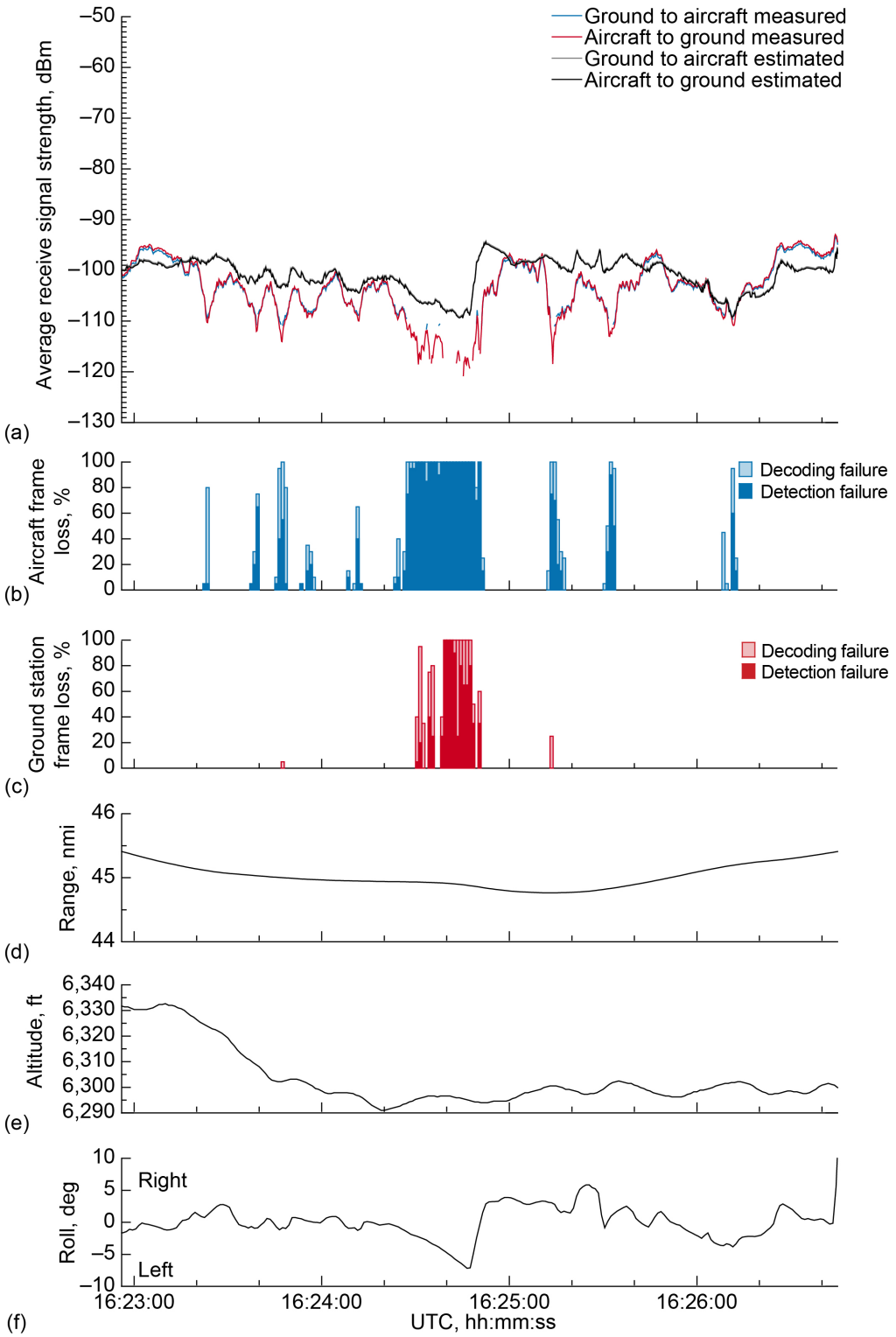

Figure 97.—Signal strength and frame loss over open freshwater at 45-nmi range and 6,500-ft altitude, 1.0° antenna elevation, traveling from waypoint E to waypoint F on December 3, 2019. (a) Average receive signal strength. (b) Aircraft frame loss. (c) Ground station frame loss. (d) Range. (e) Altitude. (f) Roll.

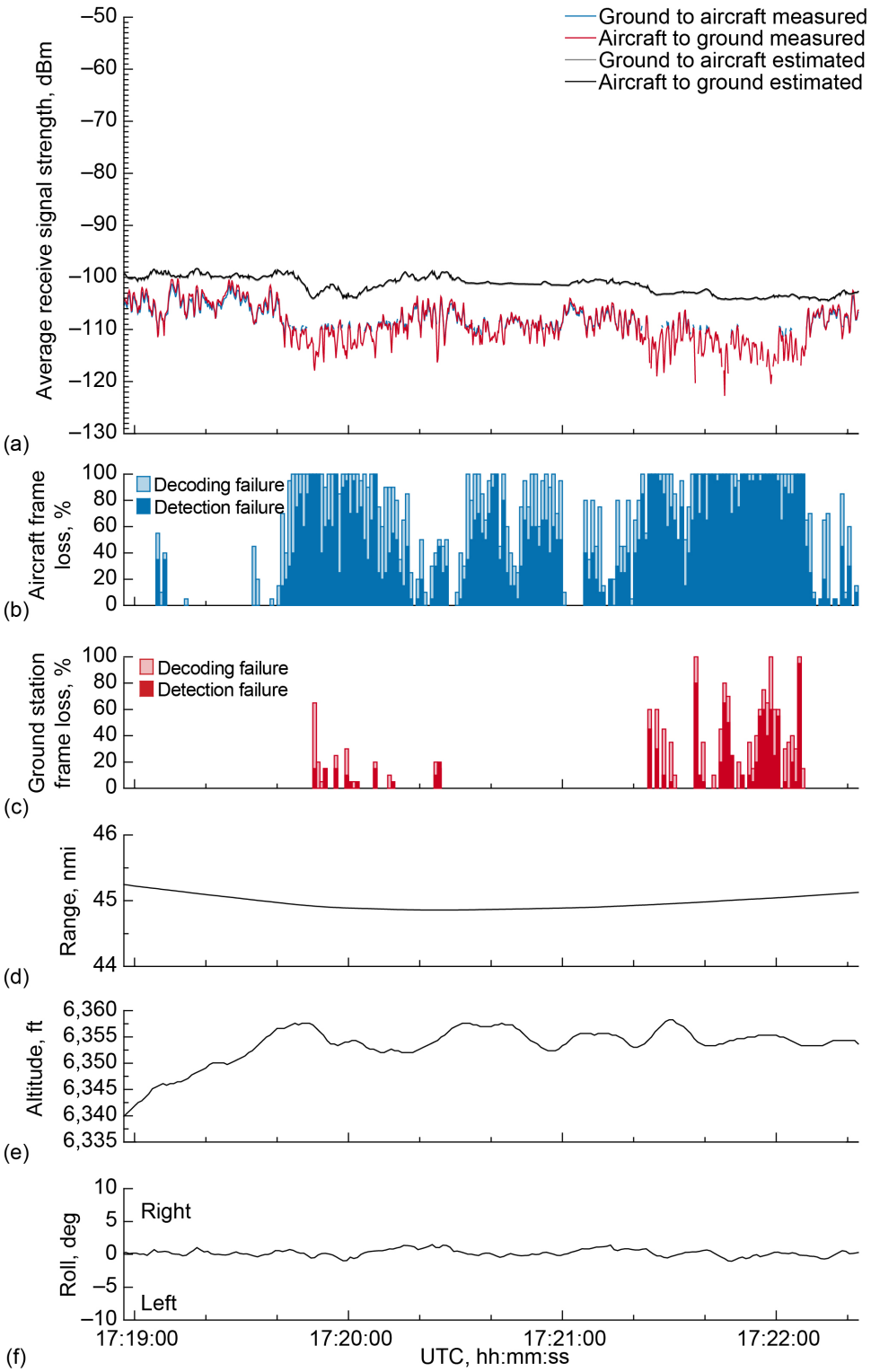

Figure 98.—Signal strength and frame loss over open freshwater at 45-nmi range and 6,500-ft altitude, 1.0° antenna elevation, traveling from waypoint E to waypoint F on December 6, 2019. (a) Average receive signal strength. (b) Aircraft frame loss. (c) Ground station frame loss. (d) Range. (e) Altitude. (f) Roll.

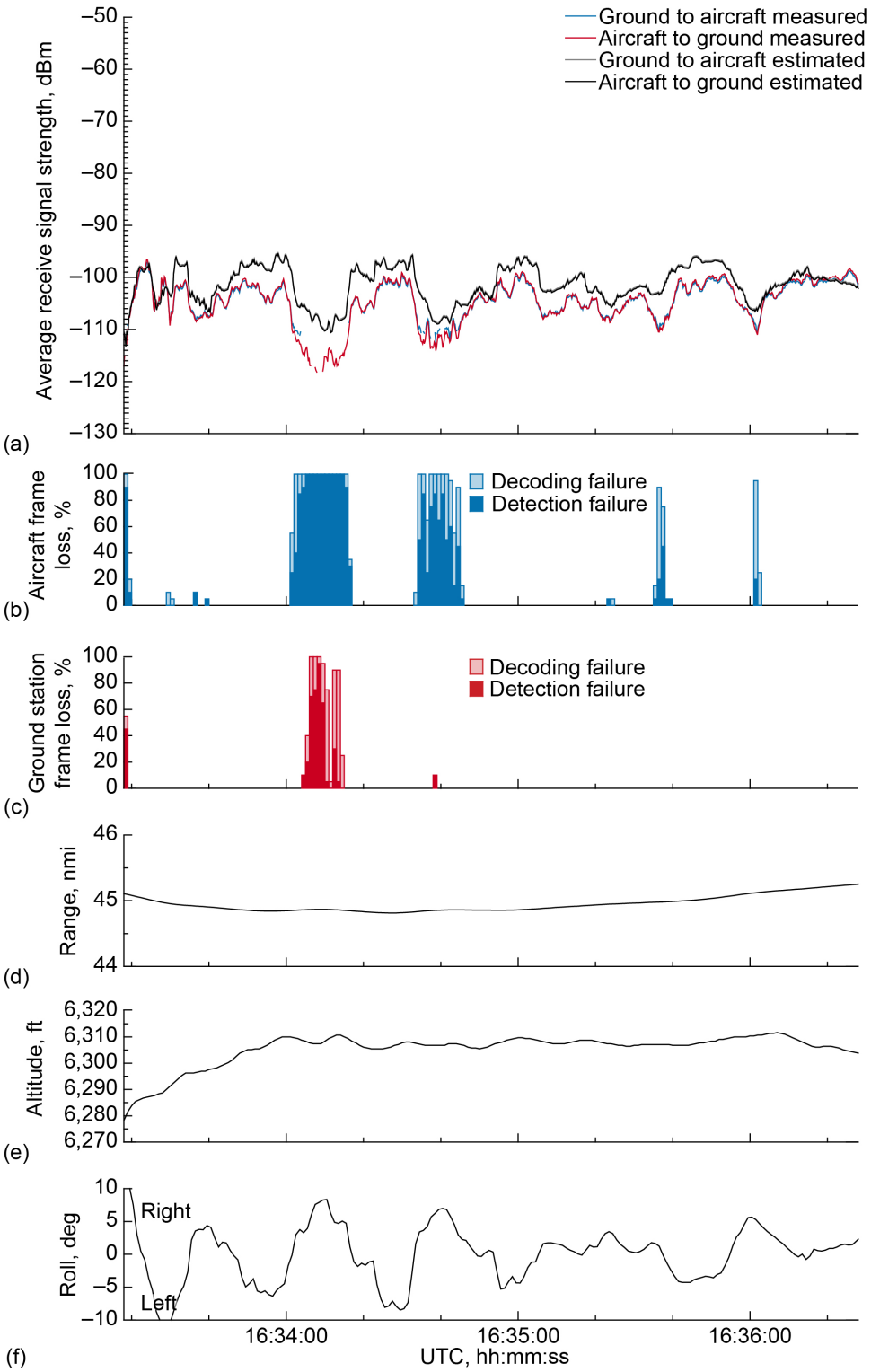

Figure 99.—Signal strength and frame loss over open freshwater at 45-nmi range and 6,500-ft altitude, 1.0° antenna elevation, traveling from waypoint F to waypoint E on December 3, 2019. (a) Average receive signal strength. (b) Aircraft frame loss. (c) Ground station frame loss. (d) Range. (e) Altitude. (f) Roll.

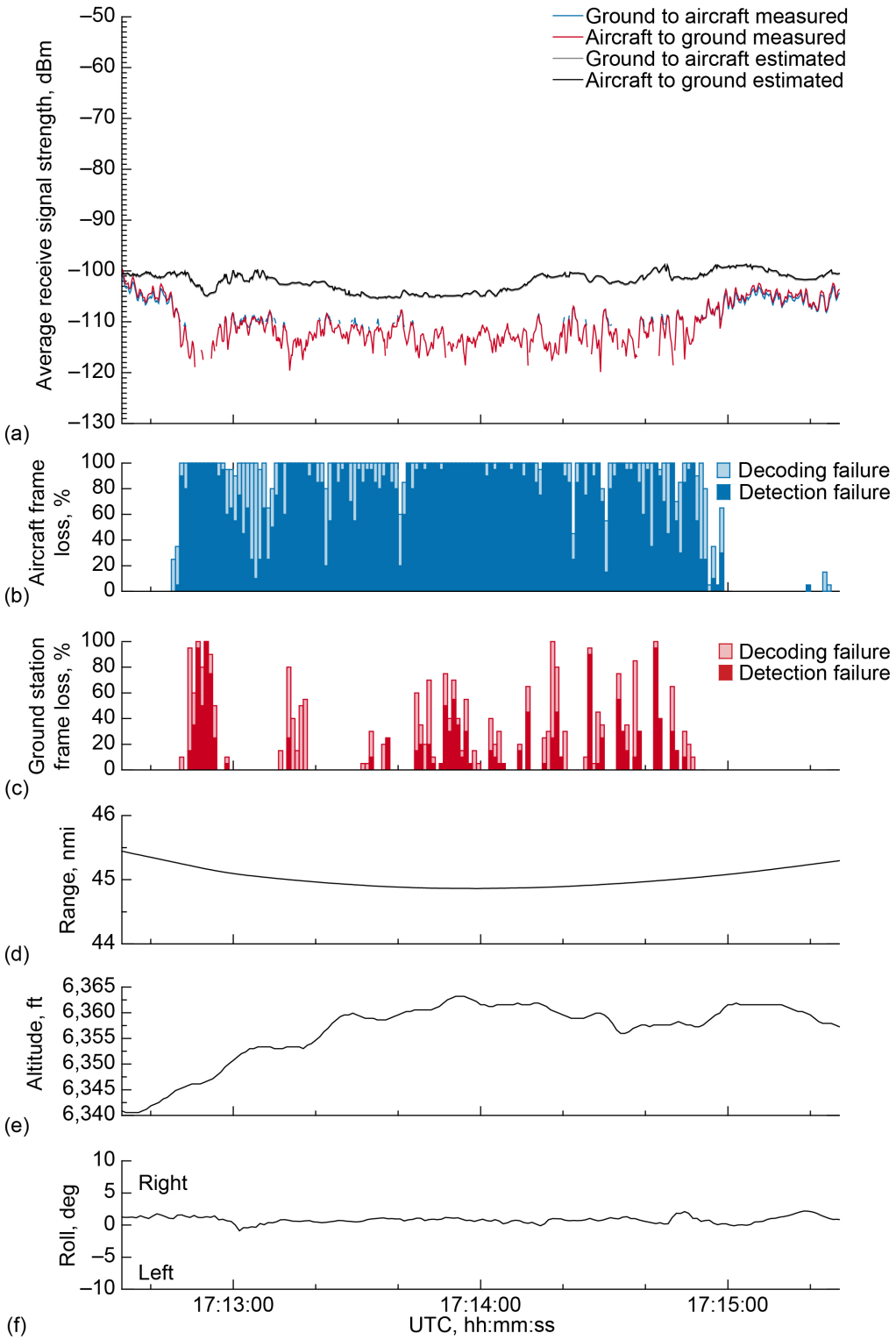

Figure 100.—Signal strength and frame loss over open freshwater at 45-nmi range and 6,500-ft altitude, 1.0° antenna elevation, traveling from waypoint F to waypoint E on December 6, 2019. (a) Average receive signal strength. (b) Aircraft frame loss. (c) Ground station frame loss. (d) Range. (e) Altitude. (f) Roll.

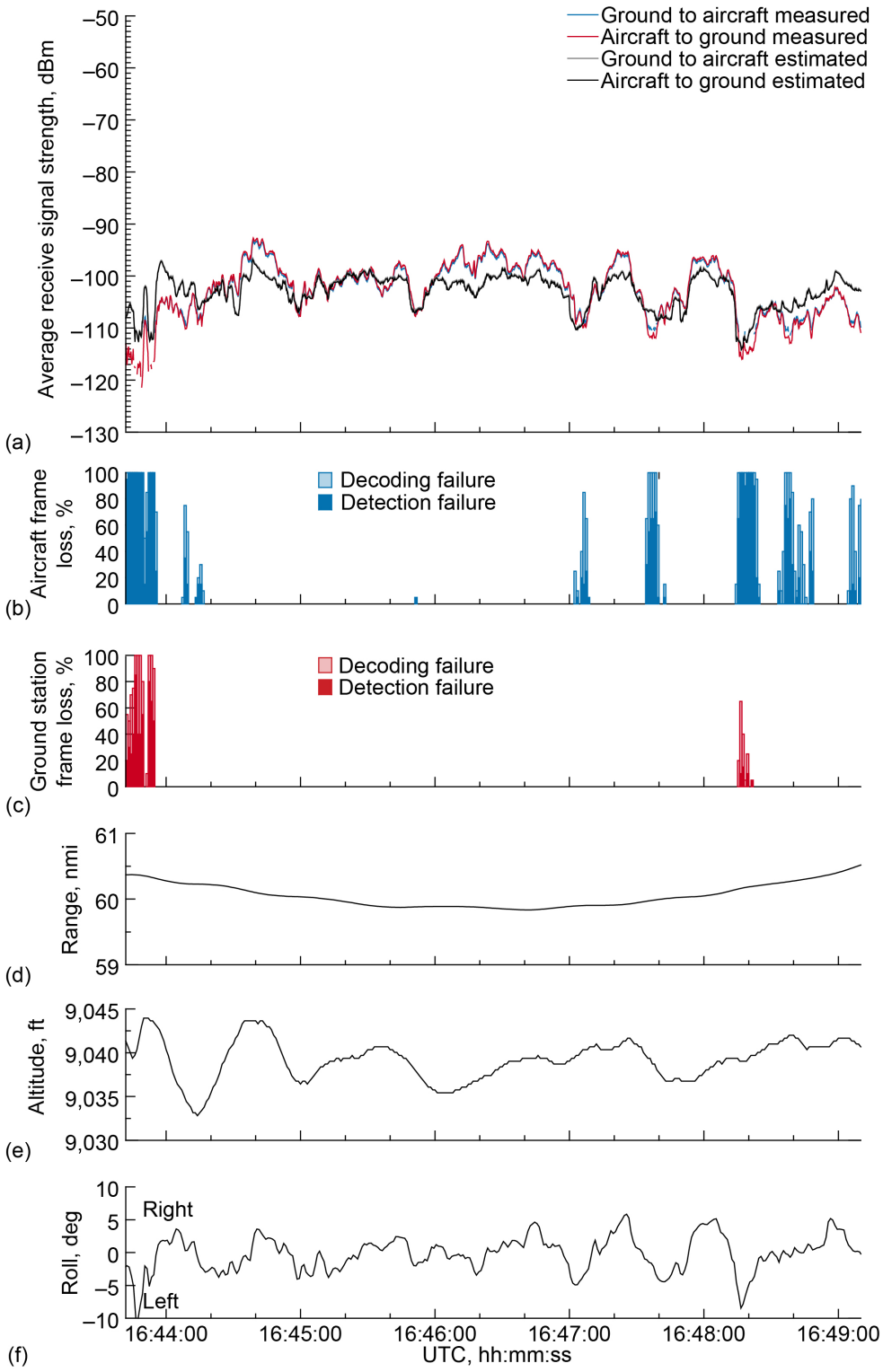

Figure 101.—Signal strength and frame loss over open freshwater at 60-nmi range and 9,000-ft altitude, 1.0° antenna elevation, traveling from waypoint G to waypoint H. (a) Average receive signal strength. (b) Aircraft frame loss. (c) Ground station frame loss. (d) Range. (e) Altitude. (f) Roll.

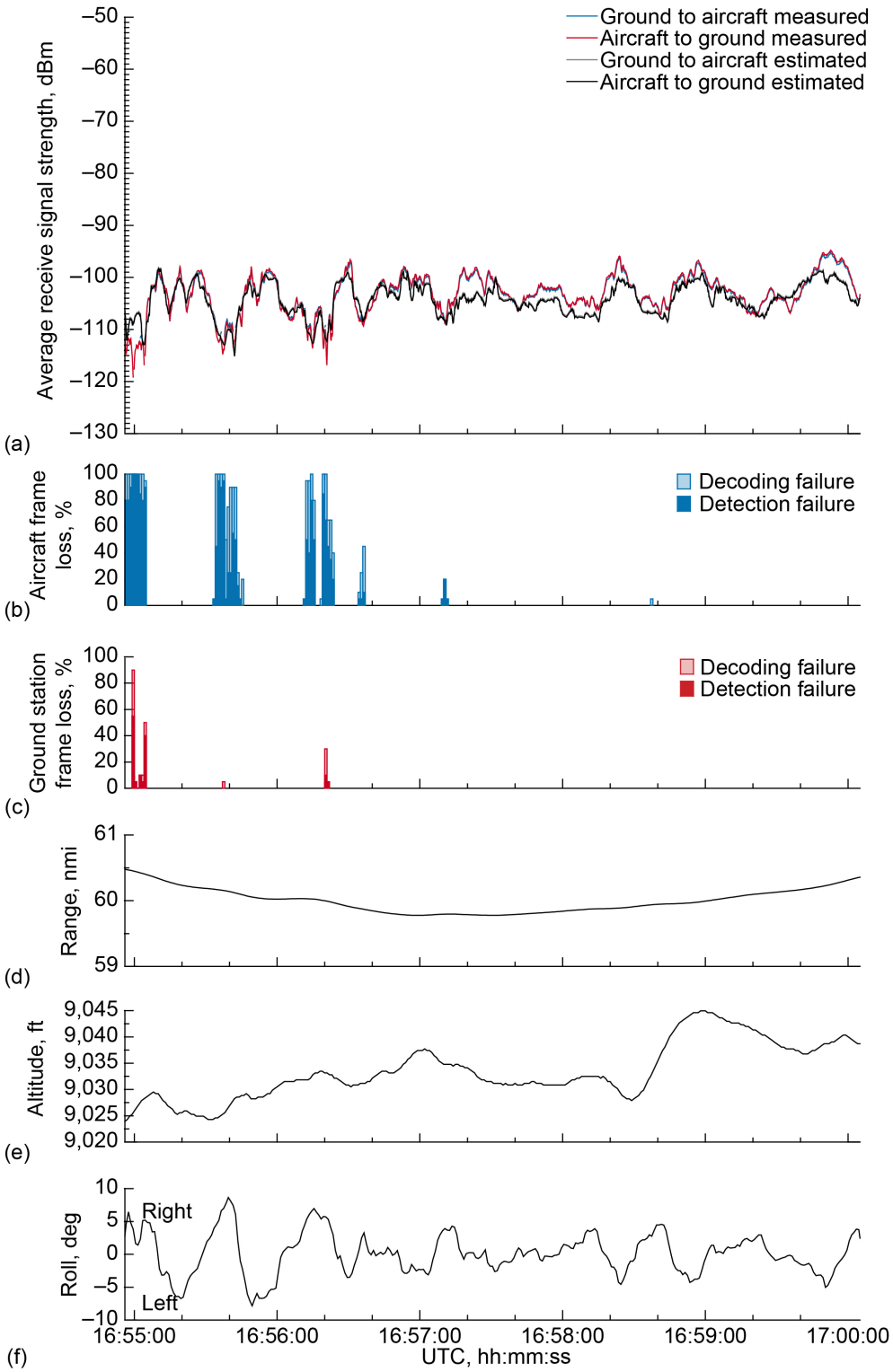

Figure 102.—Signal strength and frame loss over open freshwater at 60-nmi range and 9,000-ft altitude, 1.0° antenna elevation, traveling from waypoint H to waypoint G. (a) Average receive signal strength. (b) Aircraft frame loss. (c) Ground station frame loss. (d) Range. (e) Altitude. (f) Roll.

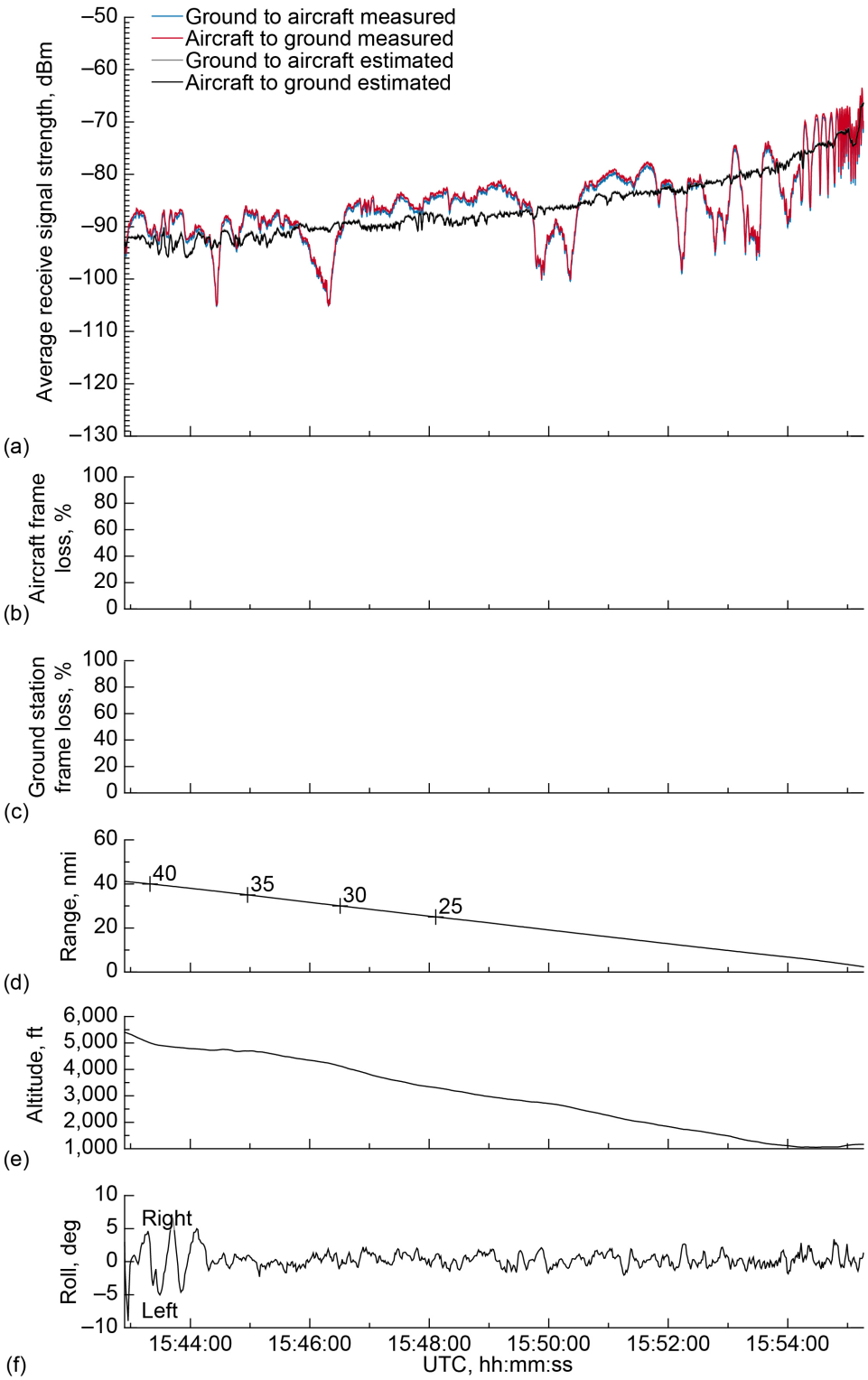

Figure 103.—Signal strength and frame loss over open freshwater during inbound, descending track on 1.0° glide slope, traveling toward ground station on December 6, 2019. (a) Average receive signal strength. (b) Aircraft frame loss. (c) Ground station frame loss. (d) Range. (e) Altitude. (f) Roll.

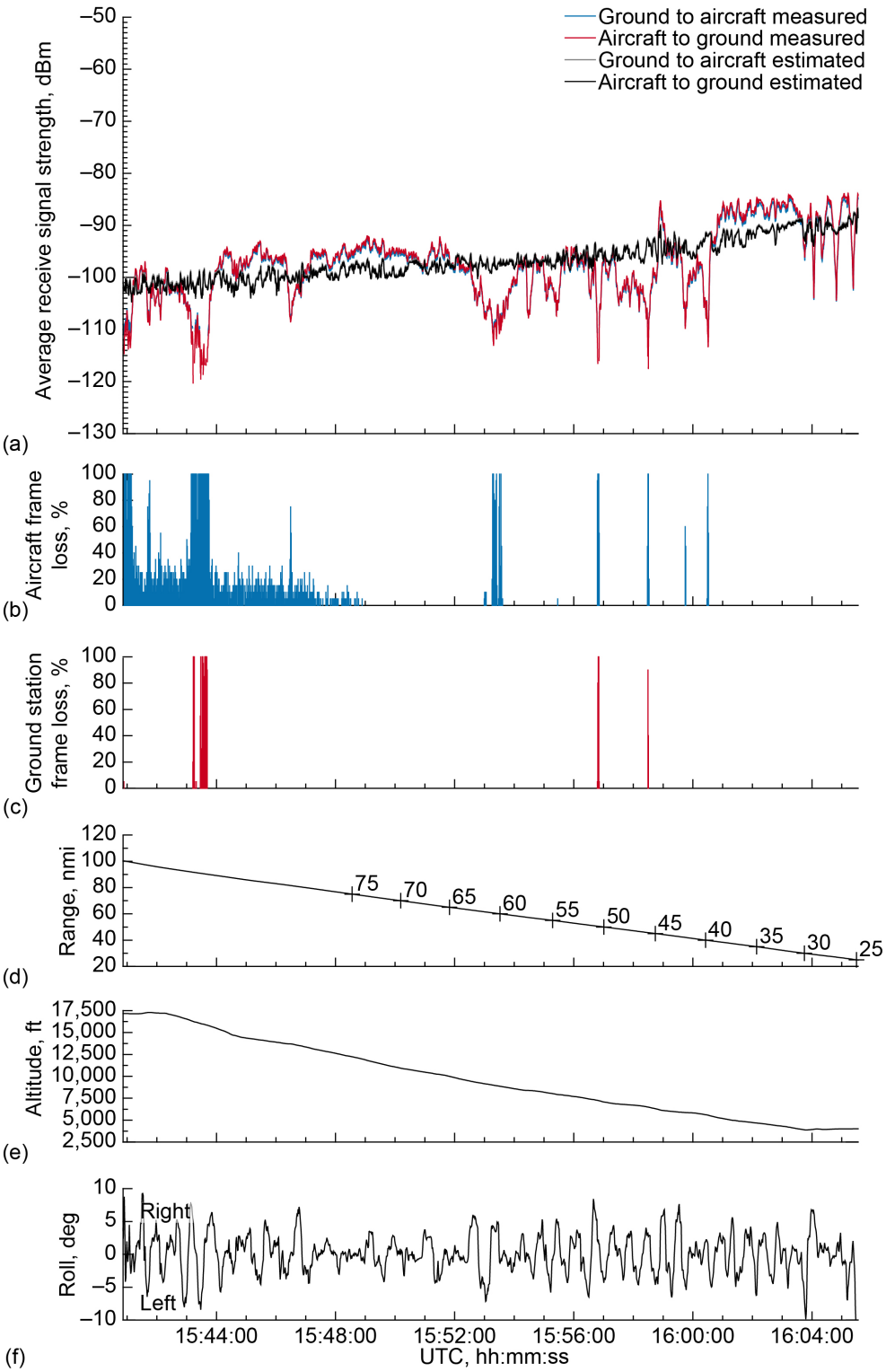

Figure 104.—Signal strength and frame loss over open freshwater during inbound, descending track on 1.0° glide slope, traveling toward ground station on December 3, 2019. (a) Average receive signal strength. (b) Aircraft frame loss. (c) Ground station frame loss. (d) Range. (e) Altitude. (f) Roll.

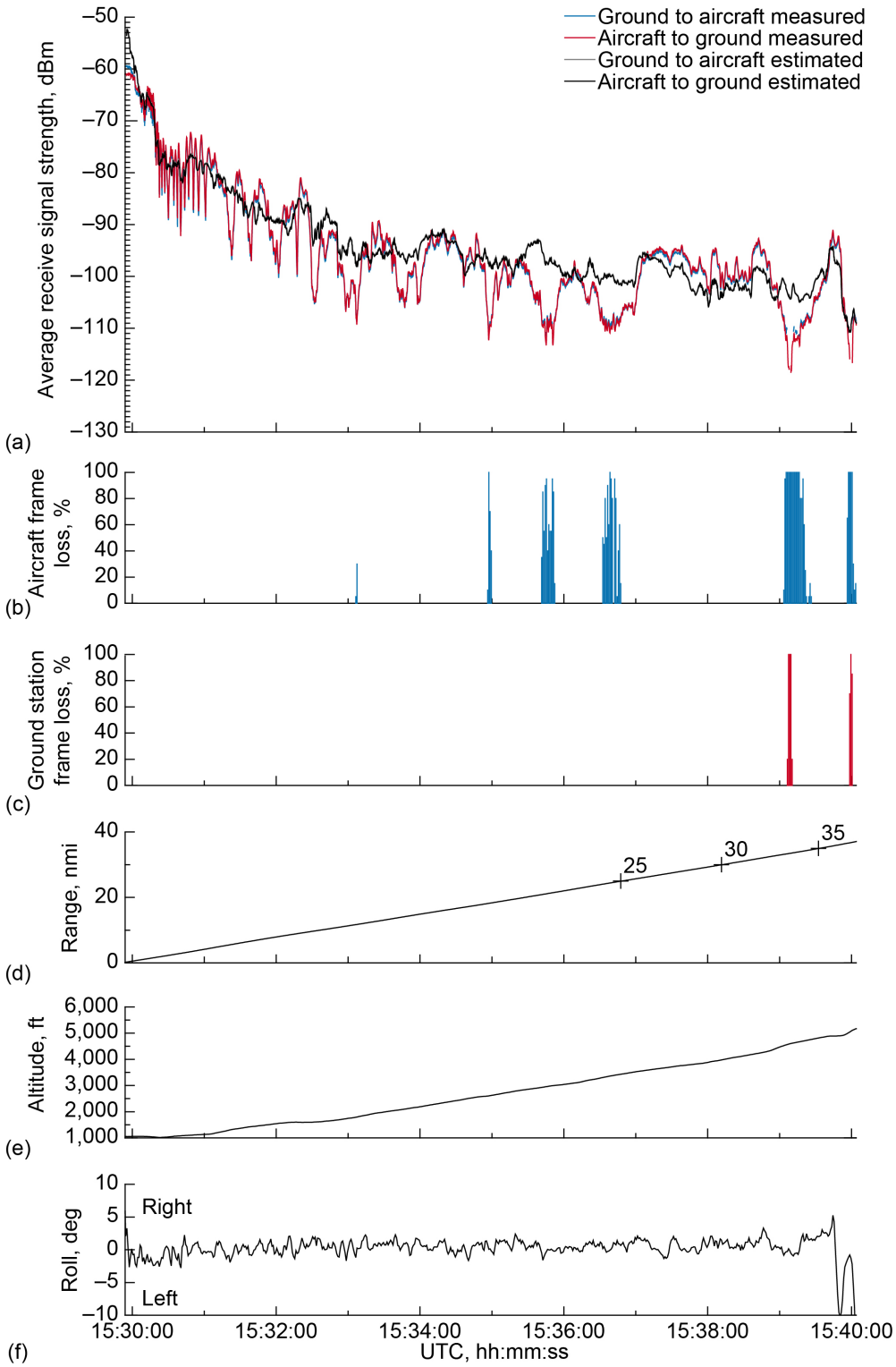

Figure 105.—Signal strength and frame loss over open freshwater during outbound, ascending track on 1.0° glide slope, traveling away from ground station on December 6, 2019. (a) Average receive signal strength. (b) Aircraft frame loss. (c) Ground station frame loss. (d) Range. (e) Altitude. (f) Roll.

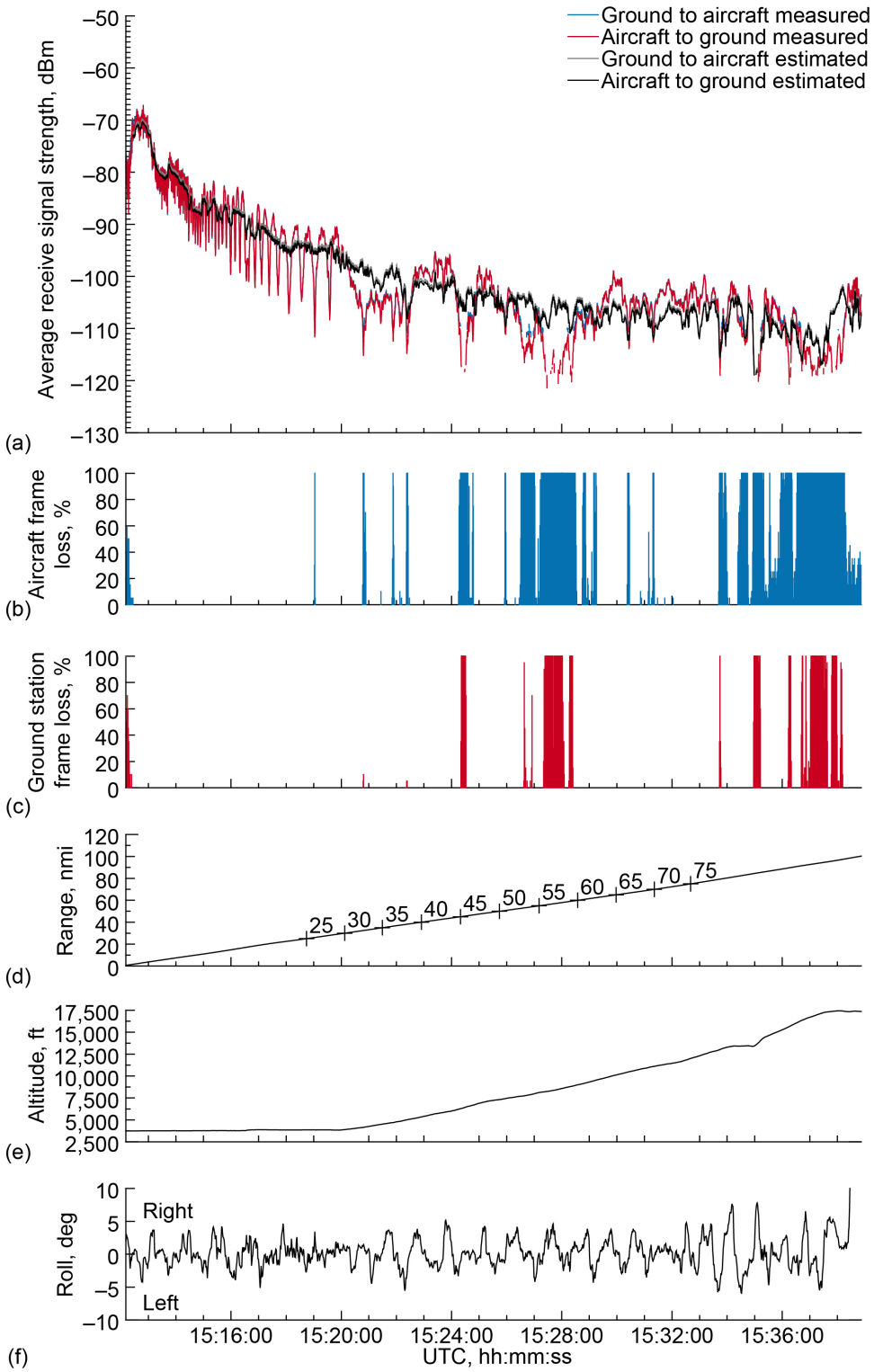

Figure 106.—Signal strength and frame loss over open freshwater during outbound, ascending track on 1.0° glide slope, traveling away from ground station on December 3, 2019. (a) Average receive signal strength. (b) Aircraft frame loss. (c) Ground station frame loss. (d) Range. (e) Altitude. (f) Roll.

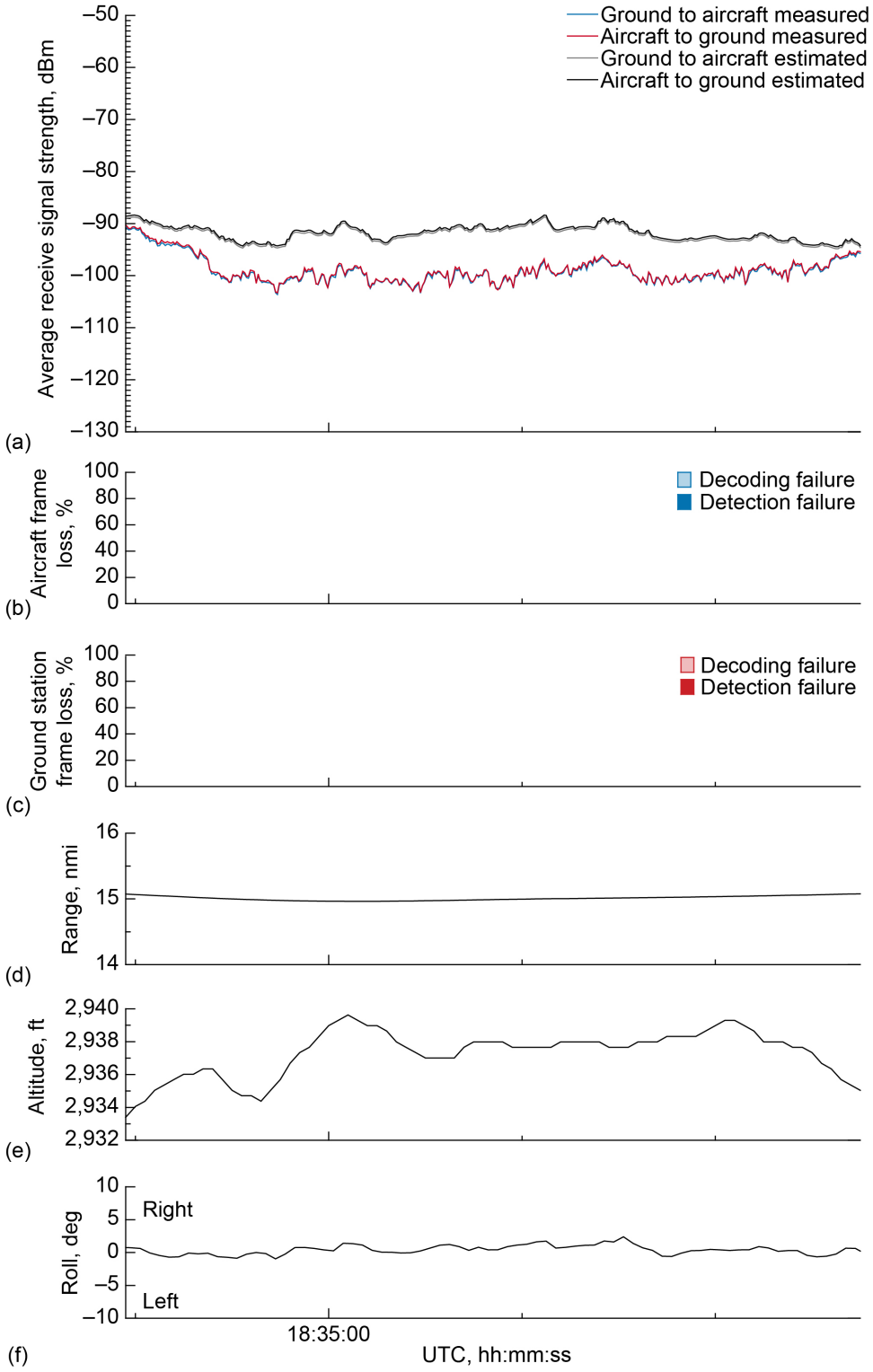

Figure 107.—Signal strength and frame loss over open freshwater at 15-nmi range and 3,000-ft altitude, 1.5° antenna elevation, traveling from waypoint A to waypoint B. (a) Average receive signal strength. (b) Aircraft frame loss. (c) Ground station frame loss. (d) Range. (e) Altitude. (f) Roll.

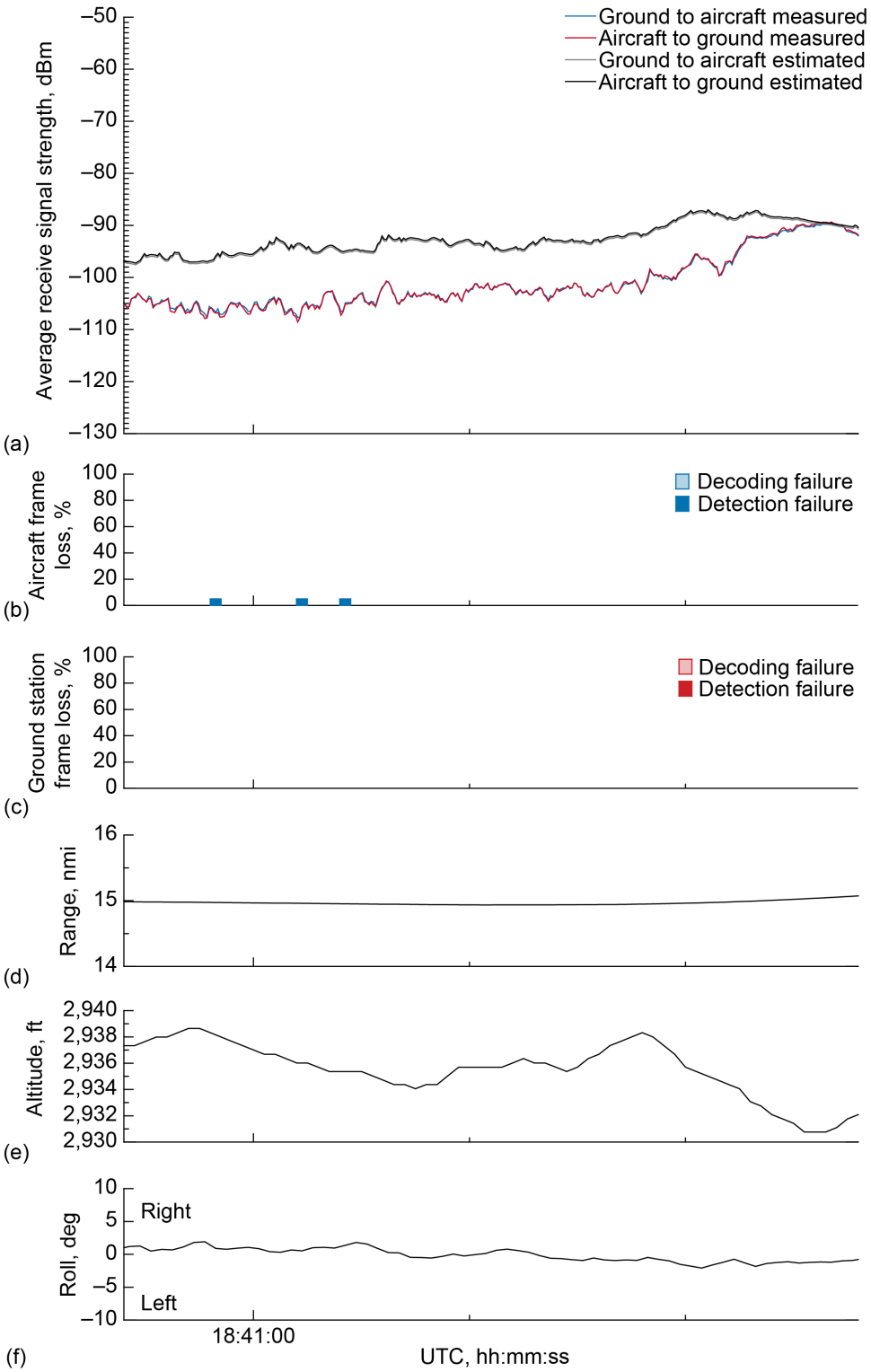

Figure 108.—Signal strength and frame loss over open freshwater at 15-nmi range and 3,000-ft altitude, 1.5° antenna elevation, traveling from waypoint B to waypoint A. (a) Average receive signal strength. (b) Aircraft frame loss. (c) Ground station frame loss. (d) Range. (e) Altitude. (f) Roll.

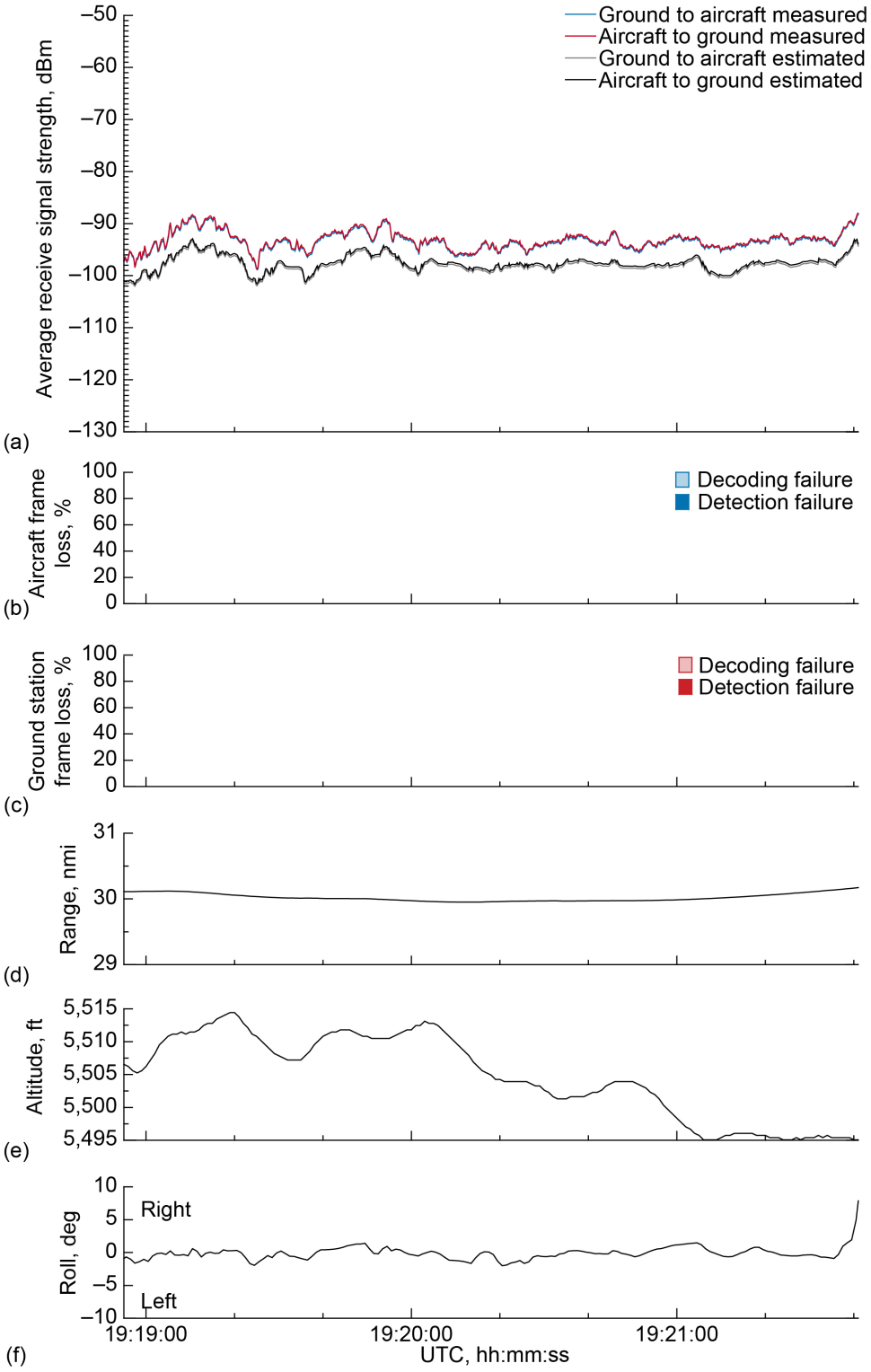

Figure 109.—Signal strength and frame loss over open freshwater at 30-nmi range and 5,500-ft altitude, 1.5° antenna elevation, traveling from waypoint C to waypoint D. (a) Average receive signal strength. (b) Aircraft frame loss. (c) Ground station frame loss. (d) Range. (e) Altitude. (f) Roll.

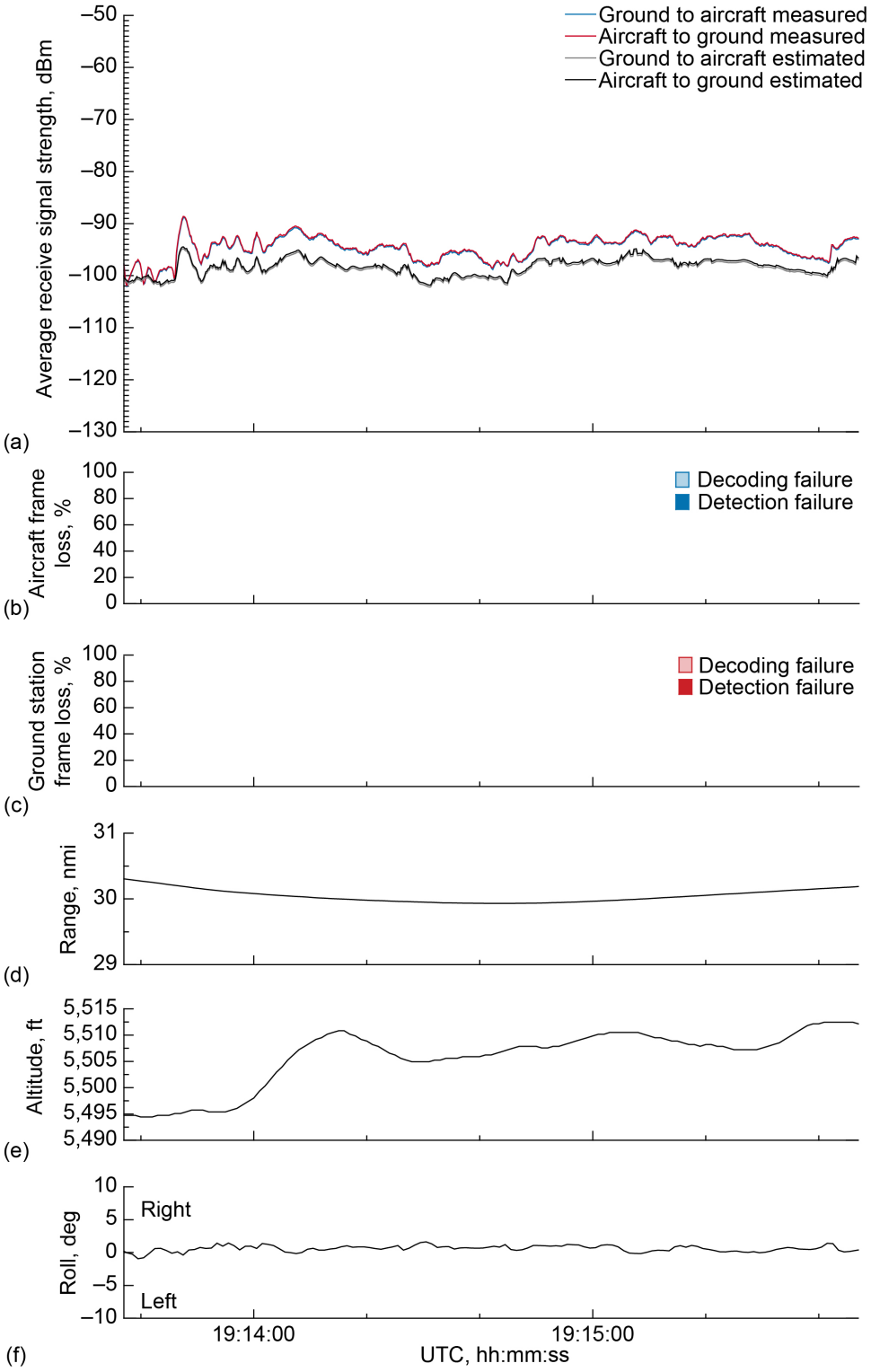

Figure 110.—Signal strength and frame loss over open freshwater at 30-nmi range and 5,500-ft altitude, 1.5° antenna elevation, traveling from waypoint D to waypoint C. (a) Average receive signal strength. (b) Aircraft frame loss. (c) Ground station frame loss. (d) Range. (e) Altitude. (f) Roll.

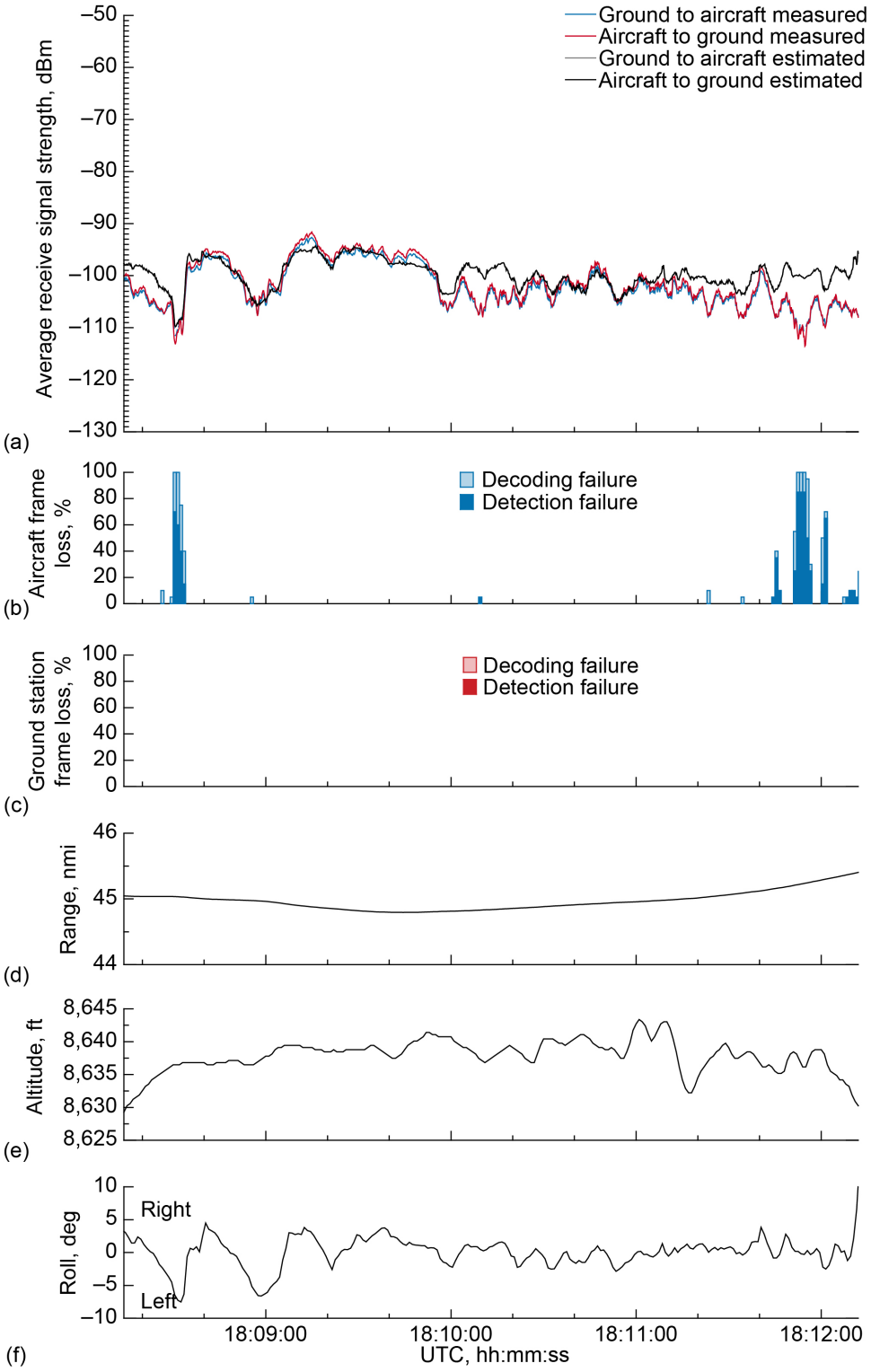

Figure 111.—Signal strength and frame loss over open freshwater at 45-nmi range and 8,500-ft altitude, 1.5° antenna elevation, traveling from waypoint E to waypoint F. (a) Average receive signal strength. (b) Aircraft frame loss. (c) Ground station frame loss. (d) Range. (e) Altitude. (f) Roll.

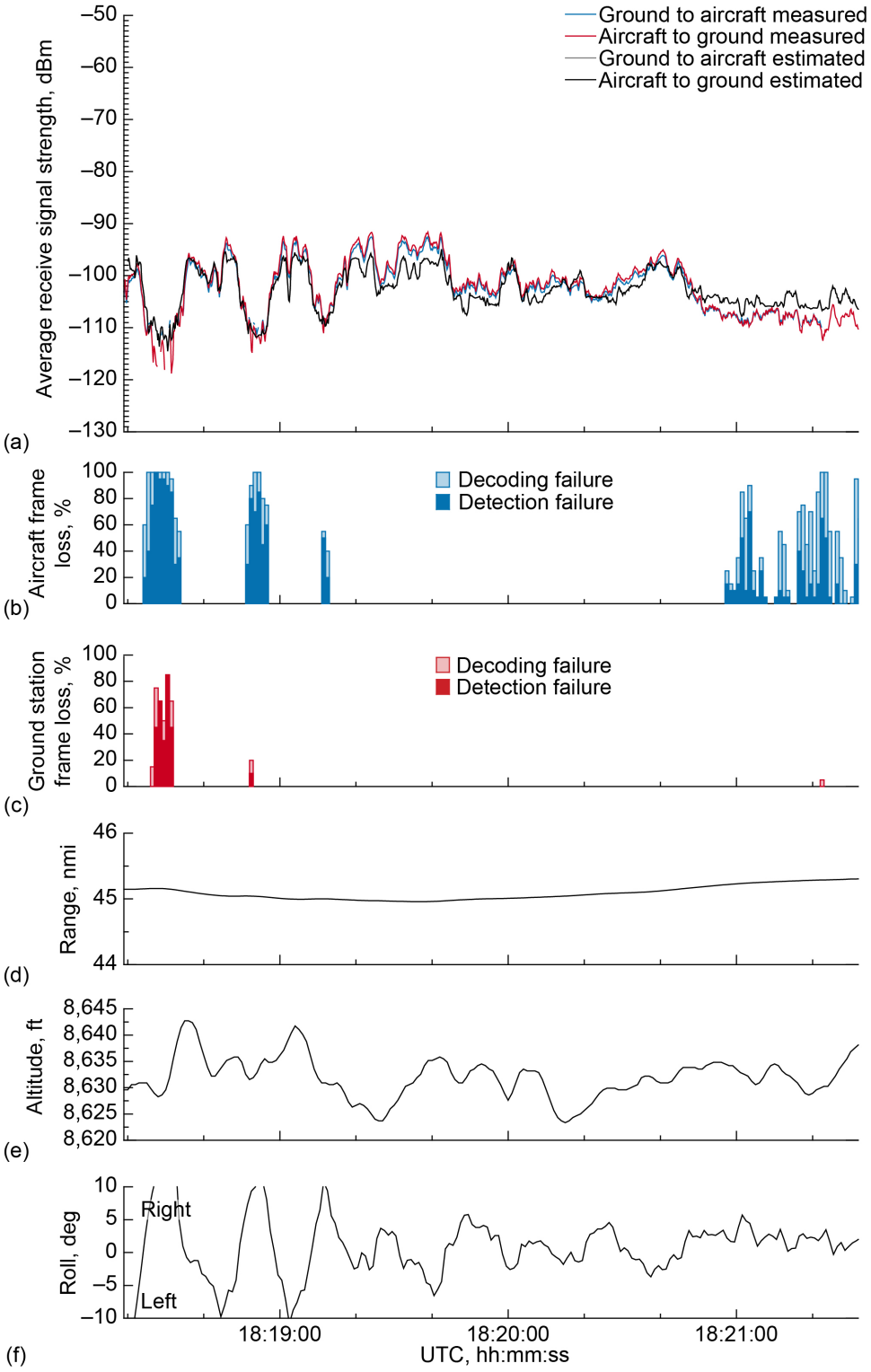

Figure 112.—Signal strength and frame loss over open freshwater at 45-nmi range and 8,500-ft altitude, 1.5° antenna elevation, traveling from waypoint F to waypoint E. (a) Average receive signal strength. (b) Aircraft frame loss. (c) Ground station frame loss. (d) Range. (e) Altitude. (f) Roll.

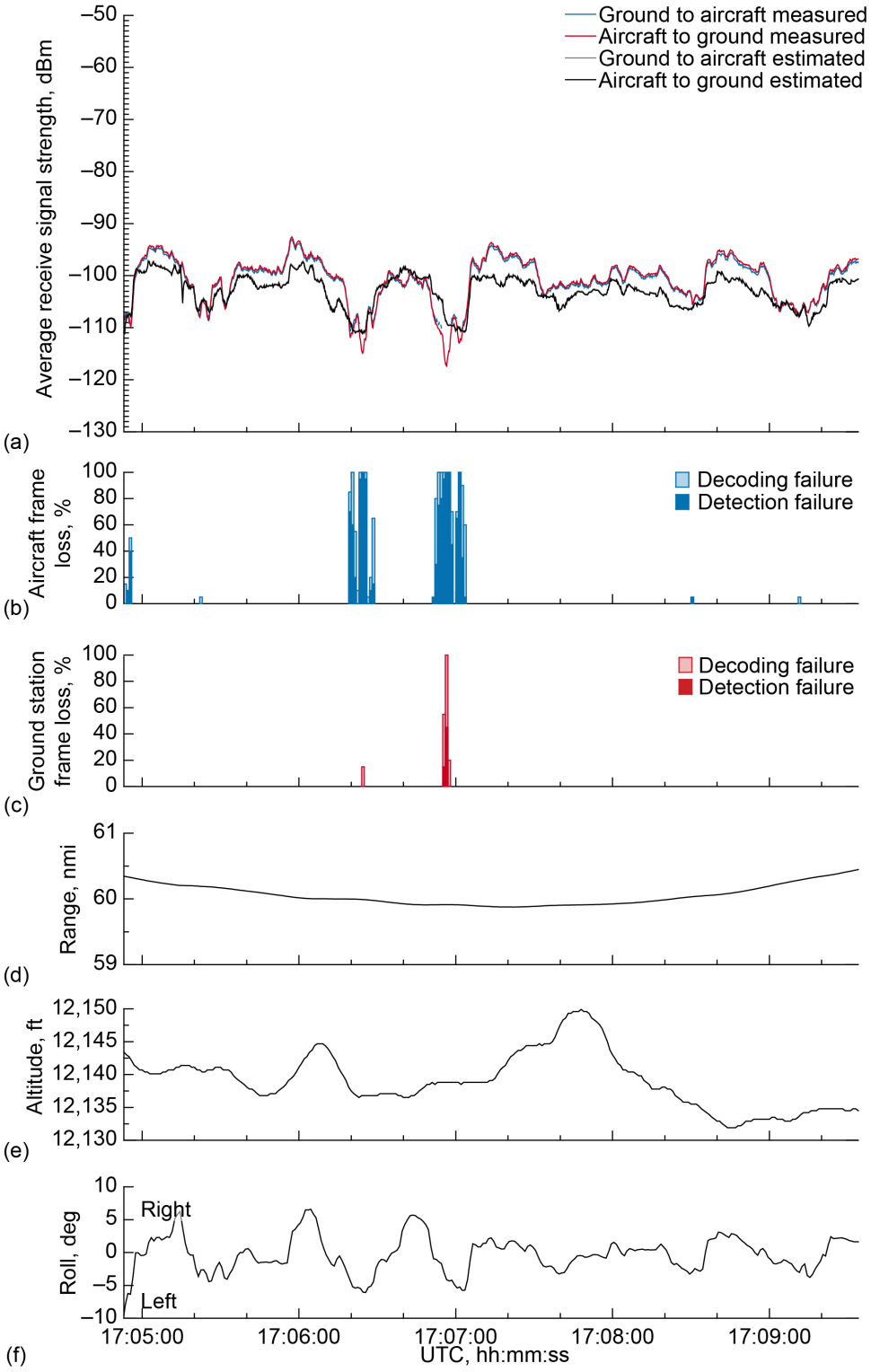

Figure 113.—Signal strength and frame loss over open freshwater at 60-nmi range and 12,000-ft altitude, 1.5° antenna elevation, traveling from waypoint G to waypoint H. (a) Average receive signal strength. (b) Aircraft frame loss. (c) Ground station frame loss. (d) Range. (e) Altitude. (f) Roll.

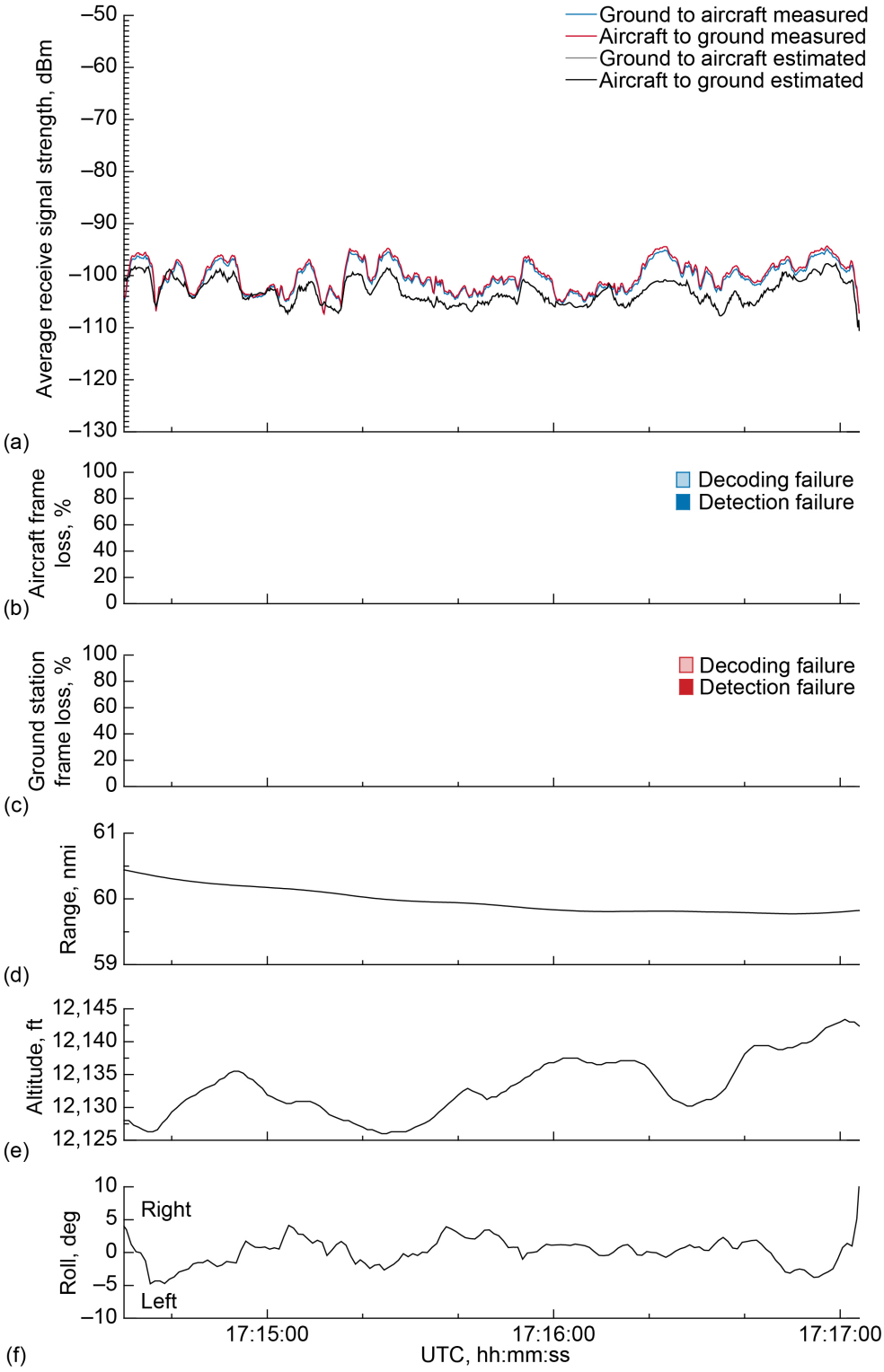

Figure 114.—Signal strength and frame loss over open freshwater at 60-nmi range and 12,000-ft altitude, 1.5° antenna elevation, traveling from waypoint H toward waypoint G. (a) Average receive signal strength. (b) Aircraft frame loss. (c) Ground station frame loss. (d) Range. (e) Altitude. (f) Roll.

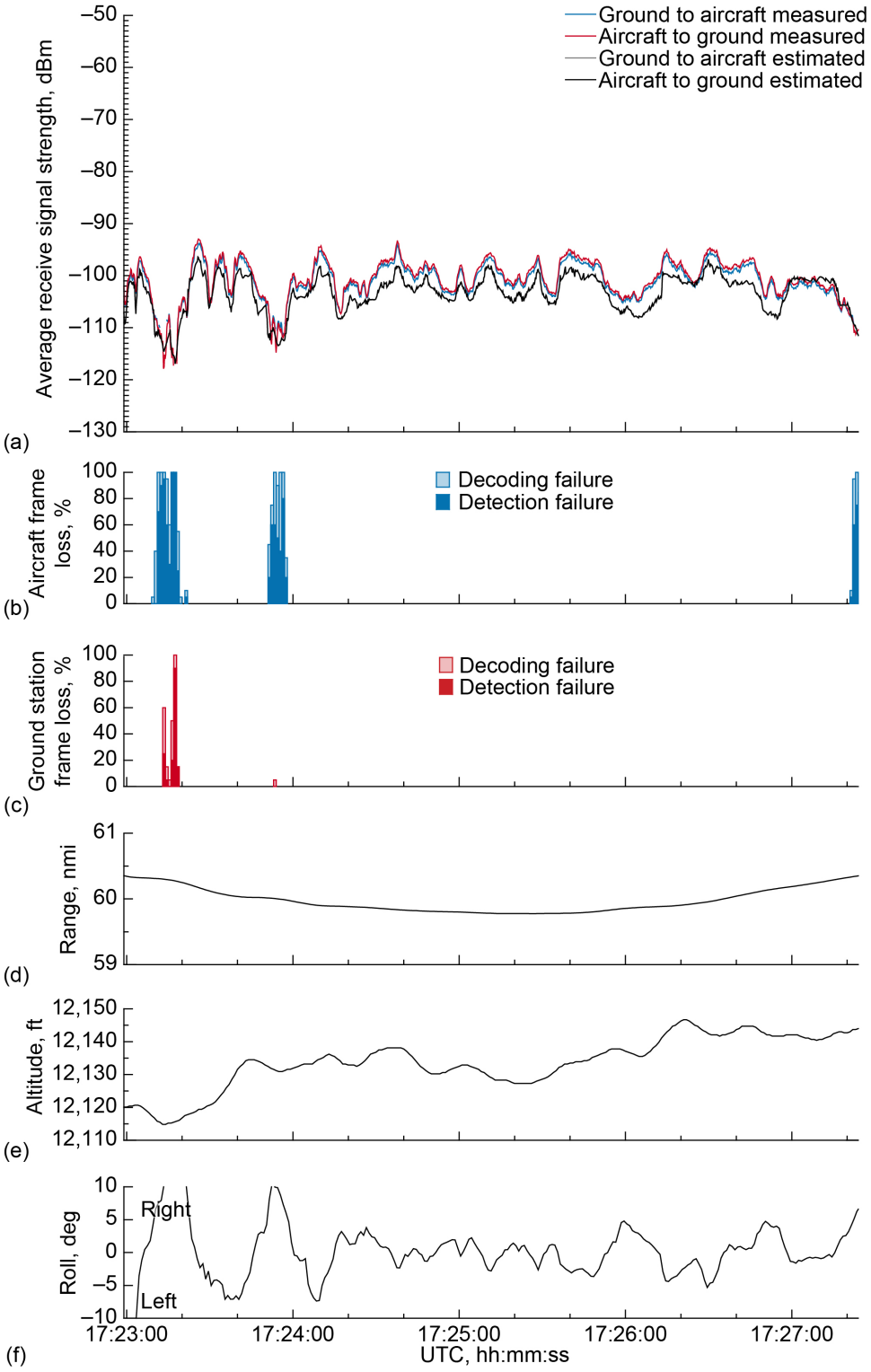

Figure 115.—Signal strength and frame loss over open freshwater at 60-nmi range and 12,000-ft altitude, 1.5° antenna elevation, traveling from waypoint H to waypoint G. (a) Average receive signal strength. (b) Aircraft frame loss. (c) Ground station frame loss. (d) Range. (e) Altitude. (f) Roll.

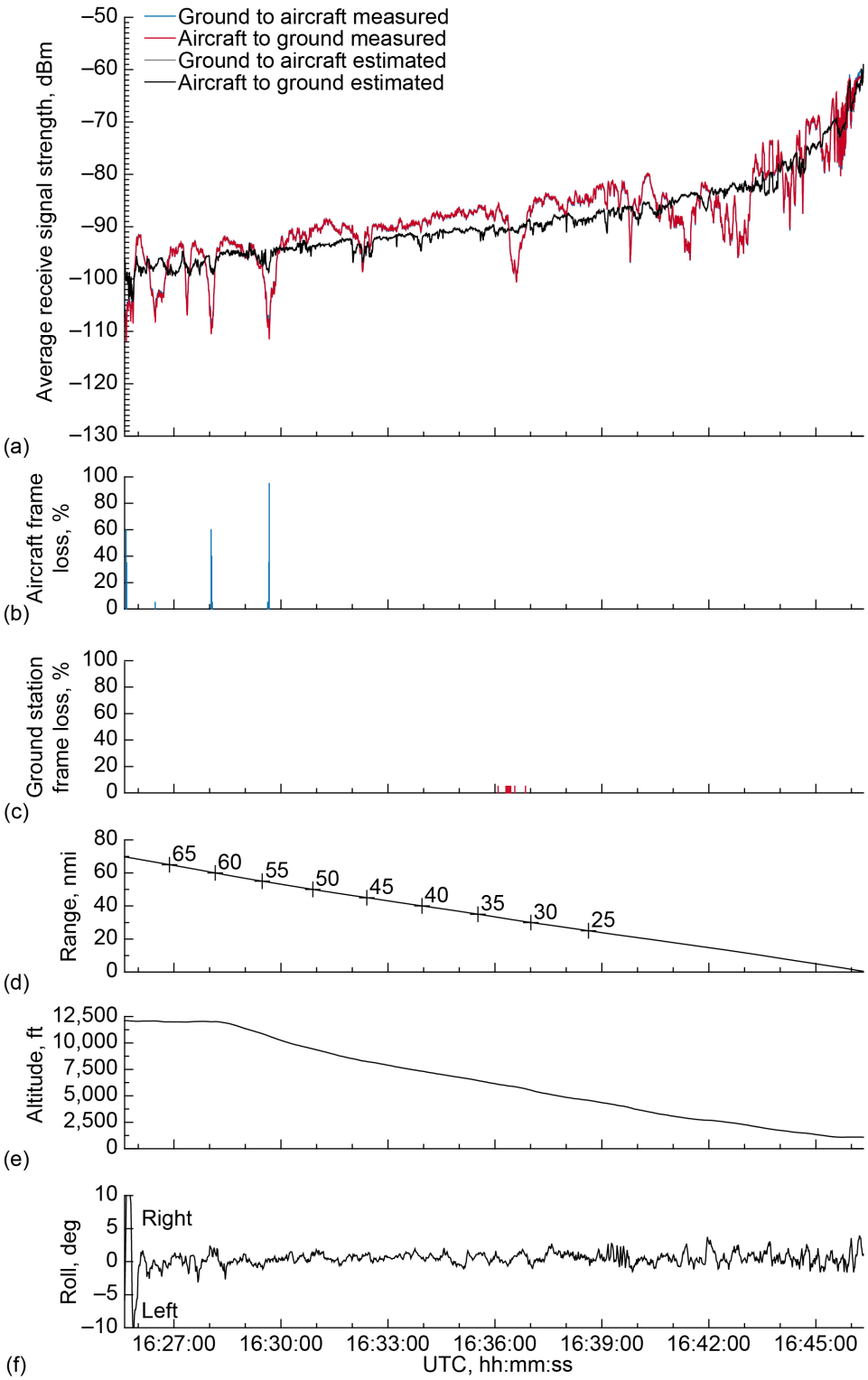

Figure 116.—Signal strength and frame loss over open freshwater during inbound, descending track on 1.5° glide slope, traveling toward ground station on December 5, 2019. (a) Average receive signal strength. (b) Aircraft frame loss. (c) Ground station frame loss. (d) Range. (e) Altitude. (f) Roll.

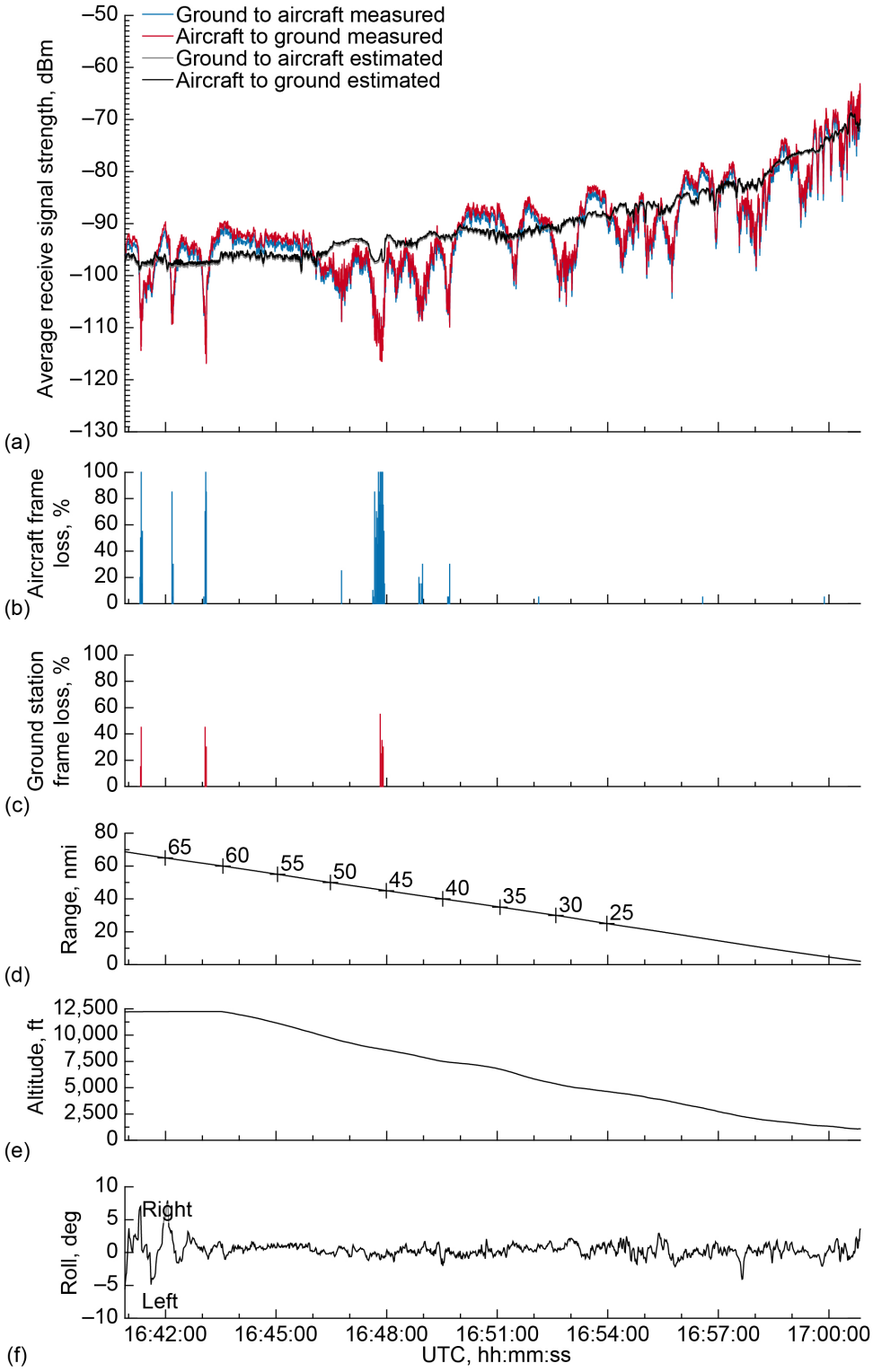

Figure 117.—Signal strength and frame loss over open freshwater during inbound, descending track on 1.5° glide slope, traveling toward ground station on December 6, 2019. (a) Average receive signal strength. (b) Aircraft frame loss. (c) Ground station frame loss. (d) Range. (e) Altitude. (f) Roll.

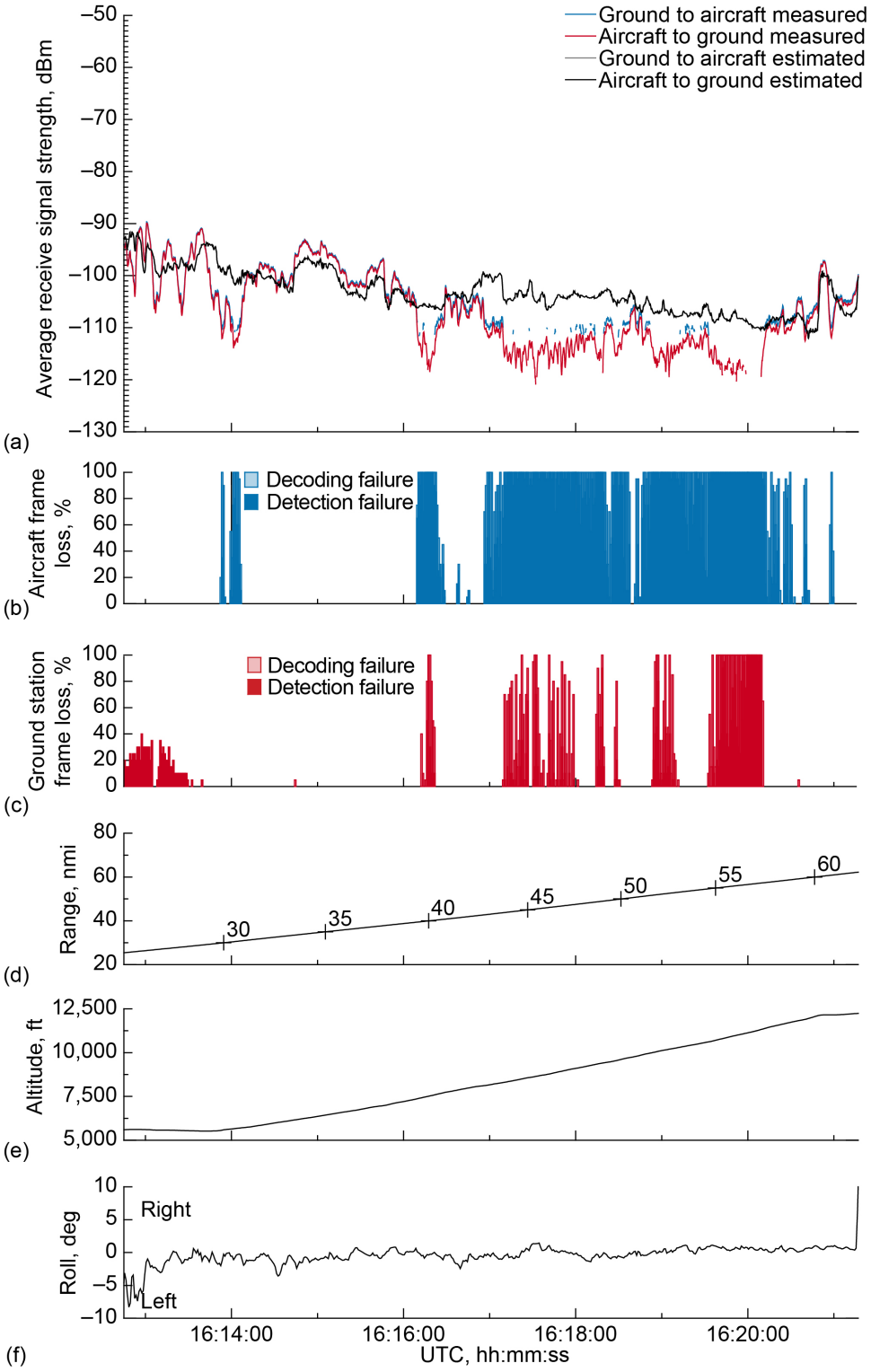

Figure 118.—Signal strength and frame loss over open freshwater during partial outbound, ascending track on 1.5° glide slope, traveling away from ground station from later in flight on December 5, 2019. (a) Average receive signal strength. (b) Aircraft frame loss. (c) Ground station frame loss. (d) Range. (e) Altitude. (f) Roll.

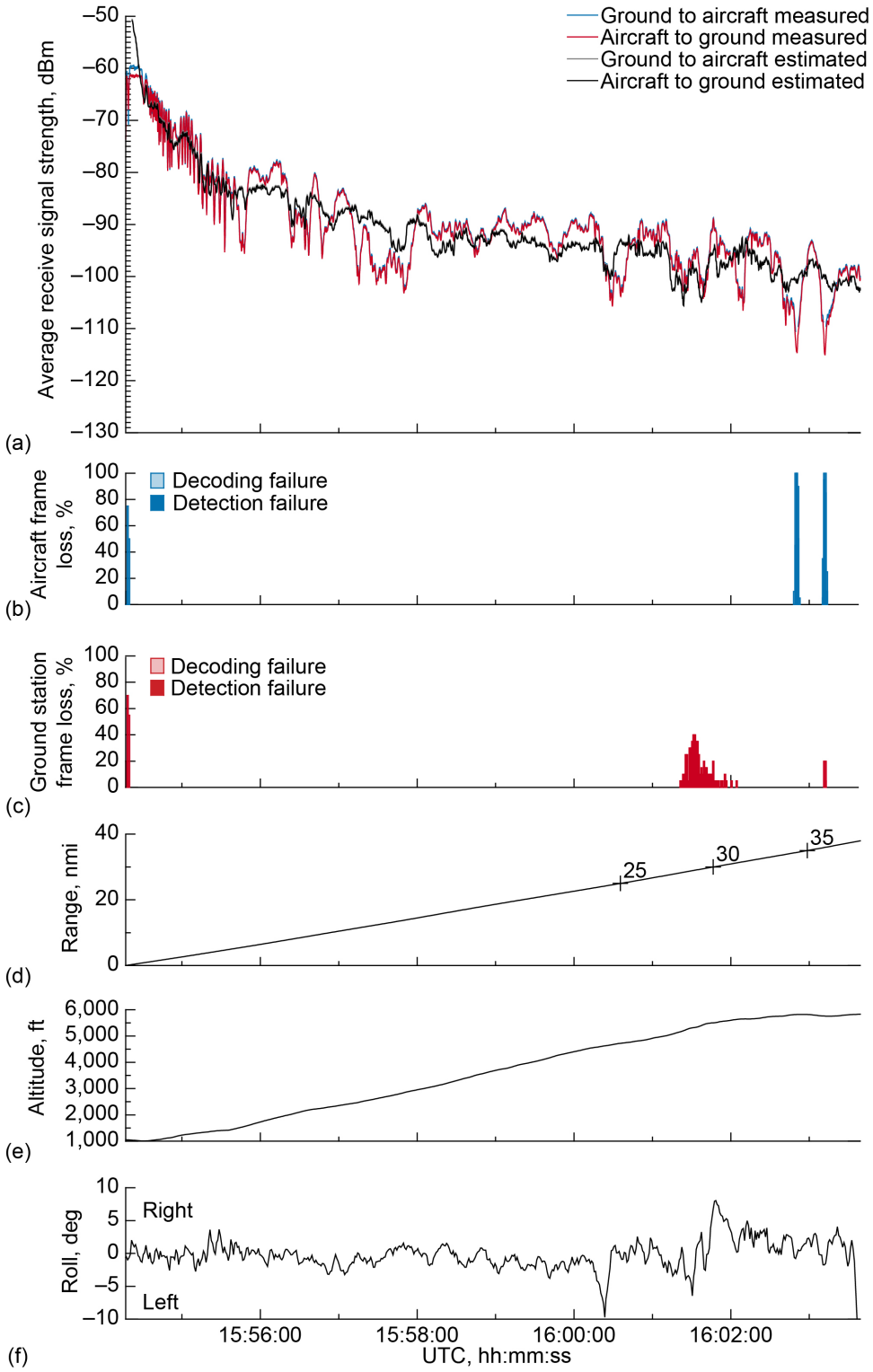

Figure 119.—Signal strength and frame loss over open freshwater during partial outbound, ascending track on 1.5° glide slope, traveling away from ground station from early in flight on December 5, 2019. (a) Average receive signal strength. (b) Aircraft frame loss. (c) Ground station frame loss. (d) Range. (e) Altitude. (f) Roll.

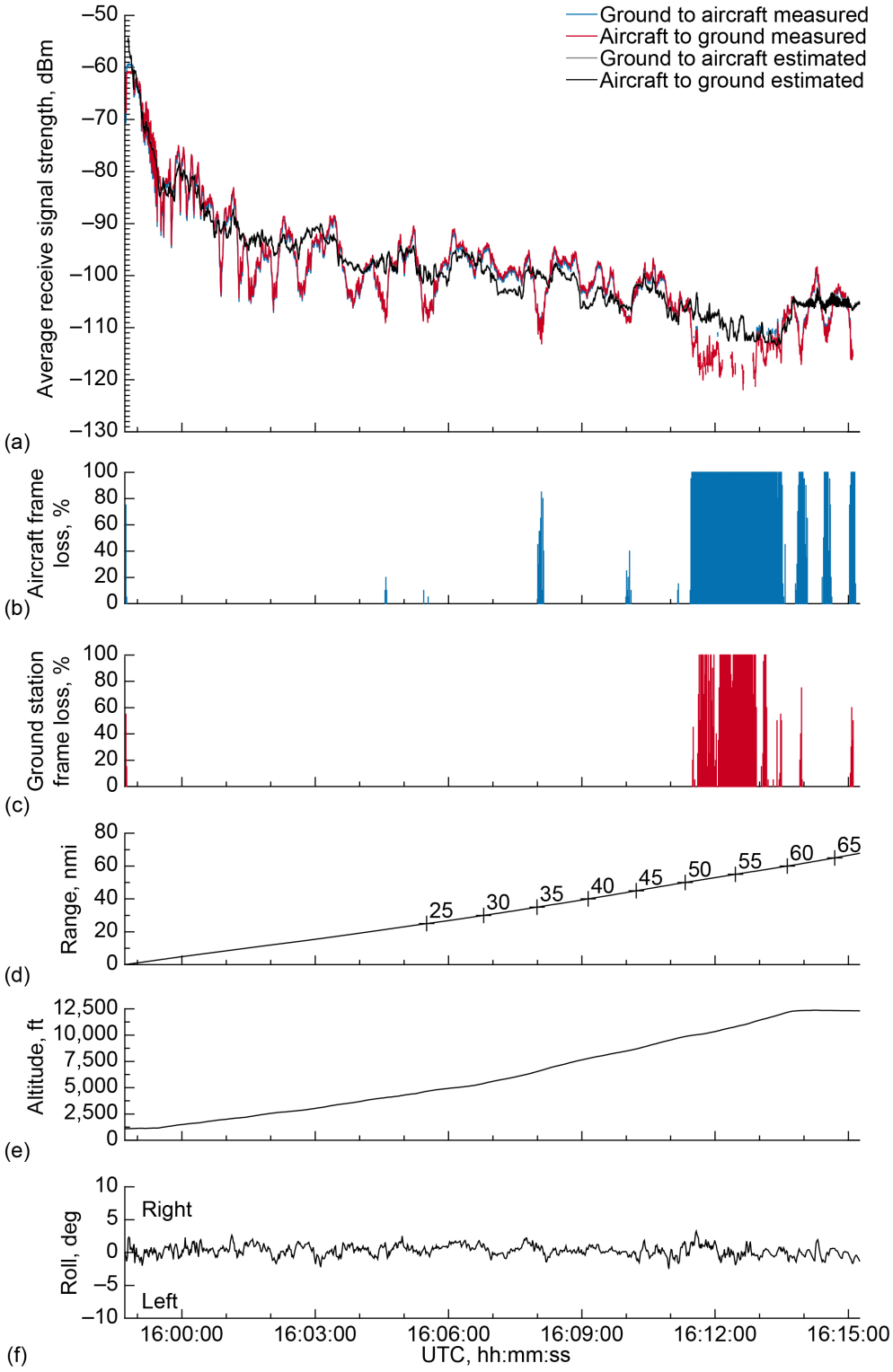

Figure 120.—Signal strength and frame loss over open freshwater during outbound, ascending track on 1.5° glide slope, traveling away from ground station on December 6, 2019. (a) Average receive signal strength. (b) Aircraft frame loss. (c) Ground station frame loss. (d) Range. (e) Altitude. (f) Roll.

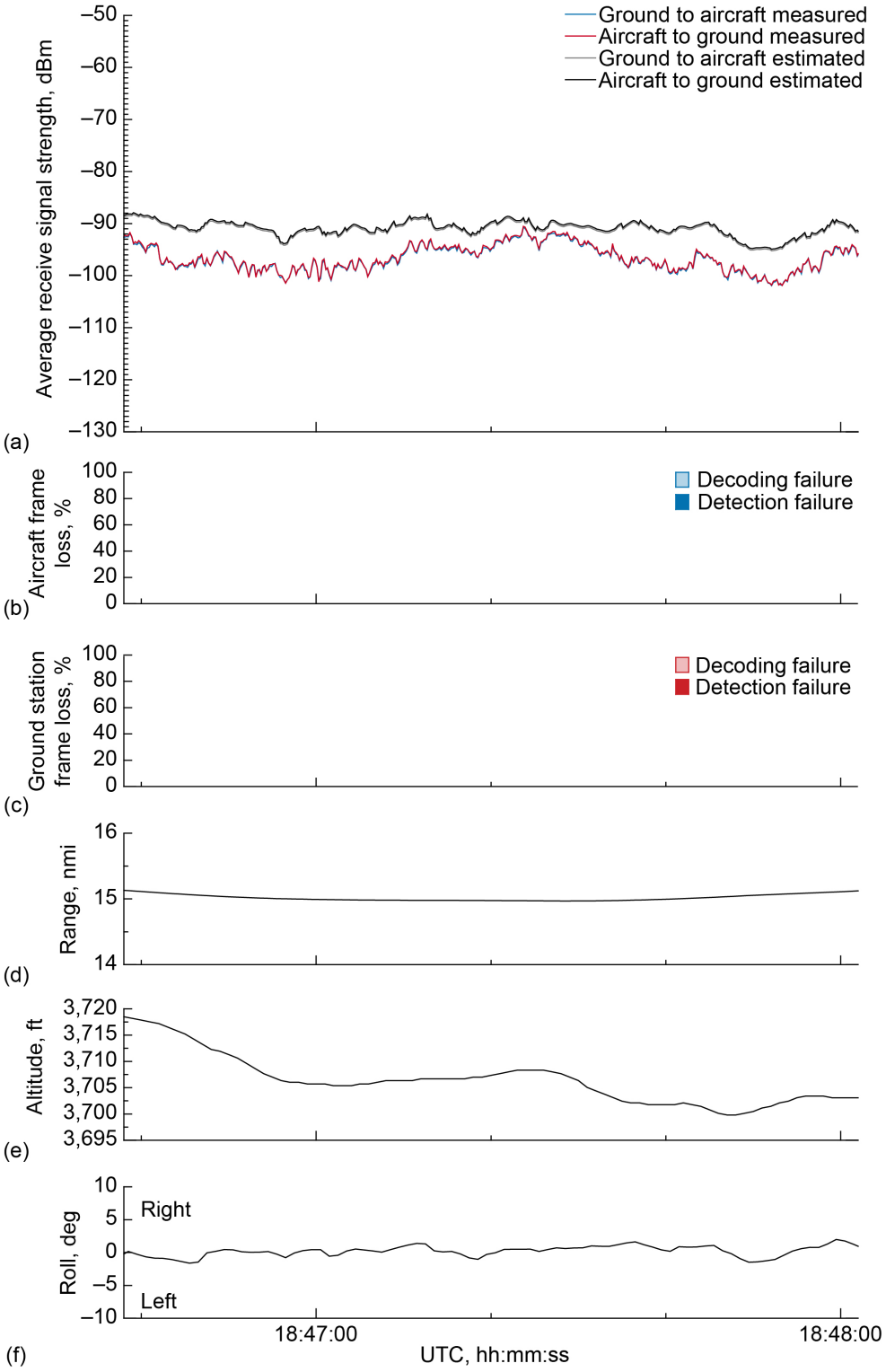

Figure 121.—Signal strength and frame loss over open freshwater at 15-nmi range and 3,500-ft altitude, 2.0° antenna elevation, traveling from waypoint A to waypoint B. (a) Average receive signal strength. (b) Aircraft frame loss. (c) Ground station frame loss. (d) Range. (e) Altitude. (f) Roll.

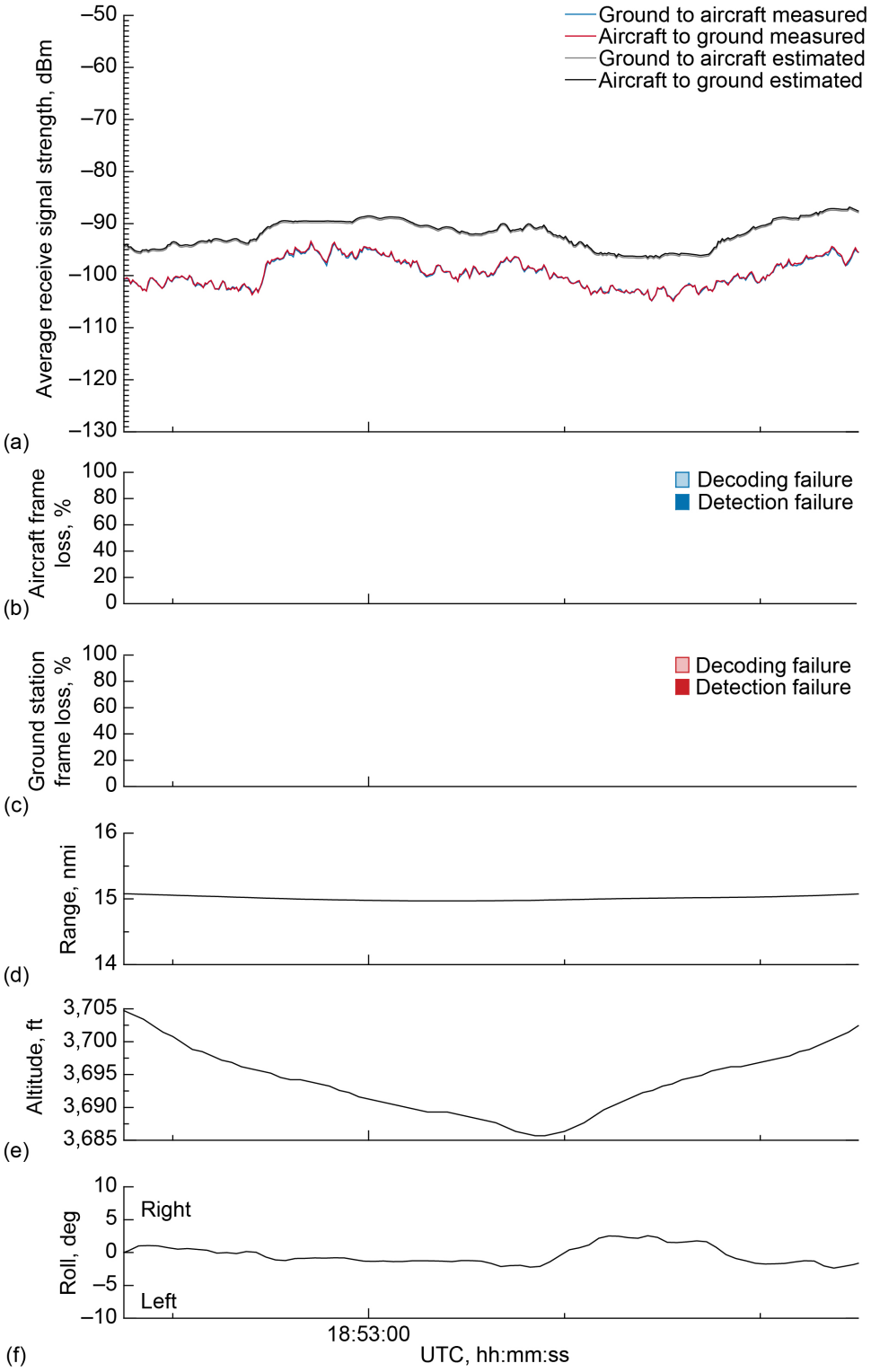

Figure 122.—Signal strength and frame loss over open freshwater at 15-nmi range and 3,500-ft altitude, 2.0° antenna elevation, traveling from waypoint B to waypoint A. (a) Average receive signal strength. (b) Aircraft frame loss. (c) Ground station frame loss. (d) Range. (e) Altitude. (f) Roll.

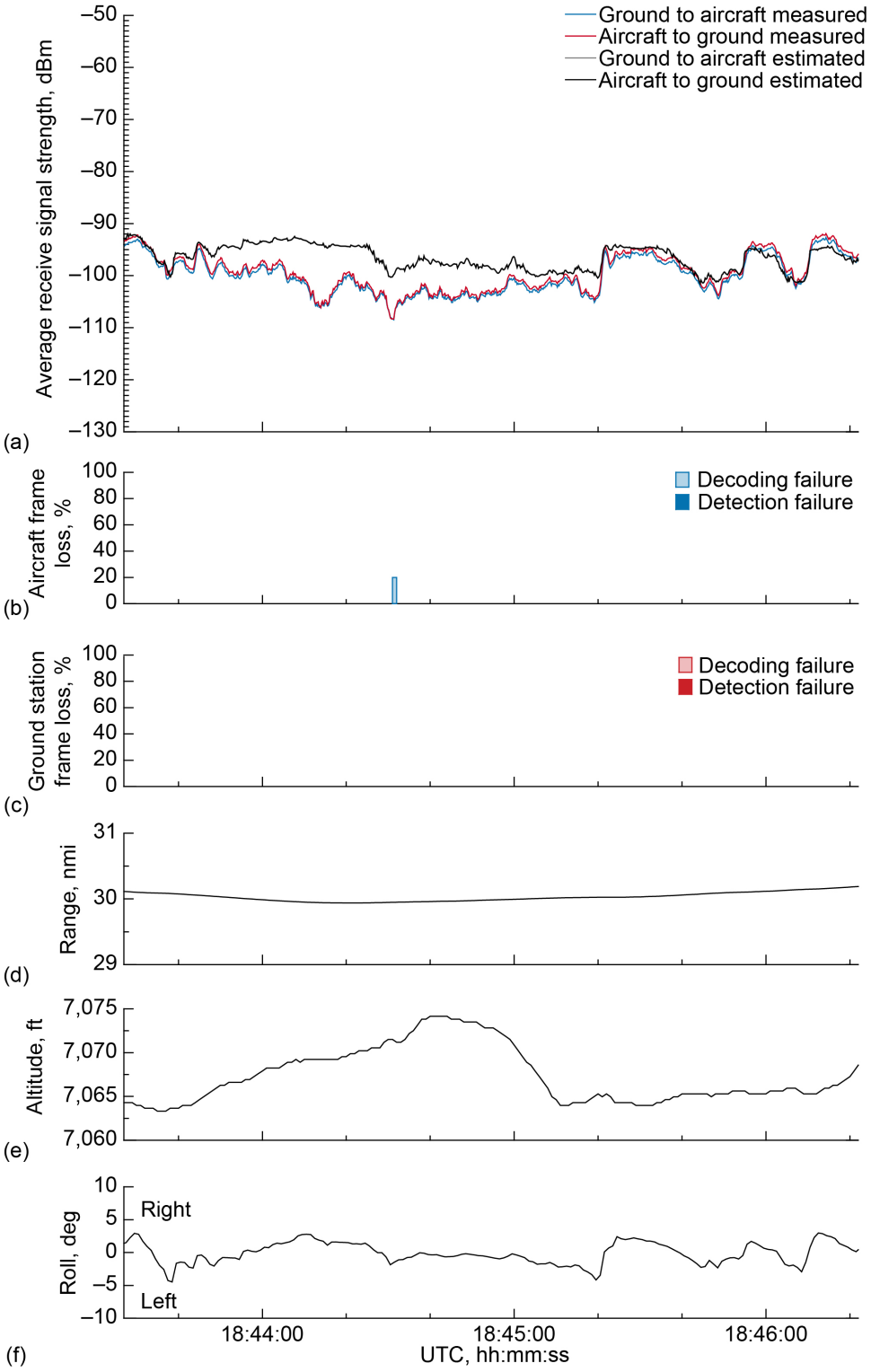

Figure 123.—Signal strength and frame loss over open freshwater at 30-nmi range and 7,000-ft altitude, 2.0° antenna elevation, traveling from waypoint C to waypoint D. (a) Average receive signal strength. (b) Aircraft frame loss. (c) Ground station frame loss. (d) Range. (e) Altitude. (f) Roll.

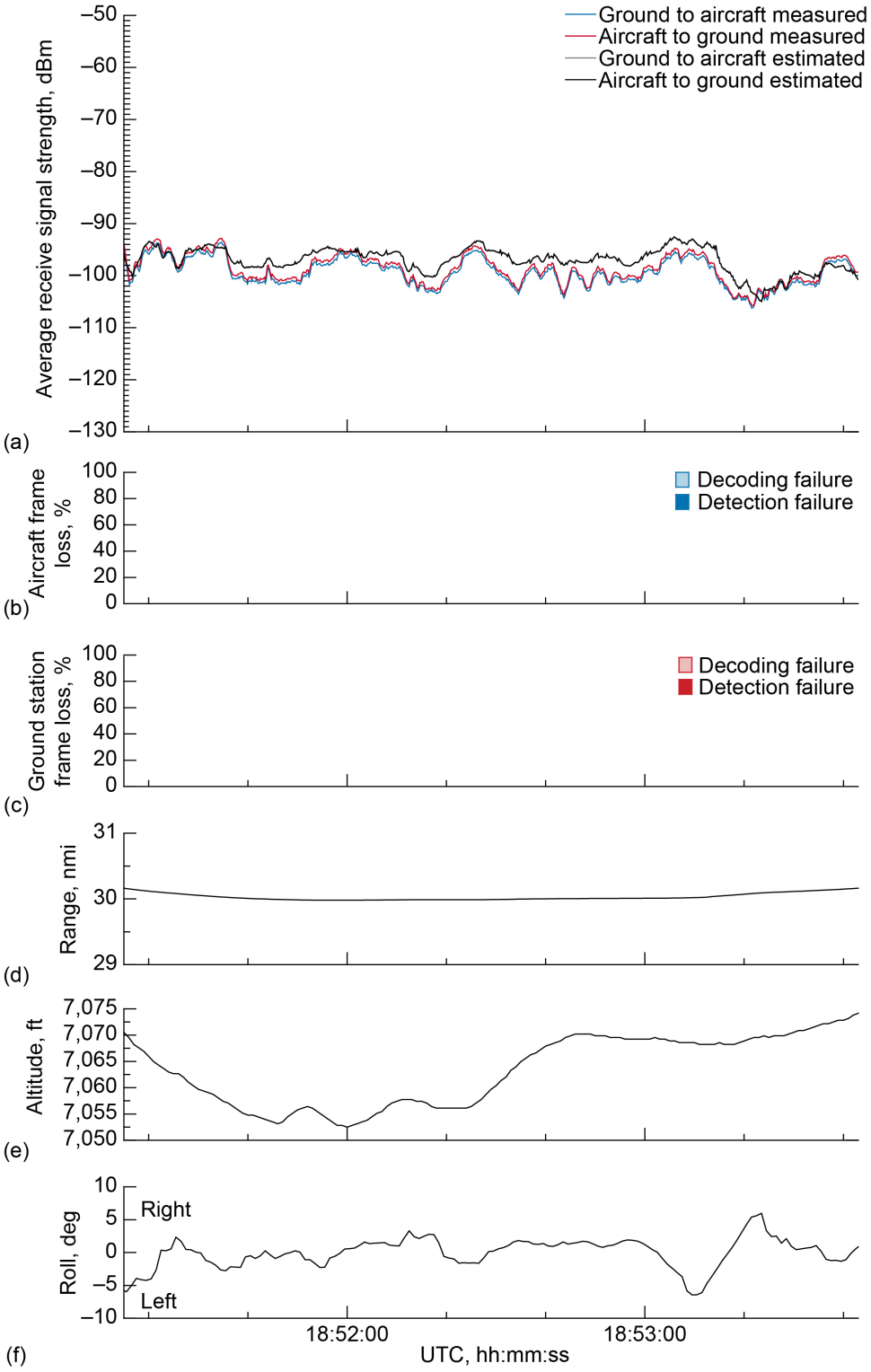

Figure 124.—Signal strength and frame loss over open freshwater at 30-nmi range and 7,000-ft altitude, 2.0° antenna elevation, traveling from waypoint D to waypoint C. (a) Average receive signal strength. (b) Aircraft frame loss. (c) Ground station frame loss. (d) Range. (e) Altitude. (f) Roll.

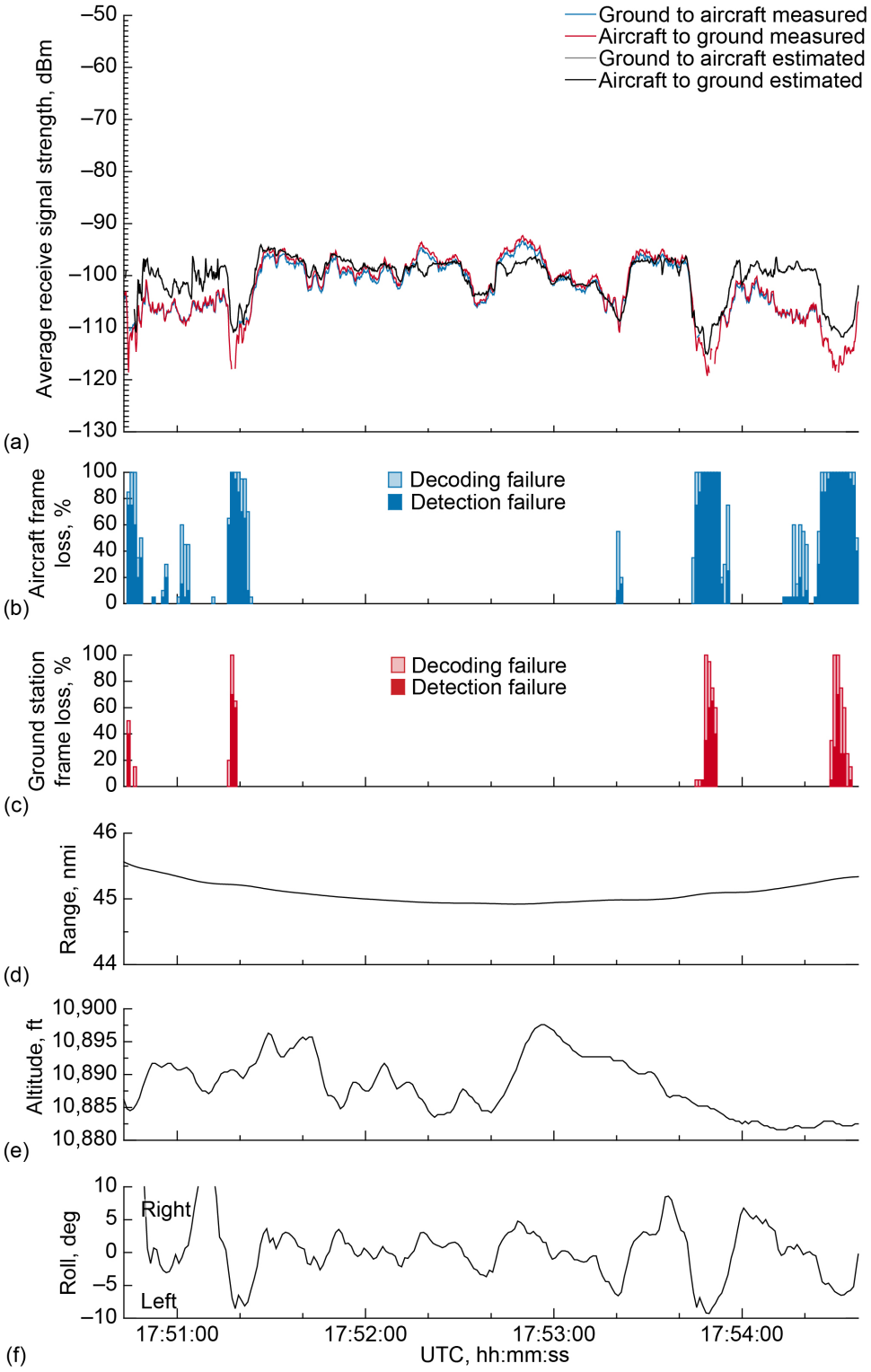

Figure 125.—Signal strength and frame loss over open freshwater at 45-nmi range and 11,000-ft altitude, 2.0° antenna elevation, traveling from waypoint E to waypoint F on December 3, 2019. (a) Average receive signal strength. (b) Aircraft frame loss. (c) Ground station frame loss. (d) Range. (e) Altitude. (f) Roll.

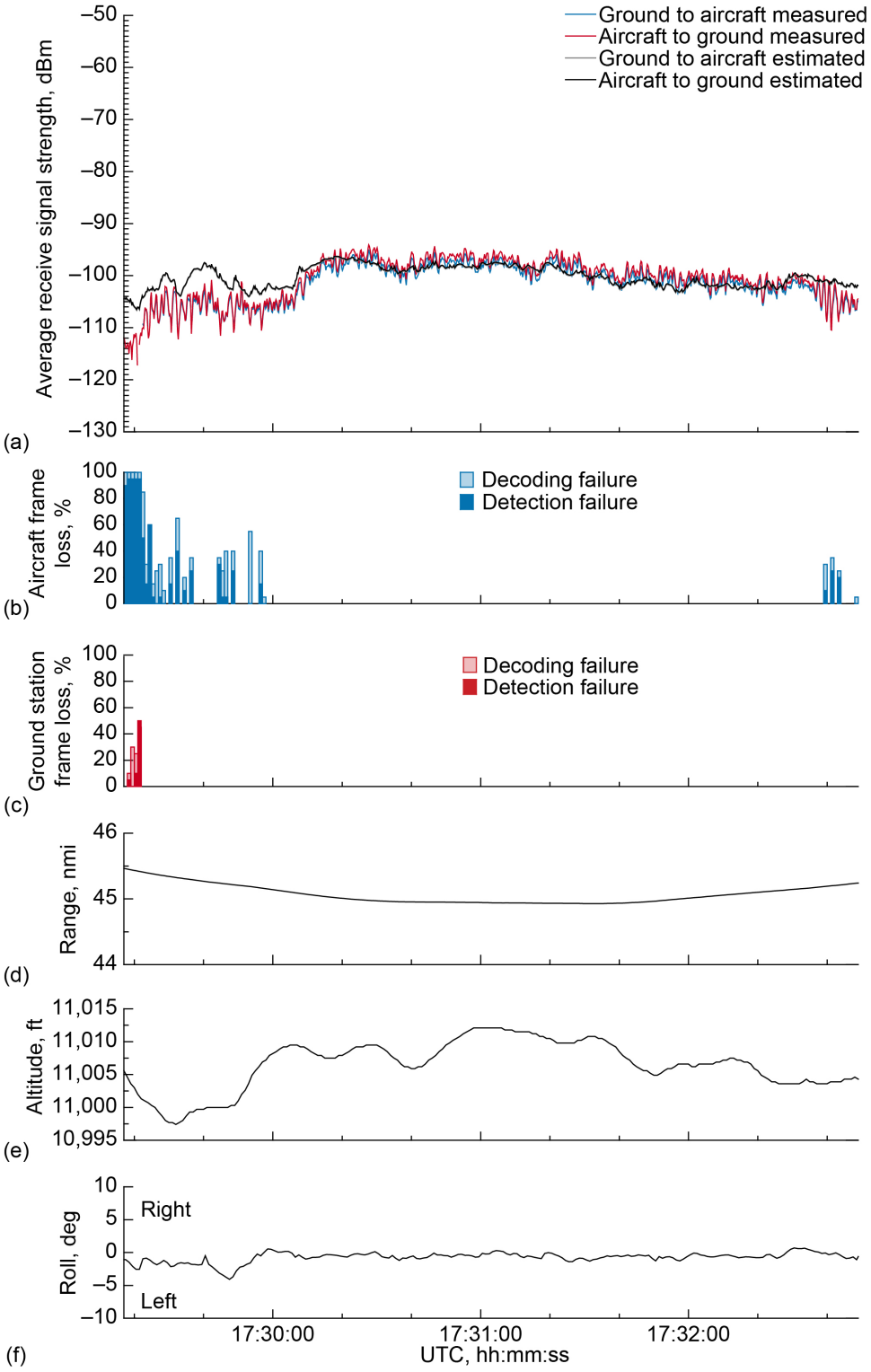

Figure 126.—Signal strength and frame loss over open freshwater at 45-nmi range and 11,000-ft altitude, 2.0° antenna elevation, traveling from waypoint E to waypoint F on December 6, 2019. (a) Average receive signal strength. (b) Aircraft frame loss. (c) Ground station frame loss. (d) Range. (e) Altitude. (f) Roll.

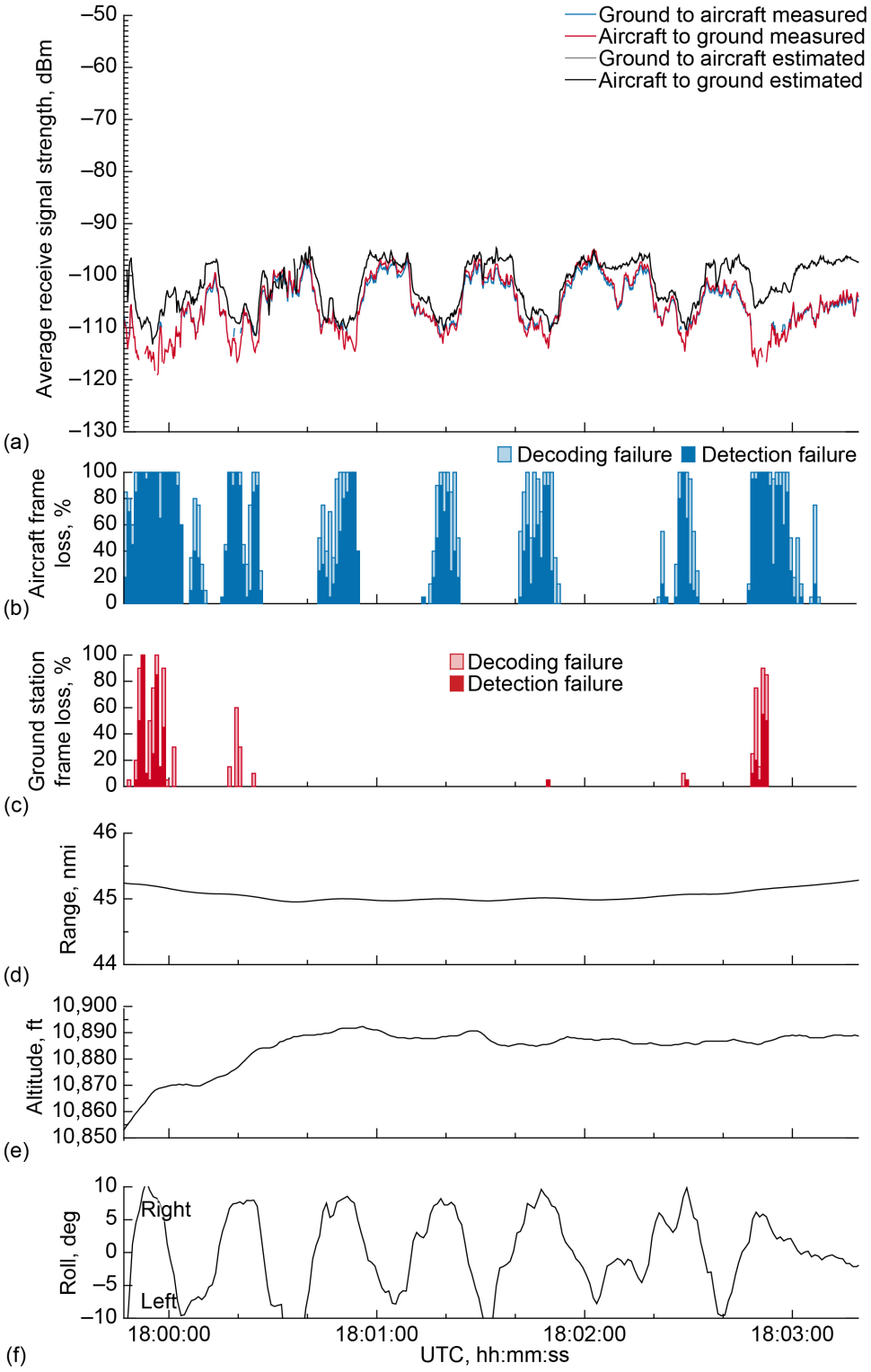

Figure 127.—Signal strength and frame loss over open freshwater at 45-nmi range and 11,000-ft altitude, 2.0° antenna elevation, traveling from waypoint F to waypoint E. (a) Average receive signal strength. (b) Aircraft frame loss. (c) Ground station frame loss. (d) Range. (e) Altitude. (f) Roll.

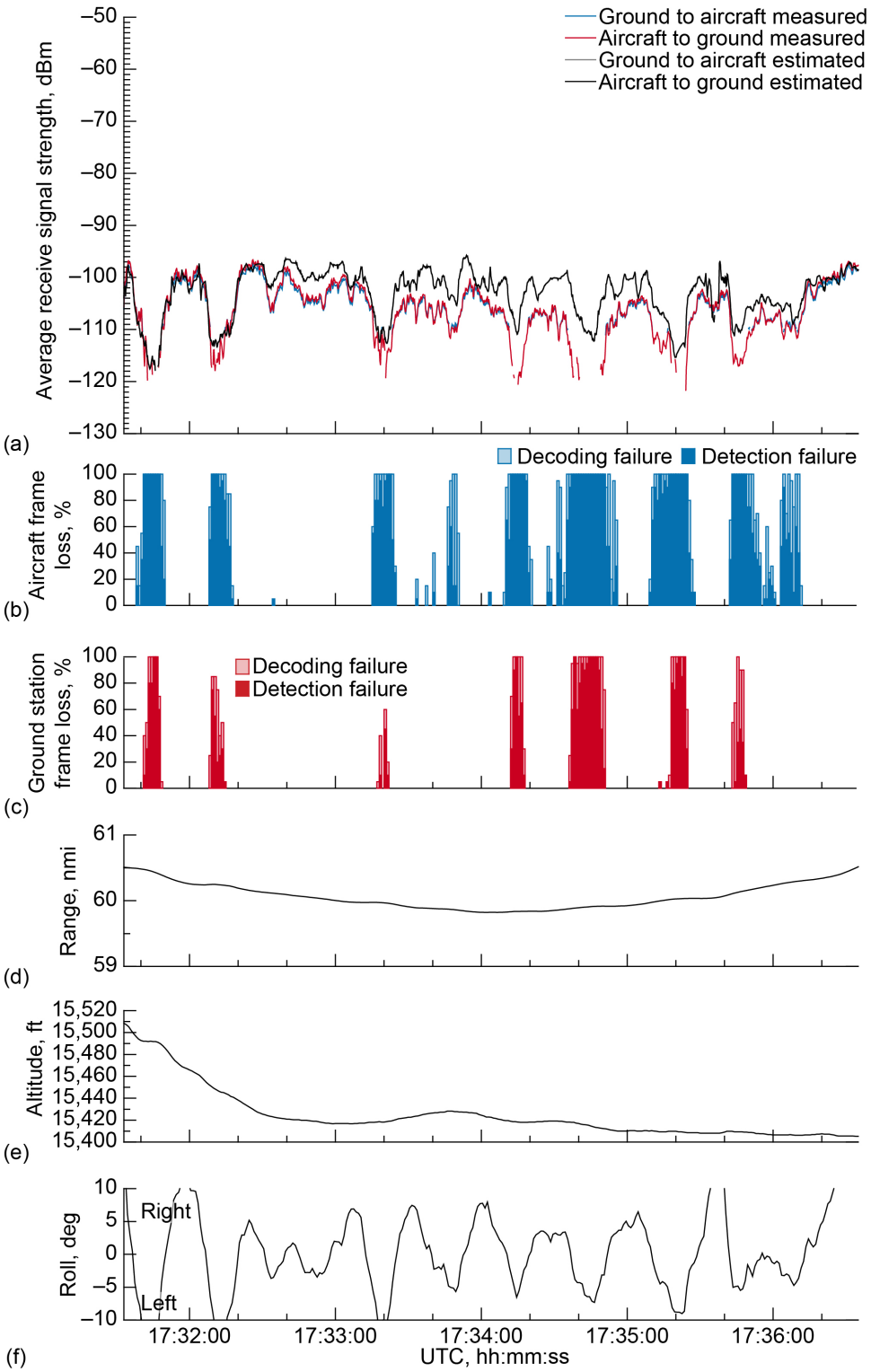

Figure 128.—Signal strength and frame loss over open freshwater at 60-nmi range and 15,500-ft altitude, 2.0° antenna elevation, traveling from waypoint G to waypoint H on December 3, 2019. (a) Average receive signal strength. (b) Aircraft frame loss. (c) Ground station frame loss. (d) Range. (e) Altitude. (f) Roll.

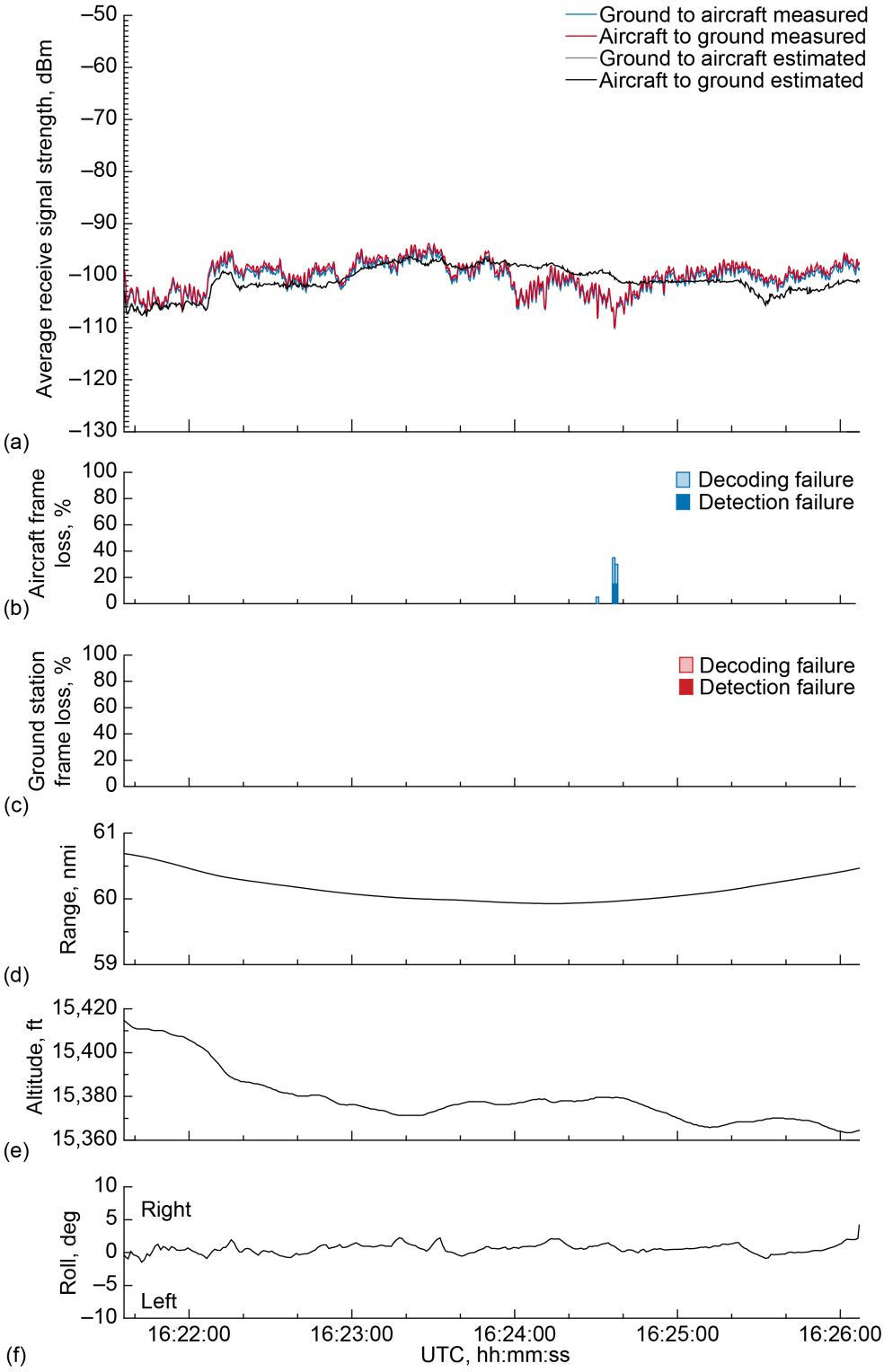

Figure 129.—Signal strength and frame loss over open freshwater at 60-nmi range and 15,500-ft altitude, 2.0° antenna elevation, traveling from waypoint G to waypoint H on December 6, 2019. (a) Average receive signal strength. (b) Aircraft frame loss. (c) Ground station frame loss. (d) Range. (e) Altitude. (f) Roll.

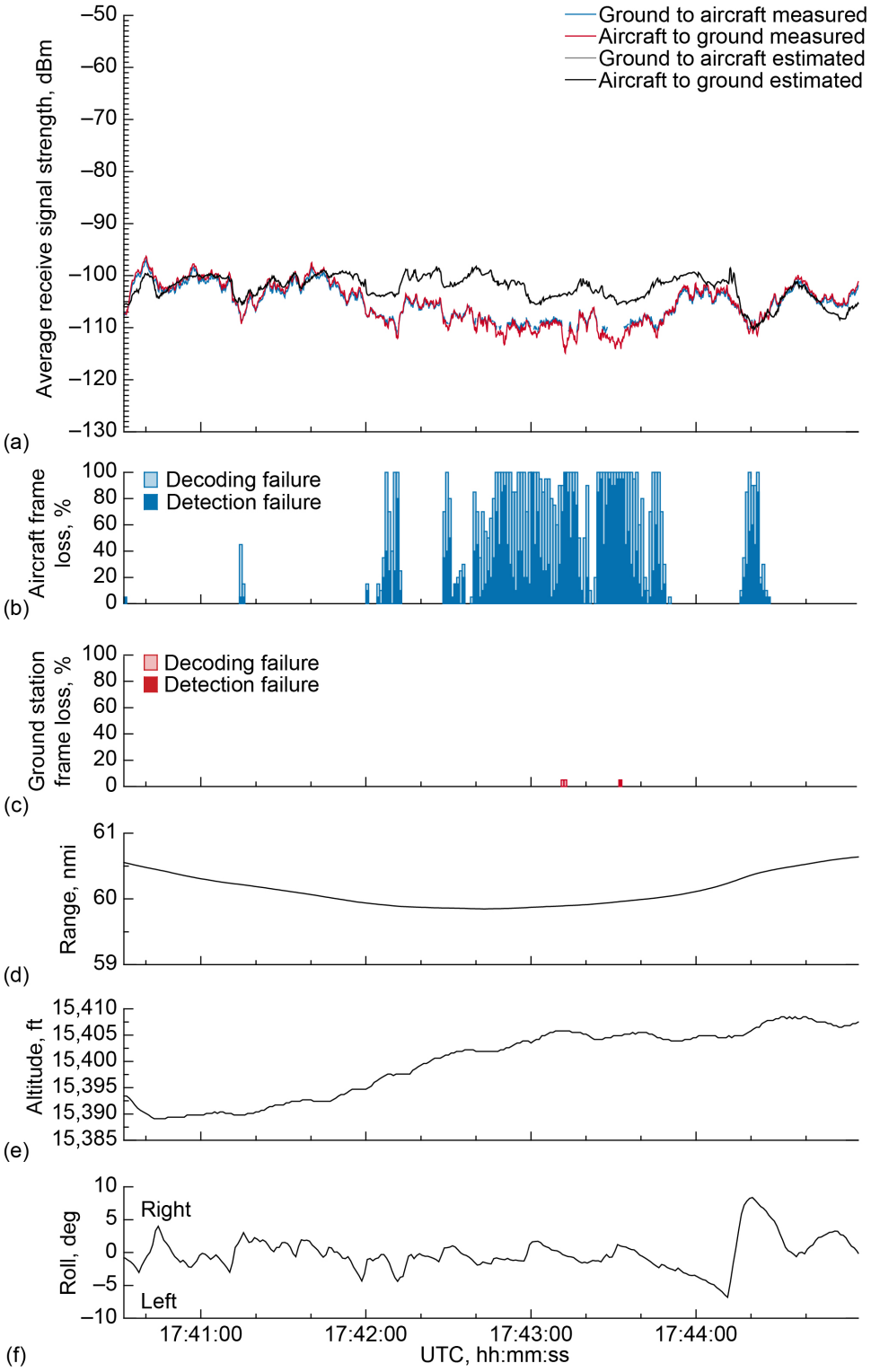

Figure 130.—Signal strength and frame loss over open freshwater at 60-nmi range and 15,500-ft altitude, 2.0° antenna elevation, traveling from waypoint H to waypoint G on December 3, 2019. (a) Average receive signal strength. (b) Aircraft frame loss. (c) Ground station frame loss. (d) Range. (e) Altitude. (f) Roll.

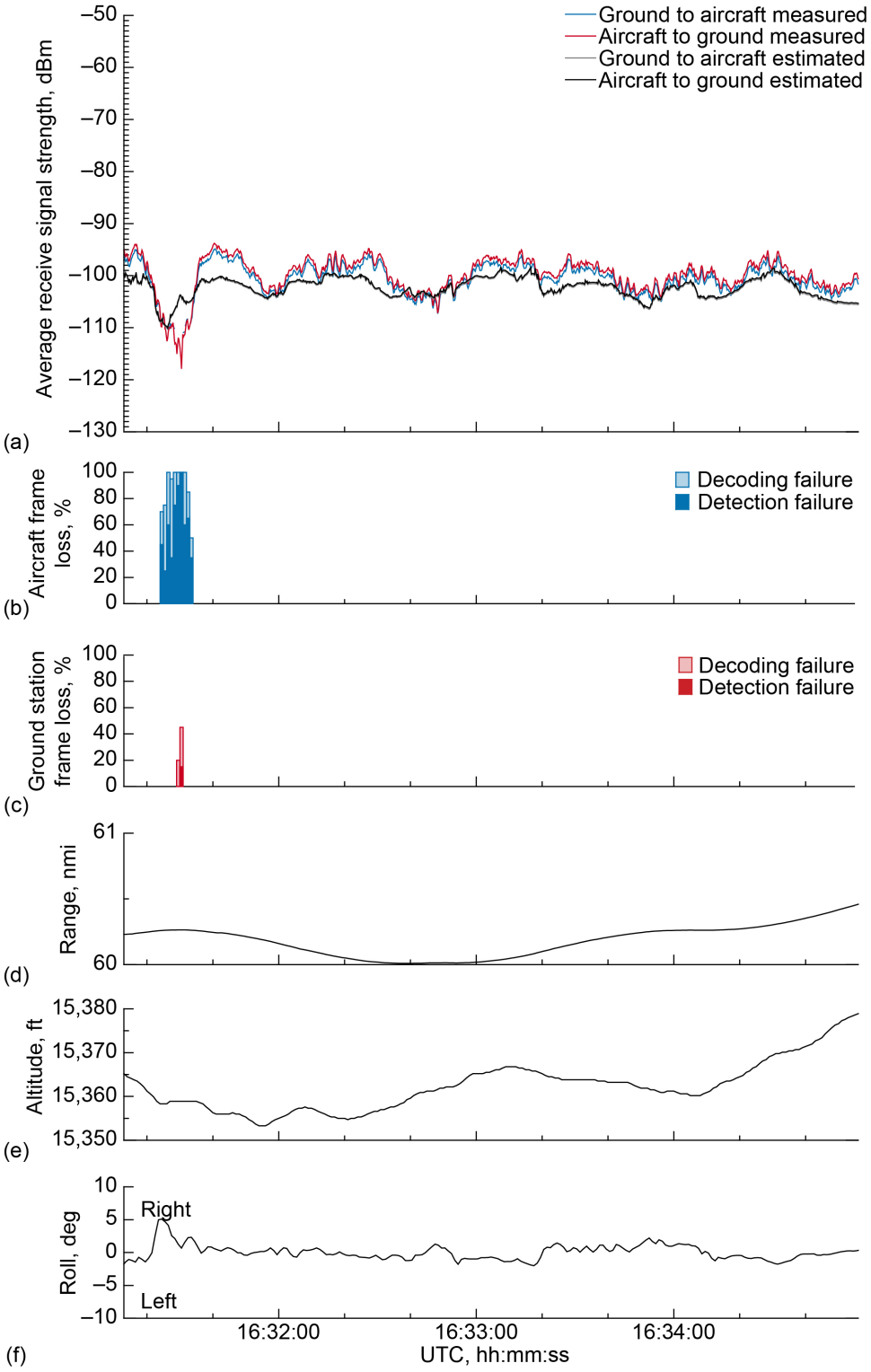

Figure 131.—Signal strength and frame loss over open freshwater at 60-nmi range and 15,500-ft altitude, 2.0° antenna elevation, traveling from waypoint H to waypoint G on December 6, 2019. (a) Average receive signal strength. (b) Aircraft frame loss. (c) Ground station frame loss. (d) Range. (e) Altitude. (f) Roll.

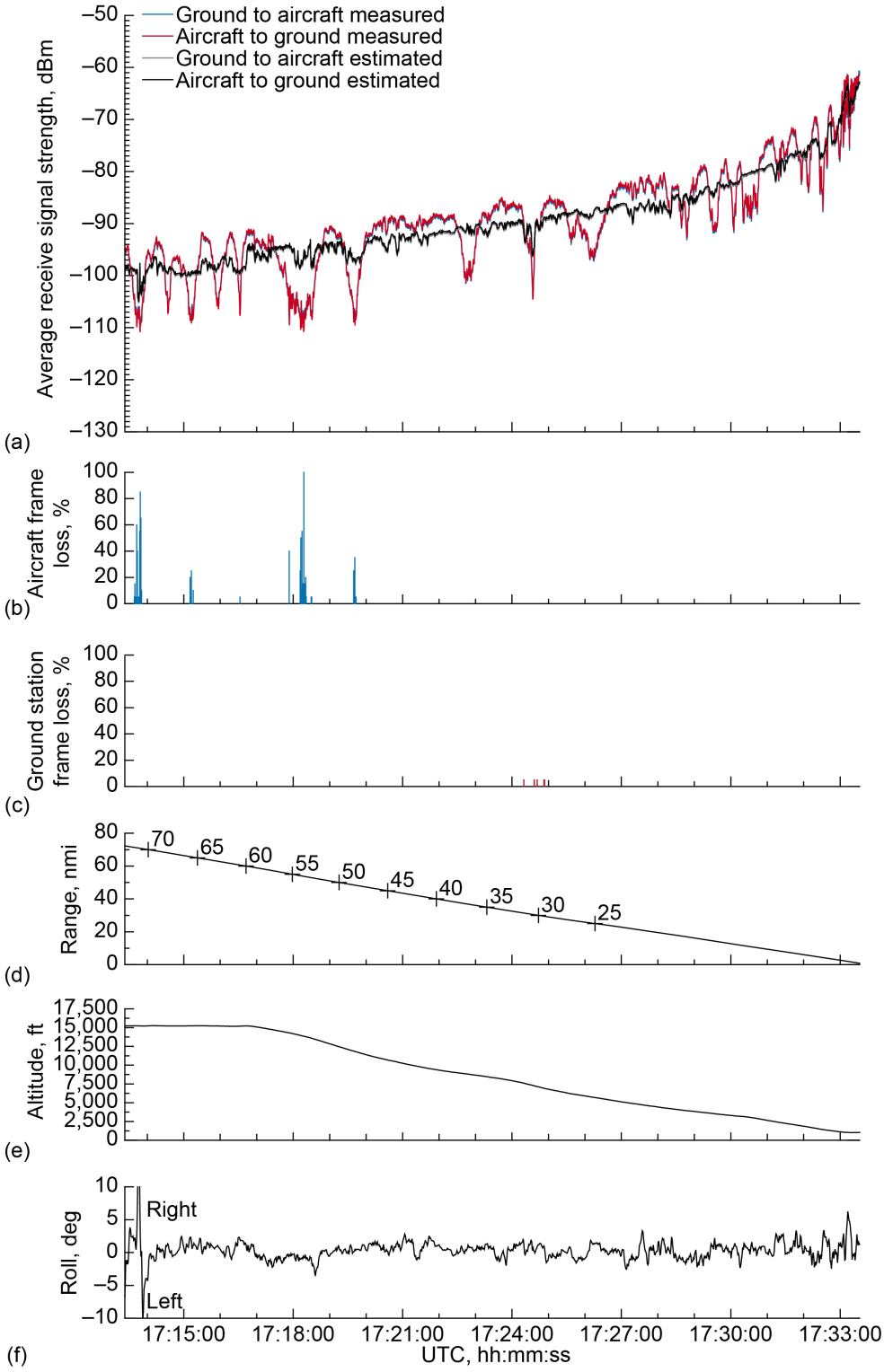

Figure 132.—Signal strength and frame loss over open freshwater during inbound, descending track on 2.0° glide slope, traveling toward ground station. (a) Average receive signal strength. (b) Aircraft frame loss. (c) Ground station frame loss. (d) Range. (e) Altitude. (f) Roll.

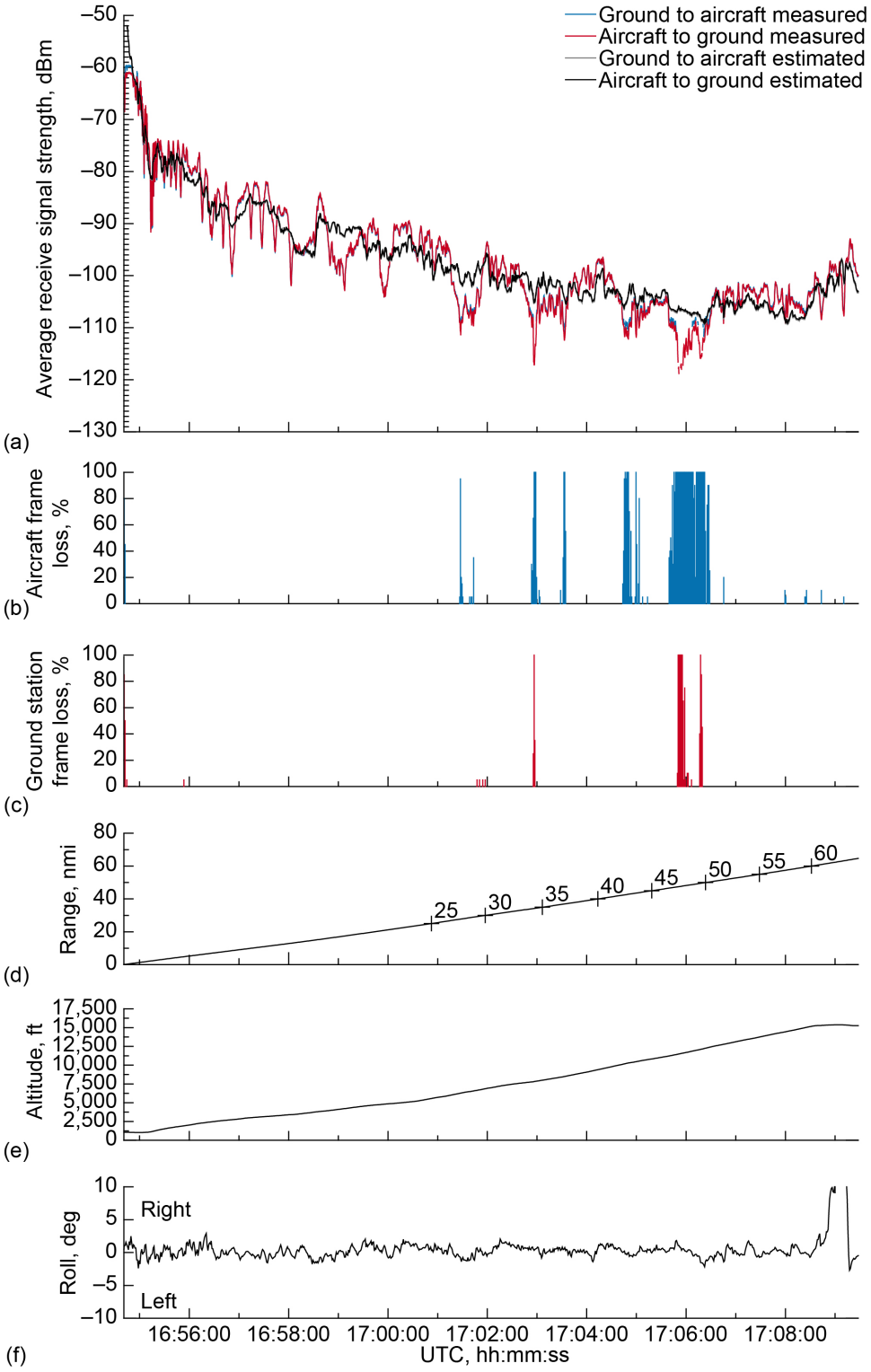

Figure 133.—Signal strength and frame loss over open freshwater during outbound, ascending track on 2.0° glide slope, traveling away from ground station. (a) Average receive signal strength. (b) Aircraft frame loss. (c) Ground station frame loss. (d) Range. (e) Altitude. (f) Roll.

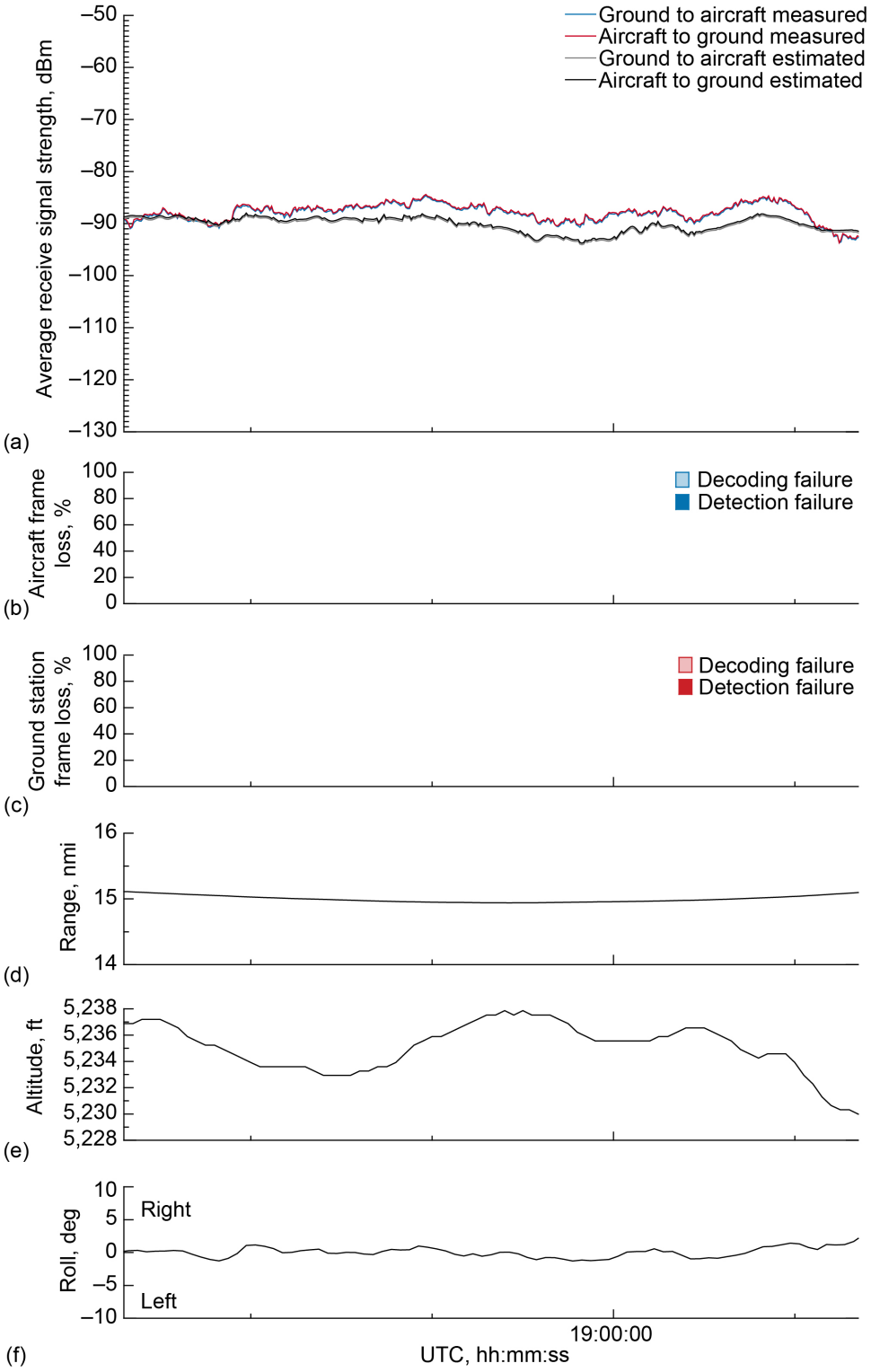

Figure 134.—Signal strength and frame loss over open freshwater at 15-nmi range and 5,000-ft altitude, 3.0° antenna elevation, traveling from waypoint A to waypoint B. (a) Average receive signal strength. (b) Aircraft frame loss. (c) Ground station frame loss. (d) Range. (e) Altitude. (f) Roll.

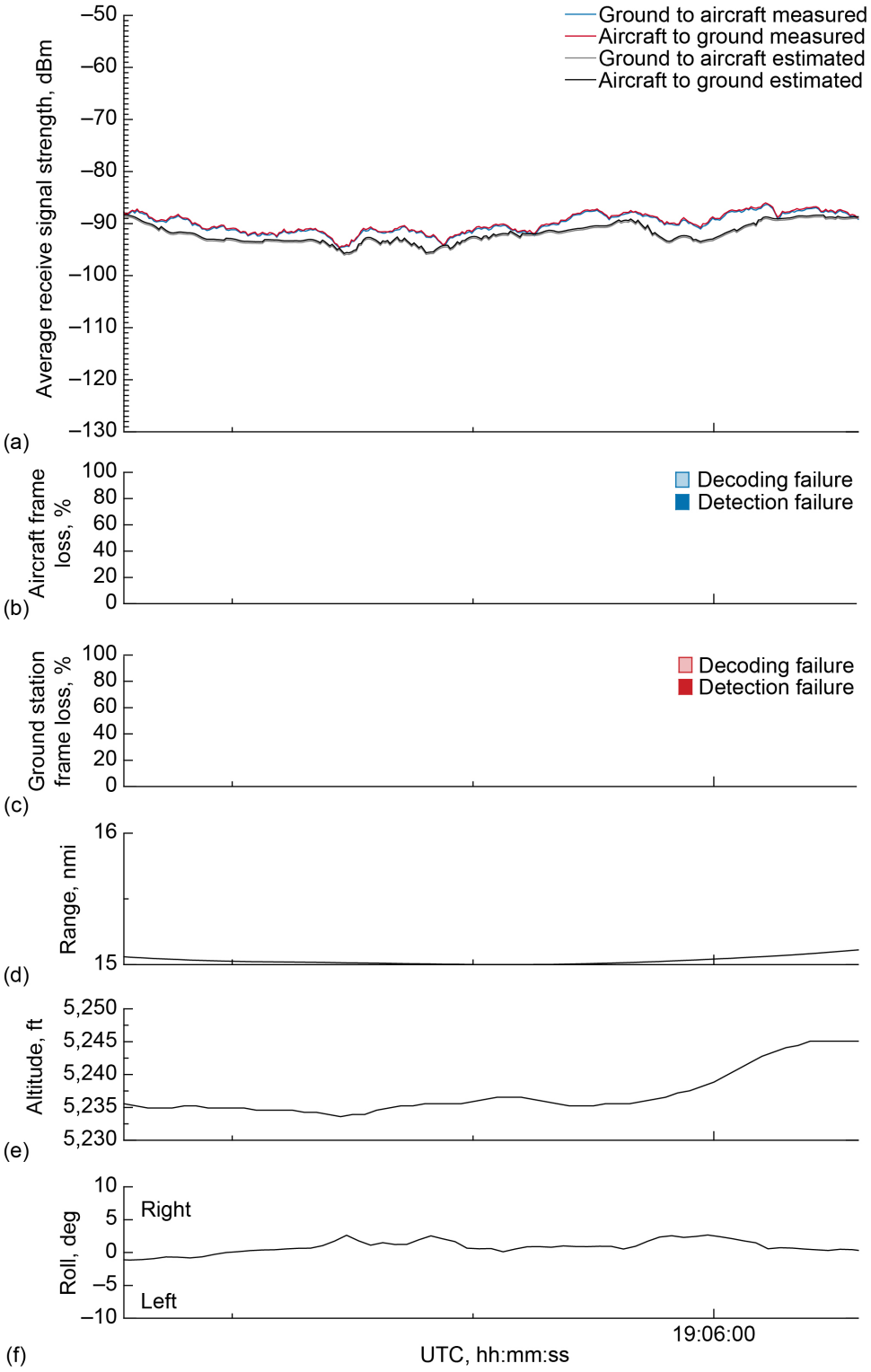

Figure 135.—Signal strength and frame loss over open freshwater at 15-nmi range and 5,000-ft altitude, 3.0° antenna elevation, traveling from waypoint B to waypoint A. (a) Average receive signal strength. (b) Aircraft frame loss. (c) Ground station frame loss. (d) Range. (e) Altitude. (f) Roll.

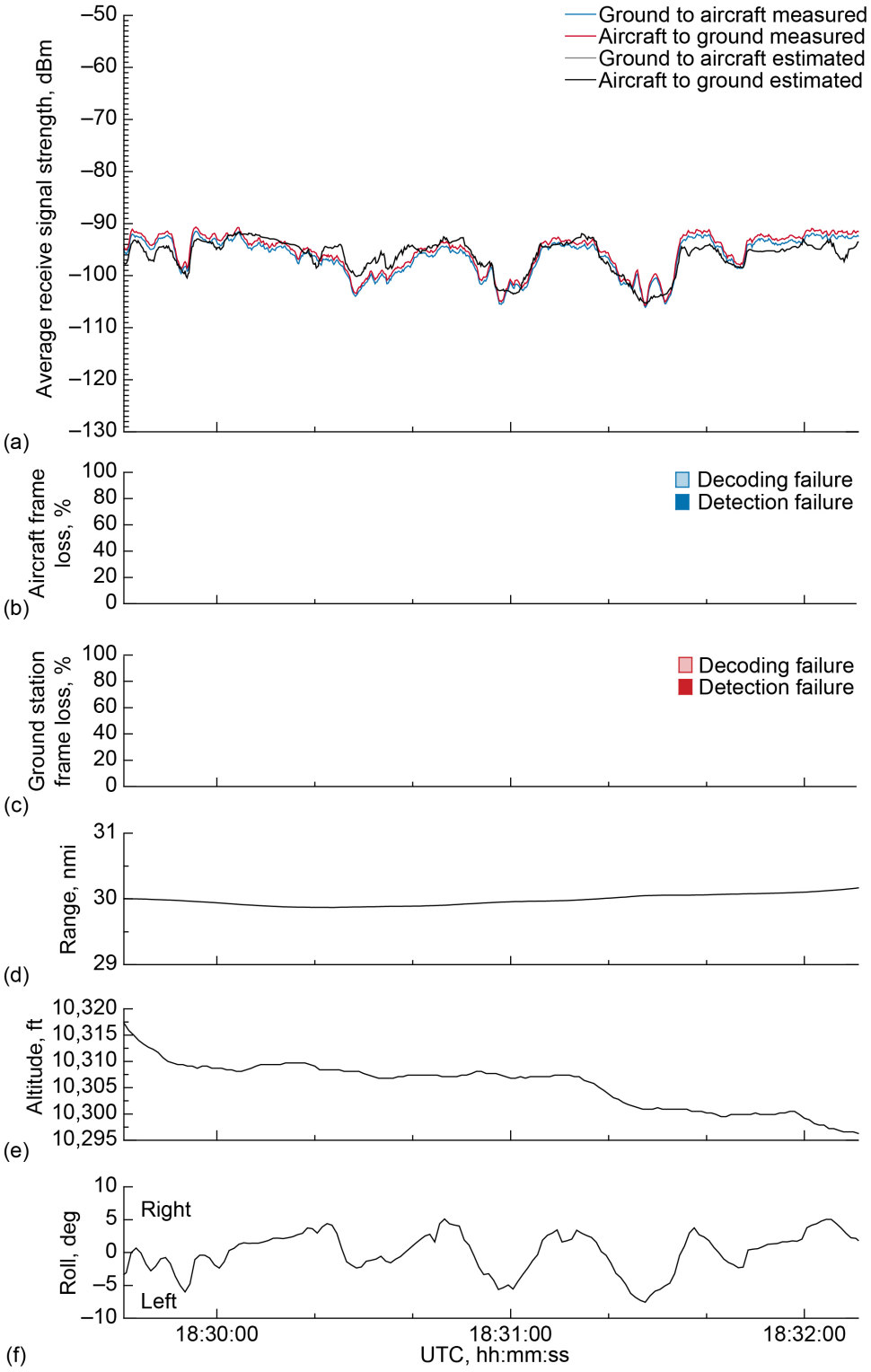

Figure 136.—Signal strength and frame loss over open freshwater at 30-nmi range and 10,500-ft altitude, 3.0° antenna elevation, traveling from waypoint C to waypoint D. (a) Average receive signal strength. (b) Aircraft frame loss. (c) Ground station frame loss. (d) Range. (e) Altitude. (f) Roll.

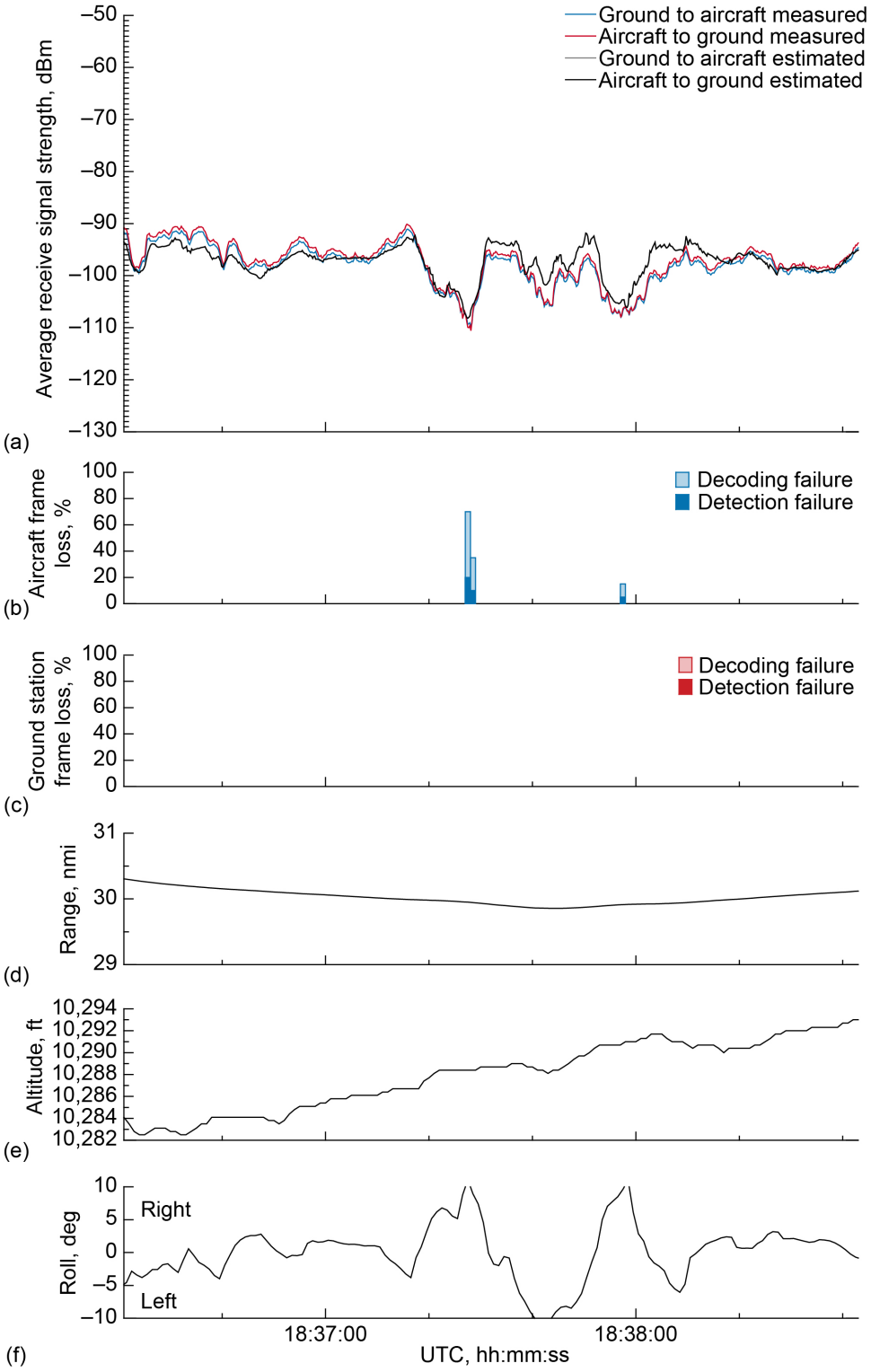

Figure 137.—Signal strength and frame loss over open freshwater at 30-nmi range and 10,500-ft altitude, 3.0° antenna elevation, traveling from waypoint D to waypoint C. (a) Average receive signal strength. (b) Aircraft frame loss. (c) Ground station frame loss. (d) Range. (e) Altitude. (f) Roll.

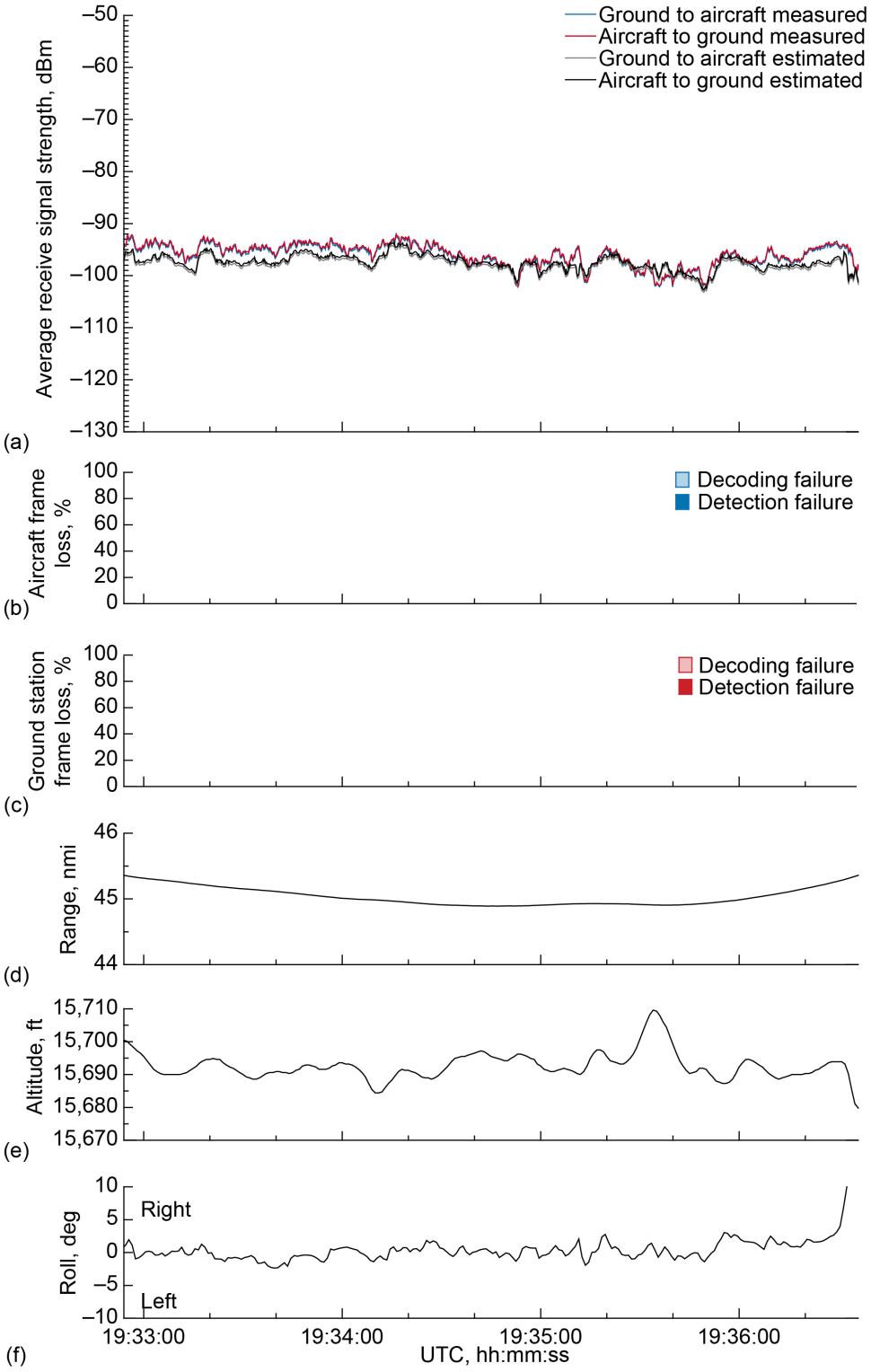

Figure 138.—Signal strength and frame loss over open freshwater at 45-nmi range and 15,500-ft altitude, 3.0° antenna elevation, traveling from waypoint E to waypoint F. (a) Average receive signal strength. (b) Aircraft frame loss. (c) Ground station frame loss. (d) Range. (e) Altitude. (f) Roll.

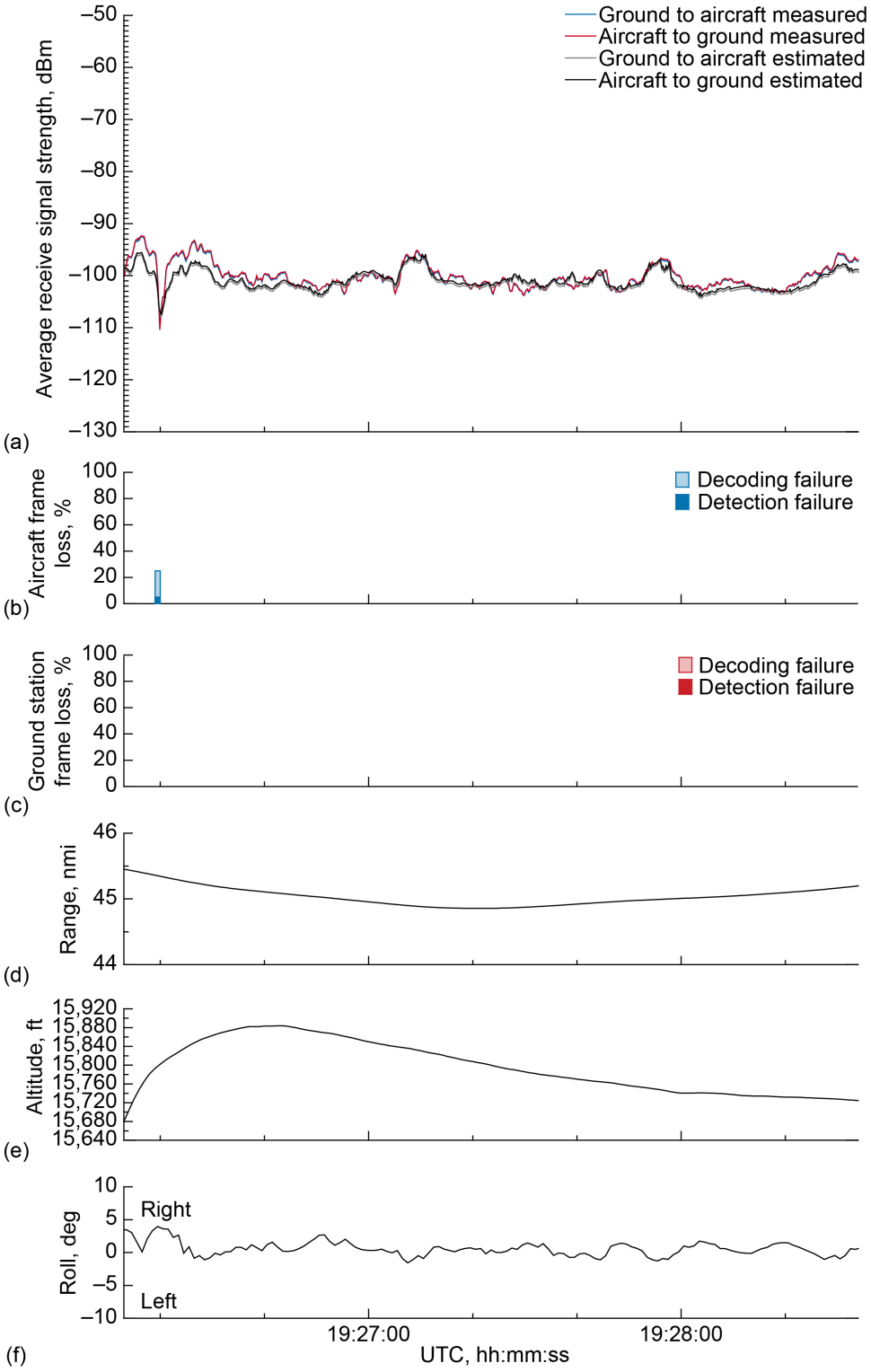

Figure 139.—Signal strength and frame loss over open freshwater at 45-nmi range and 15,500-ft altitude, 3.0° antenna elevation, traveling from waypoint F to waypoint E. (a) Average receive signal strength. (b) Aircraft frame loss. (c) Ground station frame loss. (d) Range. (e) Altitude. (f) Roll.

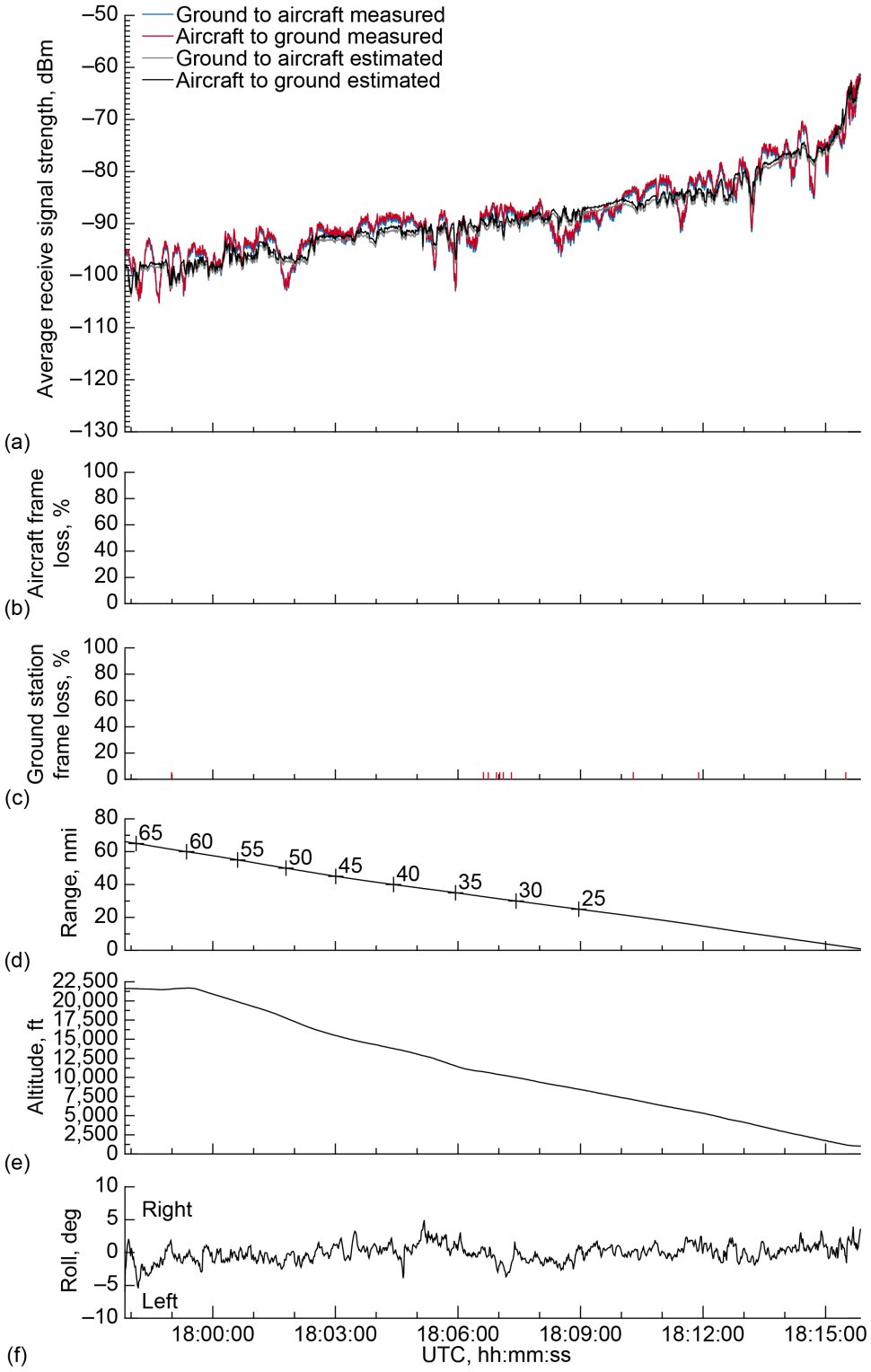

Figure 140.—Signal strength and frame loss over open freshwater during inbound, descending track on 3.0° glide slope, traveling toward ground station. (a) Average receive signal strength. (b) Aircraft frame loss. (c) Ground station frame loss. (d) Range. (e) Altitude. (f) Roll.

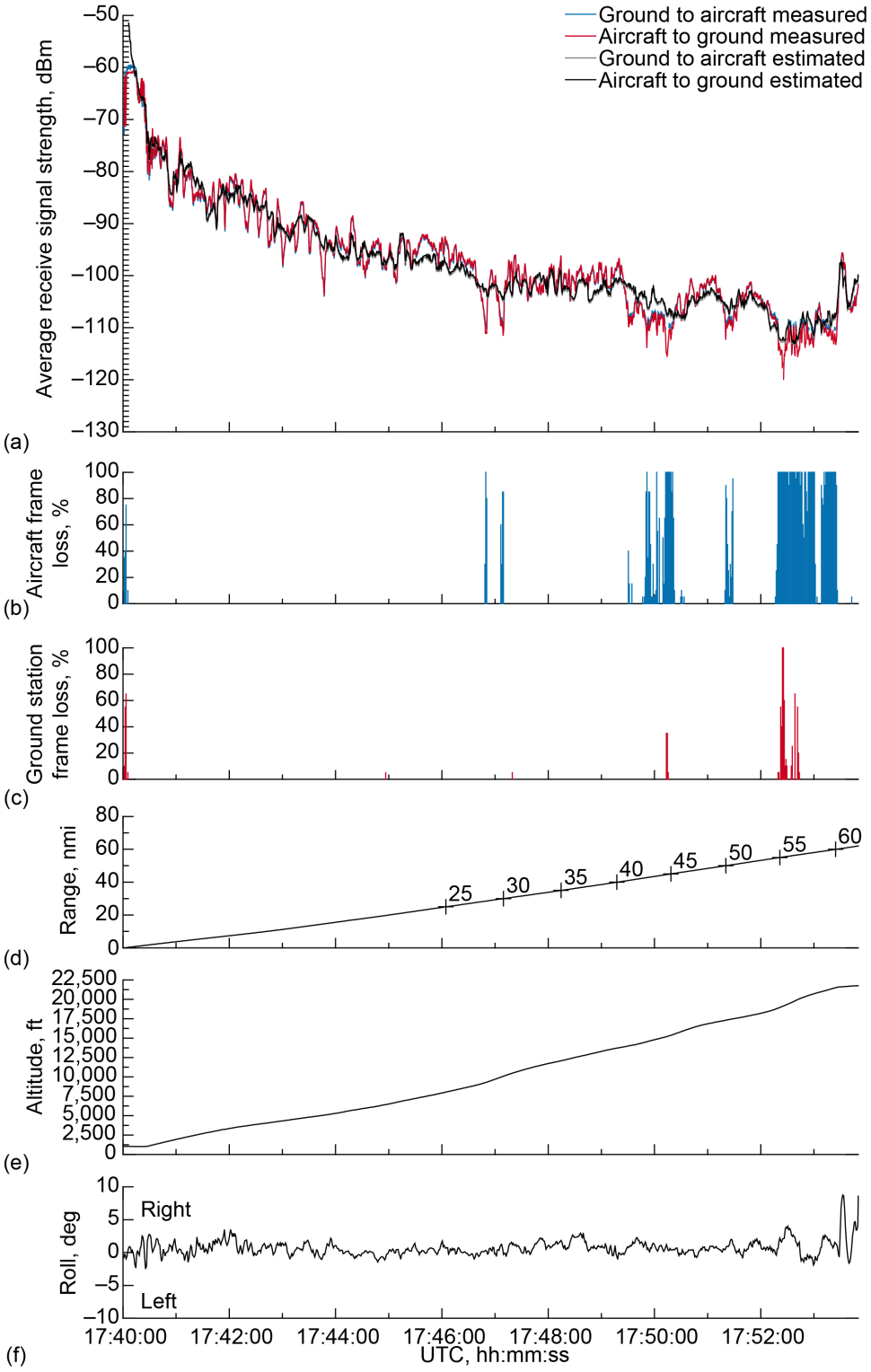

Figure 141.—Signal strength and frame loss over open freshwater during outbound, ascending track on 3.0° glide slope, traveling away from ground station. (a) Average receive signal strength. (b) Aircraft frame loss. (c) Ground station frame loss. (d) Range. (e) Altitude. (f) Roll.

3.5 Validation Test Data for Airport Surface Operations, February 19, 2020

Subsequent to the in-flight propagation measurements, the NASA GMSK CNPC test system was used to collect data during aircraft operations (taxiing) on a representative airport surface. Data from the test was also processed and included in the Excess Path Loss Assessment in Section 4.0. This was a very preliminary test performed without the engineering rigor used in the previously described tests. Still, it did validate concerns about aircraft antenna placement and solidly confirmed the need for further tests to investigate ground-specific multipath propagation issues.

For this test, the CNPC GRS was positioned at the northwest edge of the Cleveland Hopkins International Airport property (designation KCLE) in Cleveland, Ohio. The mobile tower mast supporting the GRS test antenna was elevated to 15 ft above ground level and remained stationary for the test. A full-wave dipole omnidirectional antenna providing 4.1-dBi gain was used to achieve the wide azimuthal coverage needed for the test. The NASA-owned S–3B Viking aircraft again served as the ARS using the same systems and C-band omnidirectional blade antenna as is in all previous tests. The aircraft was operated under its own power and was moved at a constant rate of speed along KCLE's 6,000- and 10,000-ft runways in both directions while CNPC radios were operated. Dwell periods were required between taxi and backtaxi runs to allow airport traffic to clear. The full path of the aircraft is displayed in Figure 142, with the reader noting that the trace includes both taxi and backtaxi paths.

Figure 143 presents the received signal strength and frame loss data from the surface operations test using GMSK CNPC waveform mode C. Vertical gray bands highlight periods of aircraft movement. Frame loss traces indicate a clear correlation to periods of aircraft movement. When stationary, the aircraft uplink and downlink both exhibited zero data frame errors and stable signal strength readings. When moving, however, the radios both recorded significant frame errors. Although the radios had difficulty decoding the CNPC signals during movement, the average received signal power levels were still detectable and, therefore, suitable for the excess path loss analysis.

Investigations into the causes of the signal errors immediately converged on multipath fading, channel delay dispersion, and the need for more frequent Doppler estimation. While these corrections were all achievable, the schedule to complete this report would not permit their inclusion in this writing. Guidance for addressing the surface operations propagation issues is presented in Subsection 2.2.1.12.2 of Reference 1. Additional test data is planned for future releases of Reference 1.

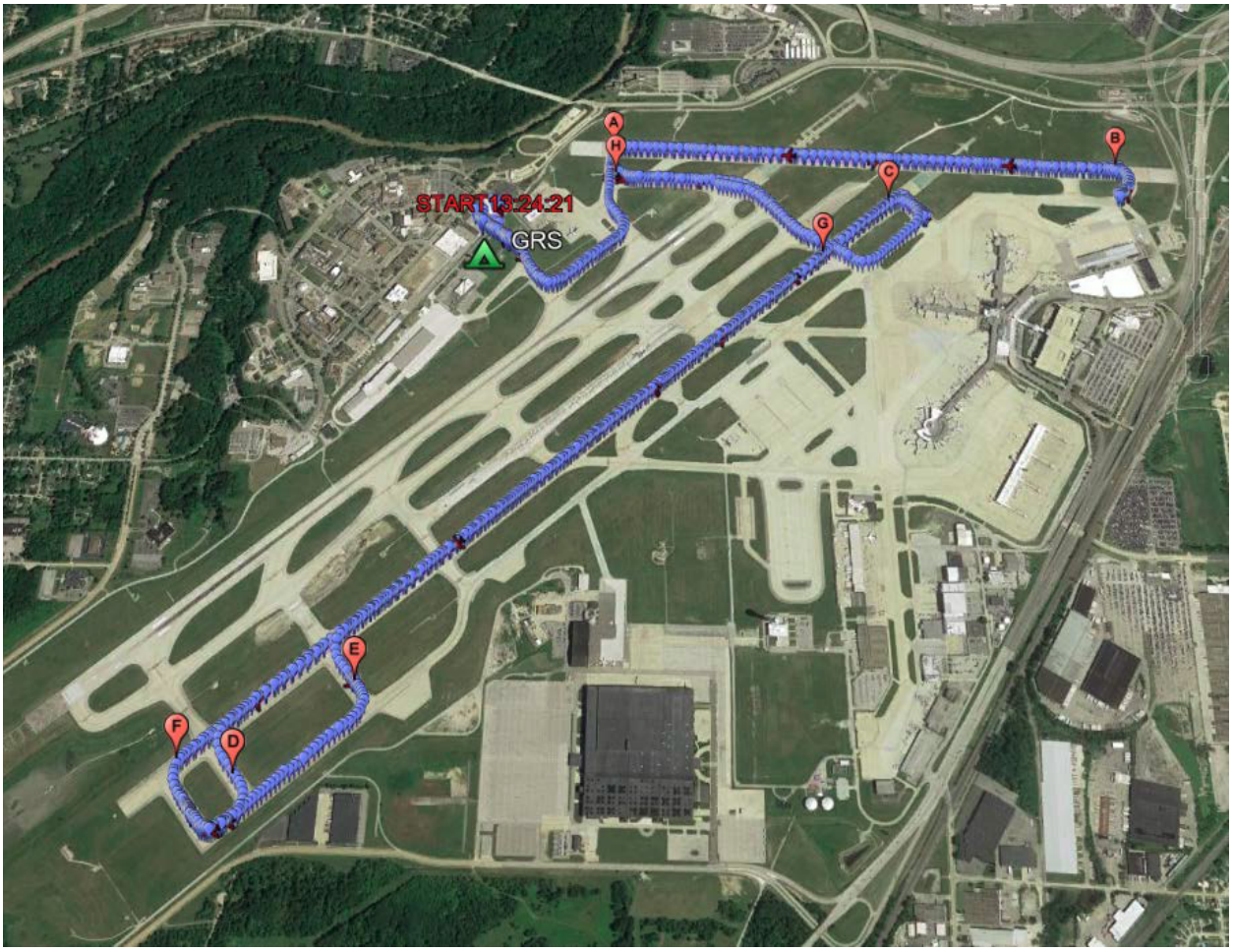

Figure 142.—View of taxiing path during surface operations test at Cleveland Hopkins Airport, February 19, 2020. Image ©2020 GoogleEarth.

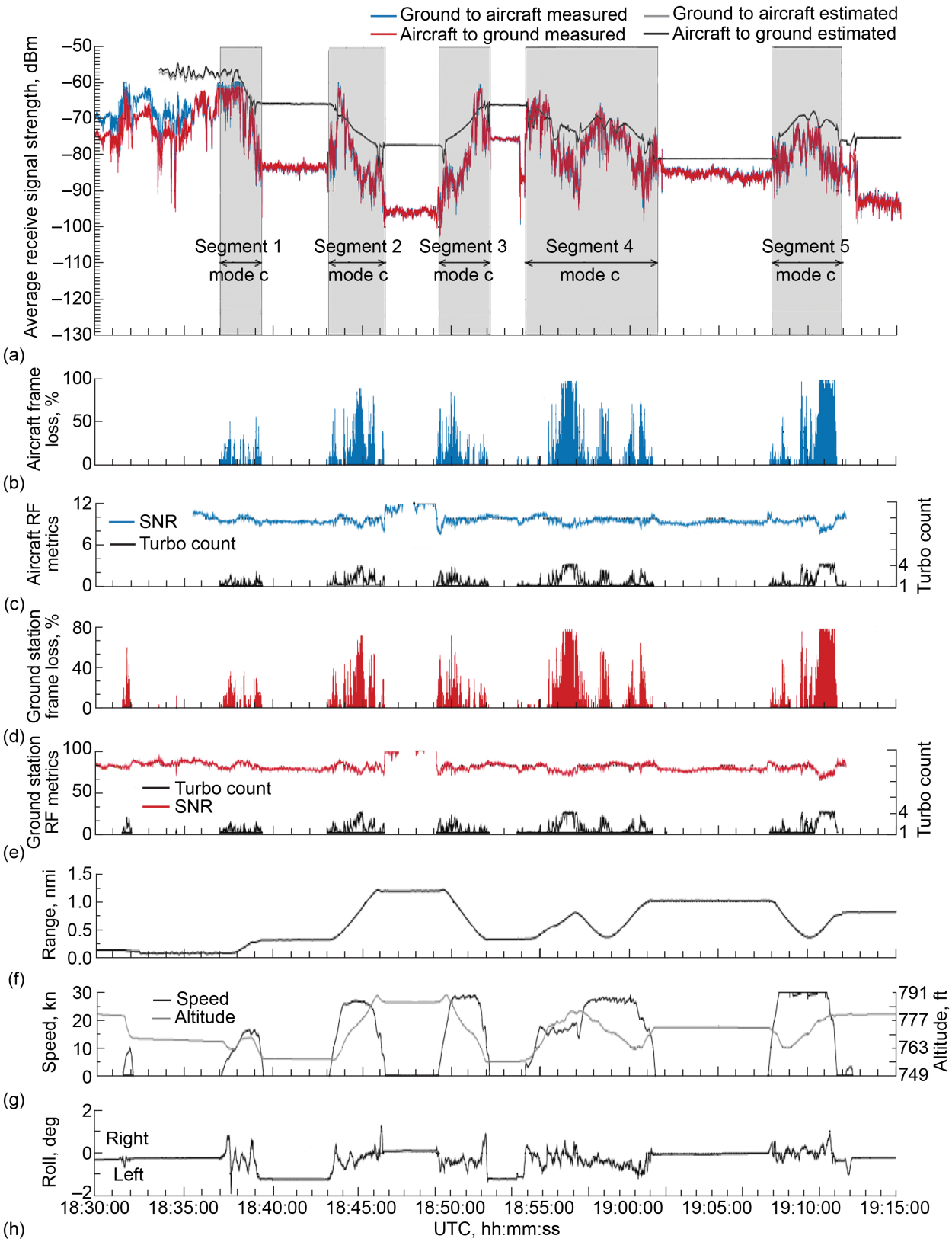

Figure 143.—Signal strength data from surface operations test, February 19, 2020. (a) Average receive signal strength. (b) Aircraft frame loss. (c) Aircraft radiofrequency (RF) metrics. Signal-to-noise ratio (SNR). (d) Ground station frame loss. (e) Ground station RF metrics. (f) Range. (g) Speed and altitude. (h) Roll.

4.0 Excess Path Loss Assessments

In addition to providing data to validate the overall performance of the CNPC ARS and GRS for the RTCA SC–228 standards (Ref. 1, Appendix S), the flight tests described in the preceding sections of this report were also used to determine the EPL that would be experienced by any link operating under similar conditions at similar frequencies. The EPL is the additional RF transmission loss in excess of that which would be predicted from the basic Friis (Ref. 3) RF transmission loss given by

$$L_{BF} = 20 \log_{10}(f) + 20 \log_{10}(r) + 32.45 \text{ dB} \quad (1)$$

where f is the operating frequency in MHz and r is the distance between the participating antennas in km. The factor of 32.45 dB is included to account for the constants and units used in the basic Friis equation. If r is measured in statute miles or nautical miles, then a factor of 36.58 or 37.80 dB, respectively, should be used. Further general discussion of link budget considerations can be found in Appendix F of Reference 4.

The EPLs are necessary to account for the received signal fading, which is the generic term describing both propagation medium refractive index effects and boundary reflection effects. The predominance of one or the other is dependent on the path length through the troposphere (which increases the variability due to the propagation medium) and the strength of the reflection from the boundary(s) (which increases the variability due to the reflection(s)). The latter is affected by the reflection coefficient of the boundary(s) (higher reflection coefficients increase the reflected signal level power) and their surface roughness (rougher surfaces scatter more energy in directions other than towards the receiving antenna).

EPLs are needed in a variety of places in RTCA standards to provide data for designers to use in their link system designs. The EPLs appear in the link budget considerations section of Appendix F in Reference 4 and in the link budget examples of Appendix L in Reference 1. The EPLs are also used in Appendix R in Reference 1 for the analysis of undesired-to-desired signal and signal-to-noise plus interference ratios for both airborne and surface operation to ensure that an appropriate amount of excess link margin is included to account for signal fading.

No propagation models or previous flight test data were available to provide this important information, so the flight tests described in the previous sections of this report were undertaken to capture these EPLs with aircraft flying over representative surface types and at ranges and altitudes that are representative of the desired operations.

The data provided in this section covers operating ranges up to 60 nmi at aircraft elevation angles that cleared the local terrain (within approximately 0.5 nmi) to the ground antenna by 1.0°, 1.5°, and 2.0° and for operations on airport surfaces.

The data is presented as graphs and tables of availability (A%), average fade duration (AFD in seconds) and level crossing rate (LCR, fades per minute). This information can be directly correlated to the availability and transaction expiration times in Reference 4 so that a designer wishing to obtain a particular Required Link Technical Performance can “look up” the EPL required to achieve that performance and then add that EPL into the basic Friis L_{BF} (see Eq. (1)) link budget to determine the total RF transmission loss for their particular design or desired operation.

The EPL was determined by subtracting the measured path loss (between the two antennas) captured during the flight tests from the calculated L_{BF} RF transmission loss based on the known exact location of the aircraft and ground antenna (slant range). A positive value of EPL indicates that the measured path loss was greater than the calculated path loss. EPLs ranging from –6 dB (i.e., 6 dB of signal enhancement) down to over 30 dB (i.e., 30 dB of fading) were measured.

The measured path loss between the two antennas was calculated from the precisely measured transmitter power, aircraft and ground antenna cable losses, and received signal strength indicator in the receiver. Note that the received signal strength indicator is taken as an average over 200 ms, therefore, the measured path loss, and subsequently, the calculated EPLs, should also be considered an average over a 200-ms period.

Both ground and aircraft antenna gains also need to be considered when calculating the measured path loss. For the ground antenna, this was done by "looking up" the gain that had been previously measured in an antenna test range for the exact azimuth and elevation of the aircraft at each sample point. For the aircraft antenna, this was not possible as its gain is significantly impacted by the presence of the aircraft's airframe.

To overcome this difficulty, the installed antenna pattern was estimated. For each received power measurement, an expected received power was calculated given the transmit power, ground and aircraft cable losses, the ground antenna gain, and L_{BF} RF transmission loss. The difference between the measured and expected received power was taken as a noisy estimate of the aircraft antenna gain at the azimuth and elevation angles resulting from the aircraft position and orientation. The gain estimates across all of the flight test datasets were separated into 0.5° by 0.5° azimuth and elevation bins. The data in each bin was then averaged to estimate the antenna's installed gain. Finally, Gaussian two-dimensional filtering was applied (standard deviation = 1) to smooth the results.

As can be seen from Figure 144, there is a significant difference between the estimate of the antenna gain when installed on the aircraft (black line) and the gain of the antenna when measured on an antenna test range (red line). The gray line indicates the raw (unfiltered) data. The pattern shown in Figure 144 is for all azimuths at an elevation angle 5° below horizontal relative to the aircraft's airframe, which is close to the angle used during the flight tests.

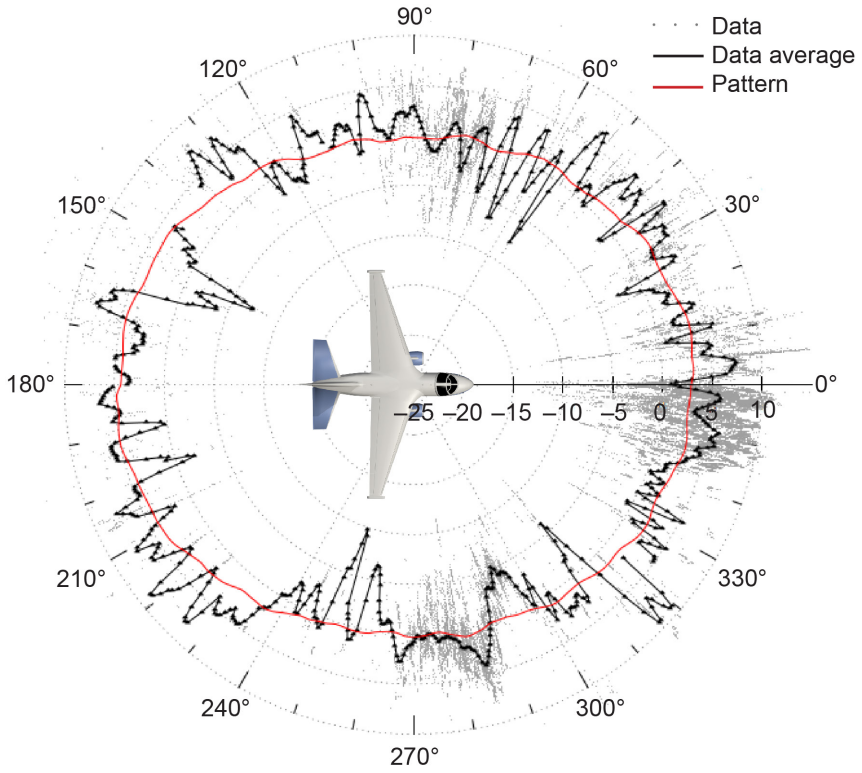

Figure 144.—Installed antenna gain estimate.

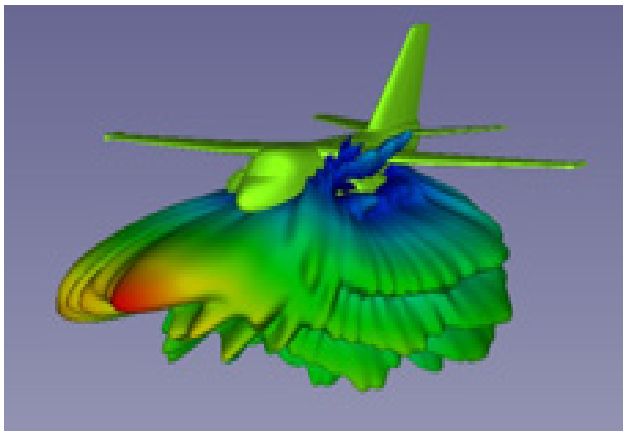

Figure 145.—Installed aircraft antenna gain simulation.

Although a simulation of the installed antenna gain was performed (Figure 145), which does confirm the significant lobing of the installed antenna, it was determined that using the estimated antenna gain based on the actual flight tests was a more precise method of calculating the true EPL. This is because, with only a 60-mm wavelength for the 5-GHz signals, even small changes in location of the antenna and airframe dimensions can have a significant impact on the exact antenna gain at a specific azimuth and elevation.

Once the EPLs had been calculated for each flight test, the data set was reduced to focus on periods of mostly straight and level flight. Since the estimated antenna pattern is less accurate in regions with limited data, periods of high maneuvering were removed from the analysis to reduce uncertainty. The outbound, ascending flight segments were found to have significant fuselage obstruction due to the aircraft's pitch and were also excluded from the analysis. The analysis thus incorporates data from the remaining 109 inbound and crosstrack flight segments described in Section 3.0.

The flight segments were categorized by the underlying terrain type (smooth plains, slightly rolling plains, and open freshwater), elevation angle (1.0°, 1.5°, and 2.0°), and range from the ground station (15, 30, 45, and 60 nmi). For the inbound segments, data within ±10 nmi of the selected ranges were included as part of that corresponding range group.

Within each category, the EPL data for each flight segment was compared to a series of reference levels from –6 to 30 dB. For each reference level, a flight segment is divided into periods of fades (where the EPL exceeds the reference level) and nonfades (where the EPL is less than the reference level). The number and length of the faded and unfaded periods are recorded for further use.

Special consideration is given to incomplete fade periods occurring at the start or end of a flight segment. In these cases, the fade began or ended outside of the segment; thus, the overall fade duration cannot be determined. Inclusion of short incomplete fades in the analysis can falsely shorten the average fade duration, while the exclusion of long incomplete fades incorrectly raises the availability. For this analysis, a conservative decision was made to include incomplete fades that are longer than the average (for that reference level) and exclude incomplete fades that are shorter than average.

Once all of the flight segments at a reference level had been analyzed, several basic quantities were calculated.

- Total number of fades (N_{faded}): The count of faded periods across all flight segments of a category at the reference level.

- Total faded duration (T_{faded}): The sum length of all faded periods across all flight segments of a category at the reference level.
- Total unfaded duration (T_{unfaded}): The sum length of all unfaded periods across all segments of a category at the reference level.

From these quantities, three parameters characterizing the EPL are computed.

- Availability (A%): The percentage of time the EPL was smaller than the reference level.

$$A\% = \frac{T_{\text{unfaded}}}{T_{\text{faded}} + T_{\text{unfaded}}}$$

- Average fade duration (AFD in seconds): The average length of time when the EPL exceeded the reference level.

$$AFD = \frac{T_{\text{faded}}}{N_{\text{faded}}}$$

- Level crossing rate (LCR, fades per minute): The number of times per minute the EPL crossed the reference level in an increasing direction, which is equivalent to the number of fades per minute.

$$LCR = \frac{N_{\text{faded}}}{T_{\text{faded}} + T_{\text{unfaded}}}$$

4.1 Excess Path Loss Values

Figure 146 to Figure 148 show the A%, AFD (in seconds), and LCR (fades per minute) for three of the terrain settings. Figure 146 was over slightly rolling plains with interdecile surface roughness ranging from 13.8 to 57.5 m. As can be seen, the A% was close to 100 percent, the AFD less than approximately 1 s, and the LCR less than one fade per minute with EPLs of greater than approximately 4 to 9 dB, depending on the range. As expected, the rough surface at the reflection point reduces the level of signal that is reflected towards the receiving antenna, so limiting the depth of the fades that can occur.

Figure 147 shows similar data but for a flight over freshwater at sea state 3 (1.6- to 4.0-ft wave height, Ref. 3) freshwater. In this test, the A% was close to 100 percent, the AFD less than approximately 1 s, and the LCR less than one fade per minute with EPLs of greater than approximately 16 to 21 dB, depending on the range. As expected, the fading over the water is more severe due to the strong dominant specular reflection from the surface of the water. It should be noted that the worst fading is not at the longest ranges. This is due to the reflection geometry where the reflected signal almost cancels the direct signal when the geometry of the reflection (due to a range and aircraft altitude combination) causes the reflected signal to exactly cancel the direct path signal due to its 180° phase difference.

Figure 148 again shows similar data but for a taxiing aircraft on the surface of an airport. In this test, the A% was close to 100 percent, the AFD less than approximately 1 s, and the LCR less than one fade per minute with EPLs of greater than 24 dB. As expected, the fading at short range on the surface is even more severe due to the even stronger dominant specular reflection, which is only slightly diminished because the surface is very smooth (less than 1 m roughness).

Table IV to Table X on the following pages provide the tabulated A%, AFD, and LCR versus EPL for 1.0°, 1.5°, and 2.0° elevation angles from the ground antenna to the airborne antenna over the various terrain types and ranges up to 60 nmi.

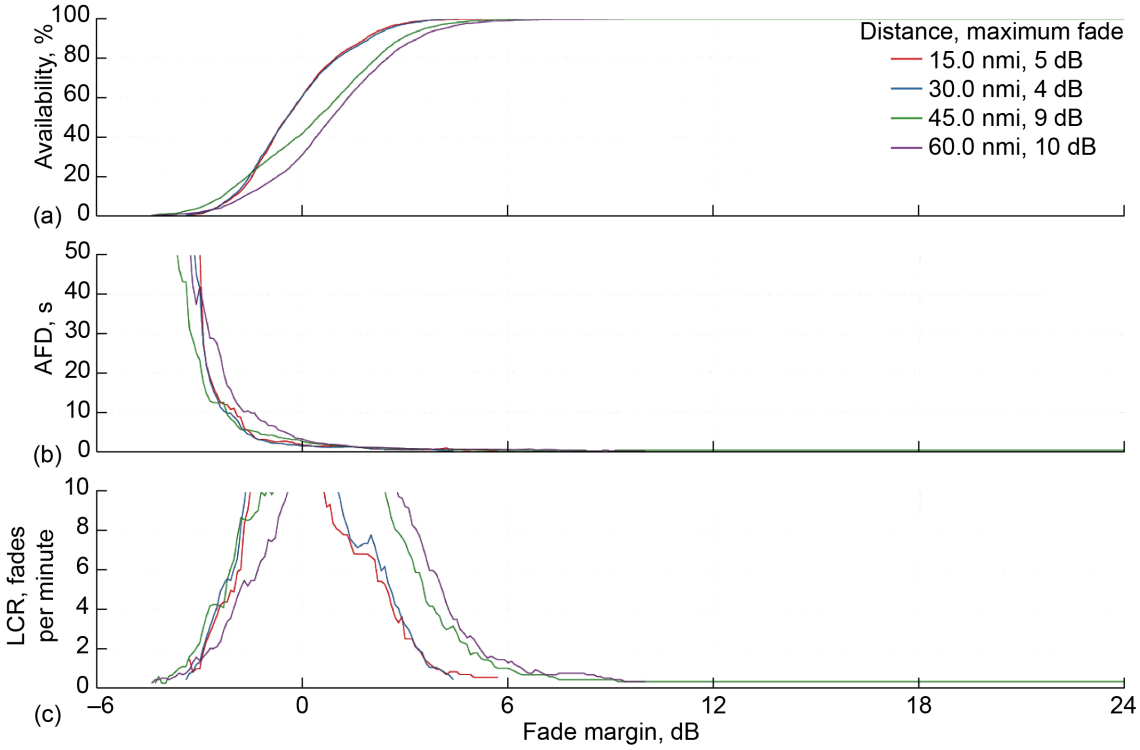

Figure 146.—Range data at 1.5° elevation over slightly rolling plain terrain. (a) Availability, (b) average fade duration (AFD), and (c) level crossing rate (LCR) versus fade margin.

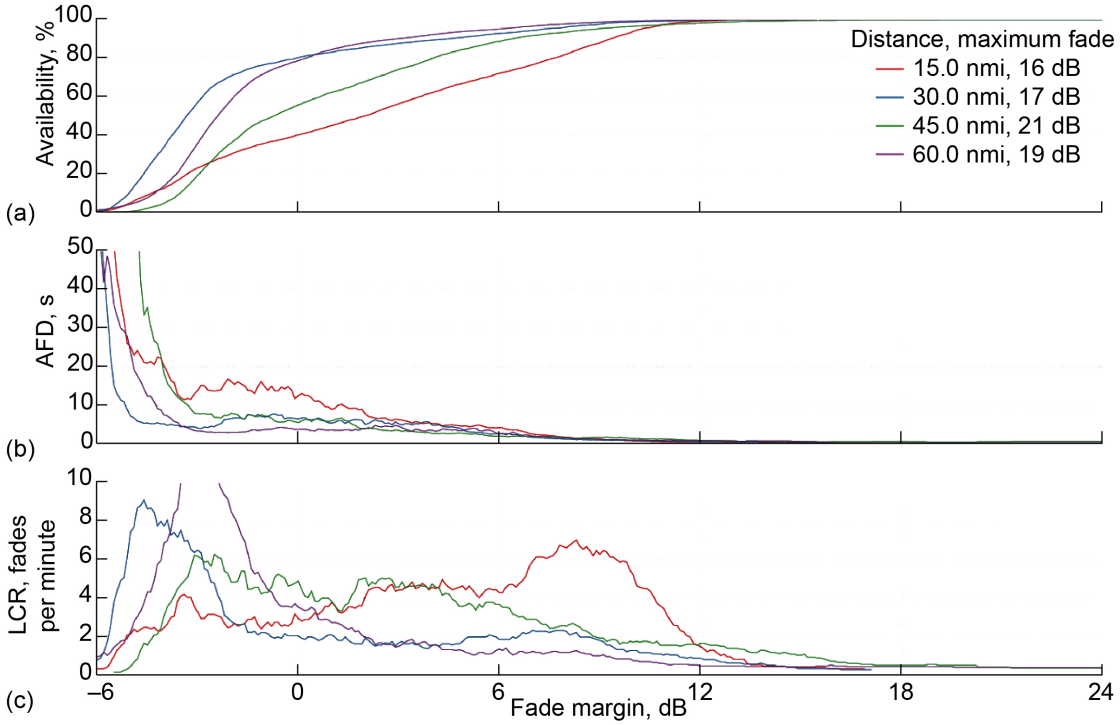

Figure 147.—Range data at 1.5° elevation over sea state 3 freshwater. (a) Availability, (b) average fade duration (AFD), and (c) level crossing rate (LCR) versus fade margin.

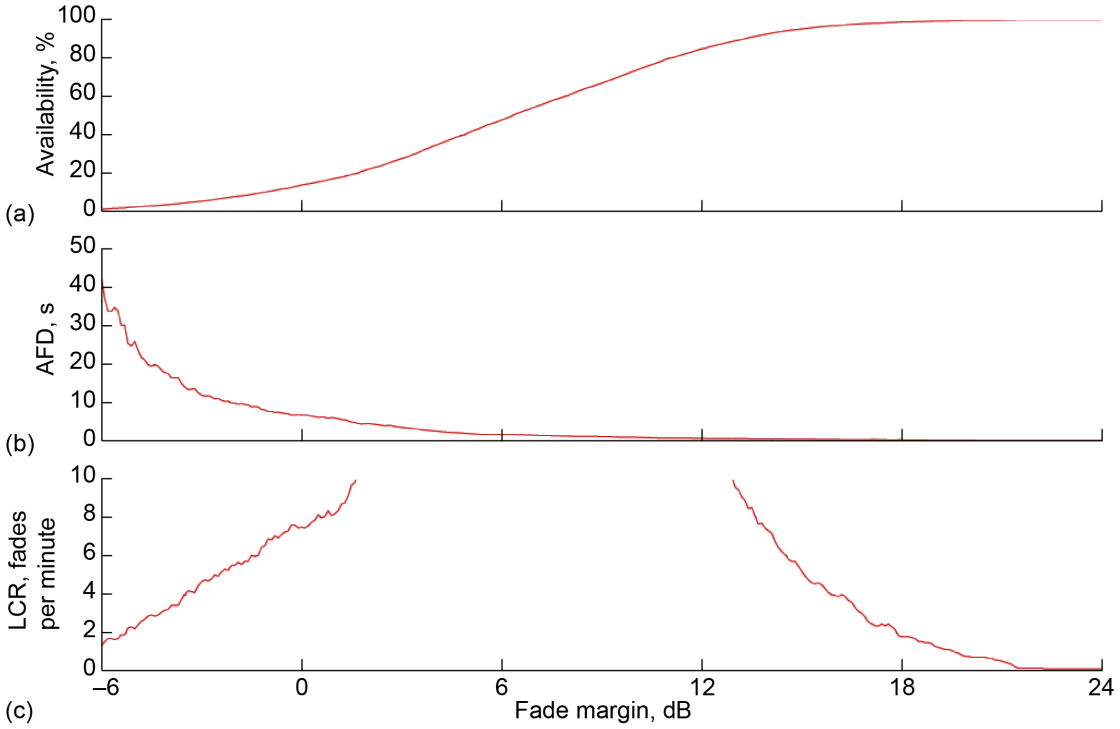

Figure 148.—Data for surface operation up to a range of 1.2 nmi with maximum fade at 24 dB. (a) Availability, (b) average fade duration (AFD), and (c) level crossing rate (LCR) versus fade margin.

TABLE IV.—AVAILABILITY (*A*%), AVERAGE FADE DURATION (*AFD*), AND LEVEL CROSSING RATE (*LCR*) AT 1.5° ELEVATION SLIGHTLY ROLLING PLAINS

Excess path loss, dB	Range, nmi at 1.5° elevation											
	15.0			30.0			45.0			60.0		
	A%	*AFD*, s	*LCR*, fades/min	*A*%	*AFD*, s	*LCR*, fades/min	*A*%	*AFD*, s	*LCR*, fades/min	*A*%	*AFD*, s	*LCR*, fades/min
–3	0.8	51.7	1.0	1.2	41.6	1.3	4.0	23.3	2.3	1.7	41.9	1.4
–2	9.8	11.1	4.9	10.5	8.9	6.1	14.4	7.8	6.5	6.8	13.7	4.1
–1	33.8	2.9	13.3	35.2	2.5	15.4	28.5	4.2	10.2	16.7	6.7	7.5
0	60.9	1.7	13.7	60.8	1.6	15.3	41.8	2.6	13.4	31.1	3.2	13.1
1	80.6	1.5	8.1	79.8	1.2	10.2	59.6	1.6	15.5	52.8	1.8	15.9
2	91.7	0.8	6.7	90.4	0.8	7.8	77.4	1.1	11.9	72.3	1.2	14.2
3	97.8	0.6	2.5	97.3	0.6	3.2	91.0	0.7	7.4	86.7	0.9	9.2
4	99.4	0.7	1.0	99.6	0.4	1.0	96.7	0.6	3.7	94.5	0.6	5.4
5	99.9	0.6	0.6	>99.9	0.2	0.4	98.9	0.4	1.8	97.8	0.6	2.5
6	>99.9	0.2	0.6	-------	-------	-------	99.5	0.4	1.0	99.0	0.6	1.3
7	-------	-------	-------	-------	-------	-------	99.8	0.3	0.7	99.6	0.5	0.8
8	-------	-------	-------	-------	-------	-------	99.9	0.4	0.4	99.7	0.3	0.8
9	-------	-------	-------	-------	-------	-------	99.9	0.3	0.4	99.9	0.3	0.5
10	-------	-------	-------	-------	-------	-------	99.9	0.4	0.3	>99.9	0.2	0.3

TABLE V.—AVAILABILITY (*A*%), AVERAGE FADE DURATION (*AFD*) AND LEVEL CROSSING RATE (*LCR*) AT 1.5° ELEVATION SEA STATE 3 FRESHWATER

Excess path loss, dB	Range, nmi at 1.5° elevation											
	15.0			30.0			45.0			60.0		
	A%	*AFD*, s	*LCR*, fades/min	*A*%	*AFD*, s	*LCR*, fades/min	*A*%	*AFD*, s	*LCR*, fades/min	*A*%	*AFD*, s	*LCR*, fades/min
–3	23.0	13.8	3.3	56.9	4.1	6.5	19.1	7.8	6.2	35.6	3.3	11.6
–2	30.1	16.1	2.5	70.7	6.6	2.8	35.9	7.9	4.8	58.2	3.0	8.5
–1	35.7	14.8	2.6	76.5	6.9	2.2	47.8	7.2	4.3	72.1	3.7	4.7
0	40.1	12.5	2.9	80.3	6.4	2.0	55.6	5.5	4.9	78.5	3.8	3.5
1	45.0	8.9	3.8	82.9	5.3	2.1	62.1	5.9	3.8	84.4	3.6	2.7
2	50.0	7.7	4.1	85.5	5.0	1.9	67.9	3.9	5.0	87.8	4.0	1.9
3	56.3	6.2	4.4	87.6	5.1	1.7	74.0	3.5	4.6	90.1	4.5	1.5
4	61.9	5.2	4.6	89.2	4.8	1.6	79.7	2.7	4.7	92.0	3.5	1.5
5	67.2	4.7	4.4	90.8	3.3	1.9	84.7	2.6	3.6	93.8	3.7	1.2
6	72.0	4.2	4.3	92.7	2.7	1.9	88.5	2.0	3.7	95.0	2.5	1.4
7	76.5	2.5	5.9	94.2	1.7	2.3	91.6	1.8	2.9	96.6	2.0	1.2
8	81.9	1.7	6.6	96.0	1.2	2.3	93.4	1.7	2.5	97.6	1.5	1.2
9	87.8	1.2	6.3	97.5	1.0	1.8	95.2	1.6	1.9	98.4	1.1	1.0
10	93.8	0.8	5.2	98.6	0.8	1.3	96.5	1.4	1.7	99.1	1.0	0.7
11	97.4	0.5	3.1	99.0	0.7	1.1	97.3	1.2	1.6	99.4	1.0	0.6
12	99.0	0.5	1.5	99.4	0.5	0.9	98.0	0.8	1.7	99.6	0.8	0.5
13	99.6	0.4	0.8	99.7	0.5	0.6	98.6	0.7	1.4	99.7	0.7	0.5
14	99.8	0.5	0.5	99.8	0.3	0.5	99.0	0.6	1.2	99.7	0.7	0.4
15	99.9	0.4	0.4	>99.9	0.2	0.3	99.3	0.5	1.0	99.8	0.6	0.4
16	>99.9	0.2	0.3	-------	------	-------	99.5	0.5	0.7	99.9	0.3	0.5
17	-------	------	-------	-------	------	-------	99.7	0.6	0.6	99.9	0.3	0.4
18	-------	------	-------	-------	------	-------	99.7	0.6	0.5	-----	------	-------
19	-------	------	-------	-------	------	-------	99.7	0.4	0.6	-----	------	-------
20	-------	------	-------	-------	------	-------	99.8	0.4	0.5	-----	------	-------
21	-------	------	-------	-------	------	-------	99.8	0.6	0.4	-----	------	-------
22	-------	------	-------	-------	------	-------	99.8	0.7	0.4	-----	------	-------

TABLE VI.—AVAILABILITY (*A*%), AVERAGE FADE DURATION (*AFD*), AND LEVEL CROSSING RATE (*LCR*) ON AIRPORT SURFACE 0.1- TO 1.2-nmi RANGE

Excess path loss, dB	*A*%	*AFD*, s	*LCR*, fades/min
–3	5.4	12.1	4.7
–2	7.8	9.9	5.5
–1	10.4	7.7	6.9
0	13.8	6.8	7.5
1	17.3	6.0	8.2
2	22.0	4.6	10.2
3	27.6	3.6	12.1
4	34.4	2.6	15.0
5	41.1	2.0	17.7
6	47.8	1.8	17.8
7	54.6	1.6	17.6
8	60.8	1.3	17.9
9	66.9	1.2	16.4
10	73.4	1.0	15.6
11	79.8	0.9	14.2
12	84.9	0.7	12.3
13	89.1	0.7	9.6
14	92.8	0.6	7.3
15	95.3	0.5	5.2
16	97.0	0.5	3.9
17	98.2	0.4	2.6
18	98.9	0.4	1.8
19	99.4	0.3	1.3
20	99.7	0.3	0.8
21	99.8	0.2	0.5
22	>99.9	0.2	0.2

TABLE VII.—AVAILABILITY (*A*%), AVERAGE FADE DURATION (*AFD)*, AND LEVEL CROSSING RATE (*LCR*) AT 1.0° ELEVATION SLIGHTLY ROLLING PLAINS

Excess path loss, dB	Range, nmi at 1.0° elevation											
	15.0			30.0			45.0			60.0		
	A%	*AFD*, s	*LCR*, fades/min	*A*%	*AFD*, s	*LCR*, fades/min	*A*%	*AFD*, s	*LCR*, fades/min	*A*%	*AFD*, s	*LCR*, fades/min
–3	0.8	58.5	0.8	2.7	20.9	2.5	4.6	31.1	1.9	6.0	13.3	4.2
–2	4.5	19.1	2.6	12.9	6.4	8.0	10.5	10.4	5.2	15.1	5.8	8.8
–1	17.5	5.4	9.2	31.2	2.8	14.5	19.4	5.7	8.5	30.6	3.3	12.6
0	38.9	2.1	17.3	56.2	1.7	15.1	32.7	2.8	14.4	49.1	2.1	14.8
1	59.3	1.6	15.6	74.1	1.4	11.3	54.2	1.7	16.7	69.3	1.5	12.1
2	77.1	1.2	11.5	85.5	1.3	6.7	75.4	1.3	11.6	82.2	1.4	7.9
3	90.5	1.0	6.4	93.3	1.1	3.8	87.8	0.9	8.1	91.4	1.1	4.9
4	96.7	0.8	2.9	97.8	0.7	2.1	95.3	0.7	4.3	96.4	0.8	3.0
5	99.3	0.7	1.0	99.4	0.5	0.9	97.8	0.7	2.1	98.4	0.8	1.4
6	>99.9	0.2	0.5	>99.9	0.2	0.4	99.0	0.6	1.2	99.0	0.7	1.0
7	-------	------	------	-------	------	------	99.3	0.8	0.7	99.5	0.8	0.6
8	-------	------	------	-------	------	------	99.4	1.2	0.5	99.5	1.0	0.5
9	-------	------	------	-------	------	------	99.4	1.5	0.4	-------	------	------

TABLE VIII.—AVAILABILITY (*A*%), AVERAGE FADE DURATION (*AFD*), AND LEVEL CROSSING RATE (*LCR*) AT 1.0° ELEVATION SEA STATE 3 FRESHWATER

Excess path loss, dB	Range, nmi at 1.0° elevation											
	15.0			30.0			45.0			60.0		
	A%	*AFD*, s	*LCR*, fades/min	*A*%	*AFD*, s	*LCR*, fades/min	*A*%	*AFD*, s	*LCR*, fades/min	*A*%	*AFD*, s	*LCR*, fades/min
–3	30.4	10.3	4.2	52.0	4.5	6.4	12.7	45.8	1.1	14.3	13.2	3.9
–2	40.3	10.8	3.5	67.4	5.1	3.8	17.0	50.8	1.1	23.5	8.5	5.3
–1	47.8	9.7	3.5	76.4	5.1	2.8	19.6	36.9	1.4	36.6	6.5	5.8
0	55.1	17.8	1.9	84.0	5.2	2.0	24.0	24.4	2.0	50.0	4.5	6.6
1	58.5	14.2	2.1	87.2	5.2	1.6	29.7	13.8	3.2	64.2	4.0	5.5
2	61.8	18.4	1.6	89.9	4.5	1.5	37.3	12.0	3.3	73.0	4.9	3.4
3	65.6	10.0	2.4	91.7	3.4	1.6	43.9	8.8	4.0	78.1	6.0	2.2
4	71.1	7.7	2.7	93.7	5.1	0.9	50.4	6.7	4.7	82.1	5.9	1.9
5	75.9	6.0	2.8	94.4	4.5	0.9	57.2	5.7	4.8	85.6	4.4	2.1
6	81.1	5.3	2.6	95.3	3.5	1.0	63.9	3.7	6.2	88.9	3.5	2.1
7	84.3	5.4	2.2	96.1	3.4	0.9	70.9	2.6	6.9	91.6	3.5	1.6
8	86.7	4.2	2.3	96.9	3.4	0.7	77.6	1.9	7.3	93.8	3.0	1.4
9	88.7	4.1	2.1	97.5	2.8	0.7	83.0	1.4	7.4	94.9	2.1	1.6
10	90.8	3.5	2.0	97.9	2.2	0.7	87.9	1.1	6.7	96.8	1.5	1.5
11	93.0	2.2	2.3	98.5	1.5	0.8	91.0	1.0	5.8	97.9	1.3	1.1
12	95.3	1.5	2.3	99.0	2.6	0.4	93.5	1.0	4.3	98.5	1.1	1.0
13	97.0	1.1	2.0	99.2	2.0	0.4	95.0	0.9	3.5	99.0	0.8	0.9
14	98.1	1.3	1.3	99.5	1.7	0.4	96.2	0.8	3.1	99.2	0.8	0.8
15	98.5	1.1	1.2	99.6	4.0	0.3	97.0	0.8	2.6	99.3	0.7	0.8
16	99.0	0.9	1.1	99.7	3.0	0.3	97.4	0.7	2.5	99.3	0.7	0.7
17	99.3	1.3	0.7	99.8	2.2	0.3	97.7	0.7	2.3	99.3	0.7	0.7
18	99.5	0.9	0.7	99.8	1.8	0.3	97.9	0.6	2.2	99.4	0.7	0.7
19	99.8	0.7	0.6	99.9	0.8	0.3	98.0	0.6	2.2	99.4	0.6	0.7
20	99.9	0.4	0.5	99.9	0.8	0.3	98.1	0.6	2.2	99.4	0.6	0.7
21	>99.9	0.2	0.5	>99.9	0.4	0.3	98.1	0.6	2.1	99.4	0.6	0.7
22	-------	------	------	>99.9	0.2	0.3	-----	------	------	99.5	0.5	0.7

TABLE IX.—AVAILABILITY (*A*%), AVERAGE FADE DURATION (*AFD*), AND LEVEL CROSSING RATE (*LCR*) AT 2.0° ELEVATION SLIGHTLY ROLLING PLAINS

Excess path loss, dB	Range, nmi at 2.0° elevation											
	15.0			30.0			45.0			60.0		
	A%	*AFD*, s	*LCR*, fades/min	*A*%	*AFD*, s	*LCR*, fades/min	*A*%	*AFD*, s	*LCR*, fades/min	*A*%	*AFD*, s	*LCR*, fades/min
–3	0.6	75.1	0.5	0.3	63.4	0.6	1.0	54.9	1.0	2.4	38.3	1.6
–2	2.6	30.2	2.1	2.5	18.9	3.0	3.7	17.3	3.2	6.6	12.1	4.7
–1	18.9	4.1	12.1	12.8	4.9	10.4	11.5	6.5	8.2	18.4	4.0	12.4
0	51.2	1.9	15.7	42.8	2.1	15.8	29.5	2.9	14.5	38.5	2.2	17.1
1	81.9	1.0	11.4	72.1	1.3	13.1	49.4	2.4	12.7	62.1	1.5	15.4
2	94.7	0.7	4.6	87.6	0.8	9.0	72.1	1.5	11.2	82.5	1.1	10.0
3	98.4	0.5	2.2	94.9	0.8	3.9	87.0	1.1	7.2	93.4	0.9	4.6
4	99.8	0.2	1.1	97.8	0.7	2.0	94.4	0.8	4.5	97.2	1.2	1.6
5	99.9	0.2	0.7	99.3	0.8	0.8	98.2	0.6	2.0	98.8	0.9	1.0
6	------	------	-------	>99.9	0.2	0.4	99.7	0.3	0.9	99.5	0.5	0.8
7	------	------	-------	-------	------	------	>99.9	0.2	0.3	99.9	0.2	0.5
8	------	------	-------	-------	------	------	-------	------	------	>99.9	0.2	0.3

TABLE X.—AVAILABILITY (*A*%), AVERAGE FADE DURATION (*AFD*), AND LEVEL CROSSING RATE (*LCR*) AT 2.0° ELEVATION SEA STATE 3 FRESHWATER

Excess path loss, dB	Range, nmi at 2.0° elevation											
	15.0			30.0			45.0			60.0		
	A%	*AFD*, s	*LCR*, fades/min	*A*%	*AFD*, s	*LCR*, fades/min	*A*%	*AFD*, s	*LCR*, fades/min	*A*%	*AFD*, s	*LCR*, fades/min
–3	28.2	17.1	2.3	18.8	12.5	3.8	10.9	14.0	3.6	15.2	8.3	6.2
–2	37.2	13.1	2.6	30.2	18.0	2.4	19.4	11.9	3.9	28.1	6.3	6.9
–1	43.2	21.2	1.4	35.3	19.9	2.1	29.5	6.1	6.8	39.5	5.9	6.4
0	46.7	17.4	1.6	41.6	11.6	3.3	40.0	4.7	7.5	48.9	5.8	5.5
1	50.4	13.7	2.0	50.4	6.9	4.6	50.1	4.1	7.1	56.5	5.5	4.9
2	53.8	12.7	2.0	60.2	5.9	4.3	58.7	3.3	7.4	62.5	5.3	4.5
3	57.4	9.7	2.4	71.9	3.9	4.6	66.3	2.6	7.7	67.9	4.8	4.3
4	62.3	6.0	3.8	79.4	3.6	3.7	72.5	2.2	7.5	73.4	3.4	4.9
5	66.8	5.0	4.0	85.3	5.3	1.9	78.4	2.0	6.6	79.6	2.4	5.3
6	73.2	2.3	7.2	90.2	2.8	2.4	83.5	2.0	5.0	85.1	2.1	4.4
7	83.8	1.1	8.7	93.3	2.4	1.9	86.7	1.7	4.7	88.7	2.1	3.5
8	92.9	0.7	6.5	96.7	1.3	1.8	90.3	1.4	4.4	91.7	1.5	3.5
9	98.0	0.7	2.2	98.6	1.4	0.9	93.7	1.0	3.7	94.4	1.3	2.7
10	99.5	0.3	1.1	99.3	1.6	0.5	96.6	0.7	3.3	96.3	1.2	2.1
11	>99.9	0.2	0.5	99.6	0.7	0.6	98.4	0.5	2.0	97.3	1.0	1.9
12	-------	------	-----	>99.9	0.2	0.4	99.0	0.5	1.5	97.9	1.0	1.5
13	-------	------	-----	-------	------	-------	99.3	0.5	1.2	98.2	1.0	1.3
14	-------	------	-----	-------	------	-------	99.3	0.5	1.0	98.4	0.9	1.3
15	-------	------	-----	-------	------	-------	99.4	0.5	1.0	98.6	1.0	1.1

References

1. RTCA, Inc.: Command and Control (C2) Data Link Minimum Operational Performance Standards (MOPS) (Terrestrial). RTCA DO–362, Revision A, 2020.
2. Shalkhauser, Kurt: Control and Non-Payload Communications Generation 7 Radio Flight Test Report. NASA/TM-20205011515, 2021. https://ntrs.nasa.gov
3. Friis, H.T.: A Note on a Simple Transmission Formula. Proc. IRE, vol. 34, no. 5, 1946, pp. 254–256.
4. RTCA, Inc.: Minimum Aviation System Performance Standards for C2 Link Systems Supporting Operations of Unmanned Aircraft Systems in U.S. Airspace. RTCA DO–377, Revision A, 2021.